Mechanisms and consequences of bacterial resistance to natural antibiotics

Thesis by

Elena Kim Perry

In Partial Fulfillment of the Requirements for the Degree of

Doctor of Philosophy in Biology

CALIFORNIA INSTITUTE OF TECHNOLOGY

Pasadena, California

2021

(Defended March 31, 2021)

Elena Kim Perry
ORCID: 0000-0002-7151-1479

ACKNOWLEDGEMENTS

I would not be where I am today without the support and guidance of many people over the years. To my parents, thank you for always encouraging me to follow my interests, from providing countless books to feed my fascination with animals and nature as a young child to helping me find internship opportunities as a high schooler. To Aunt Yung Suk, thank you for ensuring that I always had the resources to thrive. To my 8th grade science teacher, Margaret Pennock, thank you for your infectious enthusiasm and for giving me my first taste of scientific research—from designing a hypothesis, to collecting and analyzing data, to writing up a report. Our survey of local native bee populations sparked in me an interest in insects, ecology, and conservation that continues to this day. To Barry Kaplan, thank you for hosting my first research experience in a molecular biology laboratory. To Sam Droege, thank you for generously sharing your dataset and serving as the advisor for my first independent research project. To Michael Reiser, thank you for taking me on for the undergraduate summer internship where I first learned how to write a computer program, a skill that has been invaluable during my PhD. To Leo Buss, my undergraduate academic advisor, thank you for the chance to participate in your Peabody Museum course, which gave me confidence in asking my own research questions; for your feedback on my writing; for introducing me to the fascinating biology of *Podocoryne carnea* and giving me the opportunity to work in your lab; and for supporting my career aspirations. To Dong-Chan Oh and the members of the Oh lab, thank you for introducing me to the wonderful, wild world of microbes and natural product chemistry, setting me on the path that eventually led to my PhD thesis research. To Tracy Mincer and Kristen Whalen, thank you for introducing me to screen design and metabolomics. To my undergraduate senior thesis advisor, Jason Crawford, and the members of the Crawford lab, especially Hyun-Bong Park, thank you for providing me with a solid technical foundation in microbiology and chemistry, for showing me the importance of considering the environmental context that microbes live in, and for fostering my interest in how small molecules mediate interspecies interactions. To Mike Taylor and the members of the Taylor lab, thank you for welcoming me to New Zealand, introducing me to the charismatic kākāpō, and teaching me how to conduct a microbiota profiling study.

To the professors who have served on my thesis advisory committee at Caltech—Rustem Ismagilov, Sarah Reisman, Jared Leadbetter, Marianne Bronner, and Joseph Parker—thank you for

your insightful questions, advice, and support. To Joseph Parker, an extra thank you for letting me moonlight as a quasi-member of your lab and for supporting and advising my side project on the microbiotas of ants and myrmecophiles, which has been a significant and enriching part of my experience at Caltech outside of my thesis research. To Justin Bois, thank you for your thoughtful advice on data analysis and statistics. To all of the group members I have overlapped with—David Basta, Brittany Belin, Megan Bergkessel, John Ciemniecki, Kyle Costa, Kurt Dahlstrom, Daniel Dar, Will DePas, Avi Flamholz, Nate Glasser, Peter Jorth, Gargi Kulkarni, Zach Lonergan, Darcy McRose, Lucas Meirelles, Caj Neubauer, Shannon Park, Lisa Racki, Scott Saunders, Nick Shikuma, Melanie Spero, Georgia Squyres, Elise Tookmanian, Lev Tsypin, Chelsey VanDrisse, and Steven Wilbert—thank you for making the Newman lab such a welcoming, supportive, and stimulating place to work. Special thanks to my co-authors—Megan, for sharing your RNA-seq analysis pipeline, for our many scientific discussions over the years, and for the careful thought you always devoted to my questions and dilemmas; and Lucas, for being the best collaborator I could ever imagine and a great friend. To my thesis advisor, Dianne Newman, thank you for being exactly the mentor I needed—someone who is unfailingly positive and supportive, who knew how to talk me through my periodic spirals of doubt and existential angst about my research, and who gave me the freedom to pursue my own scientific ideas and explore a non-academic career path.

Finally, thank you to my husband, Shashank Gandhi, whom I met the very first day I arrived at Caltech. From spending long nights working together on homework for Justin's Data Analysis course, to acting as a sounding board for my trials and tribulations in the lab, to celebrating discoveries and successes, to helping me appreciate the importance of taking breaks for travel and exploration, you have been there with me every step of the way. I look up to the example you provide as a scientist; your creativity, passion, and dedication continually inspire me. My graduate school experience has been infinitely richer and more rewarding because of you, and I can't wait to see where our journeys will take us.

ABSTRACT

Many bacteria secrete natural antibiotics—toxic small molecules that can kill or inhibit the growth of other microorganisms. Several of these compounds have been commercialized as antimicrobial drugs, and the mechanisms and public health consequences of bacterial resistance to clinically-used antibiotics are well understood. By contrast, the role of bacterially-produced antibiotics in natural environments, where they have existed for millions of years, remains an open question. Besides potentially serving as tools of warfare between competing microbes, natural antibiotics have been proposed to serve less antagonistic functions ranging from the acquisition of nutrients to the transmission of signals between cells. Indeed, despite evidence that natural antibiotics can suppress sensitive microbes in environments such as the soil surrounding plant roots, the ecological significance of the toxicity of these molecules has sometimes been questioned. At the same time, for most natural antibiotics, the mechanisms and prevalence of resistance are either poorly characterized or entirely unknown.

This thesis addresses the molecular mechanisms and consequences of bacterial resistance to a particular class of redox-active natural antibiotics called phenazines. Phenazines are produced by a major opportunistic human pathogen, *Pseudomonas aeruginosa*, during infections, as well as by several bacterial species that associate with the roots of crops such as wheat, where they serve to protect their plant hosts against fungal pathogens. Resistance to this family of natural antibiotics is therefore potentially relevant to multiple sectors of human society. I begin by investigating the intrinsic phenazine resistance of a common soil bacterium, *Agrobacterium tumefaciens*, that does not itself produce phenazines. Using a functional genetics approach, I find that the composition of the respiratory electron transport chain plays a critical role in mitigating phenazine toxicity, one that cannot be compensated by increased expression of efflux pumps that transport phenazines out of the cell or oxidative stress responses that neutralize the toxic byproducts of phenazine redox-cycling. Subsequently, we turn to *P. aeruginosa*, the phenazine-producing opportunistic pathogen, and demonstrate that the defenses it activates against its own toxic phenazine, pyocyanin, collaterally accelerate the acquisition of resistance to certain clinical antibiotics. Other bacteria known to form multispecies infections with *P. aeruginosa* can also benefit from exposure to pyocyanin in the presence of these clinical antibiotics; we show that in at least one strain isolated from a patient, the

effect of pyocyanin on the frequency of spontaneous antibiotic-resistant mutants rivals that of disruptions in DNA repair machinery. Importantly, a growing body of reports suggests that, besides pyocyanin, other metabolites produced by bacterial pathogens can also affect the efficacy of clinical antibiotics. We review the evidence for which types of bacterial metabolites alter susceptibility to antimicrobial drugs, as well as the mechanisms underlying this phenomenon. Finally, I examine the prevalence of bacterial resistance to an agriculturally-relevant phenazine in a wheat field where the use of native phenazine producers to control crop diseases has been studied for decades. I discover that while Gram-positive bacteria are generally more susceptible to this phenazine compared to Gram-negative bacteria, the sharpness of this distinction is pH-dependent; moreover, I uncover surprising heterogeneity in phenazine resistance within certain taxonomic groups. Taken together, these findings illuminate recurring themes in mechanisms of phenazine resistance and point to an underappreciated role for natural antibiotics in the resilience of opportunistic pathogens to clinical antibiotics. This thesis also lays the groundwork for developing a predictive model of phenazine resistance across diverse bacteria, with potential implications for optimizing the use of clinical antibiotics and improving agricultural sustainability.

PUBLISHED CONTENT AND CONTRIBUTIONS

Perry, E.K., and Newman, D.K. (2019) The transcription factors ActR and SoxR differentially affect the phenazine tolerance *of Agrobacterium tumefaciens. Mol Microbiol* **112**: 199-218. doi: 10.1111/mmi.14263.

E.K.P. participated in conceptualizing the study, performed the experiments, analyzed the data, and wrote the manuscript.

Meirelles, L.A.*, Perry, E.K.*, Bergkessel, M., and Newman, D.K. (2021) Bacterial defenses against a natural antibiotic promote collateral resilience to clinical antibiotics. *PLoS Biol* **19**: e3001093. doi: 10.1371/journal.pbio.3001093.

E.K.P. participated in conceptualizing the study, designed and performed the experiments related to antibiotic resistance, analyzed the resulting data, and participated in writing the manuscript.

*Equal contribution

Perry, E.K.*, Meirelles, L.A.*, and Newman, D.K. From the soil to the clinic: the impact of microbial secondary metabolites on antibiotic tolerance and resistance. (Submitted)

E.K.P. participated in conceptualizing the theme and structure of the review, collecting the literature, and writing the manuscript.

*Equal contribution

TABLE OF CONTENTS

Chapter 1

INTRODUCTION

A brief history of natural antibiotics

For most people, the word "antibiotic" likely evokes doctors, prescriptions, and pills manufactured by pharmaceutical companies. Indeed, since the commercialization of penicillin in the 1940s, antibiotics—that is, organic molecules that kill or inhibit the growth of microorganisms—have become arguably the greatest "wonder drugs" of modern medicine, having extended the average human lifespan by 23 years and enabled the development of procedures ranging from cancer treatments to organ transplants (Hutchings *et al.*, 2019). Unfortunately, concomitantly with the rise in antibiotic use over the past century, antibiotic resistance—that is, the ability to grow in the presence of an antibiotic—has also been observed with increasing and alarming frequency in both clinical and environmental isolates of bacteria, leading to serious concerns about the future utility of antibiotics in medicine (Davies and Davies, 2010; Aminov, 2010). Yet the history of antibiotics and antibiotic resistance dates back long before the adoption of these compounds for human purposes. Phylogenetic evidence indicates that microbes have been making antibiotics and evolving resistance for hundreds of millions of years (Waglechner *et al.*, 2019). In fact, the term "antibiotic" was originally proposed to refer specifically to microbially-produced antimicrobial substances, as opposed to synthetic chemicals (Waksman, 1947). The meaning has since broadened in common parlance, but antibiotics derived from soil-dwelling microbes—including penicillin—still represent the majority of antimicrobial drugs used in clinics today (Hutchings *et al.*, 2019).

Though widespread therapeutic use of antibiotics did not come to fruition until the mid-20th century, the fact that microbes compete with each other and can hinder the growth and survival of their competitors has been recognized since at least 1874, when William Roberts of Manchester described how cultures of *Penicillium* fungi in liquid media "held in check" the growth of bacteria, and conversely, how cultures densely populated with bacteria were difficult to infect with *Penicillium* (Roberts, 1874; Foster and Raoult, 1974). Roberts also noticed that certain "races of bacteria" seemed to be antagonistic towards certain others. On the basis of these observations, he presciently wrote:

> [I]t may be assumed that, what takes place when an organic liquid is exposed to the contamination of air or water, is this: a considerable variety of germinal particles are introduced into it, and it depends on a number of conditions (composition of the liquid, its reaction, precedence, and abundance of the several germs) which of these shall grow and take a lead, and which shall partially or wholly lie dormant and unproductive. There is probably in such a case a struggle for existence and a *survival of the fittest*. And it would be hazardous to conclude because a particular organism was not found growing in a fertile infusion, that the germs of the organism were really absent from the contaminating media. (Roberts, 1874)

Roberts was followed soon after by John Tyndall of London. In 1875, approximately a decade after Louis Pasteur's seminal experiments on spontaneous generation, fermentation, and the germ theory of disease (Berche, 2012), Tyndall set up an experiment consisting of numerous test tubes containing infusions of different types of meat, fish, or vegetables, which he exposed to the air. Tyndall observed that the infusions differed in the rate at which "putrefaction" (i.e. bacterial growth) set in, and moreover, that certain types of putrid infusions were more likely to be overtaken by the growth of *Penicillium*, while others seemed to repel the fungus (Tyndall, 1876). That the latter phenomenon might be related to chemical substances produced by the bacteria was hinted at by the following:

> Another difference, pointing to differences in the life of the air, was shown by these tubes. The turbidity of the two mould-crowned ones was colourless, exhibiting a grey hue. The third tube, the middle one of the three, contained a bright yellow-green pigment, and on its surface no trace of mould was to be seen. It never cleared, but maintained its turbidity and its Bacterial life for months after the other tubes had ceased to show either. It cannot be doubted that the mould-spores fell into this tube also, but in the fight for existence the *colour-producing Bacteria* had the upper hand [emphasis added]. (Tyndall, 1876)

Tyndall repeatedly saw the appearance of such pigmented bacteria among his cultures, and noted that they "frequently show[ed] a singular power in preventing the development of mould" (Tyndall, 1876). It has since become widely appreciated by microbiologists that diverse bacteria

have evolved means of engaging in microbial warfare, often through the secretion of toxic small molecules (Tyc *et al.*, 2017; Granato *et al.*, 2019). Moreover, the chemical and biological diversity of these compounds extends far beyond those that have been coopted for use in human medicine (Bérdy, 2012). Interestingly, as Tyndall noticed, these natural antibiotics are often strikingly colored (Price-Whelan *et al.*, 2006; Charkoudian *et al.*, 2010; Glasser *et al.*, 2017).

Despite the obvious fitness benefits of suppressing one's competitors, the toxicity of natural antibiotics may sometimes represent a side effect rather than their primary purpose. Additional functions that have been demonstrated for specific natural antibiotics include nutrient acquisition (Wang *et al.*, 2011; McRose and Newman, 2021), cell-cell signaling (Dietrich *et al.*, 2006; Linares *et al.*, 2006), and conservation of energy in the absence of oxygen (Glasser *et al.*, 2014). Nevertheless, evidence accumulated over the past few decades suggests that natural antibiotics can and do also function in an inhibitory capacity in nature, and that the pressure to evolve resistance against these molecules may therefore be pervasive. For example, antibiotic production plays an essential role in the suppression of plant pathogens by certain bacteria in the rhizosphere (i.e. the region of soil immediately surrounding plant roots) (Thomashow and Weller, 1988; Handelsman and Stabb, 1996; Chin-A-Woeng *et al.*, 2003). Moreover, in many soil bacteria, antibiotic production is triggered by the presence of specific competitors (Garbeva and de Boer, 2009; Onaka *et al.*, 2011; Pérez *et al.*, 2011; Garbeva *et al.*, 2011; Traxler *et al.*, 2013; Tyc *et al.*, 2014).

As a result of their varied biological activities, even natural antibiotics that lack utility as therapeutic drugs can be highly relevant to human health and agriculture. One such class of natural antibiotics is the phenazines, a family of bacterially-produced pigments characterized by a three-ringed heterocyclic structure containing two central nitrogen atoms (Turner and Messenger, 1986). Different phenazines are distinguished by different functional groups at various positions around the rings. These chemical variations contribute to a variety of traits, including brilliant colors spanning the full spectrum of the rainbow (Turner and Messenger, 1986; Price-Whelan *et al.*, 2006). However, a key shared property is that most naturally-occurring phenazines are redox-active under physiological conditions, meaning that they can gain electrons from cellular reductants, such as NADH, and subsequently donate them to oxidants, such as molecular oxygen (Hassan and Fridovich, 1980; Price-Whelan *et al.*, 2006; Wang and Newman, 2008). It is this property that is thought to underpin their broad-spectrum antimicrobial activity, as the redox-cycling of phenazines can

generate reactive oxygen species (ROS) (Hassan and Fridovich, 1980) and interfere with components of the respiratory electron transport chain (Baron and Rowe, 1981; Voggu *et al.*, 2006).

At least four phenazines are produced by the opportunistic human pathogen *Pseudomonas aeruginosa*, which can cause serious chronic infections in immunocompromised patients (Villavicencio, 1998; Price-Whelan *et al.*, 2006). One of these phenazines, pyocyanin, confers *P. aeruginosa* with its eponymous blue-green color (the Latin "*aerugo*" refers to the color of copper rust) (Price-Whelan *et al.*, 2006). The antimicrobial activity of pyocyanin was recognized as far back as the 19th century, and in fact, after being isolated and named in 1859 by M. J. Fordos (Fordos, 1859), pyocyanin eventually became what was likely the first antibiotic to be used in a hospital, in the 1890s (Emmerich and Löw, 1899; Aminov, 2010). Unfortunately, the toxicity of pyocyanin also extends to humans, and pyocyanin is now considered to be a virulence factor that damages host tissue and enhances the severity of *P. aeruginosa* infections (Lau *et al.*, 2004). Yet while phenazines are harmful to humans in the context of infections, these natural antibiotics can be beneficial in agriculture: several rhizosphere-dwelling *Pseudomonas* species produce phenazines that efficiently suppress the growth of fungal crop pathogens. As a result, certain strains of *Pseudomonas* have received attention as potential "biocontrol" agents that might more sustainably protect crops from disease compared to synthetic fungicides (Handelsman and Stabb, 1996).

Despite these multifaceted roles of phenazines and their relevance to human interests, our understanding of how *Pseudomonas* species and certain other bacteria resist these toxins is relatively rudimentary compared to our detailed understanding of resistance to clinical antibiotics (Handelsman and Stabb, 1996; Blair *et al.*, 2015). A handful of studies have suggested that efflux (i.e. the transport of small molecules out of cells), oxidative stress responses, and/or variations in the components of the respiratory electron transport chain may help counteract the toxicity of pyocyanin (Hassan and Fridovich, 1980; Voggu *et al.*, 2006; Khare and Tavazoie, 2015; Noto *et al.*, 2017), while a comparison of 14 phylogenetically diverse bacterial species suggested that as a group, Gram-negative bacteria tend to be more resistant to pyocyanin than Gram-positive bacteria (Baron and Rowe, 1981). Additionally, a few soil bacteria have been found to possess phenazine-degrading enzymes (Yang *et al.*, 2007; Costa *et al.*, 2015; Costa *et al.*, 2018). Nevertheless, major gaps remain in our ability to predict which bacteria can resist phenazines, and our knowledge of how they do so—especially for phenazines other than pyocyanin. A deeper understanding of the molecular

mechanisms that drive phenazine resistance could inspire new approaches for the treatment of chronic *P. aeruginosa* infections, which are notoriously difficult to eradicate with traditional antibiotics (Rice, 2006; Hurley *et al.*, 2012). Furthermore, characterizing the prevalence of phenazine resistance in agricultural soils could help predict the effects of biocontrol agents on native rhizosphere bacterial communities, as well as the likelihood of phenazine resistance acquisition in target crop pathogens (Handelsman and Stabb, 1996). This thesis represents a first step towards these goals.

Overview

In Chapter 2, I investigate the molecular mechanisms of resistance to pyocyanin in a common soil bacterium and plant pathogen, *Agrobacterium tumefaciens*. Based on a phenotypic screen of ~5000 transposon insertion mutants, I find that the cellular processes involved in pyocyanin resistance fall into four general categories: 1) transcriptional regulation of stress responses, 2) central metabolism and maintenance of the proton-motive force, 3) cell wall biosynthesis and modification, and 4) transport of small molecules. I then dive deeper into the mechanisms underlying the loss-of-function phenotypes of two transcriptional regulators identified in this screen, ActR and SoxR. I show that at low concentrations of pyocyanin, appropriate preemptive regulation of the respiratory electron transport is more important for tolerance of pyocyanin toxicity than the induction of oxidative stress responses and efflux pumps.

In Chapter 3, I turn to the producer of pyocyanin, *P. aeruginosa*, and address how its ability to tolerate pyocyanin toxicity affects the acquisition of heritable antibiotic resistance. This work was done in collaboration with another graduate student in the Newman lab, Lucas Meirelles, who began by performing a genetic screen to reveal molecular mechanisms of pyocyanin tolerance in *P. aeruginosa*. Several findings from this screen overlap with those described in Chapter 2, suggesting that diverse pyocyanin-resistant bacteria may share fundamentally similar mechanisms of resistance. We reveal that a specific efflux pump induced by pyocyanin in *P. aeruginosa* confers cross-tolerance to structurally similar clinical antibiotics, such as fluoroquinolones. We then demonstrate that exposure to pyocyanin significantly increases the rate at which spontaneous antibiotic resistant mutants are detected in growing populations of *P. aeruginosa*. Lastly, we extend these findings to other opportunistic pathogens that can form multispecies infections together with *P. aeruginosa*.

In Chapter 4, together with Lucas, I review the evidence that, beyond pyocyanin, other so-called secondary metabolites (i.e. small molecules that are not directly involved in central metabolism) produced by opportunistic and enteric pathogens can affect the efficacy of clinical antibiotics. In particular, we focus on secondary metabolites that upregulate efflux pump expression and those that generate ROS, induce oxidative stress responses, or directly detoxify harmful free radicals. We posit that as a result of these interactions between diverse secondary metabolites and clinical antibiotics, the evolutionary history and ecological roots of microbial antagonism may have important consequences for how one ought to approach the diagnosis of antibiotic resistance and the optimal use of antibiotics for human benefit.

In Chapter 5, I return to the context of soil and the rhizosphere, where phenazines contribute to the suppression of crop pathogens. I describe the development of an assay that enables comparisons of phenazine susceptibility across diverse bacteria isolated from a dryland wheat field in Washington state, where the role of phenazine producers in natural suppression of crop disease has been studied for decades (Weller and Cook, 1983; Thomashow and Weller, 1988; Thomashow *et al.*, 1990). I also discuss preliminary results from this assay, including the discovery that at acidic pH, susceptibility to an agriculturally-relevant phenazine may broadly correlate with high-level phylogeny, whereas at circumneutral pH, susceptibility can vary even within the same genus.

Finally, in Chapter 6, I provide concluding remarks, including a summary of our current understanding of phenazine resistance and a few suggestions for future research directions that would build on the findings of this thesis.

References

Aminov, R.I. (2010) A brief history of the antibiotic era: lessons learned and challenges for the future. *Front Microbiol* **1**: 134.

Baron, S.S., and Rowe, J.J. (1981) Antibiotic action of pyocyanin. *Antimicrob Agents Chemother* **20**: 814–820.

Berche, P. (2012) Louis Pasteur, from crystals of life to vaccination. *Clin Microbiol Infect* **18 Suppl 5**: 1–6.

Bérdy, J. (2012) Thoughts and facts about antibiotics: where we are now and where we are heading. *J Antibiot* **65**: 385–395.

Blair, J.M.A., Webber, M.A., Baylay, A.J., Ogbolu, D.O., and Piddock, L.J.V. (2015) Molecular mechanisms of antibiotic resistance. *Nat Rev Microbiol* **13**: 42–51.

Charkoudian, L.K., Fitzgerald, J.T., Khosla, C., and Champlin, A. (2010) In living color: bacterial

pigments as an untapped resource in the classroom and beyond. *PLoS Biol* **8**.
Chin-A-Woeng, T.F.C., Bloemberg, G.V., and Lugtenberg, B.J.J. (2003) Phenazines and their role in biocontrol by *Pseudomonas* bacteria. *New Phytol* **157**: 503–523.
Costa, K.C., Bergkessel, M., Saunders, S., Korlach, J., and Newman, D.K. (2015) Enzymatic degradation of phenazines can generate energy and protect sensitive organisms from toxicity. *mBio* **6**: e01520-15.
Costa, K.C., Moskatel, L.S., Meirelles, L.A., and Newman, D.K. (2018) PhdA catalyzes the first step of phenazine-1-carboxylic acid degradation in *Mycobacterium fortuitum. J Bacteriol* **200**.
Davies, J., and Davies, D. (2010) Origins and evolution of antibiotic resistance. *Microbiol Mol Biol Rev* **74**: 417–433.
Dietrich, L.E., Price-Whelan, A., Petersen, A., Whiteley, M., and Newman, D.K. (2006) The phenazine pyocyanin is a terminal signalling factor in the quorum sensing network of *Pseudomonas aeruginosa*. *Mol Microbiol* **61**: 1308–1321.
Emmerich, R., and Löw, O. (1899) Bakteriolytische Enzyme als Ursache der erworbenen Immunität und die Heilung von Infectionskrankheiten durch dieselben. *Zeitschr f Hygiene* **31**: 1–65.
Fordos, M.J. (1859) Recherches sur la matière colorante des suppurations bleues: pyocyanine. *Rec Trav Soc d'Émul Sci Pharm* **3**: 30.
Foster, W., and Raoult, A. (1974) Early descriptions of antibiosis. *J R Coll Gen Pract* **24**: 889–894.
Garbeva, P., and Boer, W. de (2009) Inter-specific interactions between carbon-limited soil bacteria affect behavior and gene expression. *Microb Ecol* **58**: 36–46.
Garbeva, P., Silby, M.W., Raaijmakers, J.M., Levy, S.B., and Boer, W. de (2011) Transcriptional and antagonistic responses of *Pseudomonas fluorescens* Pf0-1 to phylogenetically different bacterial competitors. *ISME J* **5**: 973–985.
Glasser, N.R., Kern, S.E., and Newman, D.K. (2014) Phenazine redox cycling enhances anaerobic survival in *Pseudomonas aeruginosa* by facilitating generation of ATP and a proton-motive force. *Mol Microbiol* **92**: 399–412.
Glasser, N.R., Saunders, S.H., and Newman, D.K. (2017) The colorful world of extracellular electron shuttles. *Annu Rev Microbiol* **71**: 731–751.
Granato, E.T., Meiller-Legrand, T.A., and Foster, K.R. (2019) The evolution and ecology of bacterial warfare. *Curr Biol* **29**: R521–R537.
Handelsman, J., and Stabb, E.V. (1996) Biocontrol of soilborne plant pathogens. *Plant Cell* **8**: 1855–1869.
Hassan, H.M., and Fridovich, I. (1980) Mechanism of the antibiotic action pyocyanine. *J Bacteriol* **141**: 156–163.
Hurley, M.N., Cámara, M., and Smyth, A.R. (2012) Novel approaches to the treatment of *Pseudomonas aeruginosa* infections in cystic fibrosis. *Eur Respir J* **40**: 1014–1023.
Hutchings, M.I., Truman, A.W., and Wilkinson, B. (2019) Antibiotics: past, present and future. *Curr Opin Microbiol* **51**: 72–80.
Khare, A., and Tavazoie, S. (2015) Multifactorial competition and resistance in a two-species bacterial system. *PLoS Genet* **11**: e1005715.
Lau, G.W., Hassett, D.J., Ran, H., and Kong, F. (2004) The role of pyocyanin in *Pseudomonas aeruginosa* infection. *Trends Mol Med* **10**: 599–606.
Linares, J.F., Gustafsson, I., Baquero, F., and Martinez, J.L. (2006) Antibiotics as intermicrobial signaling agents instead of weapons. *Proc Natl Acad Sci USA* **103**: 19484–19489.
McRose, D.L., and Newman, D.K. (2021) Redox-active antibiotics enhance phosphorus

bioavailability. *Science* **371**: 1033–1037.
Noto, M.J., Burns, W.J., Beavers, W.N., and Skaar, E.P. (2017) Mechanisms of pyocyanin toxicity and genetic determinants of resistance in *Staphylococcus aureus*. *J Bacteriol* **199**.
Onaka, H., Mori, Y., Igarashi, Y., and Furumai, T. (2011) Mycolic acid-containing bacteria induce natural-product biosynthesis in *Streptomyces* species. *Appl Environ Microbiol* **77**: 400–406.
Pérez, J., Muñoz-Dorado, J., Braña, A.F., Shimkets, L.J., Sevillano, L., and Santamaría, R.I. (2011) *Myxococcus xanthus* induces actinorhodin overproduction and aerial mycelium formation by *Streptomyces coelicolor*. *Microb Biotechnol* **4**: 175–183.
Price-Whelan, A., Dietrich, L.E.P., and Newman, D.K. (2006) Rethinking "secondary" metabolism: physiological roles for phenazine antibiotics. *Nat Chem Biol* **2**: 71–78.
Rice, L.B. (2006) Challenges in identifying new antimicrobial agents effective for treating infections with *Acinetobacter baumannii* and *Pseudomonas aeruginosa*. *Clin Infect Dis* **43 Suppl 2**: S100-5.
Roberts, W. (1874) XII. Studies on biogenesis. *Philos Trans R Soc Lond* **164**: 457–477.
Thomashow, L.S., and Weller, D.M. (1988) Role of a phenazine antibiotic from *Pseudomonas fluorescens* in biological control of *Gaeumannomyces graminis* var. *tritici*. *J Bacteriol* **170**: 3499–3508.
Thomashow, L.S., Weller, D.M., Bonsall, R.F., and Pierson, L.S. (1990) Production of the antibiotic phenazine-1-carboxylic acid by fluorescent *Pseudomonas* species in the rhizosphere of wheat. *Appl Environ Microbiol* **56**: 908–912.
Traxler, M.F., Watrous, J.D., Alexandrov, T., Dorrestein, P.C., and Kolter, R. (2013) Interspecies interactions stimulate diversification of the *Streptomyces coelicolor* secreted metabolome. *mBio* **4**: e00459-13.
Turner, J.M., and Messenger, A.J. (1986) Occurrence, biochemistry and physiology of phenazine pigment production. *Adv Microb Physiol* **27**: 211–275.
Tyc, O., Berg, M. van den, Gerards, S., Veen, J.A. van, Raaijmakers, J.M., Boer, W. de, and Garbeva, P. (2014) Impact of interspecific interactions on antimicrobial activity among soil bacteria. *Front Microbiol* **5**: 567.
Tyc, O., Song, C., Dickschat, J.S., Vos, M., and Garbeva, P. (2017) The ecological role of volatile and soluble secondary metabolites produced by soil bacteria. *Trends Microbiol* **25**: 280–292.
Tyndall, J. (1876) The optical deportment of the atmosphere in relation to the phenomena of putrefaction and infection. *Philos Trans R Soc Lond* **166**: 27–74.
Villavicencio, R.T. (1998) The history of blue pus. *J Am Coll Surg* **187**: 212–216.
Voggu, L., Schlag, S., Biswas, R., Rosenstein, R., Rausch, C., and Götz, F. (2006) Microevolution of cytochrome bd oxidase in Staphylococci and its implication in resistance to respiratory toxins released by *Pseudomonas*. *J Bacteriol* **188**: 8079–8086.
Waglechner, N., McArthur, A.G., and Wright, G.D. (2019) Phylogenetic reconciliation reveals the natural history of glycopeptide antibiotic biosynthesis and resistance. *Nat Microbiol* **4**: 1862–1871.
Waksman, S.A. (1947) What is an antibiotic or an antibiotic substance? *Mycologia* **39**: 565.
Wang, Y., and Newman, D.K. (2008) Redox reactions of phenazine antibiotics with ferric (hydr)oxides and molecular oxygen. *Environ Sci Technol* **42**: 2380–2386.
Wang, Y., Wilks, J.C., Danhorn, T., Ramos, I., Croal, L., and Newman, D.K. (2011) Phenazine-1-carboxylic acid promotes bacterial biofilm development via ferrous iron acquisition. *J Bacteriol* **193**: 3606–3617.
Weller, D.M., and Cook, R.J. (1983) Suppression of take-all of wheat by seed treatments with

fluorescent pseudomonads. *Phytopathology* **73**: 463–469.

Yang, Z.-J., Wang, W., Jin, Y., Hu, H.-B., Zhang, X.-H., and Xu, Y.-Q. (2007) Isolation, identification, and degradation characteristics of phenazine-1-carboxylic acid-degrading strain *Sphingomonas* sp. DP58. *Curr Microbiol* **55**: 284–287.

C h a p t e r 2

MOLECULAR MECHANISMS OF PHENAZINE RESISTANCE IN *AGROBACTERIUM TUMEFACIENS*

This chapter is adapted from:

Perry, E.K., and Newman, D.K. (2019) The transcription factors ActR and SoxR differentially affect the phenazine tolerance *of Agrobacterium tumefaciens*. *Mol Microbiol* **112**: 199-218.

Abstract

Bacteria in soils encounter redox-active compounds, such as phenazines, that can generate oxidative stress, but the mechanisms by which different species tolerate these compounds are not fully understood. Here, we identify two transcription factors, ActR and SoxR, that play contrasting yet complementary roles in the tolerance of the soil bacterium *Agrobacterium tumefaciens* to phenazines. We show that ActR promotes phenazine tolerance by proactively driving expression of a more energy-efficient terminal oxidase at the expense of a less-efficient alternative, which may affect the rate at which phenazines abstract electrons from the electron transport chain and thereby generate reactive oxygen species. SoxR, on the other hand, responds to phenazines by inducing expression of several efflux pumps and redox-related genes, including one of three copies of superoxide dismutase and five novel members of its regulon that could not be computationally predicted. Notably, loss of ActR is far more detrimental than loss of SoxR at low concentrations of phenazines, and also increases dependence on the otherwise functionally redundant SoxR-regulated superoxide dismutase. Our results thus raise the intriguing possibility that the composition of an organism's electron transport chain may be the driving factor in determining sensitivity or tolerance to redox-active compounds.

Introduction

Soil-dwelling bacteria commonly secrete redox-active secondary metabolites, including a variety of phenazine derivatives (Turner and Messenger, 1986; Mavrodi *et al.*, 2010). Such metabolites can reversibly accept electrons from and donate electrons to a variety of substrates in

a process known as redox cycling. This property enables them to benefit their producers by promoting iron acquisition (Hernandez *et al.*, 2004; Wang *et al.*, 2011), anaerobic survival (Wang *et al.*, 2010; Glasser *et al.*, 2014), and biofilm development (Ramos *et al.*, 2010). At the same time, because of their ability to abstract electrons from redox enzymes (such as those in the respiratory electron transport chain (ETC)), reduced quinones, and other cellular reductants, and subsequently to transfer those electrons to oxygen, these metabolites can also suppress competing microbes by generating reactive oxygen species (ROS) or interfering with respiration (Hassan and Fridovich, 1980; Baron and Rowe, 1981; Baron *et al.*, 1989; Hassett *et al.*, 1992). Phenazine producers can promote crop productivity in a phenazine-dependent manner, in part by suppressing fungal plant pathogens (Audenaert *et al.*, 2002; Chin-A-Woeng *et al.*, 2003; Khare and Arora, 2011), and phenazine biosynthesis has been observed on plant roots colonized by these bacteria (Chin-A-Woeng *et al.*, 1998; Séveno *et al.*, 2001; LeTourneau *et al.*, 2018). Phenazines have also been shown to accumulate in dryland agricultural soils and the rhizosphere of cereal crops (Mavrodi *et al.*, 2012). These observations imply that tolerance of phenazines may be an important fitness determinant in certain soils and plant-associated environments. Yet aside from their producers, little is known about whether and how other soil bacteria tolerate these compounds.

Previous studies on phenazine toxicity and tolerance in bacteria have largely focused on the effects of the phenazine pyocyanin (PYO) on either generic model organisms like *Escherichia coli* or opportunistic human pathogens like *Staphylococcus aureus*. The latter frequently co-infects chronic wounds and cystic fibrosis patients along with the PYO producer *Pseudomonas aeruginosa* (Noto *et al.*, 2017), which is itself an opportunistic human pathogen found in soils and aquatic environments (Green *et al.*, 1974; Römling *et al.*, 1994; Alonso *et al.*, 1999). PYO is the most toxic among the phenazines commonly secreted by *P. aeruginosa*, presumably because of its high reactivity with oxygen (Meirelles and Newman, 2018). A comparative study of *E. coli* and *P. aeruginosa* suggested that antioxidant defenses and slower redox cycling of PYO in *P. aeruginosa* contribute to its resistance to PYO, whereas PYO-sensitive *E. coli* experiences higher levels of ROS due to faster redox cycling (Hassett *et al.*, 1992). In addition, a study based on co-evolution with *P. aeruginosa* revealed that mutations in an efflux pump regulator, a porin, and a flavodoxin $NADP^+$ reductase enzyme can modulate PYO tolerance in *E. coli* (Khare and Tavazoie, 2015). *S. aureus*, on the other hand, can escape PYO toxicity to some extent by adopting a non-respiring

phenotype, as well as by expressing genes involved in quinone detoxification (Noto *et al.*, 2017), while certain non-pathogenic staphylococci are inherently resistant to PYO due to expression of a PYO-insensitive variant of cytochrome *bd* oxidase (Voggu *et al.*, 2006). However, whether these mechanisms are at work in other bacteria that naturally tolerate phenazines is unknown, making it difficult to predict how these molecules may shape bacterial communities in soil.

To address this question, we set out to identify genes that are necessary for phenazine tolerance in *Agrobacterium tumefaciens*, a common gram-negative soil bacterium and plant pathogen. We chose *A. tumefaciens* because it is relatively tolerant of phenazines, compared to several other genetically tractable bacterial species (An *et al.*, 2006; Costa *et al.*, 2015). We employed PYO as our primary model compound because it is the most toxic among the phenazines that have been used to enhance crop productivity (Audenaert *et al.*, 2002; Chin-A-Woeng *et al.*, 2003; Khare and Arora, 2011; Meirelles and Newman, 2018). Using a forward genetic screen, we found two transcriptional regulators that both play crucial roles in tolerance of PYO, but at different concentrations and through contrasting yet complementary mechanisms. Our results point toward possible broader themes underlying tolerance of phenazines and other redox-active secondary metabolites, such as the importance of controlling their interactions with the respiratory ETC, which could have important consequences for understanding and predicting ecological impacts of these widely-produced molecules.

Results

Transposon mutagenesis reveals genes necessary for PYO tolerance

To identify genes necessary for wild-type (WT) levels of PYO tolerance, we performed random transposon insertion mutagenesis in *A. tumefaciens* NT1 using a *mariner*-based transposon that confers kanamycin resistance (Chiang and Rubin, 2002). Kanamycin-resistant mutants were screened for PYO sensitivity using a colorimetric 96-well plate assay. As WT or PYO-tolerant mutants grow to a high cell density in static liquid cultures containing 100 μM PYO, they consume the oxygen in the medium and concurrently reduce PYO from its blue oxidized form to its colorless reduced form. Conversely, PYO-sensitive mutants are unable to grow to a high enough density to fully effect the color change from blue to clear within 48 hrs (Fig. 1A). Putative PYO-sensitive

mutants were verified by comparing their growth in liquid cultures to WT across a range of PYO concentrations, from 0 to 200 μM. From roughly 5000 screened mutants, 12 (~0.2%) proved to be disproportionately sensitive to PYO; that is, while a few of these mutants exhibited growth defects even without PYO, the ratio of their growth (i.e. optical density after 24 hrs) with PYO to their growth without PYO was much lower than it was for WT (Fig. 1B).

The locus of the transposon insertion for each of the 12 verified PYO-sensitive mutants was determined using arbitrary PCR. Three of the insertions were in genes encoding transcriptional regulators, three were in genes putatively related to carbon metabolism or maintenance of protonmotive force, four were likely related to cell wall modification, and the remaining two were in a single gene, Atu2577, encoding an ABC transporter (Table S1). This list of genes important

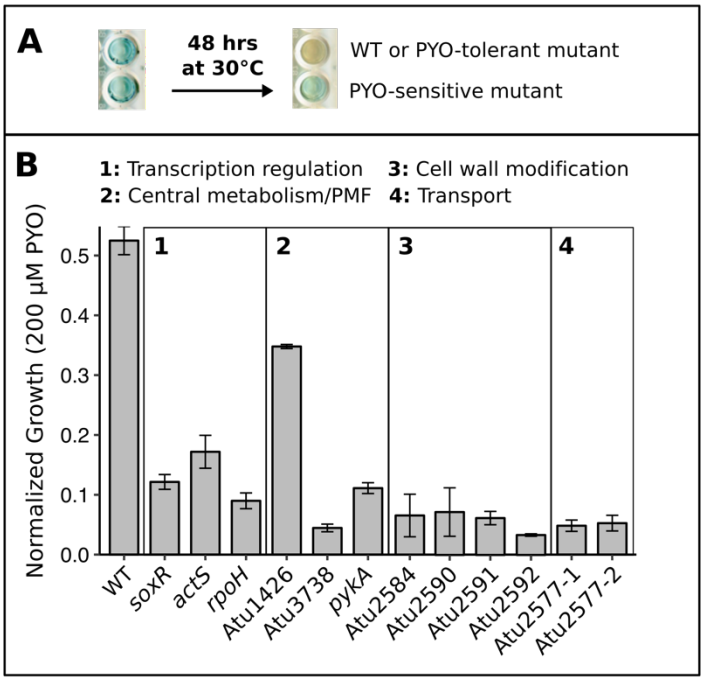

Figure 1: Transposon mutagenesis reveals genes necessary for tolerance of PYO.
A. An example 96-well plate demonstrating the colorimetric strategy used to identify PYO-sensitive transposon mutants. As WT or PYO-tolerant mutants grow to a high density over 48 hrs in static cultures, cellular reductants transform PYO from its blue oxidized form to its colorless reduced form. Wells containing PYO-sensitive mutants that cannot grow to a high density remain blue.
B. Growth of WT and the 12 PYO-sensitive transposon mutants after 24 hrs in the presence of 200 μM PYO. Cultures were either in or approaching stationary phase at this time point, and growth was normalized to growth in parallel cultures without PYO. Differences between WT and mutants were generally greater at 200 μM PYO than at lower concentrations. Mutants are named by the gene containing the transposon insertion and categorized by predicted function (see Table S1 for further details). Error bars represent standard deviations of biological replicates ($n = 3$).

for PYO tolerance is not comprehensive, as in *A. tumefaciens* NT1, approximately 24,000 transposon insertion mutants would need to be screened to achieve 99% confidence of having disrupted every gene in the genome. Nevertheless, we were particularly interested in following up on the transcriptional regulators identified in our screen, as the genes they regulate could reveal broader insights about mechanisms that are important for PYO tolerance. Specifically, we focused on the mutants with insertions in *actS*, the sensor in the *actSR* two-component sensor-response system, and *soxR*, which has previously been implicated in the oxidative stress response of *A. tumefaciens* (Eiamphungporn *et al.*, 2006) and as a sensor of redox-active antibiotics in *P. aeruginosa* and *Streptomyces coelicolor* (Dietrich *et al.*, 2006; Dietrich *et al.*, 2008; Singh *et al.*, 2013). We did not pursue the third transcriptional regulator, *rpoH*, as the transposon mutant exhibited a growth defect without PYO (Fig. S1A).

ΔactR *and* ΔsoxR *mutants are differentially sensitive to diverse redox-active small molecules*

To characterize the roles of *actSR* and *soxR* in protecting against PYO, we first generated in-frame deletions of *actS*, *actR*, and *soxR* via allelic replacement (Morton and Fuqua, 2012a). Both Δ*actS* and Δ*actR* were similarly sensitive to PYO (Fig. S1B); thus, we used Δ*actR* for all further experiments as ActR is the transcriptional regulator in this two-component system. Intriguingly, Δ*actR* and Δ*soxR* displayed strikingly different profiles of sensitivity to PYO. Δ*actR* is significantly more sensitive to PYO than WT at concentrations as low as 10 μM; conversely, Δ*soxR* is no more sensitive to PYO than WT up to at least 100 μM, and in fact grows better than WT at up to 50 μM PYO, yet its growth is severely inhibited by 200 μM PYO (Fig. 2A). Complementation by inducing expression of *actR* or *soxR* in Δ*actR* or Δ*soxR*, respectively, from a plasmid rescued PYO tolerance in each mutant (Fig. S1C).

Extending beyond PYO, we also investigated the relative sensitivity of Δ*actR* and Δ*soxR* to diverse redox-active molecules spanning a range of standard reduction potentials (E_o' vs. that of the normal hydrogen electrode) from -446 mV (paraquat) to +11 mV (methylene blue) (Fig. S2) (Wang *et al.*, 2010). For each molecule, we tested increasing concentrations until we found a dose at which the growth of either Δ*actR* or Δ*soxR* was statistically significantly different from WT. Similar to the results with PYO (E_o' -40 mV), Δ*actR* was more sensitive than either WT or Δ*soxR* to anthraquinone-2,6-disulfonate (AQDS, E_o' -184 mV), phenazine-1-carboxylic acid (PCA, E_o' -

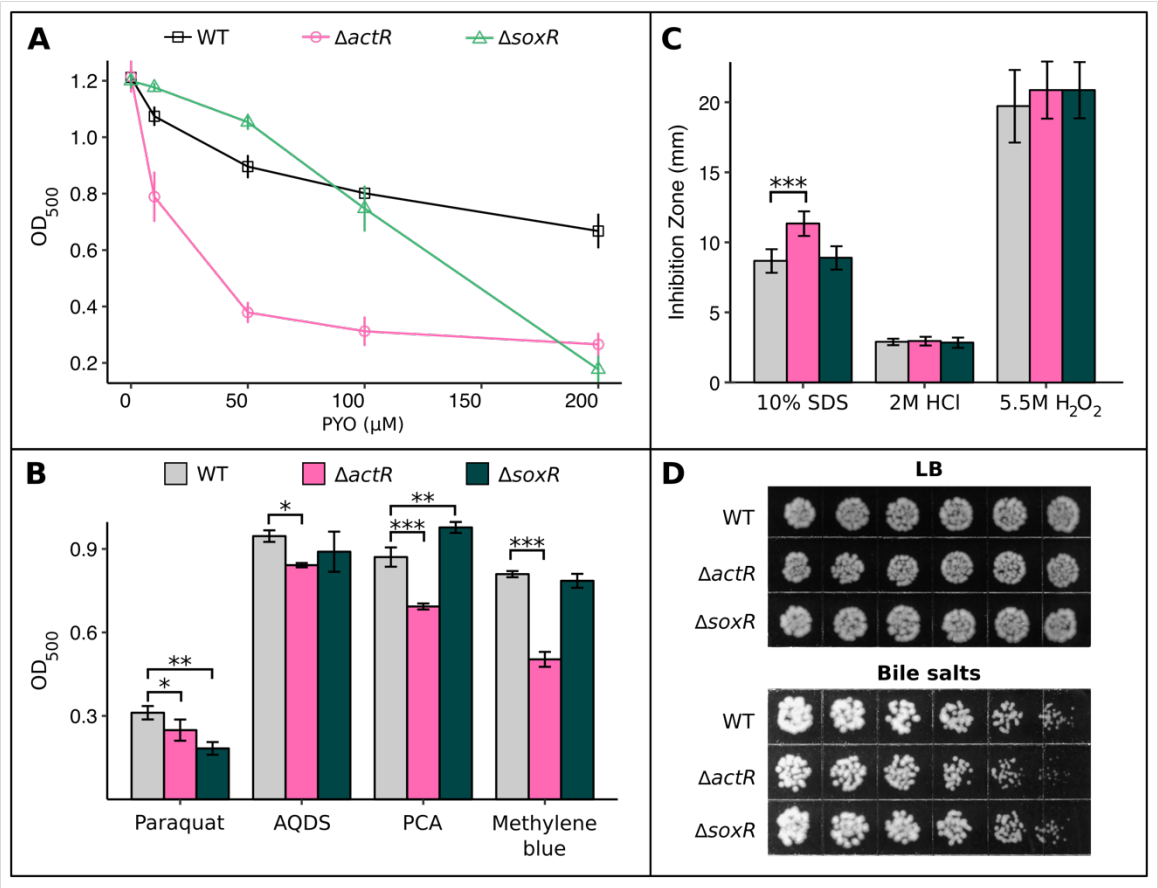

Figure 2: Δ*actR* and Δ*soxR* mutants exhibit differential sensitivity to redox-active small molecules.
A. Growth of WT, Δ*actR*, and Δ*soxR* after 24 hrs in the presence of different concentrations of PYO, measured by optical density at 500 nm ($n = 3$).
B. Growth of WT, Δ*actR*, and Δ*soxR* after 24 hrs in the presence of 20 mM paraquat, 10 mM AQDS, 500 μM PCA, or 200 μM methylene blue ($n = 3$). For each molecule, the chosen concentration was the lowest tested dose at which growth of either Δ*actR* or Δ*soxR* was statistically significantly different from WT.
C. Diameter of growth inhibition zone around a disk infused with 10% SDS, 2 M HCl, or 5.5 M H_2O_2 ($n \geq 6$). The measurements represent the diameter of the zone of clearing minus the diameter of the disk itself.
D. Growth of WT, Δ*actR*, and Δ*soxR* on agar plates containing either plain LB or a concentration gradient (low-high, left to right) of bile salts (up to 2%). Images are representative of eight biological replicates. In A and B, cultures were in stationary phase at the reported time point. In B and C, * $p < 0.05$, ** $p < 0.01$, *** $p < 0.001$ (in B, linear regression with dummy variable coding using WT as the reference group; in C, Kruskal-Wallis test followed by pairwise Wilcox rank sum test with the Benjamini-Hochberg procedure for controlling the false discovery rate). Error bars in A-C represent standard deviations of biological replicates.

114 mV), and methylene blue, whereas Δ*soxR* was no more sensitive than WT to these molecules at the tested concentrations (Fig. 2B). However, Δ*soxR* was more sensitive than Δ*actR* to paraquat. Finally, to determine whether *actR* and *soxR* specifically affect sensitivity to redox-active molecules, we tested whether these mutants were more sensitive than WT to a variety of other stresses, including detergents (SDS or bile salts), low pH (HCl), hydrogen peroxide, the membrane stressor EDTA, and osmotic stressors (myo-inositol or NaCl). Neither Δ*actR* nor Δ*soxR* was

noticeably more sensitive than WT to any of these stresses (Fig. 2C and Fig. S3), with the exception that Δ*actR* was more sensitive to detergents (Fig. 2C, D).

SoxR regulates multiple previously overlooked genes

To understand why ActR and SoxR differentially affect sensitivity to phenazines, we began to characterize the genetic mechanisms by which SoxR contributes to PYO tolerance. It is known from studies in other bacteria that redox-cycling drugs activate SoxR by directly oxidizing its [2Fe-2S] cluster (Dietrich and Kiley, 2011; Gu and Imlay, 2011; Singh *et al.*, 2013), and that oxidized SoxR binds to a conserved "SoxR box" sequence in the promoter regions of target genes (Dietrich *et al.*, 2008). Using this sequence, SoxR in *A. tumefaciens* has variously been predicted to regulate up to four putative major facilitator superfamily transporters (Atu0942, Atu2361, Atu4895, and Atu5152) along with an operon containing a superoxide dismutase (Atu4583, a.k.a. *sodBII*), ferredoxin (Atu4582), and a putative flavin reductase (Atu4581) (Eiamphungporn *et al.*, 2006; Dietrich *et al.*, 2008; Novichkov *et al.*, 2013). However, of these computationally predicted members of the SoxR regulon, SoxR-dependent expression has previously only been confirmed for Atu5152 (Eiamphungporn *et al.*, 2006) and *sodBII* (Saenkham *et al.*, 2007). SoxR has also been shown to autoregulate by binding to a SoxR box in its own promoter (Eiamphungporn *et al.*, 2006). To validate the other computationally predicted members of the SoxR regulon, we performed quantitative reverse-transcription PCR (qRT-PCR) on WT and Δ*soxR* cultures treated with either 100 μM PYO or a solvent control for 20 minutes. We expected true SoxR-regulated genes to be highly expressed only in PYO-treated WT. This was indeed the case for all but one of the genes computationally predicted to be SoxR-regulated based on the presence of a SoxR box-containing promoter (Fig. 3A, non-bolded genes). Atu4895 alone was not upregulated by PYO, suggesting that it is not in fact regulated by SoxR (Fig. S4A).

The discrepancy between the presence of a SoxR box upstream of Atu4895 and its lack of response to PYO led us to ask whether there might conversely be "cryptic" members of the SoxR regulon that lack a SoxR box but exhibit a SoxR-dependent response to PYO. Given that all of the qRT-PCR-validated, SoxR box-containing members of the SoxR regulon exhibited large fold changes in WT upon PYO treatment (Fig. 3A, non-bolded genes), we expected that any cryptic member(s) of the SoxR regulon would exhibit a similarly strong response to PYO. We therefore

performed an RNA-seq experiment to identify genes that are highly induced by PYO in WT. Based on the fold changes of *soxR* itself and the already-validated members of the SoxR regulon, we defined candidate cryptic members of the SoxR regulon as those genes with a $\log_2$ fold change > 4 in PYO-treated cultures relative to the solvent-treated control (Table S2). We then tested the resulting seven candidates for a SoxR-dependent transcriptional response by performing qRT-PCR under the four conditions described above (WT + PYO, WT – PYO, Δ*soxR* + PYO, and Δ*soxR* – PYO). Remarkably, we found that the PYO-mediated induction of three of the seven candidates (Atu4741, Atu4742, and Atu5305) was completely abolished in the absence of SoxR, while the PYO-mediated induction of two others (Atu2482 and Atu2483, annotated as *mexE* and *mexF,* respectively) appeared to partially depend on SoxR (Fig. 3A, bolded genes). Using the motif scanning program FIMO (Grant *et al.*, 2011), we confirmed the lack of a typical SoxR box upstream of these genes. Thus, we have expanded the known set of genes with SoxR-dependent regulation in *A. tumefaciens* to include five genes that could not have been found with previously applied computational methods.

Among the five identified cryptic members of the SoxR regulon, Atu4741 is particularly interesting as it is a σ^{54}-dependent Fis family transcriptional regulator, and hence could potentially be involved in regulating the other cryptic members. Although Atu4741 is annotated as *acoR* due to its similarity to the *acoR* gene in *Bacillus subtilis*, *A. tumefaciens* does not possess annotated homologs of the acetoin catabolism genes that are regulated by AcoR in *B. subtilis*, suggesting that Atu4741 plays a different regulatory role in *A. tumefaciens*. Atu4742, located just upstream of Atu4741, is predicted to encode a small (108 amino acid) hypothetical protein containing tetratricopeptide repeats, which often mediate protein-protein interactions (Zeytuni and Zarivach, 2012); this, along with its proximity to Atu4741, suggests that the two may interact. Atu5305 is annotated as a permease belonging to the major facilitator family of transporters, and thus could be involved in transporting PYO out of the cell. Finally, *mexE* and *mexF* encode homologs of the cytoplasmic membrane protein and membrane fusion protein components, respectively, of the MexEF-OprN efflux pump originally discovered in *P. aeruginosa*. In the latter, MexEF-OprN has been shown to transport chloramphenicol, fluoroquinolones, and a precursor to a quorum sensing signal (Köhler *et al.*, 1997; Lamarche and Déziel, 2011; Llanes *et al.*, 2011); it is also known to be induced by nitrosative (Fetar *et al.*, 2011) or disulfide stress (Fargier *et al.*, 2012). To our

knowledge, SoxR-dependent expression of *mexEF* has not previously been reported in other organisms; rather, in *P. aeruginosa*, *mexEF* is regulated at least in part by MexT, a LysR family transcriptional activator (Köhler *et al.*, 1999).

Functional redundancy rationalizes the ΔsoxR *phenotype*

Altogether, the SoxR regulon in *A. tumefaciens* contains five putative efflux pumps (Atu0942, Atu2361, *mexEF*, Atu5152, and Atu5305), a putative flavin reductase (Atu4581), ferredoxin (Atu4582), superoxide dismutase (*sodBII*), an uncharacterized transcriptional regulator (Atu4741), and a hypothetical protein (Atu4742). To investigate the contributions of each of these genes to PYO tolerance, we generated in-frame deletions and challenged the resulting mutants with 200 μM PYO. Only five mutants were significantly more sensitive to 200 μM PYO than WT, and no single mutant was as sensitive as Δ*soxR* itself, suggesting considerable functional redundancy among the SoxR regulon (Fig. 3B). Surprisingly, Δ*sodBII* was actually less sensitive to PYO than WT. This was counterintuitive, given that superoxide has been proposed to be a toxic byproduct of PYO treatment (Hassan and Fridovich, 1980; Hassett *et al.*, 1992; Rada and Leto, 2013; Managò *et al.*, 2015).

We wondered whether functional redundancy might explain both the surprising phenotype of Δ*sodBII* and the fact that Δ*soxR* only becomes sensitive to PYO at a relatively high dose. First, we confirmed via qRT-PCR that SoxR strongly induces expression of its regulon even at 10 μM PYO, using *soxR* itself and *sodBII* as representative examples (Fig. 3C). Thus, the tolerance of Δ*soxR* to low levels of PYO is in spite of considerable transcriptional differences between WT and Δ*soxR* under these conditions, suggesting that loss of SoxR may be compensated by functionally redundant genes outside of its regulon. Indeed, besides SoxR-regulated SodBII, *A. tumefaciens* possesses two other superoxide dismutases, SodBI and SodBIII (Saenkham *et al.*, 2007). SodBI is constitutively highly expressed at all stages of growth, whereas SodBIII is primarily expressed during stationary phase (Saenkham *et al.*, 2007). We therefore asked whether loss of SodBI would sensitize Δ*sodBII* or Δ*soxR* to lower concentrations of PYO. Indeed, while Δ*sodBI* itself was not sensitive to PYO, Δ*sodBII*/Δ*sodBI* and Δ*soxR*/Δ*sodBI* were significantly more sensitive than WT not only to high doses of PYO, but also to low doses, unlike the Δ*sodBII* and Δ*soxR* single mutants (Fig. 3D). Thus, the functions of SodBI and SodBII appear to be largely redundant at the tested

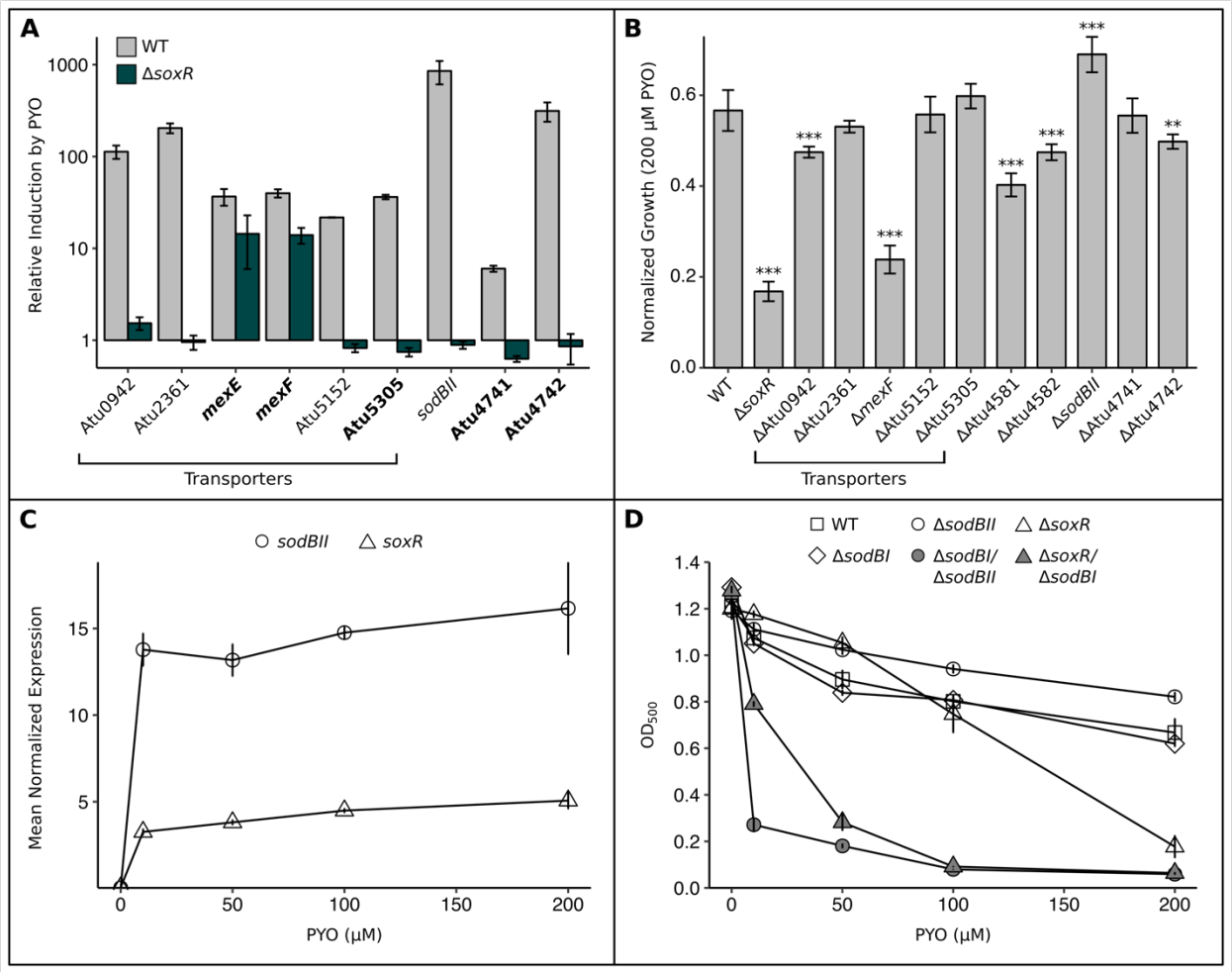

Figure 3: SoxR protects *A. tumefaciens* against PYO by upregulating functionally redundant superoxide dismutase, transporters, and redox-related genes.

A. qRT-PCR validation of putative members of the SoxR regulon, showing that induction of these genes upon a 20 min exposure to 100 µM PYO was partially or fully abrogated in the ΔSoxR mutant ($n = 3$). Bolded genes lack a SoxR box and thus could not be identified as SoxR-regulated by computational approaches in earlier studies. qRT-PCR validation was not performed for Atu4581 and Atu4582, as these genes are predicted to be co-transcribed with *sodBII* (Mao *et al.*, 2009). Expression levels were normalized to the housekeeping gene *rpoD,* and induction was calculated as the expression in the presence of PYO divided by the expression without PYO.

B. Growth of single knockout mutants for members of the SoxR regulon after 24 hrs in the presence of 200 µM PYO, normalized to growth of parallel cultures without PYO. ** $p < 0.01$, *** $p < 0.001$ ($n = 3$, linear regression with dummy variable coding using WT as the reference group).

C. Normalized expression levels of *sodBII* and *soxR* in WT after 20 min exposure to different concentrations of PYO ($n = 3$). Expression levels were determined by qRT-PCR and normalized to *rpoD*.

D. Growth of WT, Δ*sodBI*, Δ*sodBII*, Δ*soxR*, and the Δ*sodBI*/Δ*sodBII* and Δ*soxR*/Δ*sodBI* mutants after 24 hrs in the presence of different concentrations of PYO ($n \geq 3$). Error bars in all panels represent standard deviations of biological replicates. In B and D, cultures were in stationary phase at the reported time point.

concentrations of PYO, and this functional redundancy is a key factor in the tolerance of Δ*soxR* to low concentrations of PYO.

Loss of ActR causes constitutive dysregulation of the cytochrome o *and* d *ubiquinol oxidases*

Having rationalized why SoxR only becomes essential at high concentrations of PYO, we next sought to understand why the Δ*actR* mutant is hypersensitive to PYO. ActR homologs (known as ArcA, PrrA, RegA, or RoxR) are present in diverse proteobacteria and have been well-studied in several species (Elsen *et al.*, 2004; Gralnick *et al.*, 2005; Wong *et al.*, 2007; Fernández-Piñar *et al.*, 2008; Gao *et al.*, 2008; Park *et al.*, 2013; Lunak and Noel, 2015). In general, they regulate elements of the respiratory ETC in response to changes in cellular redox balance (for example, during transitions from aerobiosis to anaerobiosis), although the specific elements and directionality of regulation vary across species (Tseng *et al.*, 1996; Swem and Bauer, 2002; Elsen *et al.*, 2004; Fernández-Piñar *et al.*, 2008; Gao *et al.*, 2008). In *Sinorhizobium medicae*, which belongs to the same taxonomic order as *A. tumefaciens*, ActR regulates a glutathione S-transferase, cytochrome oxidase components, and an assimilatory nitrate reductase (Fenner *et al.*, 2004), while in *A. tumefaciens*, ActR is known to co-regulate expression of nitrite reductase and pseudoazurin,

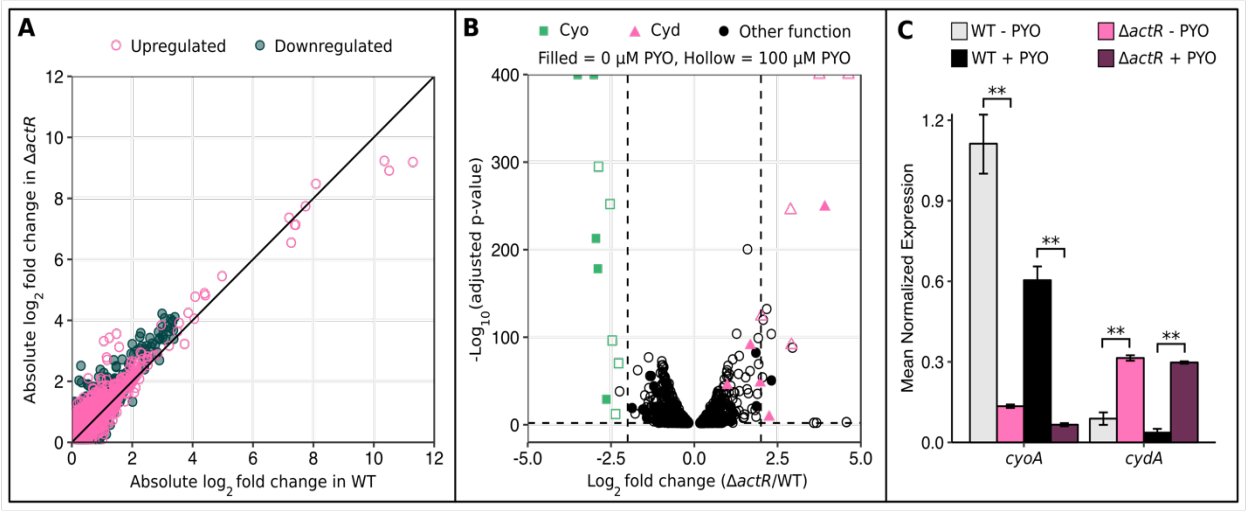

Figure 4: Expression of cytochrome *o* oxidase and cytochrome *d* oxidase is dysregulated in Δ*actR*.
A. Plot of the absolute values of $\log_2$ fold changes in gene expression upon 100 μM PYO treatment in WT against absolute values of $\log_2$ fold changes in gene expression upon 100 μM PYO treatment in Δ*actR*. Only genes that were statistically significantly differentially expressed (adjusted *p*-value < 0.01) upon PYO treatment in at least one strain are plotted. Each point represents a single gene. The black line is y = x.
B. Volcano plots of RNA-seq data comparing gene expression levels in Δ*actR* to WT, with either 0 μM PYO or 100 μM PYO. The vertical dashed lines mark a $\log_2$ fold change of -2 or 2, and the horizontal dashed line marks an adjusted p-value of 0.01. Only genes with statistical significance below the adjusted p-value cutoff are plotted.
C. qRT-PCR data confirming the expression patterns of the *cyo* and *cyd* operons in Δ*actR* vs. WT. The + PYO condition represents treatment with 100 μM PYO. Only *cyoA* and *cydA* are shown for brevity, as they are co-transcribed with other members of these operons. Expression levels were normalized to the housekeeping gene *rpoD*. ** $p < 0.01$ (Welch's *t*-test followed by the Benjamini-Hochberg procedure for controlling the false discovery rate; $n = 3$). Error bars represent standard deviations of biological replicates.

an electron donor to the denitrification pathway, during anaerobic growth (Baek *et al.*, 2008). However, to our knowledge, the ActR regulon has not been comprehensively defined in *A. tumefaciens*. Thus, to investigate how ActR contributes to PYO tolerance during aerobic growth, we performed RNA-seq to compare the transcriptomes of WT and Δ*actR* both with and without 100 μM PYO treatment. Among the genes that were up- or downregulated by PYO in each strain (comparing WT + PYO vs. WT – PYO, or Δ*actR* + PYO vs. Δ*actR* - PYO), there was a strong correlation between the fold changes in WT and Δ*actR*; in fact, there were no genes that were strongly up- or downregulated by PYO in WT but not in Δ*actR* (Fig. 4A). This suggested that ActR does not regulate a specific transcriptional response to PYO. However, we noted that among the genes that were up- or downregulated by PYO, the magnitude of the fold changes was often greater in Δ*actR* than in WT (such genes lie above the y = x line in Fig. 4A), possibly indicating that Δ*actR* was experiencing more stress than WT.

We then compared the transcriptomic profile of Δ*actR* to WT either with or without PYO (i.e. Δ*actR* + PYO vs. WT + PYO, or Δ*actR* - PYO vs. WT - PYO). Interestingly, several genes related to oxidative stress were upregulated in Δ*actR* relative to WT only upon PYO treatment, including catalase, ferredoxin I, a putative DNA oxidation protective protein, and genes involved in amino acid metabolism (Table S3). Similar to our above observation, this could imply that PYO exerts greater toxicity in Δ*actR*. We also found that two sets of genes are strongly dysregulated in Δ*actR* regardless of PYO treatment: the *cyo* operon that encodes cytochrome *o* ubiquinol oxidase (Cyo) is downregulated > 4 fold, while the *cyd* operon that encodes cytochrome *d* ubiquinol oxidase (Cyd) is upregulated > 2 fold, with the latter being exaggerated upon PYO treatment (Fig. 4B). These expression patterns were confirmed with qRT-PCR (Fig. 4C). Other elements of the ETC or central metabolism that were upregulated in Δ*actR* regardless of PYO treatment included succinate dehydrogenase, ubiquinol-cytochrome *c* reductase, and cbb_3 cytochrome *c* oxidase, along with several genes involved in sugar transport/metabolism, amino acid metabolism, fatty acid metabolism, carbon oxidation, or the tricarboxylic acid (TCA) cycle (Table S4). On the other hand, caa_3 cytochrome *c* oxidase, pseudoazurin, and biosynthetic genes for cytochrome *c* and heme were downregulated in Δ*actR* (Table S5). While the fold changes for these genes were not as dramatic as for *cyo* and *cyd*, the overall pattern suggests that ActR is broadly involved in regulating flux through central metabolic pathways in *A. tumefaciens*, as it is in *E. coli, Salmonella*

enterica, *Pseudomonas putida*, and other species (Fernández-Piñar *et al.*, 2008; Evans *et al.*, 2011; Morales *et al.*, 2013; Park *et al.*, 2013).

Downregulation of cytochrome o *ubiquinol oxidase sensitizes cells to PYO*

Given that the fold changes were most striking for the terminal ubiquinol oxidases, we next asked whether the dysregulation of these genes in Δ*actR* is causally related to PYO sensitivity. Indeed, a mutant lacking the *cyo* operon grew similarly to Δ*actR* during exponential phase across all tested concentrations of PYO (Fig. 5A, left), although it achieved a higher optical density in

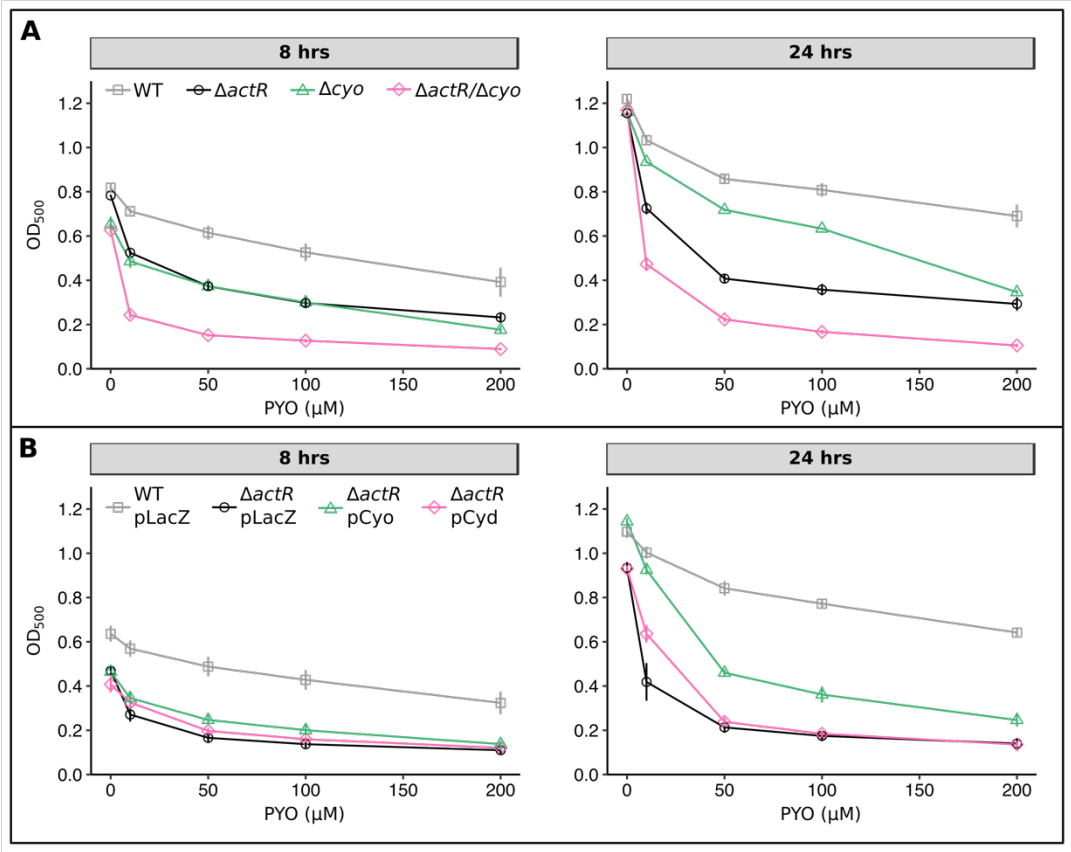

Figure 5: Loss of cytochrome *o* oxidase, but not overexpression of cytochrome *d* oxidase, increases sensitivity to PYO.
A. Growth of WT, Δ*actR*, Δ*cyo*, and Δ*actR*/Δ*cyo* after 8 hrs (left) or 24 hrs (right) in the presence of different concentrations of PYO. 8 hrs corresponds to late exponential phase while 24 hrs corresponds to stationary phase.
B. Growth of WT pLacZ (vector control for overexpression constructs), Δ*actR* pLacZ, Δ*actR* pCyo (overexpression construct for the *cyo* operon), and Δ*actR* pCyd (overexpression construct for the *cyd* operon). Overexpression was induced by adding 1 mM IPTG at the start of the experiment. Growth of Δ*actR* pCyo is statistically significantly higher than growth of Δ*actR* pLacZ at both time points and across all concentrations of PYO, except for 0 μM and 200 μM PYO after 8 hrs ($p < 0.05$, Welch's *t*-test followed by the Benjamini-Hochberg procedure for controlling the false discovery rate). All data points are plotted with error bars representing standard deviations of biological replicates ($n = 3$).

stationary phase (Fig. 5A, right), possibly due to compensatory upregulation of the *cyd* operon to levels considerably higher than that in Δ*actR* itself (Fig. S4B). Interestingly, the Δ*actR*/Δ*cyo* double mutant is more sensitive to PYO than either Δ*actR* or Δ*cyo* alone (Fig. 5A). This result likely arises from a combination of two factors: 1) total loss of *cyo* is presumably more severe than the downregulation imposed by loss of ActR; and 2) without ActR, expression of genes to compensate for total loss of *cyo* may be impaired. Conversely, overexpression of the *cyo* operon in the Δ*actR* background partially rescued tolerance to PYO, with a greater effect at the lower doses of PYO (Fig. 5B). On the other hand, increased overexpression of the *cyd* operon from an inducible plasmid-borne promoter in Δ*actR* did not further sensitize Δ*actR* to PYO, and in fact conferred a mild benefit at low doses of PYO (Fig. 5B). We therefore hypothesized that *cyd* may play a compensatory role upon abnormal downregulation of *cyo*. To further test this hypothesis, we attempted to determine whether a Δ*actR*/Δ*cyd* double mutant would be more sensitive to PYO than Δ*actR* alone, but were unable to perform this experiment due to the severe growth defect of this double mutant in liquid culture even without PYO (data not shown). Nevertheless, the *cyd* overexpression results suggest that the natural upregulation of *cyd* in Δ*actR* does not augment its PYO sensitivity, but rather is a compensatory response or else a passive side effect of losing *actR* (ActR might normally repress *cyd* during aerobic growth). Overall, ActR-mediated regulation of *cyo* appears to be important for PYO tolerance, although the fact that overexpressing *cyo* in Δ*actR* only partially rescued PYO tolerance suggests that other ActR-regulated genes likely also contribute to the Δ*actR* phenotype.

In considering candidates for other genes besides *cyo* that might contribute to the Δ*actR* phenotype, we were particularly intrigued by the upregulation of multiple dehydrogenases involved in carbon oxidation and the TCA cycle (Table S4). These enzymes oxidize various substrates while concomitantly reducing NAD+ to NADH. Thus, upregulation of these genes could lead to a higher NADH/NAD+ ratio in the cell. However, upon measuring the NADH/NAD+ ratios in exponentially growing cultures of WT and Δ*actR*, we found only a slight trend towards a higher ratio in Δ*actR*, which was not statistically significant (Fig. S5A). We also asked whether Δ*actR* exhibits increased redox cycling of PYO independently of the action of the terminal oxidases in the ETC. Specifically, we measured the rate of PYO-dependent oxygen consumption by WT and Δ*actR* in the presence of cyanide, which inhibits the terminal oxidases. This rate has previously

been correlated both with the rate of redox cycling of PYO and with PYO toxicity (Hassett *et al.*, 1992), as the apparent oxygen consumption under this condition results from reduced PYO donating electrons to oxygen and thereby generating ROS. Interestingly, we found that WT and Δ*actR* cultures treated with PYO and cyanide consumed oxygen at nearly identical rates (Fig. S5B), implying similar rates of PYO redox cycling in the two strains. However, this result does not exclude the possibility that the terminal oxidases themselves might influence the rate of PYO redox cycling.

Cellular ATP levels correlate with Cyo expression but not necessarily with PYO sensitivity

To rationalize the link between Cyo levels and phenazine tolerance, we first asked whether loss of ActR alters the rate of aerobic respiration, as Cyd possesses a much higher affinity for oxygen than Cyo (Matsushita *et al.*, 1984; D'mello *et al.*, 1996; Borisov *et al.*, 2011). We measured oxygen consumption rates in exponential-phase cultures of WT and Δ*actR* using a Clark-type electrode. These measurements revealed that WT and Δ*actR* actually consume oxygen at similar rates, both with and without PYO treatment (Fig. 6A). However, besides differing in their affinities for oxygen, Cyo and Cyd have different coupling ratios for proton translocation (2 H^+/e^- vs. 1 H^+/e^-, respectively) (Calhoun *et al.*, 1993) (Fig. 6B). Hence, given similar rates of oxygen consumption, Δ*actR* should be less efficient at generating protonmotive force (PMF) than WT. This would be expected to impair PMF-dependent processes, such as ATP synthesis via FoF1-ATP synthase. Indeed, we found that both Δ*actR* and Δ*cyo* possess less ATP than WT during exponential growth, supporting the hypothesis that the electron transport chain (ETC) is less efficient without Cyo (Fig. 6C). This difference could potentially explain why Δ*actR* is also more sensitive to detergents: tolerance of SDS and bile salts typically involves energy-intensive processes like efflux and DNA repair (Nickerson and Aspedon, 1992; Begley *et al.*, 2005). Interestingly, the ATP pools of all three strains decreased upon treatment with PYO, but this difference was only statistically significant in Δ*actR*. This could suggest that PYO decouples oxidative phosphorylation more effectively in Δ*actR*, and/or that Δ*actR* spends more ATP on defenses against PYO toxicity.

To test whether the rate of oxidative phosphorylation modulates PYO sensitivity, we treated WT and Δ*actR* with DCCD (N,N'-dicyclohexylcarbodiimide), a classical inhibitor of FoF1-ATP synthase. Both strains compensated for inhibited ATP synthesis by growing more slowly in

the presence of DCCD (Fig. S6A), and consequently the bulk ATP levels decreased only slightly (Fig. S6B). Nevertheless, we were intrigued to note that while the DCCD treatment increased sensitivity to PYO in Δ*actR*, DCCD actually improved tolerance to 10 μM PYO in WT (Fig. S6C). Thus, the link between lower rates of ATP synthesis, smaller ATP pools, and increased PYO sensitivity seems to be specific to the Δ*actR* genetic background, although it is also possible that ATP only becomes a limiting factor in PYO tolerance below a certain level.

Loss of ActR increases dependence on SodBII-mediated protection against PYO

Taken together, the above evidence suggested that PYO might exert toxic effects more readily in Δ*actR* than in WT, rather than Δ*actR* simply being deficient in responding to PYO-induced toxicity. This would be consistent with the fact that i) PYO treatment affected the ATP pool of Δ*actR* more severely, ii) inhibiting ATP synthesis decreased PYO tolerance in Δ*actR* but not in WT, and iii) several genes related to oxidative stress were more strongly transcriptionally induced by PYO in Δ*actR* than in WT. To test this hypothesis directly, we first attempted to measure whether PYO generates ROS more rapidly in Δ*actR* compared to WT, as superoxide and hydroxyl radical have previously been identified as toxic byproducts of PYO redox cycling (Hassett *et al.*, 1992; Noto *et al.*, 2017). However, we found that technical limitations prevented reliable quantification of intracellular ROS in suspensions of PYO-treated *A. tumefaciens* (see Experimental Procedures and Fig. S7). We therefore turned instead to a genetic approach to infer the relative toxicity of PYO in Δ*actR* compared to WT. Specifically, we asked whether the SoxR-regulated, functionally redundant superoxide dismutase SodBII is more important for damage control in Δ*actR* compared to WT, which could imply greater production of superoxide by PYO in Δ*actR*. Indeed, while loss of SodBII actually increased growth at all tested concentrations of PYO in the WT genetic background, loss of SodBII further sensitized Δ*actR* to PYO at concentrations above 10 μM (Fig. 6D). The trend was similar, though weaker, when comparing the effects of losing SodBII in WT versus Δ*cyo*: the growth advantage conferred by loss of SodBII was smaller for Δ*cyo* than for WT at PYO concentrations above 10 μM, suggesting increased dependency on SodBII in Δ*cyo*, albeit to a lesser extent than in Δ*actR* (Fig. S1D). Thus, the downregulation of *cyo* in Δ*actR* may contribute to its increased dependence on SodBII, though other genes are likely also involved. These findings are particularly notable given the evidence that Δ*actR* and Δ*cyo* conserve energy less efficiently than WT. Induction of SodBII, along with

the rest of the SoxR regulon, may incur significant energy costs associated with protein synthesis, especially considering that SodBII is the second-most highly expressed non-ribosomal gene in the entire *A. tumefaciens* transcriptome under PYO treatment (Table S6). Given the functional redundancy of SodBII, this cost could be gratuitous at low concentrations of PYO, which would explain why loss of either SoxR or SodBII benefits WT under those conditions. If PYO were similarly toxic in WT, Δ*actR*, and Δ*cyo*, we would have expected the comparatively energy-limited

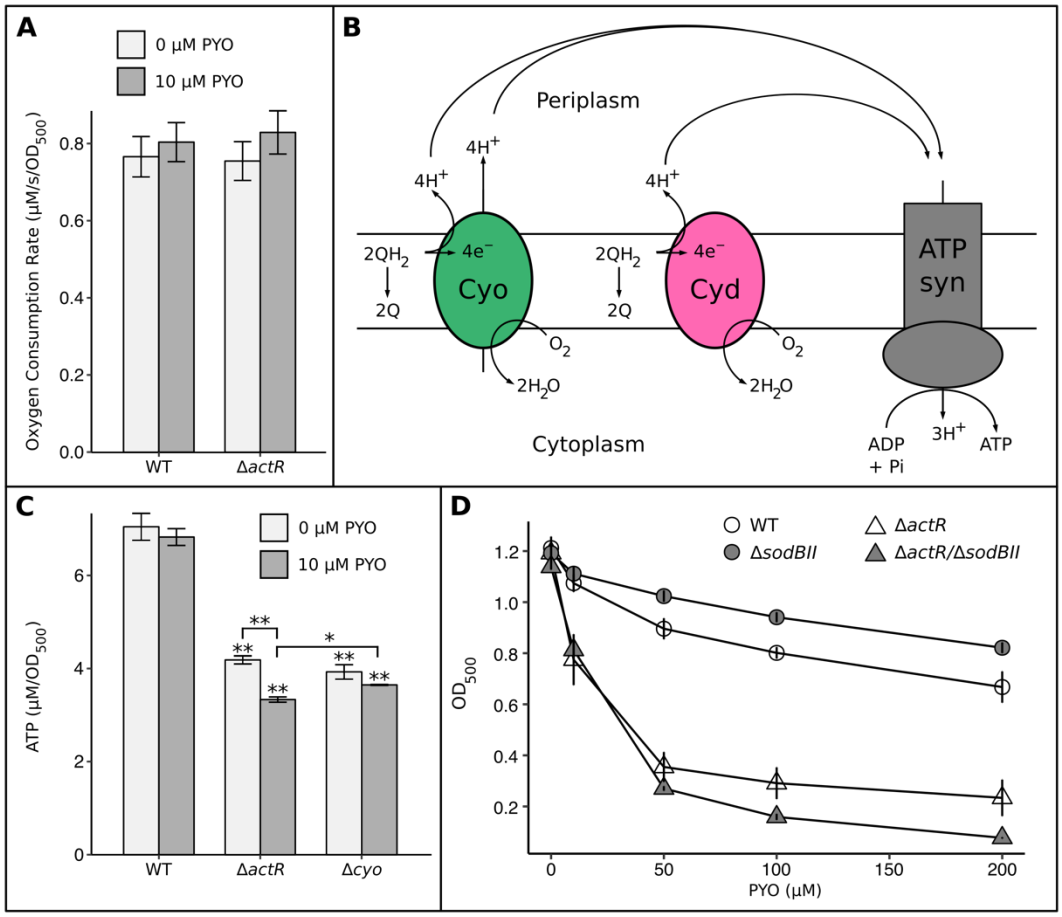

Figure 6: Loss of ActR decreases cellular ATP levels and increases dependence on SoxR-regulated SodBII.
A. Oxygen consumption rates of exponential-phase WT and Δ*actR* with and without 10 μM PYO ($n = 3$).
B. Simplified cartoon showing the relationship between Cyo, Cyd, and ATP synthase, as well as the different coupling constants of Cyo and Cyd ($2H^+/e^-$ vs. $1H^+/e^-$, respectively). QH_2 = ubiquinol (reduced), Q = ubiquinone (oxidized).
C. Bulk ATP levels in exponential phase cultures of WT, Δ*actR*, and Δ*cyoABCD*, with and without 10 μM PYO. * $p < 0.05$, * $p < 0.01$ (Welch's *t*-test followed by the Benjamini-Hochberg procedure for controlling the false discovery rate; $n = 3$).
D. Growth of WT, Δ*sodBII*, Δ*actR*, and Δ*actR*/Δ*sodBII* after 24 hrs in the presence of different concentrations of PYO, showing the increased dependency of Δ*actR* on SodBII ($n \geq 3$). Cultures were in stationary phase at this time point. Data for WT and Δ*actR* are from Fig. 2A. Error bars in A, B, and D represent standard deviations of biological replicates.

Δ*actR* and Δ*cyo* mutants to benefit even more than WT from the energy savings associated with avoiding gratuitous induction of SodBII. For this not to be the case suggests that PYO may behave differently in WT compared to Δ*actR* and Δ*cyo*, likely with increased superoxide-related toxicity in the latter two.

Discussion

Here we have identified two transcription factors in *A. tumefaciens* that contribute to tolerance of PYO and other redox-active molecules in markedly different fashions: SoxR responds to oxidative stressors by upregulating expression of transporters and redox-related genes, whereas ActR exerts its protective effect at least in part by proactively regulating a key component of the aerobic respiratory ETC. While SoxR has previously been established as an oxidative stress response regulator in *A. tumefaciens*, we have expanded its known regulon to include genes that were hidden to computational approaches—a result that should encourage caution when predicting the SoxR regulons of other bacteria. In addition, the SoxR regulon we have identified in *A. tumefaciens* exhibits considerable functional overlap with genes that also modulate PYO tolerance in *E. coli* (Hassan and Fridovich, 1980; Khare and Tavazoie, 2015), suggesting that these functional classes—efflux pumps, superoxide dismutase, and electron transfer proteins such as flavodoxin and ferredoxin—are likely to be important for PYO tolerance in diverse bacteria. Yet the finding that ActR affects phenazine tolerance is perhaps more notable, for two reasons. First, Δ*actR* is susceptible to a wide range of redox-active molecules at lower concentrations than Δ*soxR*, bringing to mind the old adage, "An ounce of prevention is worth a pound of cure." This is in contrast to the historical emphasis on studying inducible, rather than intrinsic, bacterial defenses against oxidative stress (Farr and Kogoma, 1991; Scandalios, 2002; Imlay, 2008; Chiang and Schellhorn, 2012; Imlay, 2013). Second, the correlation between the Δ*actR* phenotype and dysregulation of the ETC recalls prior studies in which phenazines appeared to directly interfere with the flow of electrons through the ETC, suggesting that phenazine toxicity and ETC composition may be intimately linked (Hassan and Fridovich, 1980; Baron and Rowe, 1981; Baron *et al.*, 1989; Voggu *et al.*, 2006; Biswas *et al.*, 2009).

ActR belongs to a family of transcription factors including ArcA, PrrA, RegA, and RoxR, which are known for their ability to respond to the redox state of the cell, and to drive or repress

the expression of different genes accordingly (Elsen *et al.*, 2004; Fenner *et al.*, 2004). Thus, in *A. tumefaciens*, it is possible that ActR not only activates *cyo* and represses *cyd* during aerobic growth, but also represses *cyo* and/or activates *cyd* under microoxic or reducing conditions. If true, this could help explain why our Δ*cyo* mutant more closely resembles Δ*actR* during exponential growth than during stationary phase: all of our RNA-seq and qPCR experiments were performed during exponential growth, when *cyo* appears to be the dominant terminal oxidase in WT, but during stationary phase, it is possible that ActR normally promotes expression of *cyd* at the expense of *cyo* as oxygen tensions drop due to high cell density. This would be beneficial as *cyd* possesses a much higher affinity for oxygen than *cyo*, and hence is generally the preferred terminal oxidase under oxygen-limited conditions (Borisov *et al.*, 2011). Under this model, *A. tumefaciens* would require ActR in order to efficiently couple oxygen respiration to oxidative phosphorylation regardless of growth phase, as without ActR, it would neither be able to fully activate *cyo* under the well-oxygenated conditions that prevail during exponential growth, nor would it be able to fully activate *cyd* under the microoxic conditions that may arise during stationary phase. In both scenarios, failure to optimize the ETC could result in energy limitation and an excess of cellular reductants, which in turn could decrease the cell's capacity to respond to oxidative damage while simultaneously promoting toxic redox cycling of PYO.

Notably, the *actR* homolog *arcA* in *E. coli* was originally named *dye* because mutations in this gene increase sensitivity to redox-active dyes such as toluidine blue O and methylene blue (Buxton *et al.*, 1983; Alvarez *et al.*, 2010). An investigation into the molecular basis of this phenotype found that overexpression of ROS-scavenging enzymes could not restore tolerance to these dyes, but that Δ*arcA* displayed normal tolerance to these dyes during respiration-independent growth (Alvarez *et al.*, 2010). The authors consequently inferred that the dominant mode of toxicity of these dyes in Δ*arcA* is not ROS production, but rather the diversion of electrons from the ETC to the redox cycling of the dye, resulting in uncoupling of oxidative phosphorylation. By contrast, superoxide production appears to be an important mechanism of toxicity for PYO, given that superoxide dismutase is required for tolerance to PYO in *A. tumefaciens*, and that loss of ActR increases dependence on the SoxR-regulated superoxide dismutase; however, redox cycling of PYO may also uncouple oxidative phosphorylation. In addition, although ArcA in *E. coli* is not known to regulate the terminal oxidases during aerobic growth (Tseng *et al.*, 1996; Park *et al.*,

2013), ectopic overexpression of *cyd* in the *E. coli* Δ*arcA* mutant restores tolerance to redox-active dyes, while ectopic overexpression of *cyo* does not (Alvarez *et al.*, 2010). This is again in contrast to our finding that overexpression of *cyo* in the *A. tumefaciens* Δ*actR* mutant restores tolerance to PYO to a greater extent than overexpression of *cyd*. Separately, Cyo itself has also previously been linked to oxidative stress tolerance in *E. coli* (Lindqvist *et al.*, 2000), with at least one study suggesting that loss of Cyo potentiates oxidant toxicity by increasing basal endogenous ROS production in *E. coli* (Brynildsen *et al.*, 2013). However, our study appears to be the first to explicitly link ActR-mediated regulation of *cyo* to intrinsic tolerance of redox-active molecules.

To our knowledge, our findings are also the first to suggest that the preemptive protection conferred by ActR may be even more important than inducible SoxR-regulated mechanisms when challenged by certain redox-active molecules; these differing mechanisms of tolerance have previously been studied separately rather than comparatively in other organisms. Nevertheless, a preemptive role for ActR homologs in oxidative stress tolerance has also been found in *Haemophilus influenzae* (Wong *et al.*, 2007) and *Shewanella oneidensis* (Wan *et al.*, 2015). In *H. influenzae*, the ActR homolog ArcA confers protection against hydrogen peroxide during low to high oxygen transitions, partially through preemptive upregulation of a putative iron storage protein (Wong *et al.*, 2007), while in *S. oneidensis*, ArcA may promote hydrogen peroxide resistance by regulating cell envelope permeability (Wan *et al.*, 2015). In *A. tumefaciens*, on the other hand, no iron-related genes are downregulated in Δ*actR* to the extent seen by Wong *et al.* in *H. influenzae*, although we have not ruled out the possibility that the few mildly downregulated iron-related genes we found (negative fold change < 2.5) might contribute to the Δ*actR* phenotype. We have also found no evidence that ActR in *A. tumefaciens* regulates homologs of the putative cell envelope-related genes identified in *S. oneidensis* by Wan *et al.* Interestingly, unlike in *S. oneidensis*, our Δ*actR* mutant was no more sensitive than WT to hydrogen peroxide in a disk diffusion assay (Fig. 2C); instead, the putative link between ActR and oxidative stress tolerance in *A. tumefaciens* seems to be specific to redox-active molecules.

Although we found that ActR does not regulate a response to PYO in *A. tumefaciens*, the ActR homolog ArcA does appear to regulate a transcriptional response to hydrogen peroxide in other organisms such as *E. coli* and *S. enterica* (Loui *et al.*, 2009; Morales *et al.*, 2013). In hydrogen peroxide-treated *E. coli*, ArcA represses flagellin (*fliC*) and stimulates expression of two

genes involved in amino acid transport and metabolism, *gltI* and *oppA* (Loui *et al.*, 2009). In *S. enterica*, ArcA responds to hydrogen peroxide treatment by downregulating several PEP-PTS and ABC transporters, while upregulating genes involved in glutathione and glycerolipid metabolism and nucleotide transport (Morales *et al.*, 2013). Consequently, hydrogen peroxide treatment oxidizes the glutathione pool to a greater extent in Δ*arcA* compared to the WT strain (Morales *et al.*, 2013). The same study also indicated that loss of ArcA leads to an approximately ten-fold increase in the NADH/NAD+ ratio during aerobic growth, with concomitantly increased ROS production (Morales *et al.*, 2013). However, loss of ActR does not appear to have this effect in *A. tumefaciens*, implying that a different mechanism underpins the PYO sensitivity of our Δ*actR* mutant. Our RNA-seq data set also provides no indication that ActR regulates glutathione reductases in *A. tumefaciens*, unlike in *S. enterica* or even the more closely related *S. medicae* (Fenner *et al.*, 2004; Morales *et al.*, 2013).

The genetic evidence linking ActR and Cyo to phenazine tolerance is particularly interesting in light of other evidence suggesting that phenazines directly interact with and accept electrons from the respiratory ETC (Hassan and Fridovich, 1980; Baron and Rowe, 1981; Baron *et al.*, 1989; Voggu *et al.*, 2006; Biswas *et al.*, 2009). Perhaps most relevant are the observations that specific sequence variants in a subunit of cytochrome *bd* oxidase confer PYO tolerance in staphylococci (Voggu *et al.*, 2006), and that cbb_3-type terminal oxidases are necessary and sufficient for normal phenazine reduction in *P. aeruginosa* (Jo *et al.*, 2017). While technical limitations prevented us from quantitatively comparing intracellular ROS formation in WT and Δ*actR*, multiple observations from our Δ*actR* mutant—such as the fact that SodBII-mediated protection is more important in the Δ*actR* background—hint that the composition of the ETC, and in particular the pool of terminal oxidases, may influence how readily phenazines can "steal" electrons and thereby exert toxic effects. Importantly, as alluded to above, the toxic effects of stealing electrons from the ETC may not be limited to the generation of ROS, as redox cycling of phenazines may subvert the coupling of electron transfer to proton pumping and hence inhibit oxidative phosphorylation. This possibility is suggested by the fact that the ATP pool in Δ*actR* shrinks upon PYO treatment. At the same time, loss of Cyo might also increase basal ROS production to levels that do not affect growth under non-stressful conditions, but that nevertheless compromise the cell's ability to cope with exogenous oxidative stress, as has been observed in *E.*

coli (Brynildsen *et al.*, 2013). To further add insult to injury, the effects of any increase in ROS production—whether basal or PYO-mediated—would be compounded by the less-efficient coupling of the ETC to oxidative phosphorylation in Δ*actR*, as many oxidative damage repair systems require ATP (Selby and Sancar, 1995; Galletto *et al.*, 2006; Heinze *et al.*, 2009; Dahl *et al.*, 2015), not to mention the energy that is presumably required to synthesize the proteins in the SoxR regulon.

Overall, we propose a model in which ActR-mediated regulation of the ETC in *A. tumefaciens* helps to preemptively mitigate PYO toxicity, likely by minimizing the ability of PYO to decouple oxidative phosphorylation and generate ROS, while also promoting efficient energy conservation to power energy-dependent defense mechanisms such as the activation of the SoxR regulon (Fig. 7). Notably, loss of ActR has also been linked to downregulation of *cyo* in *Rhizobium etli*, a fellow member of the Rhizobiaceae (Lunak and Noel, 2015). Moreover, in the much more distantly related betaproteobacterium *Burkholderia cenocepacia*, a transposon insertion in an ActR homolog (BCAL0499) dramatically increased sensitivity to PYO and PCA (Bernier *et al.*, 2018),

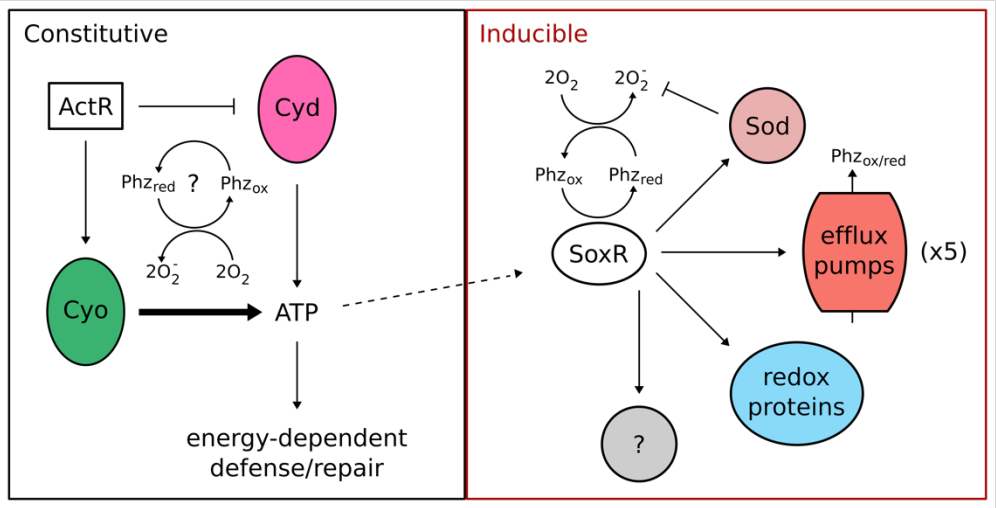

Figure 7: Proposed model for regulation of phenazine tolerance in *A. tumefaciens*.
Phenazine tolerance is regulated in both a constitutive (ActR-mediated) and inducible (SoxR-mediated) manner. ActR promotes phenazine tolerance in part by upregulating expression of cytochrome *o* oxidase (Cyo) at the expense of cytochrome *d* oxidase (Cyd) during aerobic growth. Cyo is more efficient at powering ATP synthesis and thereby supports energy-dependent defense and repair mechanisms. Levels of Cyo and Cyd may also affect how readily phenazines "steal" electrons from the electron transport chain and generate toxic superoxide radicals. Phenazines can directly oxidize and thereby activate SoxR. Activation of the SoxR regulon is likely energy dependent due to massive upregulation of several proteins, including superoxide dismutase (Sod), at least five efflux pumps, redox-related proteins such as ferredoxin, and other proteins that are as yet uncharacterized. The SoxR-regulated Sod becomes more important in the absence of ActR. Phz_{ox} = oxidized phenazines, Phz_{red} = reduced phenazines.

although this gene was not recognized as an ActR homolog in that study, nor was it further characterized; instead, we recognized this connection after performing a BLAST-P search with the BCAL0499 sequence against the *A. tumefaciens* genome. Together, these observations suggest that the role we have found for ActR in *A. tumefaciens* may extend to diverse organisms. Our results also raise the intriguing possibility that the composition of an organism's ETC may be a key determinant of its sensitivity to phenazines and other redox-active compounds. Future comparative studies will shed light on the usefulness of this principle for understanding and predicting ecological impacts of this important class of bacterial secondary metabolites.

Methods

Strains and media

All experiments with *A. tumefaciens* were performed with strain NT1, a derivative of strain C58 that lacks the pathogenicity-conferring Ti plasmid (Watson *et al.*, 1975). *A. tumefaciens* was routinely grown at 30 °C, with shaking at 250 rpm for liquid cultures. Unless otherwise stated, the medium for liquid cultures was Luria-Bertani (LB) Miller broth (Difco) buffered with 50 mM MOPS (pH 7), while solid plates were made with LB containing 1.5% agar. Kanamycin was added where appropriate at 50 µg/mL to make LB-Kan. LB was chosen as it is a commonly used rich medium and because we found that *A. tumefaciens* is highly sensitive to PYO in minimal glucose media such as AT medium (Morton and Fuqua, 2012b), possibly due to the harmful effects of superoxide on amino acid biosynthetic enzymes (Carlioz and Touati, 1986). The donor strain for transposon mutagenesis was *E. coli* β2155 pSC189, which was grown at 37 °C in LB containing 300 µM diaminopimelic acid (DAP) and 100 µg/mL carbenicillin. Molecular cloning was carried out in *E. coli* DH10b using restriction enzyme-based standard protocols, except for pCyo, which was constructed by Gibson assembly (Gibson *et al.*, 2009). Plasmids (except for pSC189) were transferred to *A. tumefaciens* by electroporation. All restriction enzymes and Gibson assembly reagents were purchased from New England Biolabs (NEB). PYO was synthesized and purified as previously described (Cheluvappa, 2014), and PCA was purchased from Princeton Biomolecular Research, Inc. For all experiments involving PYO, a 50x stock solution was made in 20 mM HCl, and the latter was used as a solvent control (2% of final culture volume) in 0 µM PYO conditions. Paraquat and AQDS were directly dissolved in MOPS-buffered LB at the desired final

concentration. Stock solutions (50x) of methylene blue and PCA were made in water, with the latter dissolved by adding an equimolar amount of NaOH.

Transposon mutagenesis screen and identification of transposon insertion loci

To generate random transposon insertion mutants, we conjugated *A. tumefaciens* with the donor strain for pSC189 as follows. First, *A. tumefaciens* and *E. coli* β2155 pSC189 were grown overnight to early stationary phase, then a 1 mL aliquot of *E. coli* was centrifuged and washed twice with LB to avoid carryover of carbenicillin and DAP. A 1 mL aliquot of *A. tumefaciens* was then added to the same microcentrifuge tube and centrifuged to generate a mixed cell pellet. The pellet was resuspended in 20 µL of LB, spotted directly on LB agar, incubated for 24 hr at 30 °C, and resuspended in 1 mL of LB by scraping and pipetting. This procedure was repeated approximately 25 times to generate independent libraries of transposon mutants. The libraries were diluted by a factor of 2×10^{-4} and 100 µL was spread on LB-Kan plates. After two days at 30 °C, colonies were picked directly into 96-well microtiter plates containing 100 µL of LB-Kan in each well. The 96-well plates were wrapped in plastic film and incubated at 30 °C for 24 hrs without shaking, in plastic containers containing damp paper towels for humidity. Subsequently, using a 48-pronged replicator flame-sterilized with ethanol, a small aliquot (1-2 µL) of each culture was transferred to a fresh 96-well plate containing 200 µL aliquots of LB-Kan + 100 µM PYO and incubated as above. After two days, the plates were assessed for the color change from blue to clear. Mutants in wells that remained blue were recovered from the original 96-well plates (that were grown without PYO) and stored at -80 °C in 15% glycerol until further analysis.

The transposon insertion location in each mutant of interest was determined using arbitrary PCR. Genomic DNA was extracted from overnight cultures of the mutants using the QIAamp DNA Mini Kit (Qiagen) and PCR-amplified in 50 µL reactions with the primers Mar4 and SS9arb1 (Table S7). 5 µL of the PCR product was treated with ExoSAP-IT (Applied Biosystems) and 1 µL of cleaned-up product was re-amplified using the nested primers Mar4-2 and arb3 (Table S7). Following gel electrophoresis in 1% agarose, 1-2 distinct bands per mutant were gel extracted with the QIAquick Gel Extraction Kit (Qiagen) and submitted for Sanger sequencing (Laragen). The resulting sequences were aligned with BLAST against the *A. tumefaciens* C58 genome on the MicroScope platform (Vallenet *et al.*, 2017).

In-frame deletion, complementation, and overexpression experiments

In-frame deletion mutants were generated via allelic replacement according to a previously published protocol (Morton and Fuqua, 2012a), using the plasmid pNPTS138 (M. R. K. Alley, unpublished), except that plating steps were done on LB agar containing 5% sucrose and/or 50 μg/mL kanamycin as appropriate. Complementation and overexpression experiments were performed by cloning the coding sequence(s) of the relevant gene(s) into the plasmid pSRKKm in place of *lacZα*, such that expression of the gene(s) of interest would be driven by the *lacI*^{q}*-lac* promoter-operator complex (Khan *et al.*, 2008). Expression from these plasmids in *A. tumefaciens* was induced by adding 1 mM isopropyl β-D-thiogalactopyranoside (IPTG) to the culture medium at the beginning of the experiment. All plasmids used in this study are described in Table S8.

Bacterial growth-based assays

To assess sensitivity to PYO or other redox-active molecules in liquid cultures, stationary-phase overnight cultures of *A. tumefaciens* were diluted to an OD_{500} of 1 in fresh medium and inoculated 1:10 (initial OD_{500} = 0.1) into 200 μL aliquots of medium containing different concentrations of the redox-active molecules in 96-well flat-bottom tissue culture plates. Each plate was then transferred to a small humidity cassette (Tecan) containing 4 mL of water and incubated in a Spark 10M plate reader (Tecan) with shaking at 30 °C for 24 hr, monitoring OD_{500} as a proxy for growth. OD_{500} measurements were corrected by subtracting the OD_{500} of "blank" wells containing the respective treatment without cells. Each strain was assessed with at least three biological replicates (derived from independent overnight cultures). Throughout this study, differences in growth after 24 hrs approximately correspond to differences in maximum achievable cell density, as cultures were either in or approaching stationary phase at this time point.

Sensitivity to acid, hydrogen peroxide, or SDS was assessed with a disk diffusion assay. Stationary-phase overnight cultures were diluted to an OD_{500} of 1, mixed 1:50 with 42 °C pre-warmed LB soft agar (0.8% agar), and evenly pipetted in 5 mL aliquots onto solid LB agar plates. Disks of Whatman #1 filter paper (7 mm diameter) were soaked in 2 M HCl, 5.5 M H_2O_2, or 10% SDS and placed in the center of the plates. Diameters of growth inhibition zones were measured after two days of incubation at room temperature.

Sensitivity to bile salts, EDTA, and osmotic stresses was assessed using a gradient plate assay. To prepare the gradient plates, 25 mL of molten LB agar containing 2% bile salts (HiMedia Laboratories), 1 mM EDTA, 0.4 M NaCl (total concentration including the salt already present in LB), or 1 M myo-inositol was poured into square grid plates (Fisherbrand) tilted by propping against their lids. Once this layer had set, the plates were topped with 30 mL of plain LB agar and left at room temperature to equilibrate for at least 24 hrs. LB-only agar plates were prepared in the same manner as a control. Exponential-phase cultures were diluted to an OD_{500} of 0.5, then diluted again 10^{-4}, and 5 µL aliquots of the suspension were spotted on the gradient plates. The plates were incubated at 30 °C for 2-3 days before imaging with an Epson Perfection V550 Photo flatbed scanner. For both the disk diffusion and gradient plate experiments, each strain was tested in duplicate at least three independent times.

RNA extraction, RNA-seq, and qRT-PCR

To obtain RNA for RNA-seq or qRT-PCR, overnight cultures (duplicate for RNA-seq, triplicate for qRT-PCR) were diluted to an OD_{500} of 0.1 and grown to exponential phase (OD_{500} ~0.5-0.7), then treated with PYO or 20 mM HCl (solvent control) for 20 min before collecting 1 mL aliquots. Cell pellets obtained by centrifuging the aliquots were flash-frozen in liquid nitrogen and stored at -80 °C until RNA extraction. RNA was extracted from the pellets using the RNeasy Mini Kit (Qiagen) with a modified protocol. Briefly, the cell pellets were resuspended in 200 µL of TE buffer (30 mM Tris-HCl, 1 mM EDTA, pH 8) containing 15 mg/mL lysozyme, plus 15 µL of 20 mg/mL proteinase K (Qiagen). After 10 min at 37 °C with occasional mixing, 700 µL of Buffer RLT containing 1% β-mercaptoethanol was added, vortexing to mix, followed by 500 µL of absolute ethanol. The manufacturer's protocol for bacteria was then followed starting at step 7 (loading the lysate onto the spin column), including the optional on-column digestion with DNase I (Qiagen). After eluting the RNA in RNase-free water, residual genomic DNA was removed with the TURBO DNA-free Kit (Invitrogen), following the manufacturer's protocol.

For RNA-seq, rRNA was depleted by treatment with the Ribo-Zero rRNA Removal Kit for Bacteria (Illumina). The remaining RNA was then fragmented to an average size of 200 bp by incubation at 94 °C for exactly 60 s with the RNA Fragmentation Buffer from the NEBNext mRNA Library Prep Master Mix Set for Illumina (NEB). Fragmentation was halted by placing the

samples on ice and adding the RNA Fragmentation Stop Buffer. The concentrations and average sizes of the fragmented RNA samples were determined using the Agilent RNA 6000 Pico Kit on an Agilent 2100 Bioanalyzer. Subsequent library preparation steps were carried out with the NEBNext Ultra II Directional RNA Library Prep Kit for Illumina (NEB), following the manufacturer's protocol for rRNA-depleted FFPE RNA. Sequencing was performed at the Millard and Muriel Jacobs Genetics and Genomics Laboratory at the California Institute of Technology to a depth of 10-15 million reads on an Illumina HiSeq2500 and processed using the Illumina HiSeq control software (HCS version 2.0). Low-quality bases were removed using Trimmomatic (LEADING:27 TRAILING:27 SLIDINGWINDOW:4:20 MINLEN:35) (Bolger *et al.*, 2014). Alignment to the *A. tumefaciens* C58 genome and calculation of the number of reads per gene was performed with Rockhopper 2 (Tjaden, 2015), with 0.04 allowed mismatches and a minimum seed length of 0.33. Differential gene expression analysis was performed using DESeq2 (Love *et al.*, 2014). Sequence data were submitted to the NCBI Sequence Read Archive under the accession number PRJNA521160.

For qRT-PCR, cDNA was synthesized from TURBO DNase-treated RNA using the iScript cDNA Synthesis Kit (Bio-Rad). The PCR reactions were set up in a 20 µL volume with iTaq Universal SYBR Green Supermix (Bio-Rad) (10 µL of the supermix, 4 µL of a 1:10 dilution of cDNA [~10 ng], 0.4 µL each of 10 µM forward and reverse primers, and 5.2 µL of water). Primers for qRT-PCR were designed using Primer-BLAST (Ye *et al.*, 2012) and are listed in Table S7. Reactions were run using a Fast 7500 Real-Time PCR System machine (Applied Biosystems). A standard curve for each primer pair was generated using known concentrations of *A. tumefaciens* genomic DNA, enabling calculation of the relative concentrations of cDNA for each gene of interest. The expression levels (relative concentrations) for each gene were normalized to the expression of the housekeeping gene *rpoD*.

Oxygen consumption rate measurements

To measure oxygen consumption rates, each overnight culture was diluted to an OD_{500} of 0.1 in four 5 mL cultures (total 20 mL) and grown to exponential phase (OD_{500} ~0.5-0.7). Meanwhile, 19 mL of MOPS-buffered LB per sample was aliquoted into autoclaved scintillation vials and pre-equilibrated by stirring with a magnetic stir bar at 500 rpm for at least 1 hr. Once the

cultures had reached exponential phase, all 20 mL of each sample was centrifuged in a 50 mL conical tube. The cell pellet was resuspended in 1 mL of MOPS-buffered LB and adjusted to an OD_{500} of 5, then 1 mL of the suspension was added to 19 mL of pre-equilibrated medium with continued stirring at 500 rpm. The concentration of oxygen in the medium was recorded over time at 1 s intervals using an OX-500 microsensor (Unisense), which was submerged to a fixed depth below the surface. After 7 min, the cultures were spiked with 10 μM PYO and the oxygen concentration was recorded for another 7 min. The measurements were calibrated by using a solution of 0.1 M sodium ascorbate + 0.1 M NaOH as the zero-oxygen reference, and MOPS-buffered LB that had equilibrated with stirring at 500 rpm for several hours as the saturated reference. The microsensor response was converted to dissolved oxygen concentration using the salinity-temperature-solubility tables provided by the manufacturer. Oxygen consumption rates were calculated using an approach similar to a previously published method (Riedel *et al.*, 2013), except that we treated only the first 2 min of each 7 min recording period as an equilibration period due to the rapid response of the microsensor, and that we fitted separate linear regressions for each 10 μM interval of oxygen concentration.

To measure PYO-mediated oxygen consumption rates in the presence of cyanide, experiments were performed as above except that 5 mM potassium cyanide (KCN) was added to the cell suspensions after the first 7 min (to ensure that cells were respiring normally prior to cyanide addition). Upon addition of cyanide, oxygen consumption halted within 10 s, and oxygen concentrations steadily rose over time due to leakage of oxygen back into the system. After 5 min of cyanide treatment, 10 μM PYO was added to the cell suspensions. As this led to no visible change in the rate of oxygen leakage/consumption, after another 5 min more PYO was added to a final concentration of 100 μM. Plating for CFUs before and after the experiments confirmed that 5 mM KCN did not kill the cells (data not shown).

NADH and NAD+ extraction and measurement

To determine the NADH/NAD+ ratios of WT and Δ*actR*, overnight cultures were diluted to an OD_{500} of 0.1 and grown to exponential phase (5 hrs) in 5 mL MOPS-buffered LB. NADH and NAD+ were then extracted and quantified according to a previously published protocol (Kern *et al.*, 2014). To monitor the progress of the enzyme-mediated colorimetric reaction, absorbance

at 570 nm was tracked in a Spark 10M plate reader (Tecan) over a period of 20 min, with the minimum possible time between readings (~45 s).

ATP measurements and ATP synthesis inhibition

To measure ATP levels, overnight cultures were diluted to an OD_{500} of 0.1 and grown to exponential phase (5 hrs) in 5 mL MOPS-buffered LB with or without 10 μM PYO. The ATP measurements were then performed using BacTiter-Glo Reagent (Promega) in opaque white 96-well plates, according to the manufacturer's instructions. Luminescence readings were taken at 30 °C using a Spark 10M plate reader (Tecan). ATP concentrations were calculated using a standard curve generated with known quantities of pure ATP dissolved in water, and were normalized to the OD_{500} of each culture. To test whether inhibiting ATP synthesis can increase sensitivity to PYO, the experiment was performed in the same manner except that the cultures were treated with 0 or 100 μM N,N-dicyclohexylcarbodiimide (DCCD), in combination with 0 or 10 μM PYO. These experiments were performed in triplicate.

Measurement of ROS production

We first measured ROS production by using electron paramagnetic resonance (EPR) spectroscopy in conjunction with the spin trap 5-tert-butoxycarbonyl-5-methyl-1-pyrroline-N-oxide (BMPO), which reacts with superoxide and hydroxyl radical to form relatively stable radical adducts (BMPO/$^{\bullet}$OOH and BMPO/$^{\bullet}$OH, respectively) (Zhao *et al.*, 2001). However, we found that this approach could only detect extracellular ROS in suspensions of *A. tumefaciens* (Fig. S7A), consistent with a previous study that used a similar spin trap to detect superoxide formation in PYO-treated *E. coli* (Hassett *et al.*, 1992). To perform these measurements, overnight cultures were first grown in AT minimal medium modified to contain 50 mM phosphate buffer and no added iron (Morton and Fuqua, 2012b). The cultures reached mid-exponential phase after approximately 20-24 hrs, at which point the cells were pelleted by centrifugation and washed twice with Chelex 100 (Bio-Rad)-treated 0.1 M phosphate buffer (pH 7.4) containing 25 μM diethylenetriaminepentaacetic acid (DTPA). The cells were then resuspended in the buffer to an OD_{500} of 1. For each sample, 176 μL of cell suspension was combined with 20 μL of 250 mM BMPO (dissolved in the phosphate buffer), 2 μL of 50% glucose (Chelex 100-treated), and 2 μL

of 10 mM PYO, and mixed by vortexing for 5 s every minute for three minutes. The sample was then loaded into a flat quartz EPR spectroscopy cuvette and the spectrum was recorded on a Bruker EMX X-band CW-EPR spectrometer starting at 10 min 30 s after the addition of PYO. The instrument settings were as follows: microwave power, 5.08 mW; microwave frequency, 9.836 GHz; modulation frequency, 100 kHz; modulation amplitude, 1 G; time constant, 81.92 msec; receiver gain, 5.02 x 10^4; sweep time, 83.89 s. Spectra shown in Fig. S6A are averages of 6 consecutive scans from single samples that are representative of at least three biological replicates, except for the cell-free and exogenous SOD control samples, for which only the initial spectrum was recorded.

To measure intracellular superoxide formation, we considered using dihydroethidium (DHE), a cell-permeable dye that reacts with superoxide to form the fluorescent derivative 2-hydroxyethidium, although it can also be nonspecifically oxidized to similarly fluorescent ethidium (Zielonka *et al.*, 2007). Unfortunately, we found that addition of PYO to DHE in cell-free phosphate buffer was sufficient to increase fluorescence, suggesting that PYO can abiotically oxidize DHE and that DHE oxidation would therefore not be a reliable reporter for intracellular superoxide (Fig. S7B). To test DHE for oxidation upon exposure to PYO, 1.5 µL of 5 mM DHE (Invitrogen) was combined in a microcentrifuge tube with 5 µL of 1 mM PYO or 5 µL of 20 mM HCl (solvent control) in 493.5 µL of Chelex 100-treated 0.1 M phosphate buffer (pH 7.4) containing 100 µM DTPA. The samples were incubated at 30 °C with shaking at 250 rpm for 1 hr. Subsequently, 200 µL of each sample was transferred to a black plastic flat transparent-bottomed 96-well plate and fluorescence (excitation at 510 nm, emission at 580 nm) was recorded in a Spark 10M plate reader (Tecan). All steps were performed in the dark or under dim lighting to minimize photooxidation of DHE.

Statistical analysis

All statistical analyses were performed using R (R Core Team, 2018). In all cases involving multiple pairwise comparisons within an experiment, the Benjamini-Hochberg procedure was used to control the false discovery rate. For Figs. 2B and 3B, statistical significance was calculated by generalized linear regression with dummy variable coding, using WT as the reference group within each treatment. The function ‘ncvTest’ from the package ‘car’ (Fox and Weisberg, 2011) was used

to verify the homoscedasticity of the residuals, while the Shapiro-Wilk normality test was used to verify the normality of the residuals. For Fig. 2C, the Shapiro-Wilk test revealed non-normality of the residuals following linear regression, so instead the Kruskal-Wallis test was performed within each treatment, followed by pairwise comparisons using the Wilcox rank sum test. For Fig. 4C, Welch's *t*-test was used to make pairwise comparisons between WT and Δ*actR* within each condition (i.e. + PYO or – PYO). For Fig. 6C, Welch's *t*-test was used to make pairwise comparisons between strains within each condition (i.e. + PYO or – PYO), as well as within strains but between conditions. For Fig. S6B, ncvTest revealed heteroscedasticity of the residuals following linear regression, so instead samples were grouped by strain and PYO treatment and Welch's *t*-test was then used to make pairwise comparisons between 0 μM and 100 μM DCCD treatments within each group. For Fig. S6C, the assumptions of linear regression were met, so linear regression was performed with a custom contrast matrix to specify comparisons between 0 μM and 100 μM DCCD treatments within each strain.

Acknowledgements

We thank all members of the Newman lab for helpful advice, discussions, and feedback on the manuscript, and Clay Fuqua for generously providing pNPTS138. We also thank the Marine Biological Laboratory Microbial Diversity Course, Class of 2017, for assistance with screening transposon mutants. This material is based upon work supported by the National Science Foundation Graduate Research Fellowship under Grant No. DGE-1745301. This work was also supported by the Millard and Muriel Jacobs Genetics and Genomics Laboratory at the California Institute of Technology (Caltech), the Caltech Electron Paramagnetic Resonance Spectroscopy Facility, and grants to D.K.N. from the ARO (W911NF-17-1-0024) and NIH (1R01AI127850-01A1).

References

Alonso, A., Rojo, F., and Martínez, J.L. (1999) Environmental and clinical isolates of *Pseudomonas aeruginosa* show pathogenic and biodegradative properties irrespective of their origin. *Environ Microbiol* **1**: 421–430.

Alvarez, A.F., Malpica, R., Contreras, M., Escamilla, E., and Georgellis, D. (2010) Cytochrome *d* but not cytochrome *o* rescues the toluidine blue growth sensitivity of *arc* mutants of *Escherichia coli*. *J Bacteriol* **192**: 391–399.

An, D., Danhorn, T., Fuqua, C., and Parsek, M.R. (2006) Quorum sensing and motility mediate interactions between *Pseudomonas aeruginosa* and *Agrobacterium tumefaciens* in biofilm cocultures. *Proc Natl Acad Sci* **103**: 3828–3833.

Audenaert, K., Pattery, T., Cornelis, P., and Höfte, M. (2002) Induction of systemic resistance to *Botrytis cinerea* in tomato by *Pseudomonas aeruginosa* 7NSK2: role of salicylic acid, pyochelin, and pyocyanin. *Mol Plant-Microbe Interact* **15**: 1147–1156.

Baek, S.H., Hartsock, A., and Shapleigh, J.P. (2008) *Agrobacterium tumefaciens* C58 uses ActR and FnrN to control *nirK* and *nor* expression. *J Bacteriol* **190**: 78–86.

Baron, S.S., and Rowe, J.J. (1981) Antibiotic action of pyocyanin. *Antimicrob Agents Chemother* **20**: 814–820.

Baron, S.S., Terranova, G., and Rowe, J.J. (1989) Molecular mechanism of the antimicrobial action of pyocyanin. *Curr Microbiol* **18**: 223–230.

Begley, M., Gahan, C.G.M., and Hill, C. (2005) The interaction between bacteria and bile. *FEMS Microbiol Rev* **29**: 625–651.

Bernier, S.P., Son, S., and Surette, M.G. (2018) The Mla pathway plays an essential role in the intrinsic resistance of *Burkholderia cepacia* complex species to antimicrobials and host innate components. *J Bacteriol* **200**: e00156-18.

Biswas, L., Biswas, R., Schlag, M., Bertram, R., and Götz, F. (2009) Small-colony variant selection as a survival strategy for *Staphylococcus aureus* in the presence of *Pseudomonas aeruginosa*. *Appl Environ Microbiol* **75**: 6910–6912.

Bolger, A.M., Lohse, M., and Usadel, B. (2014) Trimmomatic: a flexible trimmer for Illumina sequence data. *Bioinformatics* **30**: 2114–2120.

Borisov, V.B., Gennis, R.B., Hemp, J., and Verkhovsky, M.I. (2011) The cytochrome *bd* respiratory oxygen reductases. *Biochim Biophys Acta - Bioenerg* **1807**: 1398–1413.

Brynildsen, M.P., Winkler, J.A., Spina, C.S., MacDonald, I.C., and Collins, J.J. (2013) Potentiating antibacterial activity by predictably enhancing endogenous microbial ROS production. *Nat Biotechnol* **31**: 160–165.

Buxton, R.S., Drury, L.S., and Curtis, C.A.M. (1983) Dye sensitivity correlated with envelope protein changes in *dye* (*sfrA*) mutants of *Escherichia coli* K12 defective in the expression of the sex factor F. *J Gen Microbiol* **129**: 3363–3370.

Calhoun, M.W., Oden, K.L., Gennis, R.B., Mattos, M.J.T. de, and Neijssel, O.M. (1993) Energetic efficiency of *Escherichia coli*: effects of mutations in components of the aerobic respiratory chain. *J Bacteriol* **175**: 3020–3025.

Carlioz, A., and Touati, D. (1986) Isolation of superoxide dismutase mutants in *Escherichia coli*: is superoxide dismutase necessary for aerobic life? *EMBO J* **5**: 623–630.

Cheluvappa, R. (2014) Standardized chemical synthesis of *Pseudomonas aeruginosa* pyocyanin. *MethodsX* **1**: 67–73.

Chiang, S.L., and Rubin, E.J. (2002) Construction of a *mariner*-based transposon for epitope-tagging and genomic targeting. *Gene* **296**: 179–185.

Chiang, S.M., and Schellhorn, H.E. (2012) Regulators of oxidative stress response genes in *Escherichia coli* and their functional conservation in bacteria. *Arch Biochem Biophys* **525**: 161–169.

Chin-A-Woeng, T.F.C., Bloemberg, G. V., and Lugtenberg, B.J.J. (2003) Phenazines and their role in biocontrol by *Pseudomonas* bacteria. *New Phytol* **157**: 503–523.

Chin-A-Woeng, T.F.C., Bloemberg, G. V, Bij, A.J. van der, Drift, K.M.G.M. van der, Schripsema, J., Kroon, B., *et al.* (1998) Biocontrol by phenazine-1-carboxamide-producing *Pseudomonas*

chlororaphis PCL1391 of tomato root rot caused by *Fusarium oxysporum* f. sp. *radicis-lycopersici*. *Mol Plant-Microbe Interact* **11**: 1069–1077.

Costa, K.C., Bergkessel, M., Saunders, S., Korlach, J., and Newman, D.K. (2015) Enzymatic degradation of phenazines can generate energy and protect sensitive organisms from toxicity. *mBio* **6**: 1–10.

D'mello, R., Hill, S., and Poole, R.K. (1996) The cytochrome *bd* quinol oxidase in *Escherichia coli* has an extremely high oxygen affinity and two oxygen-binding haems: implications for regulation of activity in vivo by oxygen inhibition. *Microbiology* **142**: 755–763.

Dahl, J.-U., Gray, M.J., and Jakob, U. (2015) Protein quality control under oxidative stress conditions. *J Mol Biol* **427**: 1549–1563.

Dietrich, L.E.P., and Kiley, P.J. (2011) A shared mechanism of SoxR activation by redox-cycling compounds. *Mol Microbiol* **79**: 1119–1122.

Dietrich, L.E.P., Price-Whelan, A., Petersen, A., Whiteley, M., and Newman, D.K. (2006) The phenazine pyocyanin is a terminal signalling factor in the quorum sensing network of *Pseudomonas aeruginosa*. *Mol Microbiol* **61**: 1308–1321.

Dietrich, L.E.P., Teal, T.K., Price-Whelan, A., and Newman, D.K. (2008) Redox-active antibiotics control gene expression and community behavior in divergent bacteria. *Science (80-)* **321**: 1203–1206.

Eiamphungporn, W., Charoenlap, N., Vattanaviboon, P., and Mongkolsuk, S. (2006) *Agrobacterium tumefaciens* soxR is involved in superoxide stress protection and also directly regulates superoxide-inducible expression of itself and a target gene. *J Bacteriol* **188**: 8669–8673.

Elsen, S., Swem, L.R., Swem, D.L., and Bauer, C.E. (2004) RegB/RegA, a highly conserved redox-responding global two-component regulatory system. *Microbiol Mol Biol Rev* **68**: 263–279.

Evans, M.R., Fink, R.C., Vazquez-Torres, A., Porwollik, S., Jones-Carson, J., McClelland, M., and Hassan, H.M. (2011) Analysis of the ArcA regulon in anaerobically grown *Salmonella enterica sv.* Typhimurium. *BMC Microbiol* **11**: 58.

Fargier, E., Aogáin, M., Mooij, M.J., Woods, D.F., Morrissey, J.P., and Dobson, A.D.W. (2012) MexT functions as a redox-responsive regulator modulating disulfide stress resistance in *Pseudomonas aeruginosa*. *J Bacteriol* **194**: 3502–3511.

Farr, S.B., and Kogoma, T. (1991) Oxidative stress responses in *Escherichia coli* and *Salmonella typhimurium*. *Microbiol Rev* **55**: 561–585.

Fenner, B.J., Tiwari, R.P., Reeve, W.G., Dilworth, M.J., and Glenn, A.R. (2004) *Sinorhizobium medicae* genes whose regulation involves the ActS and/or ActR signal transduction proteins. *FEMS Microbiol Lett* **236**: 21–31.

Fernández-Piñar, R., Ramos, J.L., Rodríguez-Herva, J., and Espinosa-Urgel, M. (2008) A two-component regulatory system integrates redox state and population density sensing in *Pseudomonas putida*. *J Bacteriol* **190**: 7666–7674.

Fetar, H., Gilmour, C., Klinoski, R., Daigle, D.M., Dean, C.R., and Poole, K. (2011) *mexEF-oprN* multidrug efflux operon of *Pseudomonas aeruginosa*: regulation by the MexT activator in response to nitrosative stress and chloramphenicol. *Antimicrob Agents Chemother* **55**: 508–514.

Fox, J., and Weisberg, S. (2011) *An R companion to applied regression*. 2nd ed., Sage, Thousand Oaks, CA.

Galletto, R., Amitani, I., Baskin, R.J., and Kowalczykowski, S.C. (2006) Direct observation of individual RecA filaments assembling on single DNA molecules. *Nature* **443**: 875–878.

Gao, H., Wang, X., Yang, Z.K., Palzkill, T., and Zhou, J. (2008) Probing regulon of ArcA in

Shewanella oneidensis MR-1 by integrated genomic analyses. *BMC Genomics* **9**: 42.
Gibson, D.G., Young, L., Chuang, R.-Y., Venter, J.C., Hutchison III, C.A., and Smith, H.O. (2009) Enzymatic assembly of DNA molecules up to several hundred kilobases. *Nat Methods* **6**: 343–345.
Glasser, N.R., Kern, S.E., and Newman, D.K. (2014) Phenazine redox cycling enhances anaerobic survival in *Pseudomonas aeruginosa* by facilitating generation of ATP and a proton-motive force. *Mol Microbiol* **92**: 399–412.
Gralnick, J.A., Brown, C.T., and Newman, D.K. (2005) Anaerobic regulation by an atypical Arc system in *Shewanella oneidensis*. *Mol Microbiol* **56**: 1347–1357.
Grant, C.E., Bailey, T.L., and Noble, W.S. (2011) FIMO: Scanning for occurrences of a given motif. *Bioinformatics* **27**: 1017–1018.
Green, S.K., Schroth, M.N., Cho, J.J., Kominos, S.K., and Vitanza-Jack, V.B. (1974) Agricultural plants and soil as a reservoir for *Pseudomonas aeruginosa*. *Appl Microbiol* **28**: 987–991.
Gu, M., and Imlay, J.A. (2011) The SoxRS response of *Escherichia coli* is directly activated by redox-cycling drugs rather than by superoxide. *Mol Microbiol* **79**: 1136–1150.
Hassan, H.M., and Fridovich, I. (1980) Mechanism of the antibiotic action of pyocyanine. *J Bacteriol* **141**: 156–163.
Hassett, D.J., Charniga, L.L., Bean, K., Ohman, D.E., and Scohen, M. (1992) Response of *Pseudomonas aeruginosa* to pyocyanin: mechanisms of resistance, antioxidant defenses, and demonstration of a manganese-cofactored superoxide dismutase. *Infect Immun* **60**: 328–336.
Heinze, R.J., Giron-Monzon, L., Solovyova, A., Elliot, S.L., Geisler, S., Cupples, C.G., *et al.* (2009) Physical and functional interactions between *Escherichia coli* MutL and the Vsr repair endonuclease. *Nucleic Acids Res* **37**: 4453–4463.
Hernandez, M.E., Kappler, A., and Newman, D.K. (2004) Phenazines and other redox-active antibiotics promote microbial mineral reduction. *Appl Environ Microbiol* **70**: 921–928.
Imlay, J.A. (2008) Cellular defenses against superoxide and hydrogen peroxide. *Annu Rev Biochem* **77**: 755–776.
Imlay, J.A. (2013) The molecular mechanisms and physiological consequences of oxidative stress: lessons from a model bacterium. *Nat Rev Microbiol* **11**: 443–454.
Jo, J., Cortez, K.L., Cornell, W.C., Price-Whelan, A., and Dietrich, L.E.P. (2017) An orphan *cbb3*-type cytochrome oxidase subunit supports *Pseudomonas aeruginosa* biofilm growth and virulence. *Elife* **6**: e30205.
Kern, S.E., Price-Whelan, A., and Newman, D.K. (2014) Extraction and measurement of NAD(P)+ and NAD(P)H. In *Pseudomonas Methods and Protocols*. Filloux, A., and Ramos, J.-L. (eds). Springer New York, New York, NY. pp. 311–323.
Khan, S.R., Gaines, J., Roop, R.M., and Farrand, S.K. (2008) Broad-host-range expression vectors with tightly regulated promoters and their use to examine the influence of TraR and TraM expression on Ti plasmid quorum sensing. *Appl Environ Microbiol* **74**: 5053–5062.
Khare, A., and Tavazoie, S. (2015) Multifactorial competition and resistance in a two-species bacterial system. *PLoS Genet* **11**: e1005715.
Khare, E., and Arora, N.K. (2011) Dual activity of pyocyanin from *Pseudomonas aeruginosa* — antibiotic against phytopathogen and signal molecule for biofilm development by rhizobia. *Can J Microbiol* **57**: 708–713.
Köhler, T., Epp, S.F., Curty, L.K., and Pechère, J.-C. (1999) Characterization of MexT, the regulator of the MexE-MexF-OprN multidrug efflux system of *Pseudomonas aeruginosa*. *J Bacteriol* **181**: 6300–6305.

Köhler, T., Michéa-Hamzehpour, M., Henze, U., Gotoh, N., Curty, L.K., and Pechère, J.-C. (1997) Characterization of MexE-MexF-OprN, a positively regulated multidrug efflux system of *Pseudomonas aeruginosa*. *Mol Microbiol* **23**: 345–354.

Lamarche, M.G., and Déziel, E. (2011) MexEF-OprN efflux pump exports the *Pseudomonas* quinolone signal (PQS) precursor HHQ (4-hydroxy-2-heptylquinoline). *PLoS One* **6**: e24310.

LeTourneau, M.K., Marshall, M.J., Cliff, J.B., Bonsall, R.F., Dohnalkova, A.C., Mavrodi, D. V, *et al.* (2018) Phenazine-1-carboxylic acid and soil moisture influence biofilm development and turnover of rhizobacterial biomass on wheat root surfaces. *Environ Microbiol* **20**: 2178–2194.

Lindqvist, A., Membrillo-Hernández, J., Poole, R.K., and Cook, G.M. (2000) Roles of respiratory oxidases in protecting *Escherichia coli* K12 from oxidative stress. *Antonie Van Leeuwenhoek* **78**: 23–31.

Llanes, C., Kohler, T., Patry, I., Dehecq, B., Delden, C. Van, and Plesiat, P. (2011) Role of the MexEF-OprN efflux system in low-level resistance of *Pseudomonas aeruginosa* to ciprofloxacin. *Antimicrob Agents Chemother* **55**: 5676–5684.

Loui, C., Chang, A.C., and Lu, S. (2009) Role of the ArcAB two-component system in the resistance of *Escherichia coli* to reactive oxygen stress. *BMC Microbiol* **14**: 1–14.

Love, M.I., Huber, W., and Anders, S. (2014) Moderated estimation of fold change and dispersion for RNA-seq data with DESeq2. *Genome Biol* **15**: 550.

Lunak, Z.R., and Noel, K.D. (2015) Quinol oxidase encoded by *cyoABCD* in *Rhizobium etli* CFN42 is regulated by ActSR and is crucial for growth at low pH or low iron conditions. *Microbiology* **161**: 1806–1815.

Managò, A., Becker, K.A., Carpinteiro, A., Wilker, B., Soddemann, M., Seitz, A.P., *et al.* (2015) *Pseudomonas aeruginosa* pyocyanin induces neutrophil death via mitochondrial reactive oxygen species and mitochondrial acid sphingomyelinase. *Antioxid Redox Signal* **22**: 1097–1110.

Mao, F., Dam, P., Chou, J., Olman, V., and Xu, Y. (2009) DOOR: A database for prokaryotic operons. *Nucleic Acids Res* **37**: 459–463.

Matsushita, K., Patel, L., and Kaback, H.R. (1984) Cytochrome *o* type oxidase from *Escherichia coli*. Characterization of the enzyme and mechanism of electrochemical proton gradient generation. *Biochemistry* **23**: 4703–4714.

Mavrodi, D. V., Mavrodi, O. V., Parejko, J.A., Bonsall, R.F., Kwak, Y.S., Paulitz, T.C., *et al.* (2012) Accumulation of the antibiotic phenazine-1-carboxylic acid in the rhizosphere of dryland cereals. *Appl Environ Microbiol* **78**: 804–812.

Mavrodi, D. V, Peever, T.L., Mavrodi, O. V, Parejko, J.A., Raaijmakers, J.M., Lemanceau, P., *et al.* (2010) Diversity and evolution of the phenazine biosynthesis pathway. *Appl Environ Microbiol* **76**: 866–879.

Meirelles, L.A., and Newman, D.K. (2018) Both toxic and beneficial effects of pyocyanin contribute to the lifecycle of *Pseudomonas aeruginosa*. *Mol Microbiol* **110**: 995–1010.

Morales, E.H., Collao, B., Desai, P.T., Calderón, I.L., Gil, F., Luraschi, R., *et al.* (2013) Probing the ArcA regulon under aerobic/ROS conditions in *Salmonella enterica* serovar Typhimurium. *BMC Genomics* **14**.

Morton, E.R., and Fuqua, C. (2012a) Genetic manipulation of *Agrobacterium*. *Curr Protoc Microbiol* **25**: 3D.2.1-3D.2.15.

Morton, E.R., and Fuqua, C. (2012b) Laboratory maintenance of *Agrobacterium*. *Curr Protoc*

Microbiol **24**: 3D.1.1-3D.1.6.

Nickerson, K.W., and Aspedon, A. (1992) Detergent-shock response in enteric bacteria. *Mol Microbiol* **6**: 957–961.

Noto, M.J., Burns, W.J., Beavers, W.N., and Skaar, E.P. (2017) Mechanisms of pyocyanin toxicity and genetic determinants of resistance in *Staphylococcus aureus*. *J Bacteriol* **199**: 1–13.

Novichkov, P.S., Kazakov, A.E., Ravcheev, D.A., Leyn, S.A., Kovaleva, G.Y., Sutormin, R.A., *et al.* (2013) RegPrecise 3.0 – a resource for genome-scale exploration of transcriptional regulation in bacteria. *BMC Genomics* **14**: 745 BMC Genomics.

Park, D.M., Akhtar, S., Ansari, A.Z., Landick, R., and Kiley, P.J. (2013) The bacterial response regulator ArcA uses a diverse binding site architecture to regulate carbon oxidation globally. *PLoS Genet* **9**: e1003839.

R Core Team (2018) R: A language and environment for statistical computing.

Rada, B., and Leto, T.L. (2013) Pyocyanin effects on respiratory epithelium: relevance in *Pseudomonas aeruginosa* airway infections. *Trends Microbiol* **21**: 73–81.

Ramos, I., Dietrich, L.E.P., Price-Whelan, A., and Newman, D.K. (2010) Phenazines affect biofilm formation by *Pseudomonas aeruginosa* in similar ways at various scales. *Res Microbiol* **161**: 187–191.

Riedel, T.E., Berelson, W.M., Nealson, K.H., and Finkel, S.E. (2013) Oxygen consumption rates of bacteria under nutrient-limited conditions. *Appl Environ Microbiol* **79**: 4921–4931.

Römling, U., Wingender, J., Müller, H., and Tümmler, B. (1994) A major *Pseudomonas aeruginosa* clone common to patients and aquatic habitats. *Appl Environ Microbiol* **60**: 1734–1738.

Saenkham, P., Eiamphungporn, W., Farrand, S.K., Vattanaviboon, P., and Mongkolsuk, S. (2007) Multiple superoxide dismutases in *Agrobacterium tumefaciens*: functional analysis, gene regulation, and influence on tumorigenesis. *J Bacteriol* **189**: 8807–8817.

Scandalios, J. (2002) Oxidative stress responses – what have genome-scale studies taught us? *Genome Biol* **3**: reviews1019.1-1019.6.

Selby, C.P., and Sancar, A. (1995) Structure and function of transcription-repair coupling factor. I. Structural domains and binding properties. *J Biol Chem* **270**: 4882–4889.

Séveno, N.A., Morgan, J.A.W., and Wellington, E.M.H. (2001) Growth of *Pseudomonas aureofaciens* PGS12 and the dynamics of HHL and phenazine production in liquid culture, on nutrient agar, and on plant roots. *Microb Ecol* **41**: 314–324.

Singh, A.K., Shin, J.-H., Lee, K.-L., Imlay, J.A., and Roe, J.-H. (2013) Comparative study of SoxR activation by redox-active compounds. *Mol Microbiol* **90**: 983–996.

Swem, D.L., and Bauer, C.E. (2002) Coordination of ubiquinol oxidase and cytochrome *cbb*$_3$ oxidase expression by multiple regulators in *Rhodobacter capsulatus*. *J Bacteriol* **184**: 2815–2820.

Tjaden, B. (2015) De novo assembly of bacterial transcriptomes from RNA-seq data. *Genome Biol* **16**: 1.

Tseng, C.-P., Albrecht, J., and Gunsalus, R.P. (1996) Effect of microaerophilic cell growth conditions on expression of the aerobic (*cyoABCDE* and *cydAB*) and anaerobic (*narGHJI*, *frdABCD*, and *dmsABC*) respiratory pathway genes in *Escherichia coli*. *J Bacteriol* **178**: 1094–1098.

Turner, J.M., and Messenger, A.J.M. (1986) Occurence, biochemistry and physiology of phenazine pigment production. *Adv Microb Physiol* **27**: 211–275.

Vallenet, D., Calteau, A., Cruveiller, S., Gachet, M., Lajus, A., Josso, A., *et al.* (2017) MicroScope in 2017: an expanding and evolving integrated resource for community expertise of

microbial genomes. *Nucleic Acids Res* **45**: D517–D528.
Voggu, L., Schlag, S., Biswas, R., Rosenstein, R., Rausch, C., and Götz, F. (2006) Microevolution of cytochrome *bd* oxidase in staphylococci and its implication in resistance to respiratory toxins released by *Pseudomonas*. *J Bacteriol* **188**: 8079–8086.
Wan, F., Mao, Y., Dong, Y., Ju, L., Wu, G., and Gao, H. (2015) Impaired cell envelope resulting from arcA mutation largely accounts for enhanced sensitivity to hydrogen peroxide in Shewanella oneidensis. *Sci Rep* **5**: 10228.
Wang, Y., Kern, S.E., and Newman, D.K. (2010) Endogenous phenazine antibiotics promote anaerobic survival of *Pseudomonas aeruginosa* via extracellular electron transfer. *J Bacteriol* **192**: 365–369.
Wang, Y., Wilks, J.C., Danhorn, T., Ramos, I., Croal, L., and Newman, D.K. (2011) Phenazine-1-carboxylic acid promotes bacterial biofilm development via ferrous iron acquisition. *J Bacteriol* **193**: 3606–3617.
Watson, B., Currier, T.C., Gordon, M.P., Chilton, M.-D., and Nester, E.W. (1975) Plasmid required for virulence of *Agrobacterium tumefaciens*. *J Bacteriol* **123**: 255–264.
Wong, S.M.S., Alugupalli, K.R., Ram, S., and Akerley, B.J. (2007) The ArcA regulon and oxidative stress resistance in *Haemophilus influenzae*. *Mol Microbiol* **64**: 1375–1390.
Ye, J., Coulouris, G., Zaretskaya, I., Cutcutache, I., Rozen, S., and Madden, T.L. (2012) Primer-BLAST: a tool to design target-specific primers for polymerase chain reaction. *BMC Bioinformatics* **13**: 134.
Zeytuni, N., and Zarivach, R. (2012) Structural and functional discussion of the tetra-trico-peptide repeat, a protein interaction module. *Structure* **20**: 397–405.
Zhao, H., Joseph, J., Zhang, H., Karoui, H., and Kalyanaraman, B. (2001) Synthesis and biochemical applications of a solid cyclic nitrone spin trap: a relatively superior trap for detecting superoxide anions and glutathiyl radicals. *Free Radic Biol Med* **31**: 599–606.
Zielonka, J., Vasquez-Vivar, J., and Kalyanaraman, B. (2007) Detection of 2-hydroxyethidium in cellular systems: a unique marker product of superoxide and hydroethidine. *Nat Protoc* **3**: 8–21.

Supplementary Tables and Figures

Table S1: PYO-sensitive transposon insertion mutants identified in this study.

Mutant	Transposon Insertion Site	Gene Product
soxR	*soxR*, bp 6-7	transcriptional regulator
actS	*actS*, bp 1007-1008	two-component sensor kinase
rpoH	*rpoH*, bp 87-88	RNA polymerase factor sigma-32
Atu1426	Atu1426, bp 170-171	enolase/phosphoenolpyruvate hydratase
Atu3738	Atu3738, bp 11-12	potassium/proton antiporter
pykA	*pykA*, bp 1129-1130	pyruvate kinase
Atu2584	Atu2584, bp 548-549	hypothetical protein with high sequence similarity to rhizobial NodB-like proteins that modify cell wall polysaccharides
Atu2590	Atu2590, bp 35-36	putative glycosyltransferase belonging to the MurG superfamily
Atu2591	Atu2591, bp 42-43	putative glycosyltransferase belonging to the RfaB superfamily

Atu2592	Atu2592, bp 878-879	putative glycosyltransferase belonging to the MurG superfamily
Atu2577-1	Atu2577, bp 2288-2289	ABC transporter, nucleotide binding/ATPase protein
Atu2577-2	Atu2577, bp 1010-1011	ABC transporter, nucleotide binding/ATPase protein

Table S2: Top 15 genes (by fold change) upregulated by PYO in WT. The fold change is for PYO-treated cultures relative to cultures treated with the solvent control. Base Mean = mean of normalized transcript counts across all replicates and conditions. Bolded genes were previously computationally predicted to be regulated by SoxR on the basis of a SoxR box-containing promoter. Genes that were confirmed to be regulated by SoxR are highlighted in green.

Gene	Base Mean	Log_2 Fold Change	Adjusted p-value	Product
Atu4582	8108	11.30	2.22E-170	ferredoxin
Atu4581	3644	10.51	1.89E-114	putative flavin reductase
Atu4583 (*sodBII*)	106513	10.35	0	superoxide dismutase
Atu5305	1548	8.08	9.83E-149	hypothetical protein
Atu2361	10590	7.74	0	MFS permease
Atu5152	932	7.41	1.60E-117	hypothetical protein
Atu4742	4465	7.38	0	hypothetical protein
Atu3915 (*soxR*)	8621	7.27	0	MerR family transcriptional regulator
Atu0942	29490	7.19	0	MFS permease
Atu4316	2029	4.98	0	ABC transporter permease
Atu2482 (*mexE*)	34410	4.42	0	AcrB/AcrD/AcrF family protein
Atu2483 (*mexF*)	19007	4.39	0	HlyD family secretion protein
Atu1475	1784	4.08	0	hypothetical protein
Atu4741	6479	4.06	0	putative transcriptional regulator
Atu4366	343	3.86	3.24E-82	short chain dehydrogenase

Table S3: Genes that were expressed at least 2-fold more highly in Δ*actR* than in WT only upon PYO treatment. The fold change is for Δ*actR* relative to WT. Base Mean = mean of normalized transcript counts across all replicates and conditions.

Gene	Base Mean	Log2 Fold Change	Adjusted p-value	Product
Atu3298	542	2.95	9.59E-89	C4-dicarboxylate transporter DctA
Atu4080	1096	2.31	2.21E-104	glutamine amidotransferase
Atu2511	1697	2.17	5.82E-133	D-alanine aminotransferase
Atu4311	90	1.85	6.14E-10	sarcosine oxidase delta subunit
Atu4642	24522	1.60	3.41E-201	catalase
Atu2510	1005	1.54	5.97E-55	aminopeptidase
Atu3180	179	1.51	1.61E-12	ABC transporter permease
Atu2733	132	1.50	1.79E-09	hypothetical protein
Atu3329	2939	1.35	2.48E-79	beta alanine-pyruvate transaminase

Atu4732	324	1.25	2.32E-15	fimbrial chaperone
Atu8166	341	1.21	4.54E-12	hypothetical protein
Atu4073	1211	1.18	6.68E-38	glycogen debranching protein
Atu4709	36	1.16	4.10E-03	NAD-dependent formate dehydrogenase subunit delta
Atu2248	985	1.16	2.90E-30	hypothetical protein
Atu3790	151	1.13	3.70E-07	potassium-transporting ATPase subunit A
Atu3340	250	1.12	2.74E-10	trehalose/maltose ABC transporter permease
Atu3472	87	1.10	1.04E-04	2-oxoisovalerate dehydrogenase subunit beta
Atu0727	2186	1.09	3.92E-45	ferredoxin I
Atu3038	169	1.08	2.87E-07	dipeptide ABC transporter ATPase
Atu0236	373	1.08	8.07E-13	hypothetical protein
Atu0496	363	1.06	6.67E-12	putative universal stress protein
Atu4077	4410	1.05	8.76E-59	glycogen branching protein
Atu4076	1716	1.04	6.31E-38	glucose-1-phosphate adenylyltransferase
Atu4074	4597	1.02	3.87E-56	phosphoglucomutase
Atu3039	358	1.02	1.32E-11	hydantoinase beta subunit-like protein
Atu3037	136	1.01	1.68E-05	dipeptide ABC transporter permease
Atu2477	1029	1.00	1.01E-23	DNA oxidation protective protein

Table S4: Genes that were statistically significantly upregulated in Δ*actR* vs. WT regardless of PYO treatment. Values listed in the table are for PYO-treated Δ*actR* relative to PYO-treated WT. Base Mean = mean of normalized transcript counts across all replicates and conditions. Genes are ordered by decreasing magnitude of fold change between Δ*actR* and WT, and are highlighted with colors according to their function. Pink = genes related to the respiratory ETC; green = genes related to amino acid metabolism, including proteases; blue = genes related to sugar transport/metabolism; purple = genes related to fatty acid metabolism; orange = genes related to carbon oxidation, glycolysis, and the TCA cycle.

Gene	Base Mean	Log2 Fold Change	Adjusted p-value	Product
Atu4090	2240	4.63	0.00E+00	ABC transporter permease
Atu4089	1925	3.75	0.00E+00	ABC transporter permease
Atu8036	554	2.92	1.07E-91	protein YBGT-like protein
Atu4092	2595	2.89	5.99E-246	cytochrome d oxidase subunit II
Atu4081	2514	2.07	1.36E-120	aspartate racemase
Atu4314	552	2.05	7.30E-55	serine hydroxymethyltransferase
Atu4091	3678	2.02	1.44E-124	cytochrome d oxidase
Atu4088	837	1.93	4.88E-70	transcriptional regulator
Atu0143	1520	1.92	9.53E-100	MFS permease
Atu4310	380	1.90	4.97E-36	sarcosine oxidase beta subunit
Atu4313	180	1.83	1.29E-17	sarcosine oxidase gamma subunit
Atu4447	306	1.73	5.54E-19	sorbitol ABC transporter substrate-binding protein
Atu4312	1016	1.67	5.02E-62	sarcosine oxidase alpha subunit

Atu2249	567	1.62	8.95E-37	hypothetical protein
Atu3342	695	1.59	2.95E-41	trehalose utilization-like protein
Atu4315	114	1.47	1.95E-08	formyltetrahydrofolate deformylase
Atu3343	1005	1.35	3.64E-39	trehalose utilization-like protein
Atu3341	325	1.34	1.06E-16	trehalose/maltose ABC transporter ATPase
Atu0649	1691	1.33	8.93E-59	cyclopropane-fatty-acyl-phospholipid synthase
Atu4660	582	1.28	1.07E-25	alpha-galactosidase
Atu0543	7394	1.27	1.19E-104	flaB
Atu3338	1077	1.21	2.33E-37	trehalose/maltose ABC transporter substrate-binding protein
Atu0726	4368	1.15	2.40E-75	ring hydroxylating dioxygenase, alpha-subunit
Atu3471	350	1.15	3.85E-13	branched-chain alpha-keto acid dehydrogenase subunit E2
Atu3339	338	1.13	5.35E-13	trehalose/maltose ABC transporter permease
Atu1338	2909	1.10	1.28E-09	3-oxoacyl-(acyl carrier protein) reductase
Atu4078	7728	1.01	4.18E-68	glycogen phosphorylase
Atu4661	277	0.99	4.95E-09	alpha-galactoside ABC transporter substrate-binding protein
Atu2200	11449	0.98	6.88E-63	cold shock protein
Atu8170	9043	0.97	2.35E-60	hypothetical protein
Atu1567	1372	0.95	7.00E-25	glutathione-independent formaldehyde dehydrogenase
Atu1865	3965	0.93	1.17E-28	hypothetical protein
Atu5489	783	0.92	2.16E-13	hypothetical protein
Atu2631	2010	0.91	1.34E-30	hypothetical protein
Atu1632	9825	0.90	1.39E-52	dimethylglycine dehydrogenase
Atu3894	180	0.87	3.03E-05	sugar ABC transporter permease
Atu3506	2431	0.86	1.60E-27	hypothetical protein
Atu4442	496	0.84	9.55E-11	hypothetical protein
Atu0063	2389	0.83	6.24E-25	ABC transporter, substrate binding protein (sugar)
Atu0542	682	0.82	1.81E-12	flagellin
Atu3474	279	0.82	9.90E-07	acyl-CoA dehydrogenase
Atu1174	1835	0.81	6.36E-24	H+ translocating pyrophosphate synthase
Atu1805	4548	0.81	3.79E-36	hypothetical protein
Atu4708	534	0.78	5.77E-10	formate dehydrogenase alpha subunit
Atu4727	756	0.75	2.47E-11	hypothetical protein
Atu5450	5849	0.73	5.59E-34	hypothetical protein
Atu3893	106	0.73	3.34E-03	sugar ABC transporter permease
Atu5270	77	0.72	9.36E-03	permease component of C4 dicarboxylate transporter
Atu3336	1843	0.72	1.05E-19	hypothetical protein
Atu1864	4280	0.71	1.63E-18	putative homoserine/homoserine lactone efflux protein

Atu1777	6119	0.71	6.67E-30	hypothetical protein
Atu4728	8613	0.71	1.63E-05	ABC transporter permease
Atu5449	13865	0.71	7.79E-39	heat-shock protein
Atu0373	471	0.69	2.46E-07	methyl-accepting chemotaxis protein
Atu3891	286	0.69	2.57E-05	hypothetical protein
Atu0738	1062	0.67	1.41E-10	chemotaxis methyl-accepting protein
Atu4014	16149	0.67	2.87E-32	transcriptional regulator
Atu0591	12637	0.64	1.76E-29	ABC transporter, substrate binding protein (alpha-glucoside)
Atu4061	732	0.63	1.99E-08	exopolysaccharide production repressor protein
Atu3895	170	0.62	2.91E-03	sugar ABC transporter ATPase
Atu1832	926	0.62	2.40E-09	membrane protein associated metalloendopeptidase
Atu0545	4409	0.61	1.79E-21	flagella associated protein
Atu0108	4839	0.60	1.98E-21	putative metalloprotease M20 family
Atu0590	1735	0.60	6.22E-14	transcriptional regulator repressor
Atu0064	549	0.60	1.70E-06	ABC transporter, membrane spanning protein (sugar)
Atu4062	736	0.60	8.80E-08	hypothetical protein
Atu0476	1401	0.59	1.48E-11	aquaporin
Atu0517	1013	0.58	3.63E-09	Chemotaxis protein histidine kinase
Atu2768	1085	0.58	7.83E-09	hypothetical protein
Atu0871	5443	0.57	1.06E-20	branched-chain-amino-acid aminotransferase
Atu0984	1007	0.57	3.09E-08	aminopeptidase N
Atu5052	22384	0.55	9.03E-20	small heat shock protein
Atu1661	1362	0.54	4.06E-09	soluble pyridine nucleotide transhydrogenase
Atu5053	3354	0.53	6.22E-14	hypothetical protein
Atu3185	795	0.51	2.31E-06	glycerol-3-phosphate ABC transporter substrate-binding protein
Atu1392	15199	0.47	6.00E-19	citrate synthase
Atu2617	1342	0.46	1.85E-07	chemotaxis protein
Atu3896	234	0.46	8.13E-03	sugar ABC transporter ATPase
Atu2644	2277	0.46	3.55E-09	succinate dehydrogenase hydrophobic membrane anchor
Atu8094	1653	0.44	8.99E-08	hypothetical protein
Atu2827	819	0.43	1.50E-04	hypothetical protein
Atu1405	617	0.43	3.02E-04	transcriptional regulator, GntR family
Atu0526	2120	0.42	1.58E-07	methyl-accepting chemotaxis protein
Atu1210	1939	0.42	3.05E-07	putative 2,3-cyclic nucleotide 2-phosphodiesterase/3-nucleotidase
Atu3898	763	0.41	3.72E-04	DeoR family transcriptional regulator
Atu0573	1619	0.40	5.35E-05	transcriptional regulator
Atu3596	5621	0.39	3.82E-10	electron transfer flavoprotein alpha subunit

Atu2645	2303	0.36	3.61E-06	succinate dehydrogenase cytochrome B-556 subunit
Atu2643	6452	0.36	1.25E-08	succinate dehydrogenase flavoprotein subunit
Atu3595	3695	0.36	2.03E-07	electron transfer flavoprotein subunit beta
Atu4319	2386	0.35	1.06E-05	AraC family transcriptional regulator
Atu2196	5340	0.35	1.41E-08	aspartate aminotransferase A
Atu3695	4263	0.34	1.35E-07	hypothetical protein
Atu1616	9523	0.34	2.67E-09	fumarate hydratase
Atu0767	4159	0.33	1.20E-06	cytochrome c oxidase subunit II
Atu2239	1761	0.32	3.00E-04	ubiquinol-cytochrome C reductase iron-sulfur subunit
Atu2223	802	0.31	5.77E-03	methyl-accepting chemotaxis protein
Atu2642	3397	0.31	1.61E-05	succinate dehydrogenase iron-sulfur
Atu1717	869	0.29	5.89E-03	long-chain fatty acid transport protein
Atu0594	3253	0.29	2.91E-05	alpha-glucosidase
Atu1870	14872	0.28	2.98E-07	isocitrate dehydrogenase
Atu0768	5078	0.27	1.81E-04	cytochrome-c oxidase chain I
Atu2675	4519	0.26	5.78E-04	hypothetical protein
Atu3706	2778	0.26	1.00E-03	D-3-phosphoglycerate dehydrogenase
Atu2685	14712	0.25	1.77E-05	aconitate hydratase
Atu1426	7399	0.24	1.01E-04	enolase
Atu2238	2861	0.22	3.24E-03	ubiquinol-cytochrome c reductase cytochrome b subunit
Atu1307	1977	0.22	7.56E-03	dihydroorotase
Atu0592	2054	0.21	8.63E-03	ABC transporter, membrane spanning protein
Atu2348	6953	0.21	8.02E-04	sugar binding protein
Atu0977	51857	0.20	1.05E-03	serine protease DO-like protease
Atu2682	17487	0.19	8.74E-04	hypothetical protein

Table S5: Genes that were statistically significantly downregulated in Δ*actR* vs. WT regardless of PYO treatment. Values listed in the table are for PYO-treated Δ*actR* relative to PYO-treated WT. Base Mean = mean of normalized transcript counts across all replicates and conditions. Genes are ordered by decreasing magnitude of fold change between Δ*actR* and WT. Genes mentioned in the main text because of their relevance to the respiratory ETC are highlighted in pink.

Gene	Base Mean	Log2 Fold Change	Adjusted p-value	Product
Atu0142	2962	-2.88	1.43E-295	cytochrome o ubiquinol oxidase subunit II
Atu0141	3309	-2.53	8.03E-253	cytochrome O ubiquinol oxidase subunit I
Atu0140	874	-2.46	5.49E-97	cytochrome o ubiquinol oxidase subunit III
Atu0138	89	-2.36	6.03E-13	surfeit 1
Atu0139	645	-2.27	5.64E-71	cytochrome o ubiquinol oxidase subunit IV
Atu4171	1181	-1.70	4.77E-63	cold-shock dead-box protein A
Atu4096	142	-1.43	1.03E-08	nicotinate-nucleotide pyrophosphorylase

Atu1528	731	-1.38	2.85E-27	nitrogen fixation protein FixI
Atu2333	2854	-1.37	9.58E-78	ATP-dependent RNA helicase
Atu1529	238	-1.36	3.00E-13	nitrogen fixation protein FixH
Atu1155	400	-1.32	1.98E-19	hypothetical protein
Atu3122	576	-1.30	3.51E-21	cold shock protein
Atu4097	474	-1.29	1.58E-21	L-aspartate oxidase
Atu1798	155	-1.27	1.99E-08	ankyrin repeat protein
Atu3124	434	-1.25	6.16E-17	hypothetical protein
Atu1221	984	-1.23	3.30E-29	hypothetical protein
Atu1536	268	-1.21	1.36E-11	cytochrome C oxidase, FixO chain
Atu2112	168	-1.20	3.81E-08	soluble lytic transglycosylase
Atu1530	1171	-1.17	2.85E-29	nitrogen fixation protein FixG
Atu5384	640	-1.15	4.16E-21	hypothetical protein
Atu4372	247	-1.08	9.70E-09	ribose ABC transporter permease
Atu1537	1510	-1.04	8.66E-07	cytochrome-c oxidase, FixN chain
Atu5126	740	-1.03	1.10E-19	ABC transporter nucleotide binding/ATPase(putrescine)
Atu3998	220	-1.00	1.62E-07	8-amino-7-oxononanoate synthase
Atu1535	58	-0.99	3.28E-03	cytochrome c oxidase, FixQ chain
Atu4695	595	-0.99	4.94E-14	oligopeptide ABC transporter substrate-binding protein
Atu3771	431	-0.97	1.35E-11	ferrochelatase
Atu0895	7152	-0.95	9.15E-58	ABC transporter, substrate binding protein
Atu1956	22144	-0.94	1.01E-68	DNA-directed RNA polymerase beta chain
Atu2273	651	-0.93	1.92E-15	hypothetical protein
Atu3817	403	-0.92	1.78E-10	dehydratase
Atu2833	4918	-0.92	1.04E-45	transcription termination factor Rho
Atu1601	1118	-0.91	1.03E-05	oxygen-independent coproporphyrinogen III oxidase
Atu5108	287	-0.91	2.25E-07	conjugal transfer coupling protein TraG
Atu2806	489	-0.91	1.09E-11	hypothetical protein
Atu2804	2183	-0.90	3.68E-31	cobaltochelatase subunit
Atu2805	1465	-0.90	9.38E-26	cobalamin synthesis protein
Atu2283	816	-0.88	1.60E-04	pseudoazurin
Atu0885	176	-0.88	1.96E-05	hypothetical protein
Atu1923	14379	-0.87	3.51E-54	DNA-directed RNA polymerase alpha subunit
Atu2803	698	-0.84	2.56E-13	Cobalamin biosynthesis associated protein
Atu2673	2180	-0.83	1.25E-25	hypothetical protein
Atu4609	3074	-0.82	1.15E-31	glycosyltransferase
Atu1771	286	-0.81	1.27E-06	hypothetical protein
Atu5516	1337	-0.81	6.38E-18	hypothetical protein

Atu3191	768	-0.81	2.30E-10	outer membrane protein
Atu5162	590	-0.80	1.34E-08	type IV secretion protein AvhB1
Atu1955	33189	-0.79	1.03E-43	DNA-directed RNA polymerase beta' chain
Atu0663	385	-0.78	2.00E-07	hypothetical protein
Atu3121	8101	-0.77	1.01E-39	cold shock protein
Atu1654	117	-0.77	1.47E-03	nitroreductase
Atu2183	2132	-0.76	9.49E-23	lipopolysaccharide core biosynthesis mannosyltransferase
Atu2801	780	-0.76	9.76E-12	precorrin-2 C20 methyltransferase
Atu2835	1143	-0.76	1.37E-14	uroporphyrinogen decarboxylase
Atu2834	285	-0.76	4.89E-06	hypothetical protein
Atu0107	369	-0.75	1.61E-06	hypothetical protein
Atu1534	460	-0.75	3.76E-07	cytochrome-c oxidase, FixP chain
Atu2085	5294	-0.73	7.85E-32	UDP-3-0-(3-hydroxymyristoyl) N-acetylglucosamine deacetylase
Atu5127	414	-0.70	7.90E-07	ABC transporter membrane spanning protein (mannopine)
Atu0033	2568	-0.69	3.74E-22	two component sensor kinase
Atu2824	935	-0.69	9.89E-12	hypothetical protein
Atu0070	1714	-0.69	4.02E-17	ribonucleoside-diphosphate reductase 2 alpha chain
Atu2394	3017	-0.68	2.43E-03	Regulator of Biofilm formation, Fnr Family
Atu2792	184	-0.68	8.38E-04	hypothetical protein
Atu5110	109	-0.68	5.43E-03	conjugal transfer protein
Atu0983	225	-0.68	2.84E-04	hypothetical protein
Atu3230	375	-0.67	8.05E-06	hypothetical protein
Atu0769	848	-0.67	2.03E-10	protoheme IX farnesyltransferase
Atu5161	800	-0.66	1.14E-07	hypothetical protein
Atu2073	1393	-0.66	1.39E-13	membrane protein
Atu0365	744	-0.66	3.21E-09	hypothetical protein
Atu2710	1129	-0.65	7.82E-11	hypothetical protein
Atu4667	534	-0.64	4.78E-07	ABC transporter permease
Atu0250	344	-0.64	2.61E-05	hypothetical protein
Atu4608	4774	-0.64	3.10E-24	hypothetical protein
Atu4098	778	-0.64	1.90E-08	quinolinate synthetase
Atu2026	1377	-0.64	1.39E-12	exodeoxyribonuclease V
Atu8135	2663	-0.64	5.43E-16	hypothetical protein
Atu2800	556	-0.63	4.80E-07	precorrin-3B C17-methyltransferase
Atu2471	136	-0.61	6.53E-03	hypothetical protein
Atu0106	11129	-0.60	2.10E-23	cold shock protein
Atu0345	1829	-0.60	8.82E-14	DNA mismatch repair protein, MutS family
Atu0034	4246	-0.60	5.26E-21	two component response regulator

Atu0071	839	-0.59	2.42E-08	ribonucleoside-diphosphate reductase 2 beta chain
Atu2287	144	-0.59	6.48E-03	outer membrane heme receptor
Atu3203	2501	-0.58	4.53E-15	RND multidrug efflux membrane permease
Atu5130	355	-0.58	9.65E-05	attachment protein
Atu0012	7125	-0.58	1.20E-21	DNA gyrase subunit B
Atu0032	266	-0.58	6.08E-04	hypothetical protein
Atu2730	7718	-0.56	3.48E-21	beta (1-->2) glucan biosynthesis protein
Atu5129	1722	-0.56	5.08E-12	ABC transporter substrate binding protein (mannopine)
Atu5001	1437	-0.56	1.90E-10	replication protein B
Atu4666	677	-0.56	2.11E-05	HlyD family secretion protein
Atu5128	444	-0.55	8.22E-05	ABC transporter membrane spanning protein (mannopine)
Atu1447	3047	-0.55	7.51E-15	two component sensor kinase
Atu3229	259	-0.54	1.86E-03	hypothetical protein
Atu1658	1096	-0.53	5.86E-08	conserved protein involved in phosphoglycerol modification of cyclic glucan
Atu0973	1235	-0.53	6.64E-09	cycH protein
Atu2303	694	-0.53	3.47E-06	hypothetical protein
Atu2494	443	-0.52	1.39E-04	NAD(P)+ transhydrogenase beta chain
Atu1445	863	-0.51	1.25E-06	two component sensor kinase
Atu2129	380	-0.51	4.90E-04	hypothetical protein
Atu3704	2031	-0.51	1.03E-10	hypothetical protein
Atu0721	2154	-0.50	1.95E-10	hypothetical protein
Atu3202	3935	-0.49	5.04E-14	RND multidrug efflux transporter
Atu4491	1679	-0.49	3.73E-09	hypothetical protein
Atu2380	583	-0.49	6.13E-05	hypothetical protein
Atu4619	1063	-0.49	3.67E-07	ATP-dependent DNA helicase
Atu2320	487	-0.49	2.30E-04	transcriptional regulator, TetR family
Atu5469	562	-0.48	1.03E-04	DNA polymerase IV
Atu3325	756	-0.48	1.69E-05	exopolysaccharide production protein
Atu2057	2428	-0.48	9.28E-11	DNA helicase II
Atu5000	1652	-0.48	6.13E-08	replication protein A
Atu1262	16332	-0.47	7.08E-14	histone-like protein
Atu8200	3772	-0.47	1.07E-10	hypothetical protein
Atu1074	606	-0.47	1.33E-04	NAD/NADP dependent oxidoreductase
Atu5170	283	-0.47	7.31E-03	type IV secretion protein AvhB9
Atu0900	620	-0.46	1.05E-04	hypothetical protein
Atu5165	1769	-0.46	5.78E-06	type IV secretion protein AvhB4
Atu1131	43210	-0.46	3.23E-15	outer membrane protein
Atu1683	1453	-0.45	2.26E-07	hypothetical protein

Atu0933	729	-0.45	9.93E-05	beta-lactamase class D
Atu1877	4170	-0.45	4.18E-10	OmpA family protein
Atu1242	1157	-0.44	6.58E-06	cytochrome oxidase assembly factor
Atu2692	2234	-0.44	1.19E-07	intracellular septation protein
Atu2728	4808	-0.43	1.78E-09	beta (1-->2) glucan export ATP-binding protein
Atu1602	891	-0.43	9.86E-05	transcriptional activator, Crp family
Atu3396	4110	-0.43	1.31E-09	ABC transporter substrate-binding protein
Atu1825	1610	-0.43	5.53E-06	cysteine desulfurase
Atu1467	436	-0.42	2.00E-03	hypothetical protein
Atu8142	743	-0.42	4.95E-04	hypothetical protein
Atu4026	14058	-0.42	5.49E-13	hypothetical protein
Atu5167	485	-0.42	4.41E-03	type IV secretion protein AvhB6
Atu2163	6391	-0.41	7.59E-12	hypothetical protein
Atu2521	1143	-0.41	2.85E-05	Protein regulated by acid pH
Atu5122	806	-0.41	1.92E-04	3-ketoacyl-ACP reductase
Atu2463	740	-0.41	2.50E-04	hypothetical protein
Atu2181	1052	-0.41	2.85E-05	hypothetical protein
Atu1077	1260	-0.39	3.73E-05	DNA repair protein
Atu3326	1373	-0.39	5.38E-05	exopolysaccharide production protein
Atu0898	602	-0.39	1.72E-03	hypothetical protein
Atu3295	803	-0.39	5.08E-04	hypothetical protein
Atu2653	450	-0.39	5.00E-03	Uroporphyrinogen III synthase HEM4
Atu1874	11481	-0.38	5.09E-09	RecA protein
Atu3507	2784	-0.38	3.23E-07	hypothetical protein
Atu2779	1792	-0.36	8.78E-06	gamma-glutamyl phosphate reductase
Atu2652	1401	-0.36	9.33E-05	porphobilinogen deaminase
Atu5124	1920	-0.35	1.17E-05	glutamate-1-semialdehyde aminotransferase
Atu0720	2876	-0.35	5.42E-06	ribonuclease HII
Atu2168	2744	-0.35	1.69E-05	DNA primase
Atu2522	696	-0.34	3.11E-03	agrobacterium chromosomal virulence protein B
Atu2780	1666	-0.34	7.80E-05	gamma-glutamyl kinase
Atu4499	683	-0.33	3.99E-03	hypothetical protein
Atu2001	7332	-0.33	3.74E-07	excinuclease ABC subunit B
Atu0974	639	-0.32	7.84E-03	cytochrome-c biosynthesis heme-carrier protein cycJ
Atu1780	1051	-0.31	1.66E-03	ATP-dependent DNA helicase
Atu1032	905	-0.31	5.48E-03	hypothetical protein
Atu0975	1765	-0.30	4.18E-04	cytochrome c-type synthesis protein
Atu1395	2869	-0.30	6.47E-05	LexA repressor

Atu0998	1891	-0.30	5.05E-04	undecaprenyl pyrophosphate phosphatase, possible bacitracin resistance protein
Atu4498	1078	-0.29	3.11E-03	hypothetical protein
Atu4178	2418	-0.29	2.60E-04	hypothetical protein
Atu5123	2497	-0.28	2.42E-04	acetolactate synthase catalytic subunit
Atu1433	4200	-0.28	7.83E-05	arylesterase
Atu1300	1132	-0.26	7.31E-03	MFS permease
Atu1446	1385	-0.26	3.78E-03	two component response regulator
Atu1028	6244	-0.24	1.13E-04	hypothetical protein
Atu1715	2517	-0.20	9.33E-03	exopolysaccharide production negative regulator

Table S6: Top six most highly expressed non-ribosomal genes in *A. tumefaciens* NT1 WT upon treatment with 100 µM PYO. Expression values were calculated in a manner similar to RPKM (reads per kilobase per million mapped reads) values except that they were normalized to the upper quartile of gene expression instead of total mapped reads (Tjaden, 2015).

Gene	**Product**	**Expression**
rnpB	RNase P RNA	53179
sodBII	superoxide dismutase	25726
hspL	small heat shock protein	15130
Atu1020	outer membrane protein	14239
groEL	GroEL chaperonin	13833
groES	co-chaperonin GroES	12884

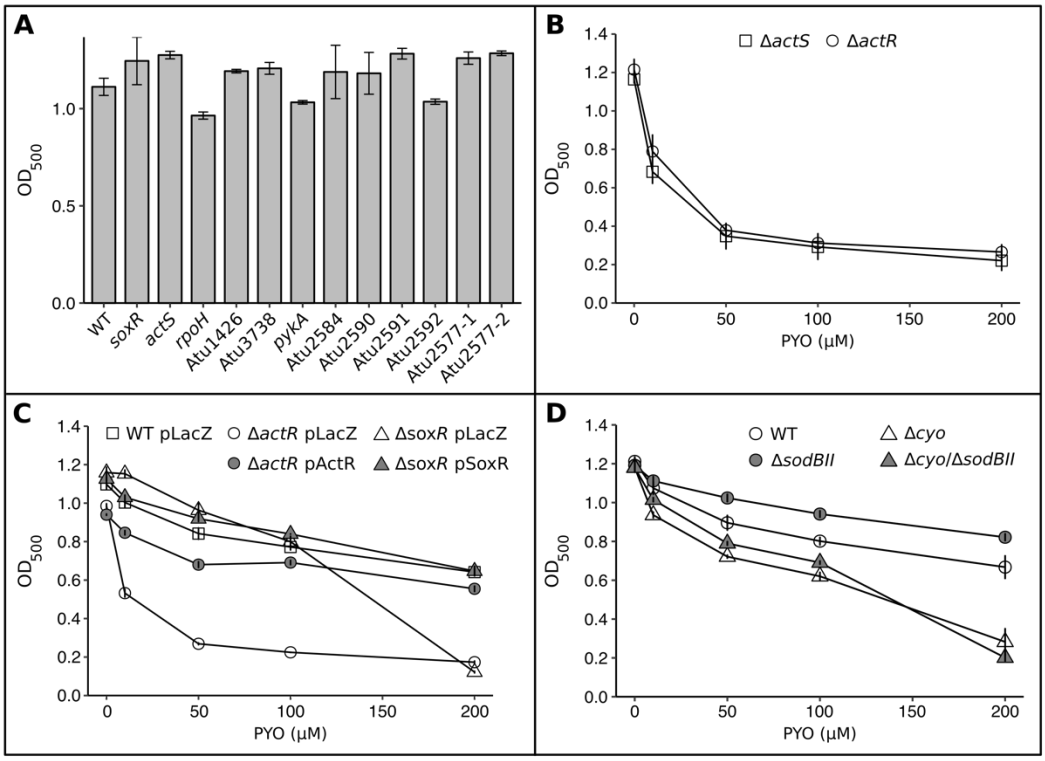

Figure S1: Supplemental data from growth-based PYO sensitivity assays.
A. Growth of WT and PYO-sensitive transposon mutants after 24 hrs without PYO treatment.
B. Growth of Δ*actS* and Δ*actR* after 24 hrs in the presence of different concentrations of PYO.
C. Growth of WT pLacZ (vector control for overexpression constructs), Δ*actR* pLacZ, Δ*actR* pActR (overexpression vector for ActR), Δ*soxR* pLacZ, and Δ*soxR* pSoxR (overexpression vector for SoxR) after 24 hrs in the presence of different concentrations of PYO, showing complementation of the Δ*actR* and Δ*soxR* clean deletion mutants. Expression from the vectors was induced by adding 1 mM IPTG at the start of the experiment.
D. Growth of WT, Δ*sodBII*, Δ*cyo*, and Δ*cyo*/Δ*sodBII* after 24 hrs in the presence of different concentrations of PYO, showing that Δ*cyo* is slightly more dependent on SodBII than WT (i.e. it does not gain as large of a growth advantage upon loss of SodBII). Error bars in all panels represent standard deviations of biological replicates ($n = 3$).

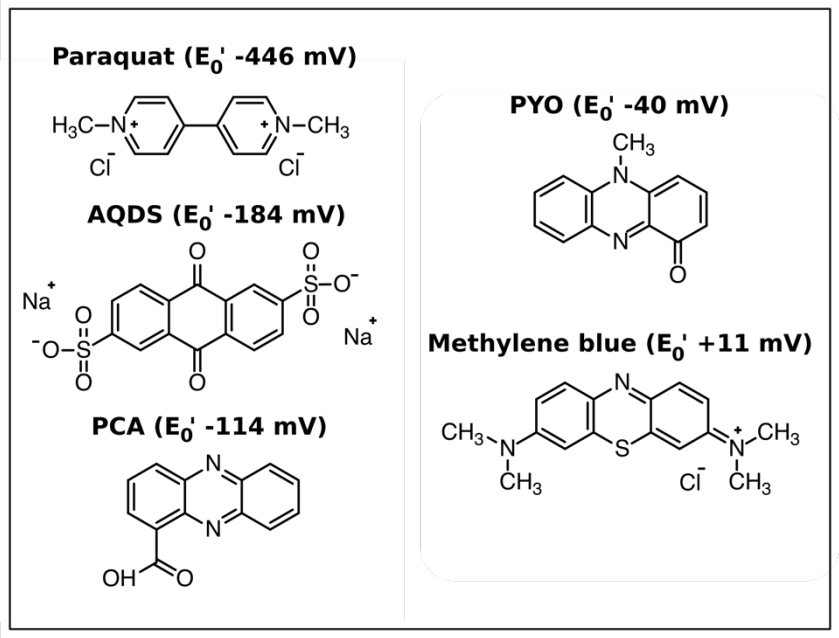

Figure S2: Structures and standard reduction potentials (E_0') of the redox-active molecules tested in this study.
Reduction potentials are versus that of the normal hydrogen electrode (NHE).

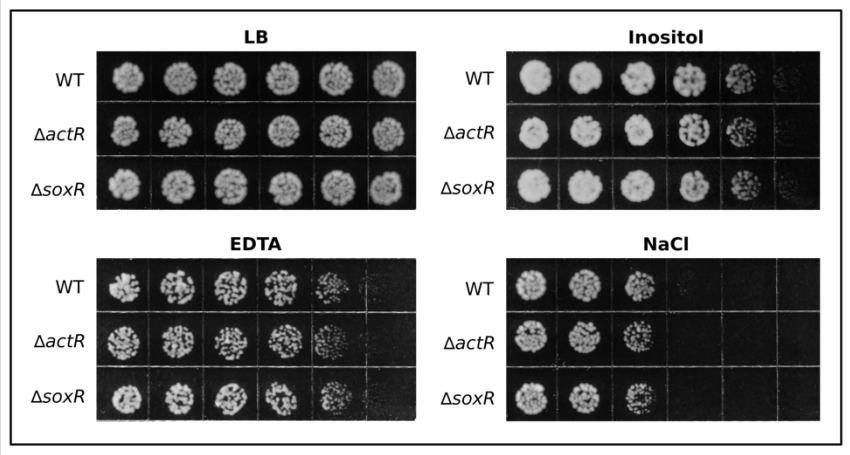

Figure S3: Supplemental gradient plate assays.
Growth of WT, Δ*actR*, and Δ*soxR* on agar plates containing either plain LB or a concentration gradient (low-high, left to right) of EDTA (up to 1 mM), myo-inositol (up to 1 M), or NaCl (up to 0.4 M). Images are representative of eight biological replicates.

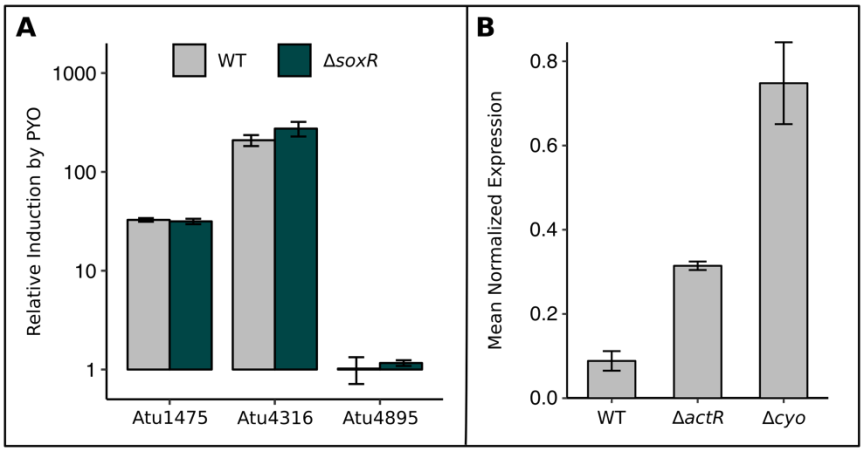

Figure S4: Supplemental qRT-PCR data for SoxR regulon candidates and *cydA*.
A. Relative induction by 100 µM PYO of Atu1475, Atu4316, and Atu4895 in WT and Δ*soxR*, showing that these three genes are not regulated by SoxR.
B. Relative expression of *cydA* in WT, Δ*actR*, and Δ*cyo* without PYO treatment. Expression was normalized to the housekeeping gene *rpoD*.

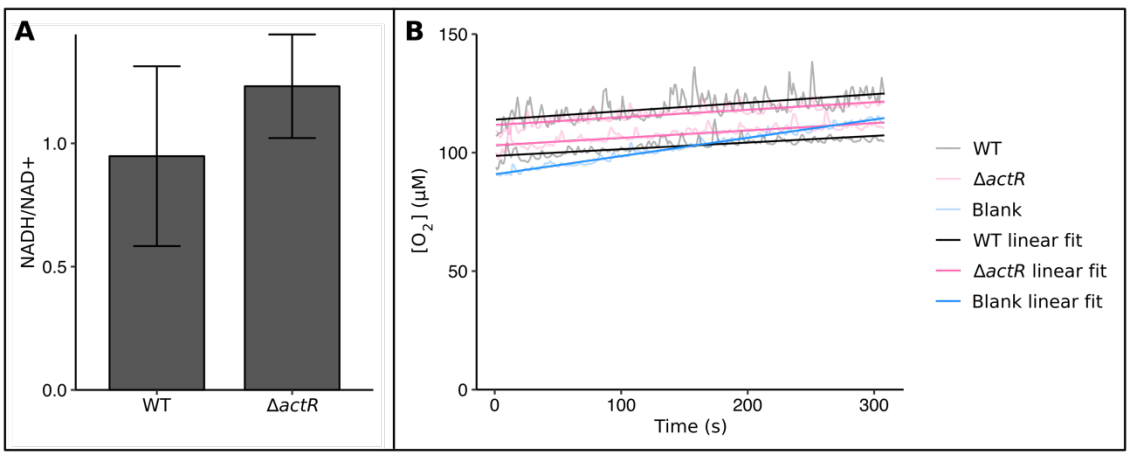

Figure S5: Loss of ActR does not significantly alter the NADH/NAD+ ratio or PYO-mediated cyanide-insensitive oxygen consumption rate.
A. NADH and NAD+ were extracted and quantified from exponential phase cultures of WT and Δ*actR*. The slight increase in the mean NADH/NAD+ ratio in Δ*actR* is not statistically significant ($p > 0.05$, Welch's t-test, $n = 4$).
B. Exponential phase cultures of WT or Δ*actR* in LB were treated with 5 mM potassium cyanide for 5 min to inhibit terminal oxidase activity; this concentration was sufficient to fully inhibit respiration. After 5 min, 10 µM PYO was added, and after another 5 min, an additional 90 µM PYO was added. The concentration of oxygen over time is plotted such that t = 0 is approximately the time of the second PYO addition. The concentration of oxygen over time was also plotted for a blank sample (cell-free) with a similar starting concentration of oxygen. Each sample was fitted with a linear regression. The positive slope of the blank reference represents the rate of oxygen leakage into the system. The slope for the culture samples is a function of the leak rate minus the consumption rate. Hence, PYO-mediated oxygen consumption resulted in shallower slopes for the culture samples compared to the blank sample, although their rates of oxygen consumption were slower than the rate of oxygen leakage back into the system (resulting in a net positive slope). Two biological replicates are plotted for each strain.

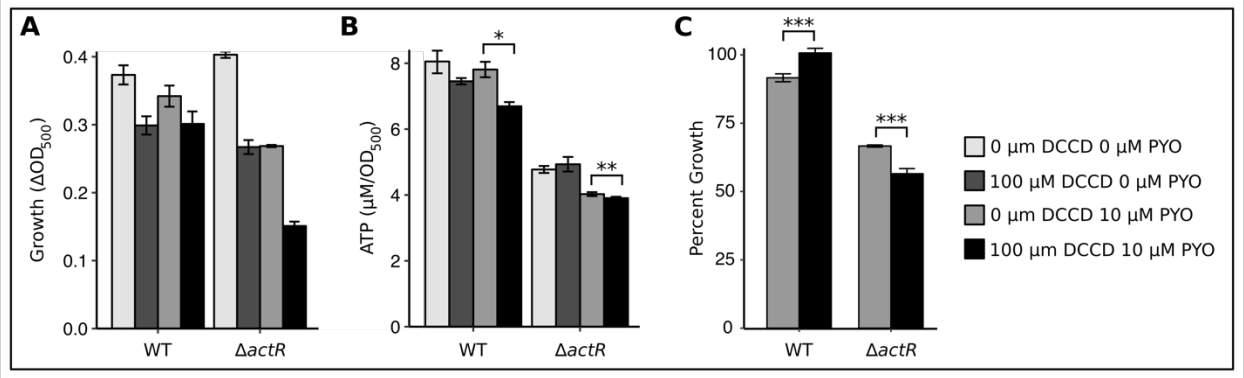

Figure S6: Inhibition of ATP synthesis does not necessarily correlate with PYO sensitivity. Data in all panels is from the same experiment ($n = 3$).
A. Growth of WT and Δ*actR* after 5 hrs of treatment with +/- 100 μM DCCD combined with +/- 10 μM PYO. The difference between the OD_{500} at 5 hrs and initial OD_{500} was taken as a proxy for growth.
B. ATP levels after 5 hrs of treatment.
C. Percent growth of each strain in 10 μM PYO relative to its growth in 0 μM PYO, with or without 100 μM DCCD, after 5 hrs. * $p < 0.05$, ** $p < 0.01$, *** $p < 0.001$ (in B, Welch's *t*-test followed by the Benjamini-Hochberg procedure to control the false discovery rate; in C, linear regression with custom contrast matrix to specify comparisons between 0 μM and 100 μM DCCD conditions). Legend on the right applies to all panels.

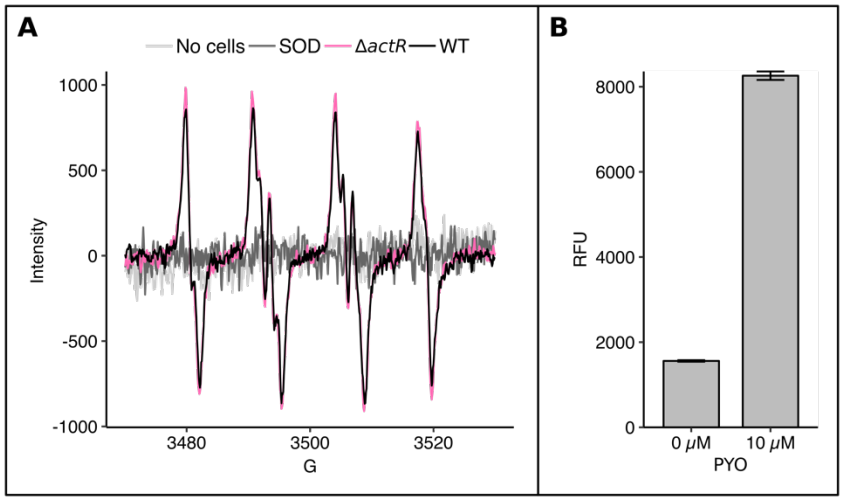

Figure S7: EPR spectra and DHE oxidation in the presence of PYO.
A. EPR spectra of 1) a cell-free sample containing 100 μM PYO + 0.5% glucose (light gray); 2) WT + 100 μM PYO + 0.5% glucose + exogenous superoxide dismutase (SOD) (100 units) (dark gray); 3) Δ*actR* + 100 μM PYO + 0.5% glucose (pink); 4) WT + 100 μM PYO + 0.5% glucose (black). G = Gauss. EPR signal intensity is directly proportional to the quantity of radicals in a sample (Eaton *et al.*, 2010). All spectra were collected using 25 mM BMPO as the spin trap for superoxide and hydroxyl radical. The cell-free and SOD control spectra are single scans while the other two spectra are averages of six consecutive scans and are representative of at least three biological replicates. The complete loss of signal upon addition of cell-impermeable SOD indicates that the signal from PYO-treated cell suspensions represents only extracellular superoxide.
B. Fluorescence (510ex/580em) of 15 μM dihydroethidium (DHE) after 1 hr of incubation with 0 μM or 10 μM PYO in cell-free phosphate buffer. Increased fluorescence in the PYO-treated sample indicates abiotic DHE oxidation, suggesting that DHE oxidation would not be a reliable reporter for intracellular superoxide. RFU = relative fluorescence units.

Table S7: Primers used in this study. Primers with "us" or "ds" were used to amplify the upstream or downstream flanking regions of the given gene, respectively, which were subsequently joined by overlap extension PCR and cloned into pNPTS138.

Primer	Sequence	Cut site
SS9arb1	GACCACGAGACGCCACACTNNNNNNNNNNCATGC	
Mar4	TAGGGTTGAGTGTTGTTCCAGTT	
arb3	GACCACGAGACGCCACACT	
Mar4-2	TCACCGTCATGGTCTTTGTAGTC	
soxR-us-F	GTAAAAATT-GAATTC-CACCGAAGAGCTGACCATCAAG	EcoRI
soxR-us-R	GAATAAGGGGCGGCTCAGCCGC-TCTGGCTCCTGCTTCCG	
soxR-ds-F	CGGAAGCAGGAGCCAGA-GCGGCTGAGCCGCCCCTTATTC	
soxR-ds-R	GTAAAAATT-ACTAGT-CCGACCGAAGACGGCATATTCCG	SpeI
actS-us-F	CTTGGTGCCATCATTCTCGAC	EcoRI (downstream)
actS-us-R	CGCTTCAACGTGGATGGTAAAG-CGTCTTCTCCTTTACCCTTTTC	
actS-ds-F	GAAAAGGGTAAAGGAGAAGACG-CTTTACCATCCACGTTGAAGCG	
actS-ds-R	GTAAAAATT-ACTAGT-TGCGCCGATGCATGTTG	SpeI
actR-us-F	GTAAAAATT-GGATCC-GCGTCGTCGCCAAGGAAATG	BamHI
actR-usR	CGCACTTTTACTGGAAATGCT-GTTTCCGGCCTTCCGGCAAC	
actR-ds-F	GTTGCCGGAAGGCCGGAAAC-AGCATTTCCAGTAAAAGTGCG	
actR-ds-R	GTAAAAATT-ACTAGT-CGCCAAATTGTGCGAAGGAG	SpeI
sodBI-us-F	GTAAAAATT-GGATCC-AATGGCTGAATACGGTGC	BamHI
sodBI-us-R	GAAAAATTCCGTTCGCCAAGCC-GGTTTTTACTCCTTTTTGCAGC	
sodBI-ds-F	GGCTTGGCGAACGGAATTTTTC	
sodBI-ds-R	GTAAAAATT-ACTAGT-GAATTGCTTGTCACTGAGTG	SpeI
sodBII-us-F	GTAAAAATT-GGATCC-TCGAAACCGTGCTTCTGCGC	BamHI
sodBII-us-R	GGGTCGGTGGGGCTCAAA-GGGGTATTCCTTTGTCAACTGTT	
sodBII-ds-F	AACAGTTGACAAAGGAATACCCC-TTTGAGCCCCACCGACCC	
sodBII-ds-R	GTAAAAATT-ACTAGT-ACGCGGCGAGATCGTCGG	SpeI
Atu0942-us-F	GTAAAAATT-GAATTC-CAAGGACGAACATCGCTGTG	EcoRI
Atu0942-us-R	GGTTCACTTTTTCTGGAAATGCT-GCGGGCTTTTTTATCCGATG	
Atu0942-ds-F	AGCATTTCCAGAAAAAGTGAACC	
Atu0942-ds-R	GTAAAAATT-ACTAGT-GATCGAACTTGCCTCGTCAG	SpeI
Atu2361-us-F	GTAAAAATT-GGATCC-CTACGAGCCGCAGAATTTCG	BamHI
Atu2361-us-R	CCCACCCCACGCTGCGCC-GGAACGTCCTTCGATAGTGT	
Atu2361-ds-F	ACACTATCGAAGGACGTTCC-GGCGCAGCGTGGGGTGGG	
Atu2361-ds-R	GTAAAAATT-ACTAGT-GGAATAGAGTGCATCGGATTCC	SpeI
mexF-us-F	GTAAAAATT-GAATTC-TCAACCCGATCTATGCAAGC	EcoRI
mexF-us-R	GCGGTGGATGGGGTGCGGCG-ATCCAGTCCCTCTCCGGG	

mexF-ds-F	CGCCGCACCCCATCCACCGC	
mexF-ds-R	GTAAAAATT-ACTAGT-GTTTTCCGTCCAACCTGCC	SpeI
Atu5152-us-F	GTAAAAATT-GGATCC-AGCCATTGGGATTGATGTCG	BamHI
Atu5152-us-R	CCACGTCAAAGGAGGGCGTC-ATTCCCGACCGCACTTGGTG	
Atu5152-ds-F	CACCAAGTGCGGTCGGGAAT-GACGCCCTCCTTTGACGTGG	
Atu5152-ds-R	GTAAAAATT-ACTAGT-CGTAGTGGTCATTGAGCTTGG	SpeI
Atu5305-us-F	TGCAGACCAATGTCGAATTC	EcoRI
Atu5305-us-R	GCATCCAACGGATCCACAT-GAGCCGCGACCGTCTTGC	
Atu5305-ds-F	ATGTGGATCCGTTGGATGC	
Atu5305-ds-R	GTAAAAATT-ACTAGT-GTAACGGTTGCGGCACATAG	SpeI
Atu4581-us-F	GTAAAAATT-GGATCC-CACGGAAAACGGCGTCAAC	BamHI
Atu4581-us-R	GGGAGAGAAAATCCCTAGTTGAG-ACCGCCATCGATCAGCCTG	
Atu4581-ds-F	CTCAACTAGGGATTTTCTCTCCC	
Atu4581-ds-R	GTAAAAATT-ACTAGT-CCCGCGCCACAATATTTTC	SpeI
Atu4582-us-F	GTAAAAATT-GGATCC-TGTCCGAGGAGACGCTGAAG	BamHI
Atu4582-us-R	ATGAGACATGCAGTGCCGGG-GGGGATGCTCAAATGGAGTTG	
Atu4582-ds-F	CCCGGCACTGCATGTCTCAT	
Atu4582-ds-R	GTAAAAATT-ACTAGT-GCCGCCTTTCTAAATGTCCG	SpeI
Atu4741-us-F	GTAAAAATT-GGATCC-GAACTGCTGGAAGAAAACCG	BamHI
Atu4741-us-R	CTGTGGCATATGCCTCACCT-AAACCACCGGCTCTAGACAG	
Atu4741-ds-F	AGGTGAGGCATATGCCACAG	
Atu4741-ds-R	GTAAAAATT-ACTAGT-CACAGGCATAAACGGCAACG	SpeI
Atu4742-us-F	GTAAAAATT-GAATTC-ATTTCCAACAACAGGCACGG	EcoRI
Atu4742-us-R	CGACTGAACTTCCGCTGCCA-CGTTATTCCGTTGCAATGG	
Atu4742-ds-F	TGGCAGCGGAAGTTCAGTCG	
Atu4742-ds-R	GTAAAAATT-ACTAGT-CATGTTCTGGCTCGTCTTCAG	SpeI
CyoABCD-us-F	GTAAAAATT-GGATCC-CGATCTGGAGGAAGATCAGC	BamHI
CyoABCD-us-R	GCCGCTGATTTATCGCTGC-GACGACCAGATTGCAGCCGC	
CyoABCD-ds-F	GCAGCGATAAATCAGCGGC	
CyoABCD-ds-R	GTAAAAATT-ACTAGT-GGTTCTAAGGAAAAGCCCACC	SpeI
pSRK-actR-F	GTAAAAATT-CAT-ATGAAGATTGAAGACCAGACCC	NdeI
pSRK-actR-R	GTAAAAATT-GCTAGC-TCACTTCGGAGCGCGTTTC	NheI
pSRK-soxR-F	GTAAAAATT-CAT-ATGGAAAATACCATCTTCAAACAC	NdeI
pSRK-soxR-R	GTAAAAATT-GCTAGC-TTATTCAGCGGAGACGAGG	NheI
Cyo-pSRK-Gib-F	GAATTGTGAGCGGATAACAATTTCACACAGGAAACAGCATATGAACCCTT CGGGCGAC	Used with NdeI/NheI-cut pSRKKm
surf1-pSRK-Gib-R	CCTGAACCGACGACCGGGTCGAATTTGCTTTCGAATTGTCAATCAGCATCC CGTTTCG	Used with NdeI/NheI-cut pSRKKm
pSRK-Cyd-F	GTAAAAATT-CAT-ATGCTGCCGGCGCTGCTCTG	NdeI

pSRK-Atu8036-R	GTAAAAATT-GCTAGC-TCATTTTTCCGGCTTCGCTTCG	NheI
soxR-qpcr-F	CTGTCGGTGGGGGATGTTG	
soxR-qpcr-R	GATGATAACGACGCTGGTTGC	
sodBII-qpcr-F	CTTCTGGGAGATCATGGGGC	
sodBII-qpcr-R	CGAGGGCGAAATTCTGCTTG	
Atu0942-qpcr-F	GCGGGTTTTTATAGCTGGGC	
Atu0942-qpcr-R	AGATGAGGCAGCACAGAAGC	
Atu2361-qpcr-F	TTTTACACCATCCCCTCGCA	
Atu2361-qpcr-R	CTGCCAGATTGAAGATGCCG	
mexE-qpcr-F	CGCTGGTGAAGGAAGGTGAC	
mexE-qpcr-R	CACGGTCGAGTTCCGTCTTT	
mexF-qpcr-F	ACCGACGCCTATGACATCAC	
mexF-qpcr-R	TAATCACCTGCGCCGAAGAC	
Atu5152-qpcr-F	GGTTGGAGCCGTATTGTTGC	
Atu5152-qpcr-R	CCACAGAATGAAACCCAGCG	
Atu5305-qpcr-F	CCATAGCGAGCCCAAATCCA	
Atu5305-qpcr-R	AGTCACCTCAGTCTCGTTGC	
Atu4741-qpcr-F	GAAGCCACGGAAAATCGTCG	
Atu4741-qpcr-R	CATCTCACCGTCCCCTGAAC	
Atu4742-qpcr-F	CCATCAGGCAGAATCCCGAC	
Atu4742-qpcr-R	CACTGCCACGCCTTCTATCC	
CyoA-qpcr-F	GAGATGCCGTCGTAGACACC	
CyoA-qpcr-R	AACTCCTTCTTCGTTCCCGC	
CydA-qpcr-F	CGAAGCAATGTGGGAAACCG	
CydA-qpcr-R	TTTGCGTATCAAGCGAACGG	
Atu4316-qpcr-F	TGGCATAAACGCCGATGACT	
Atu4316-qpcr-R	CCAGATCATCACGCTCTCCC	
Atu1475-qpcr-F	AACGCCTGAACCCGATTTTG	
Atu1475-qpcr-R	GTCCGTATGGAACGTCGTGA	
Atu4895-qpcr-F	GGGCTCACTGCAAAACCAAC	
Atu4895-qpcr-R	TCCCAAATGCCAAGAGCGAC	

Table S8: Strains and plasmids used in this study. All *A. tumefaciens* mutants were constructed from the NT1 parent strain.

Strain/Plasmid	**Notes**	**Reference/Source**
E. coli		
DH10b	Cloning strain	Invitrogen
β2155	Δ*dapA*::*erm* (Erm^r) *pir*::RP4 [::*kan* (Km^r) from SM10]	(Dehio and Meyer, 1997)

A. tumefaciens		
NT1	non-pathogenic derivative of strain C58; carries pDCI41E33 (plasmid with *traG*::*lacZ* fusion)	(Watson *et al.*, 1975; Shaw *et al.*, 1997)
soxR	*mariner* transposon insertion in *soxR*	This study
actS	*mariner* transposon insertion in *actS*	This study
rpoH	*mariner* transposon insertion in *rpoH*	This study
Atu1426	*mariner* transposon insertion in Atu1426	This study
Atu3738	*mariner* transposon insertion in Atu3738	This study
pykA	*mariner* transposon insertion in *pykA*	This study
Atu2584	*mariner* transposon insertion in Atu2584	This study
Atu2590	*mariner* transposon insertion in Atu2590	This study
Atu2591	*mariner* transposon insertion in Atu2591	This study
Atu2592	*mariner* transposon insertion in Atu2592	This study
Atu2577-1	*mariner* transposon insertion in Atu2577	This study
Atu2577-2	*mariner* transposon insertion in Atu2577	This study
Δ*soxR*	clean deletion of *soxR* coding sequence	This study
Δ*actS*	clean deletion of *actS* coding sequence	This study
Δ*actR*	clean deletion of *actR* coding sequence	This study
Δ*actR*/Δ*soxR*	clean deletion of *actR* and *soxR* coding sequences	This study
Δ*sodBI*	clean deletion of *sodBI* coding sequence	This study
Δ*sodBII*	clean deletion of *sodBII* coding sequence	This study
Δ*sodBI*/Δ*sodBII*	clean deletion of *sodBI* and *sodBII* coding sequences	This study
Δ*soxR*/Δ*sodBI*	clean deletion of *soxR* and *sodBI* coding sequences	This study
ΔAtu0942	clean deletion of Atu0942 coding sequence	This study
ΔAtu2361	clean deletion of Atu2361 coding sequence	This study
Δ*mexF*	clean deletion of *mexF* coding sequence	This study
ΔAtu5152	clean deletion of Atu5152 coding sequence	This study
ΔAtu5305	clean deletion of Atu5305 coding sequence	This study
ΔAtu4581	clean deletion of Atu4581 coding sequence	This study
ΔAtu4582	clean deletion of Atu4582 coding sequence	This study
ΔAtu4741	clean deletion of Atu4741 coding sequence	This study
ΔAtu4742	clean deletion of Atu4742 coding sequence	This study
Δ*cyo*	clean deletion of cytochrome *o* oxidase biosynthesis operon	This study
Plasmid		
pSC189	R6K suicide plasmid carrying *mariner* transposon with hyperactive transposase; Ap^R Km^R	(Chiang and Rubin, 2002)
pNPTS138	ColE1 suicide plasmid; *sacB*; Km^R	Constructed by M.R.K. Alley; gift of C. Fuqua
pNPTS138::soxRdel	pNPTS138 carrying flanking regions of *soxR* for clean deletion	This study
pNPTS138::actSdel	pNPTS138 carrying flanking regions of *actS* for clean deletion	This study
pNPTS138::actRdel	pNPTS138 carrying flanking regions of *actR* for clean deletion	This study

pNPTS138::sodBIdel	pNPTS138 carrying flanking regions of *sodBI* for clean deletion	This study
pNPTS138::sodBIIdel	pNPTS138 carrying flanking regions of *sodBII* for clean deletion	This study
pNPTS138::Atu0942del	pNPTS138 carrying flanking regions of Atu0942 for clean deletion	This study
pNPTS138::Atu2361del	pNPTS138 carrying flanking regions of Atu2361 for clean deletion	This study
pNPTS138::mexFdel	pNPTS138 carrying flanking regions of *mexF* for clean deletion	This study
pNPTS138::Atu5152del	pNPTS138 carrying flanking regions of Atu5152 for clean deletion	This study
pNPTS138::Atu5305del	pNPTS138 carrying flanking regions of Atu5305 for clean deletion	This study
pNPTS138::Atu4581del	pNPTS138 carrying flanking regions of Atu4581 for clean deletion	This study
pNPTS138::Atu4582del	pNPTS138 carrying flanking regions of Atu4582 for clean deletion	This study
pNPTS138::Atu4741del	pNPTS138 carrying flanking regions of Atu4741 for clean deletion	This study
pNPTS138::Atu4742del	pNPTS138 carrying flanking regions of Atu4742 for clean deletion	This study
pNPTS138::cyoABCDdel	pNPTS138 carrying flanking regions of *cyoABCD* for clean deletion	This study
pLacZ	alias for pSRKKm; broad host range P_{lac} vector; $lacI^{Q}$; Km^{R}	(Khan *et al.*, 2008)
pActR	pSRKKm carrying P_{lac}-*actR*	This study
pSoxR	pSRKKm carrying P_{lac}-*soxR*	This study
pCyo	pSRKKm carrying P_{lac}-*cyoABCD-surf1* (*surf1* is co-transcribed with the other *cyo* genes)	This study
pCyd	pSRKKm carrying P_{lac}-*cydDCAB*-Atu8036 (Atu8036 is co-transcribed with the other *cyd* genes)	This study

Supplementary References

Dehio, C., and Meyer, M. (1997) Maintenance of broad-host-range incompatibility group P and group Q plasmids and transposition of Tn5 in *Bartonella henselae* following conjugal plasmid transfer from *Escherichia coli*. *J Bacteriol* **179**: 538–540.

Eaton, G.R., Eaton, S.S., Barr, D.P., and Weber, R.T. (2010) *Quantitative EPR*. SpringerWienNewYork, New York.

Shaw, P.D., Ping, G., Daly, S.L., Cha, C., Cronan Jr., J.E., Rinehart, K.L., and Farrand, S.K. (1997) Detecting and characterizing *N*-acyl-homoserine lactone signal molecules by thin-layer chromatography. *Proc Natl Acad Sci* **94**: 6036–6041.

Chapter 3

PHENAZINE-MEDIATED COLLATERAL RESILIENCE TO CLINICAL ANTIBIOTICS IN OPPORTUNISTIC PATHOGENS

This chapter is adapted from:

Meirelles, L.A.*, Perry, E.K.*, Bergkessel, M, and Newman, DK. (2021) Bacterial defenses against a natural antibiotic promote collateral resilience to clinical antibiotics. *PLoS Biol* **19**: e300193.

Abstract

Bacterial opportunistic human pathogens frequently exhibit intrinsic antibiotic tolerance and resistance, resulting in infections that can be nearly impossible to eradicate. We asked whether this recalcitrance could be driven by these organisms' evolutionary history as environmental microbes that engage in chemical warfare. Using *Pseudomonas aeruginosa* as a model, we demonstrate that the self-produced antibiotic pyocyanin activates defenses that confer collateral tolerance specifically to structurally-similar synthetic clinical antibiotics. Non-pyocyanin-producing opportunistic pathogens, such as members of the *Burkholderia cepacia* complex, likewise display elevated antibiotic tolerance when co-cultured with pyocyanin-producing strains. Furthermore, by widening the population bottleneck that occurs during antibiotic selection and promoting the establishment of a more diverse range of mutant lineages, pyocyanin increases apparent rates of mutation to antibiotic resistance to a degree that can rival clinically-relevant hypermutator strains. Together, these results reveal an overlooked mechanism by which opportunistic pathogens that produce natural toxins can dramatically modulate the efficacy of clinical antibiotics and the evolution of antibiotic resistance, both for themselves and other members of clinically-relevant polymicrobial communities.

Introduction

The emergence and spread of bacterial resistance to clinical antibiotics is a growing public health concern worldwide (Fair and Tor, 2014). Moreover, it is increasingly appreciated that antibiotic tolerance can also contribute to the failure of treatments for infections (Brauner *et al.*, 2016) and that tolerance can lead to the evolution of resistance (Levin-Reisman *et al.*, 2017; Windels

et al., 2019). Yet bacterial resilience to antibiotics is anything but new: microbes in environments like soil have been producing natural antibiotics and evolving mechanisms of tolerance and resistance for millions of years (Martinez, 2009; Davies and Davies, 2010). Here, we define tolerance as the ability to survive a transient exposure to an otherwise lethal antibiotic concentration, and resistance as the ability to grow in the presence of an antibiotic, similar to recent recommendations (Kester and Fortune, 2014; Brauner *et al.*, 2016; Balaban *et al.*, 2019).

Considering that most of the antibiotics used today are derived from microbially-produced molecules, we hypothesized that molecular defenses that originally evolved to protect cells from a natural antibiotic in the environment might also promote tolerance and/or resistance to structurally- or mechanistically-similar clinical drugs. Indeed, several clinical antibiotic resistance genes are thought to have originated in non-pathogenic soil bacteria, but it has often been assumed that intermediate steps of horizontal gene transfer are necessary in order for such genes to be acquired by human pathogens (Davies and Davies, 2010). In this study, we asked whether there could be a direct link between production of natural antibiotics by an opportunistic human pathogen and its recalcitrance to clinical antibiotic treatment due to shared protective mechanisms. In addition, we sought to determine whether in the presence of such a natural antibiotic producer, recalcitrance to clinical antibiotics could also be observed in other opportunistic pathogens found together with it in polymicrobial infections. Given that many opportunistic pathogens share their natural environment (e.g. soil), we posited that the evolutionary legacy of natural-antibiotic-mediated ecological interactions between these microbial species could have important implications for antibiotic tolerance and resistance in the clinical context.

One organism that is well-suited to testing these hypotheses is the opportunistic pathogen *Pseudomonas aeruginosa*, which is notorious for causing chronic lung infections in cystic fibrosis (CF) patients, as well as other types of infections in immunocompromised hosts (Driscoll *et al.*, 2007). *P. aeruginosa* produces several redox-active, heterocyclic compounds known as phenazines (Laursen and Nielsen, 2004). Phenazines have been shown to provide multiple benefits for their producers, including by: (i) serving as an alternative electron acceptor in the absence of oxygen, thereby promoting redox homeostasis and anaerobic survival (Glasser *et al.*, 2014), which is particularly relevant for oxidant-limited biofilms (Saunders *et al.*, 2020); (ii) acting as signaling molecules (Dietrich *et al.*, 2006); (iii) promoting iron acquisition (Wang *et al.*, 2011); and (iv) killing

competitor species (Korgaonkar *et al.*, 2013). In addition, despite possessing broad-spectrum antimicrobial activity (Laursen and Nielsen, 2004), including against *P. aeruginosa* itself (Meirelles and Newman, 2018), phenazines have recently been shown to promote tolerance to clinical antibiotics under some circumstances, via mechanisms that have yet to be characterized (Schiessl *et al.*, 2019; Zhu *et al.*, 2019). Here, we sought to assess potential broader implications of this phenomenon by investigating whether phenazine-mediated tolerance to clinical antibiotics in *P. aeruginosa* is driven by cellular defenses that evolved to mitigate self-induced toxicity. We also tested whether phenazine production by *P. aeruginosa* could promote antibiotic tolerance in other clinically-relevant opportunistic pathogens from the *Burkholderia* and *Stenotrophomonas* genera. Finally, we explored the ramifications of phenazine-induced tolerance for the evolution of heritable antibiotic resistance, both in *P. aeruginosa* and in a clinical isolate from the *Burkholderia cepacia* complex.

Results

Mechanisms of tolerance to the self-produced natural antibiotic PYO in P. aeruginosa

We started by characterizing the defense mechanisms *P. aeruginosa* has evolved to tolerate its most toxic self-produced phenazine, pyocyanin (PYO) (Laursen and Nielsen, 2004; Meirelles and Newman, 2018). To do so in an unbiased fashion, we performed a genome-wide transposon sequencing (Tn-seq) screen in which the mutant library was exposed to PYO under starvation to maximize PYO toxicity (Meirelles and Newman, 2018), and tolerance of the pooled mutants to PYO was assessed following re-growth (Fig. 1A). This revealed five broad categories of genes that significantly affect tolerance to PYO: (i) efflux system repressors, (ii) protein damage responses, (iii) membrane or cell wall biosynthesis, (iv) oxidative stress responses, and (v) carbon metabolism and transport (Fig. 1B). We validated the screen results by constructing and testing chromosomal clean deletion mutants for four of these genes (Fig. 1C).

The fitness effects of different transposon insertions largely aligned with what is thought to be the primary mode of PYO toxicity, which is the generation of reactive oxygen species (ROS)

(Muller, 2002; Rada and Leto, 2013). For example, the fact that transposon insertions in different genes within the "carbon metabolism and transport" category had opposite effects on fitness likely reflects conflicting priorities for cells challenged with ROS-generating toxins: on one hand, limiting flux through the electron transport chain decreases the potential for ROS generation, but on the other

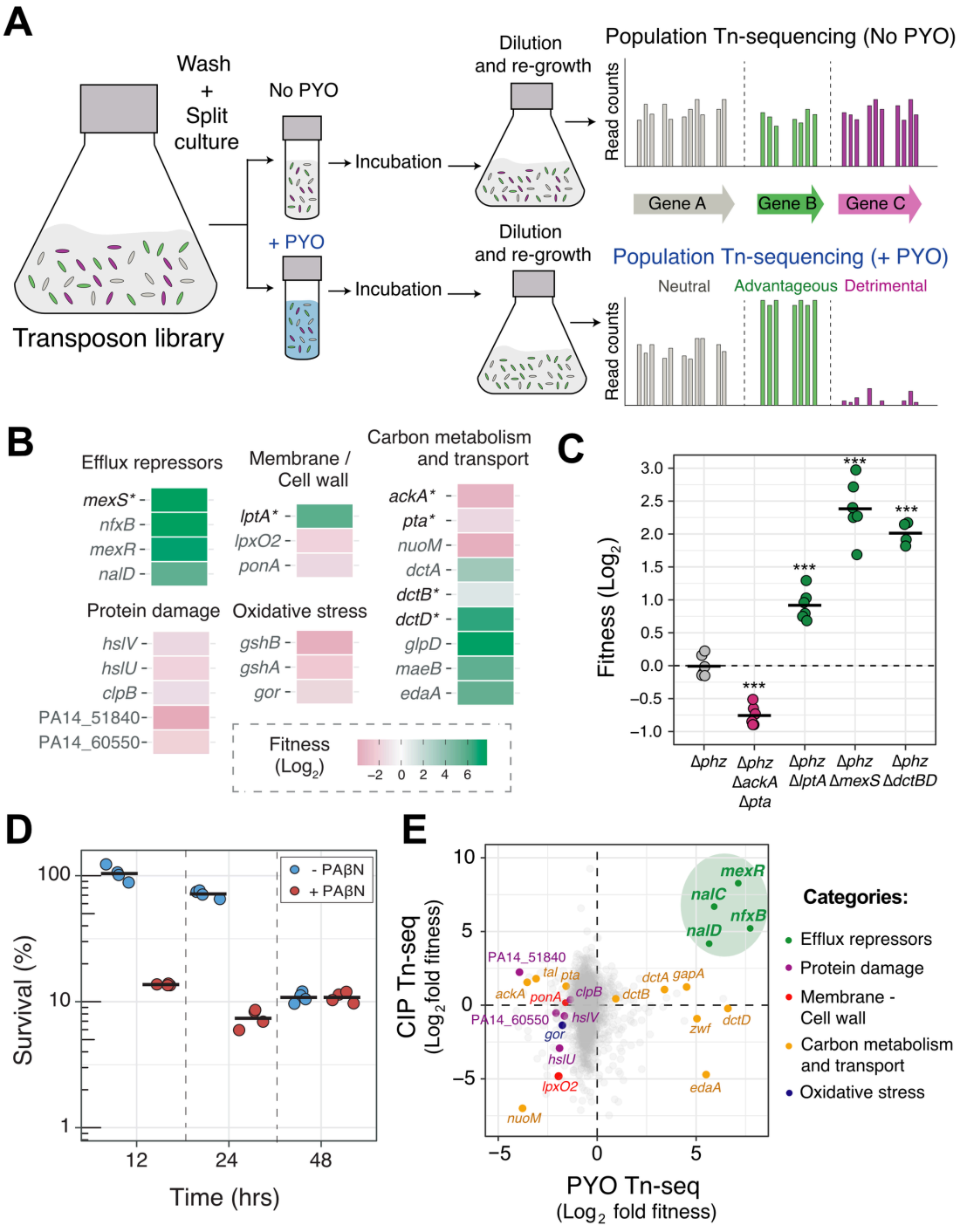

Figure 1 (see next page for legend).

Figure 1: Mechanisms of tolerance to the self-produced natural antibiotic PYO in *P. aeruginosa*.
A. Genome-wide transposon sequencing (Tn-seq) experimental design. Cells were incubated with and without PYO under nutrient starvation for maximum PYO toxicity (Meirelles and Newman, 2018) (see Methods for details). Bar graphs shown are hypothetical representations of the expected results for genes with different fitness effects and are not derived from the obtained data.
B. Statistically-significant fitness effects of transposon insertions in different representative genes under conditions that maximize PYO toxicity (for full dataset, see S1 Table).
See Methods for details on calculation of fitness. Asterisks show genes for which chromosomal clean deletion mutants were constructed and validated.
C. Tn-seq validations. Chromosomal clean deletion mutants were exposed to PYO under carbon starvation, similar to the conditions used for the Tn-seq experiment. Survival of each strain was measured by colony forming units (CFUs) and compared to the survival of the parent Δ*phz* strain for fitness calculation (see Methods for details). Statistical significance was calculated using one-way ANOVA with Tukey's HSD multiple-comparison test, with asterisks showing significant differences relative to Δ*phz* (*** $p < 0.001$). Data points represent independent replicates and black horizontal lines mark the mean fitness for each strain.
D. Tolerance to PYO toxicity in the presence and absence of the efflux inhibitor PAβN. Each data point represents an independent biological replicate (n = 4), and the horizontal black lines mark the mean survival for each condition and time point.
E. Fitness correlation analysis between PYO tolerance Tn-seq (this study) and CIP persistence Tn-seq (Cameron *et al.*, 2018). Efflux repressors present in both datasets are highlighted in green. For full analysis, see S1 Table.

hand, proton-motive force is required to pump the toxin out, and NADH is needed to power reductases involved in repair of oxidative damage. The need to counteract oxidative stress would also explain why transposon insertions in genes related to protein damage repair and glutathione synthesis or reduction led to decreased fitness in the presence of PYO (Fig. 1B). Finally, for genes related to cell wall/membrane synthesis, the transposon insertions may have altered cellular permeability and thereby either increased or decreased PYO influx.

However, the strongest hits in our Tn-seq were transposon insertions in transcriptional repressors of resistance-nodulation-division (RND) efflux system genes (Fig. 1B, S1 Table), which would cause overexpression of the downstream efflux pumps. These insertions dramatically increased fitness in the presence of PYO, suggesting that one of the most effective defenses against PYO toxicity is to decrease the intracellular concentration of the toxin. While transposon insertions in the genes encoding the efflux pump proteins themselves did not have strong effects in our screen (S1 Table), this is likely due to partial functional redundancy among the various efflux systems (Lister *et al.*, 2009). Indeed, when we challenged starved *P. aeruginosa* with PYO in the presence of the broad-spectrum RND efflux inhibitor phenylalanine-arginine β-naphthylamide (PAβN), cell death was accelerated, confirming that efflux pumps are necessary for minimizing PYO toxicity (Fig. 1D).

Mutations in the efflux system repressors identified in our Tn-seq screen are commonly found in clinical isolates that are resistant to synthetic fluoroquinolone antibiotics, as the efflux systems regulated by these repressors efficiently export this class of drugs (Llanes *et al.*, 2004; Sobel *et al.*, 2005). We therefore asked whether the mechanisms used by *P. aeruginosa* to tolerate PYO toxicity might overlap more broadly with those that confer tolerance to fluoroquinolones. To address this question, we compared our dataset to a recent Tn-seq study that screened for genes that affect *P. aeruginosa* survival in the presence of the broad-spectrum fluoroquinolone ciprofloxacin (Cameron *et al.*, 2018). Across the two datasets, we observed similar fitness effects for insertions in a small number of genes within the "protein damage response," "membrane/cell wall," and "oxidative stress response" categories, but the most dramatic fitness increases in both experiments were caused by insertions in a shared set of efflux system repressors (Fig. 1E, S1 Table). These results highlighted the potential for a conserved molecular route to increased tolerance against both a natural antibiotic, PYO, and a synthetic clinical antibiotic, ciprofloxacin.

PYO induces expression of specific efflux systems, conferring cross-tolerance to fluoroquinolones

Given that cellular processes involved in PYO tolerance have also been implicated in ciprofloxacin tolerance, we asked whether exposure to PYO could promote an increase in tolerance to ciprofloxacin and related clinical antibiotics, including other synthetic fluoroquinolones. Importantly, such an effect would require that PYO induces the expression of shared defense mechanisms. We have previously established that PYO upregulates expression of not only the oxidative stress response genes *ahpB* (a thiol-specific peroxidase) and *katB* (a catalase) (Meirelles and Newman, 2018), but also at least two efflux systems known to pump fluoroquinolones, *mexEF-oprN* and *mexGHI-opmD* (Dietrich *et al.*, 2006; Meirelles and Newman, 2018). We confirmed these expression patterns by performing qRT-PCR on the WT strain that produces PYO, a Δ*phz* mutant that does not produce PYO, and Δ*phz* treated with exogenous PYO (S1, S2 and S3 Figs). Notably, phenazines and fluoroquinolones both contain at least one aromatic ring, unlike other antibiotics that are not thought to be pumped by *mexEF-oprN* and *mexGHI-opmD*, such as aminoglycosides (Lister *et al.*, 2009) (Fig. 2A). Thus, structural similarities could account for why efflux pumps that likely evolved to export natural antibiotics such as PYO can also transport certain classes of synthetic antibiotics. To determine whether PYO also induces other efflux systems known to pump clinical antibiotics besides fluoroquinolones, we performed qRT-PCR on representative genes from all 11

major RND efflux systems in the *P. aeruginosa* genome. These measurements confirmed that *mexEF-oprN* and *mexGHI-opmD* are the only two efflux systems significantly induced by PYO, and that the induction is PYO dose-dependent (Fig. 2B, S2 and S3 Fig). The *mexGHI-opmD* system in

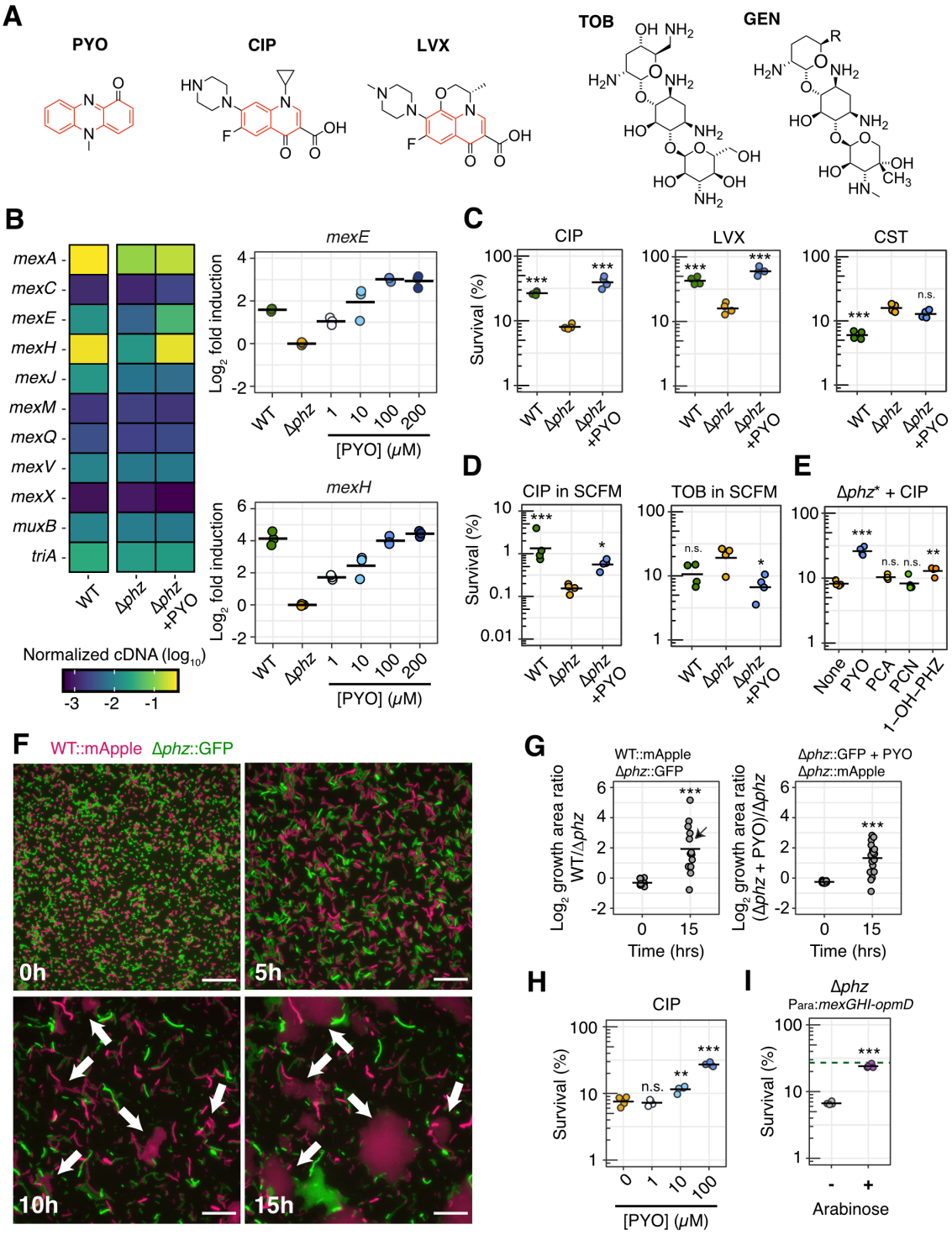

Figure 2 (see next page for legend).

Figure 2: PYO induces expression of specific efflux systems, conferring cross-tolerance to fluoroquinolones.
A. Structures of PYO, two representative fluoroquinolones (CIP = ciprofloxacin, LVX = levofloxacin) and two representative aminoglycosides (GEN = gentamicin, TOB = tobramycin). PYO and fluoroquinolones are pumped by MexEF-OprN and MexGHI-OpmD, while aminoglycosides are not (Llanes *et al.*, 2004; Lister *et al.*, 2009). Rings with an aromatic character are highlighted in red.
B. Normalized cDNA levels for genes within operons coding for the 11 main RND efflux systems in *P. aeruginosa* (left; n = 3), and PYO-dose-dependent changes in expression of *mexEF-oprN* and *mexGHI-opmD* systems (right; n = 3). For full qRT-PCR dataset, see S1, S2 and S3 Figs.
C. Effect of PYO on tolerance to CIP (1 μg/mL), LVX (1 μg/mL) and CST (colistin, 16 μg/mL) in glucose minimal medium (n = 4).
D. Effect of PYO on tolerance to CIP (1 μg/mL) and TOB (40 μg/mL) in SCFM (n = 4). PYO itself was not toxic under the experimental conditions (Meirelles and Newman, 2018) (S4C Fig). WT made 50-80 μM PYO as measured by absorbance of the culture supernatant at 691 nm. See S5A Fig. for experimental design. (**E)** Effect on tolerance to CIP (1 μg/mL) caused by the presence of the four main phenazines produced by *P. aeruginosa* (PYO = pyocyanin, PCA = phenazine-1-carboxylic acid, PCN = phenazine-1-carboxamide and 1-OH-PHZ = 1-hydroxyphenazine) (n = 4). For this experiment, a Δ*phz** strain that cannot produce or modify any phenazine was used (see Methods).
F-G. Effect of PYO on lag during outgrowth after exposure to CIP. A representative field of view over different time points (F; magenta = WT::mApple, green = Δ*phz*::GFP) is shown together with the quantification of growth area on the agarose pads at time 0 hrs and 15 hrs (G). For these experiments, a culture of each strain tested was grown and exposed to CIP (10 μg/mL) separately, then cells of both cultures were washed, mixed and placed together on a pad and imaged during outgrowth. The pads did not contain any PYO or CIP (see Methods and S5D Fig. for details). White arrows in the displayed images point to regions with faster recovery of WT growth. The field of view displayed is marked with a black arrow in the quantification plot. The results for the experiment with swapped fluorescent proteins are shown in S4E Fig. See S4C Fig. for complementary data about effects of PYO on lag. Scale bar: 20 μm.
H. Tolerance of Δ*phz* to CIP (1 μg/mL) in stationary phase in the presence of different concentrations of PYO (n = 4).
I. Tolerance of Δ*phz* to CIP (1 μg/mL) upon artificial induction of the *mexGHI-opmD* operon with arabinose (n = 4). The dashed green line marks the average survival of PYO-producing WT under similar conditions (without arabinose).
Statistics: C, D, E, H – One-way ANOVA with Tukey's HSD multiple-comparison test, with asterisks showing significant differences relative to untreated Δ*phz* (no PYO); G, I – Welch's unpaired t-test (* $p < 0.05$, ** $p < 0.01$, *** $p < 0.001$, n.s. $p > 0.05$). In all panels with quantitative data, black horizontal lines mark the mean value for each condition. Individual data points represent independent biological replicates, except for in panel G, where the data points represent different fields of view.

particular reached expression levels comparable to the constitutively-expressed *mexAB-oprM* efflux system (Fig. 2B, S2 Fig), which plays an important role in the intrinsic antibiotic tolerance and resistance of *P. aeruginosa* (Lister *et al.*, 2009).

To assess whether the induction of efflux pumps and oxidative stress responses by PYO could increase the tolerance of *P. aeruginosa* to clinical drugs such as ciprofloxacin, we grew cultures with or without clinically-relevant concentrations of PYO (Wilson *et al.*, 1988) and performed a survival assay following treatment with different antibiotics. Importantly, we hypothesized that PYO would not be a universal antagonist to all clinical antibiotics. Instead, we

expected tolerance to increase only for drugs affected by the defense mechanisms induced by PYO in the cells. Indeed, compared to the non-PYO-producing Δ*phz* mutant, the PYO-producing WT strain and PYO-treated Δ*phz* were more tolerant to both ciprofloxacin and another fluoroquinolone, levofloxacin (Fig. 2C). On the other hand, PYO did not confer increased tolerance to: (i) aminoglycosides (Fig. 2D, S4B Fig), which are not substrates for the efflux pumps upregulated by PYO (Lister *et al.*, 2009); or (ii) colistin (polymyxin E) (Fig. 2C), an antimicrobial peptide that permeabilizes the outer membrane of the cell by interacting with the lipopolysaccharide and causing displacement of divalent cations (Fair and Tor, 2014). Similar to aminoglycosides, colistin is not known to be pumped by the PYO-induced efflux systems (Lister *et al.*, 2009); moreover, efflux rarely impacts polymyxin efficacy (Olaitan *et al.*, 2014). PYO itself was not toxic under the experimental conditions used in our tolerance assays (Meirelles and Newman, 2018) (S4C Fig). Aside from PYO, 1-hydroxyphenazine was the only other phenazine made by *P. aeruginosa* that increased tolerance to ciprofloxacin under our conditions, albeit to a lesser extent than PYO (Fig. 2E). We also tested whether the presence of PYO could affect the minimum inhibitory concentration (MIC) for ciprofloxacin, as the classical definition of antibiotic tolerance also stipulates that increased survival in the presence of an antibiotic is not accompanied by an increase in MIC (Brauner *et al.*, 2016; Balaban *et al.*, 2019). When we determined the MIC for ciprofloxacin according to standard clinical protocols (Determination of minimum inhibitory concentrations (MICs) of antibacterial agents by broth dilution, 2003) for our *P. aeruginosa* strain in the presence or absence of PYO, we saw no consistent difference at a detection limit of a two-fold increase in MIC (S7 Table), supporting the interpretation that the effect of PYO on *P. aeruginosa* is primarily an increase in antibiotic tolerance (i.e. survival without the ability to grow) rather than phenotypic resistance. Importantly, PYO also induced ciprofloxacin tolerance when *P. aeruginosa* was grown in synthetic cystic fibrosis sputum medium (SCFM) (Fig. 2D), suggesting that PYO production could contribute to antibiotic tolerance of this bacterium in CF patients. Together, these results indicate that PYO preferentially induces tolerance to fluoroquinolones.

Under *in vitro* conditions, PYO is typically produced in early stationary phase (Dietrich *et al.*, 2006). However, the heterogeneous nature of physiological conditions in infections (Kopf *et al.*, 2016; Winstanley *et al.*, 2016) could lead to intermixing of PYO-producing and -non-producing cells *in vivo*. We therefore tested whether exogenous PYO could increase the fluoroquinolone tolerance

of cells harvested during log phase, which did not make PYO. To limit the growth of the no-antibiotic control, we exposed these cells to the antibiotics under nitrogen depletion. PYO still increased tolerance to both ciprofloxacin and levofloxacin under these conditions, suggesting that the induced tolerance phenotype does not depend on the previous growth phase of growth-arrested cells (Meirelles and Newman, 2018) (S4B Fig). Next, to visualize the recovery of cell growth after a transient exposure to ciprofloxacin, we performed a time-lapse microscopy assay (S4D Fig). Interestingly, WT *P. aeruginosa* and PYO-treated Δ*phz* exhibited a shorter lag phase compared to non-PYO-treated Δ*phz* following ciprofloxacin treatment (Fig. 2F-G and S4E-F Fig), suggesting that PYO-induced defenses may help minimize cellular damage during the antibiotic treatment. We also found that addition of PYO to Δ*phz* increased ciprofloxacin tolerance in a dose-dependent manner (Fig. 2H), mirroring the dose-dependent induction of *mexEF-oprN* and *mexGHI-opmD* (Fig. 2B).

Given that PYO-induced efflux pumps transport specific substrates (Lister *et al.*, 2009), we asked if increased drug efflux could be the primary mechanism underlying PYO-mediated tolerance to fluoroquinolones. At high concentrations of ciprofloxacin, addition of the efflux inhibitor PAβN eliminated the survival advantage of PYO-treated cells, indicating that efflux pump activity is necessary for the PYO-mediated increase in antibiotic tolerance (S4G Fig). Next, we constructed a Δ*phz* strain with the *mexGHI-opmD* operon under the control of an arabinose-inducible promoter (P_{ara}:*mexGHI-opmD*). We verified that the transcription levels of *mexGHI-opmD* under arabinose induction were comparable to when PYO is present (S5 Fig). Indeed, arabinose induction of *mexGHI-opmD* expression increased ciprofloxacin tolerance to near-WT levels (Fig. 2I), suggesting that induction of this efflux system is sufficient to confer the PYO-mediated increase in tolerance. On the other hand, arabinose induction of the oxidative stress response genes *ahpB* or *katB* did not significantly increase tolerance of Δ*phz* to ciprofloxacin (S6A-B Fig); however, the levels of induction achieved for these two genes with arabinose were lower than those observed in the presence of PYO (S1 and S5 Figs). Importantly, the clinical relevance of *mexGHI-opmD* was previously not well known, as to our knowledge, there have been no reports of clinical mutants with constitutive overexpression of this efflux system. Taken together, our results demonstrate that PYO-mediated regulation of *mexGHI-opmD* expression modulates tolerance to a particular class of clinically used antibiotics in *P. aeruginosa*.

PYO promotes the evolution of antibiotic resistance in P. aeruginosa

Previous studies have demonstrated that mutations conferring antibiotic tolerance or persistence promote the evolution of antibiotic resistance (Levin-Reisman *et al.*, 2017; Windels *et al.*, 2019). Moreover, tolerance mutations can (i) interact synergistically with resistance mutations to increase bacterial survival during antibiotic treatment (Levin-Reisman *et al.*, 2019) and (ii) promote the establishment of resistance mutations during combination drug therapy (Liu *et al.*, 2020). To assess whether antibiotic tolerance induced by PYO could similarly promote the establishment of resistance mutations in populations of *P. aeruginosa* undergoing extended exposure to a clinical antibiotic, we next performed a series of fluctuation tests (Fig. 3A). In clinical settings, antibiotic resistance is likely to result in treatment failure if a pathogen can grow at antibiotic concentrations above a threshold commonly referred to as a "breakpoint." We adopted this criterion by selecting mutants on antibiotic concentrations equal to or higher than the breakpoints defined by the European Committee on Antimicrobial Susceptibility Testing (EUCAST) (EUCAST, 2020). Furthermore, we added PYO to our cultures either prior to the antibiotic selection step and/or concurrently with the antibiotic selection, in order to distinguish between the effects of preemptive versus continuous induction of PYO-regulated cellular defenses. Finally, while mutation rates inferred from fluctuation tests have sometimes been assumed to correlate with the per-base mutation rate across the genome (Bridges, 1980; Kohanski *et al.*, 2010), the results from these assays are also affected by the number of unique possible mutations that permit growth under the selection condition (Luria and Delbrück, 1943). To encompass both possibilities in this study, we use the term μ_{app} (apparent rate of mutation) as a proxy for the likelihood of evolving antibiotic resistance. We calculated this parameter using standard methods for fluctuation test analysis (see Methods).

Regardless of whether PYO was added prior to or concurrently with the antibiotic selection, PYO significantly increased μ_{app} for resistance to ciprofloxacin in log-phase cultures (Fig. 3B, S2 and S3 Table). The same trends were also observed in stationary-phase cultures, albeit with smaller effect sizes (S7A Fig). These results indicate that pre-treatment with PYO is sufficient but not necessary to increase μ_{app} for ciprofloxacin resistance. Adding PYO at both stages of the fluctuation test generally resulted in an even greater increase in μ_{app} (Fig. 3B, S7A Fig), and the increase in μ_{app} when PYO was added prior to antibiotic selection was dose-dependent (Fig. 3C). Cultures that were selected on levofloxacin similarly displayed an increased μ_{app} upon PYO treatment, though the

impact of pre-treatment vs. co-treatment with PYO varied across biological replicates (Fig. 3B, S2 and S3 Table). More importantly, PYO significantly increased μ_{app} for cultures that were grown in liquid SCFM and selected on SCFM plates containing ciprofloxacin (Fig. 3D, S3 Table), suggesting that PYO produced by *P. aeruginosa* could promote mutation to antibiotic resistance in chronically infected lungs of CF patients (Palmer *et al.*, 2007).

Because PYO did not increase tolerance to aminoglycosides (Fig. 2D, S4B Fig), we hypothesized that PYO would not promote mutation to aminoglycoside resistance if the induction of shared defense mechanisms was required for the observed increases in μ_{app}. On the other hand, if PYO affected μ_{app} primarily by acting as a mutagen, pre-treatment with PYO before antibiotic selection would be expected to increase μ_{app} by a similar proportion for resistance to all classes of antibiotics. To differentiate between these modes of action, we repeated the fluctuation tests using gentamicin and tobramycin, representative members of the aminoglycoside class that disrupt protein translation (Fair and Tor, 2014). Cultures that were pre-exposed to PYO consistently exhibited significant increases in μ_{app} for gentamicin resistance (Fig. 3E, S2 and S3 Table). For tobramycin resistance, on the other hand, pre-treatment with PYO only significantly increased μ_{app} in one out of four biological replicates (Fig. 3E, S2 and S3 Table). In addition, for both aminoglycosides, adding PYO to the antibiotic selection plates had no effect on μ_{app} in most replicates (Fig. 3E, S2 and S3 Table). These differing responses to PYO depending on the choice of clinical antibiotic suggested that the observed changes in μ_{app} were related to PYO-induced cellular defenses more so than a mutagenic effect of PYO. In fact, previous studies have suggested that gentamicin generates ROS more readily than tobramycin (Smith *et al.*, 1980; Prayle *et al.*, 2010). This could account for why the effect of pre-exposure to PYO on μ_{app} for resistance was greater for gentamicin than for tobramycin, given that PYO primes cells to detoxify ROS by inducing oxidative stress responses (S1 Fig). For resistance to fluoroquinolones, on the other hand, simultaneous induction of multiple defenses is likely necessary to recapitulate the increases in μ_{app} upon exposure to PYO. Overexpression of individual oxidative stress genes induced by PYO did not increase μ_{app} for ciprofloxacin resistance, while overexpression of the *mexGHI-opmD* efflux system only mildly increased μ_{app} in a subset of biological replicates (S7B Fig). Interestingly, the latter result contrasted with our finding that induction of *mexGHI-opmD* was sufficient to recapitulate PYO-mediated increases in fluoroquinolone tolerance. Together, our data suggest that while tolerance and resistance

can be mechanistically interrelated, overcoming the barrier to growing in the presence of an antibiotic in some cases requires a different or broader set of defenses than is required for temporary

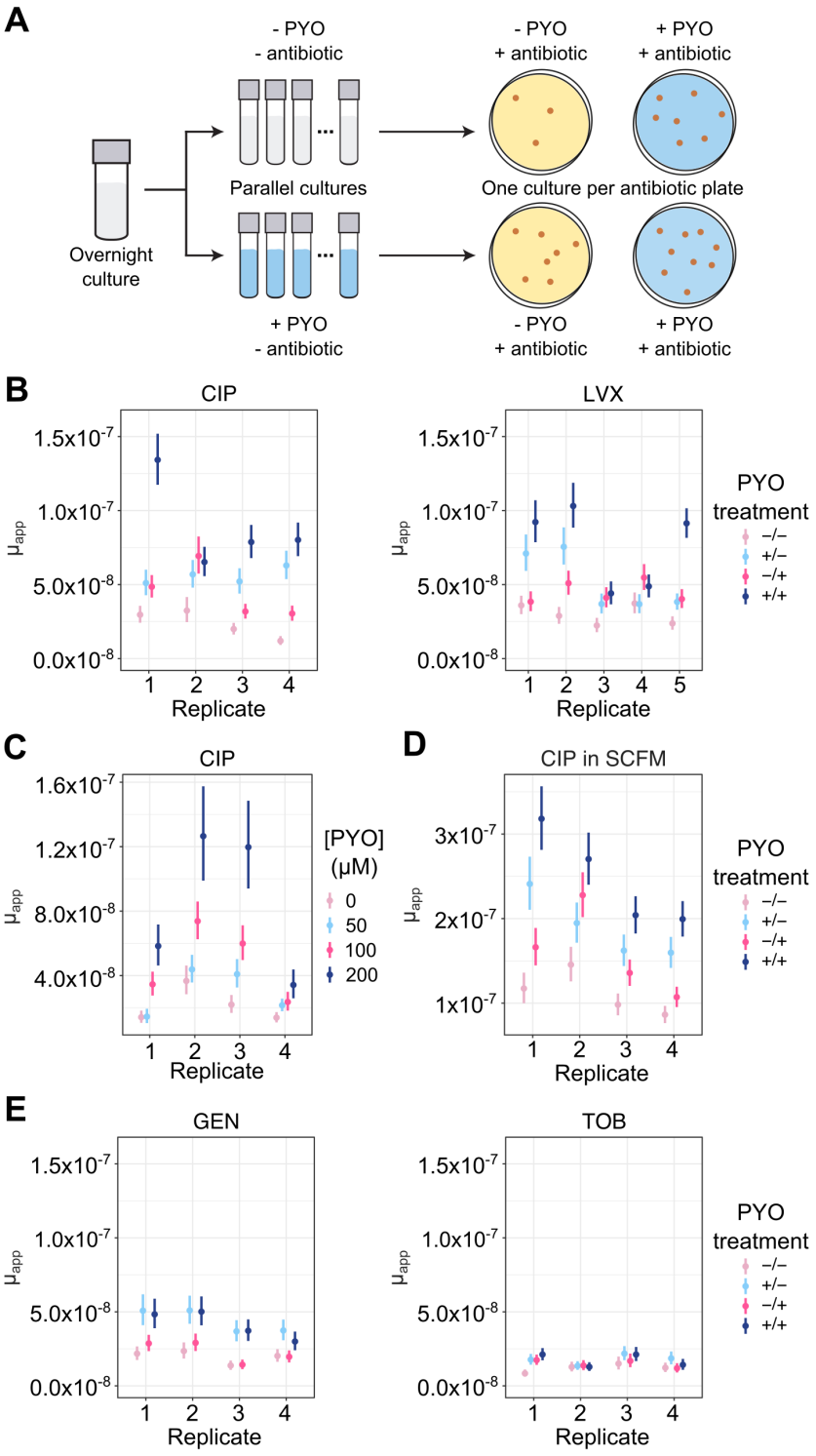

Figure 3 (see next page for legend).

Figure 3: PYO increases the apparent rate of mutation to antibiotic resistance in *P. aeruginosa*.
A. Experimental design for fluctuation tests to determine the effect of PYO (100 μM unless otherwise noted) on apparent mutation rates. For panels B-E, mutation rates were calculated using an established maximum likelihood-based method that accounts for the effects of plating a small proportion of the total culture volume (see Methods for details). Each data point in those panels represents a single biological replicate comprising 44 parallel cultures, and the vertical lines represent the 84% confidence intervals. Lack of overlap in these confidence intervals corresponds to statistical significance at the $p < 0.05$ threshold (Zheng, 2017). For statistical significance as determined by a likelihood ratio test, see S2 Table. In B, D, and E, the PYO treatments correspond to the following: -/- denotes no PYO pre-treatment (in the liquid culture stage) or co-treatment (in the antibiotic agar plates), +/- denotes PYO pre-treatment but no co-treatment, -/+ denotes PYO co-treatment without pre-treatment, and +/+ denotes both PYO pre-treatment and co-treatment.
B. Apparent mutation rates of log-phase Δ*phz* grown in glucose minimal medium and plated on MH agar containing ciprofloxacin (CIP, 0.5 μg/mL; n = 4) or levofloxacin (LVX, 1 μg/mL; n = 5), with or without pre- and/or co-exposure to PYO relative to the antibiotic selection step.
C. The apparent rate of mutation to resistance for Δ*phz* cells that were pre-treated with different concentrations of PYO and plated onto CIP (0.5 μg/mL).
D. Apparent mutation rates of log-phase Δ*phz* grown in SCFM and plated on SCFM agar containing CIP (1 μg/mL; n = 4) with or without pre- and/or co-exposure to PYO.
E. Apparent mutation rates of log-phase Δ*phz* grown in glucose minimal medium and plated during onto MH agar containing gentamicin (GEN, 16 μg/mL; n = 4) or tobramycin (TOB, 4 μg/mL; n = 4), with or without pre- and/or co-exposure to PYO.

survival under growth-arrested conditions. Nevertheless, PYO-induced defense mechanisms appear to contribute to both types of resilience to antibiotic treatment.

We envisioned at least three ways in which, under antibiotic selection, PYO-induced defense mechanisms could lead to the apparent increases in mutation rates: A) by enhancing the growth of pre-existing "partially-resistant" mutants during exposure to the antibiotic; B) by increasing the proportion of cells that survive and subsequently mutate to resistance while still in the presence of the antibiotic; or C) by a combination of A and B. To distinguish between these scenarios, we implemented a two-pronged approach. First, to explore the possibility of scenario A, we isolated and characterized several mutants from the fluctuation test plates containing ciprofloxacin. We re-grew the isolates under non-selective conditions both with and without PYO treatment and calculated the percentage of CFUs that could subsequently be recovered on ciprofloxacin plates relative to non-selective plates, as a metric for each isolate's level of resistance. We defined as "partially-resistant" those isolates for which only a subset of the population could grow under the antibiotic selection without PYO treatment, as evidenced by lower CFU counts on antibiotic plates compared to non-selective plates. Second, to determine the relative likelihoods of scenario A and scenario B, we examined the fit of our fluctuation test data to different formulations of the theoretical Luria-

Delbrück (LD) distribution. Specifically, we compared mathematical models that make different assumptions regarding whether mutants arise prior to or during the antibiotic selection.

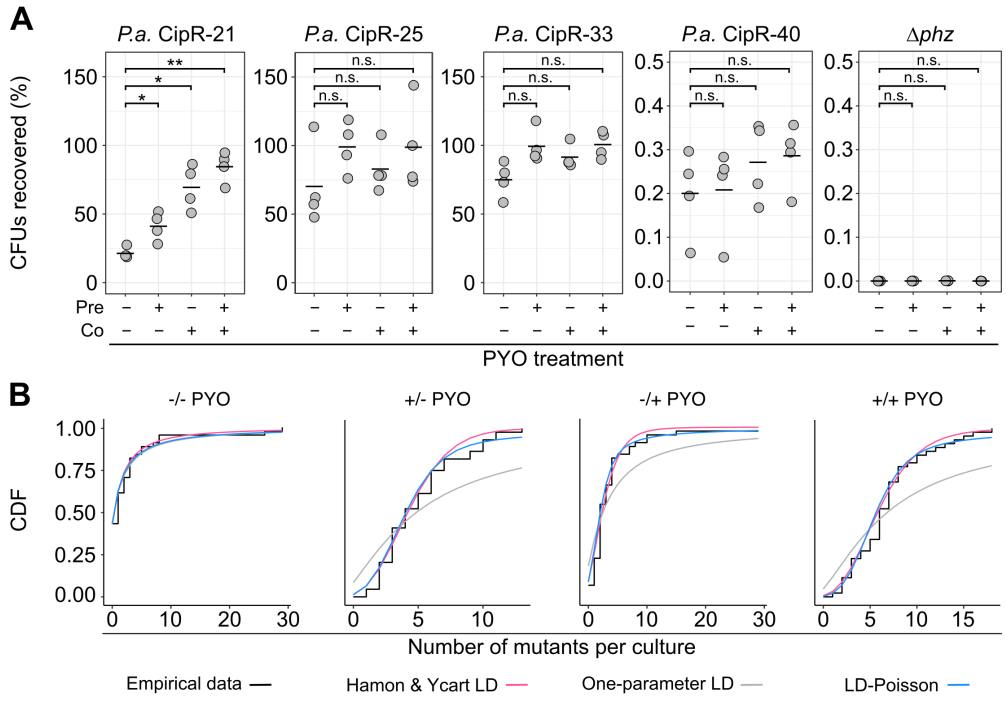

Figure 4. PYO promotes the growth of partially-resistant mutants and the occurrence of post-plating mutations.

A. Putative ciprofloxacin-resistant mutants of *P. aeruginosa* (*P.a.*) isolated from fluctuation test plates were grown to mid-log phase in liquid glucose minimal medium with or without 100 µM PYO, before plating for CFUs on non-selective agar plates, plates containing ciprofloxacin alone (0.5 µg/mL), and plates containing ciprofloxacin and PYO. Plotted values represent the percentage of CFUs recovered on the ciprofloxacin plates, calculated relative to total CFUs counted on non-selective plates. On the x-axis, "pre" denotes the presence of PYO in the liquid cultures and "co" denotes the presence of PYO in the agar plates. Data points represent independent biological cultures (n = 4). Black horizontal lines mark the mean values for each condition.

B. Goodness-of-fit of different mathematical models for *P. aeruginosa* Δ*phz* fluctuation test data. Data from the fluctuation tests performed on ciprofloxacin are plotted for different combinations of PYO in liquid (pre-treatment) and PYO in agar (co-exposure to antibiotic selection). The empirical cumulative distribution functions of the data (black) are plotted against 1) a variation of the Luria-Delbrück model fit with two parameters, *m* (the expected number of mutations per culture) and *w* (the relative fitness of mutant cells vs. WT), as implemented by Hamon and Ycart (2012) (pink); 2) a mixed Luria-Delbrück and Poisson distribution fit with two parameters, *m* and *d* (the number of generations that occur post-plating), allowing for the possibility of post-plating mutations, as implemented by Lang and Murray (2008) (blue); 3) the basic Luria-Delbrück distribution model fit only with *m*, as implemented by Lang and Murray (2008) (gray). In each condition, the plotted experimental data represent the biological replicate with the lowest chi-square goodness-of-fit *p*-value (i.e. least-good fit) for the Hamon & Ycart model, demonstrating that this model was still a reasonable fit for these samples.

Statistics: A – Welch's unpaired t-tests with Benjamini-Hochberg correction for controlling false discovery rate (* $p < 0.05$, ** $p < 0.01$, *** $p < 0.001$, n.s. $p > 0.05$).

We identified multiple partially-resistant mutants for which the percentage of CFUs recovered on ciprofloxacin plates following growth under non-selective conditions increased when the isolate was either pre-exposed or co-exposed to PYO (Fig. 4A), although the trends were not always statistically significant. Importantly, CFUs for the Δ*phz* parent strain were below the level of detection on the ciprofloxacin plates even in the presence of PYO, confirming that PYO-induced defenses alone, in the absence of a resistance mutation, were insufficient to enable growth under the selection condition used for the fluctuation tests (Fig. 4A). In addition, for all characterized partially-resistant mutants, the MIC for ciprofloxacin was higher than for the parent strain (S7 Table). For some of these mutants, the MIC determined according to standard clinical protocols (Determination of minimum inhibitory concentrations (MICs) of antibacterial agents by broth dilution, 2003) matched the ciprofloxacin concentration originally used for selection, even in the presence of PYO, but this is not surprising, as the relatively dilute inoculum (5×10^5 CFU/mL) and short incubation time (18 hrs) used for standard MIC assays can preclude detection of weak growth at a given antibiotic concentration. As a further validation of our assay for detection of partially-resistant mutants, we also tested isolates with distinct colony morphologies that were not enriched on the PYO-containing antibiotic plates relative to PYO-free antibiotic plates in the original fluctuation tests. As expected, these mutants were fully resistant to ciprofloxacin at the original selection concentration (S8A Fig), meaning that the same number of CFUs grew on both antibiotic plates and non-selective plates even in the absence of PYO. Interestingly, the effect of PYO on ciprofloxacin resistance varied across different partially-resistant isolates (Fig. 4A). This suggests that PYO does not universally raise the level of resistance of the entire population, but rather interacts synergistically with specific types of mutations conferring partial resistance. Such heterogeneity could account for why the effect of PYO in the fluctuation tests varied across biological replicates, as the degree of benefit conferred by PYO would depend on the specific mutations that randomly occurred in each replicate. We also repeated the stationary phase ciprofloxacin tolerance assay with the partially-resistant isolates and found that tolerance was likewise differentially affected by PYO (S8B Fig). Interestingly, the tolerance and resistance phenotypes shared no obvious underlying pattern, again suggesting that cellular processes that affect resistance do not always equally effect tolerance, and vice versa. Nevertheless, our results demonstrate that under antibiotic selection, a subset of partially-resistant mutants benefits from exposure to PYO.

Whole-genome sequencing revealed that the partially-resistant isolates contained mutations either in the efflux pump repressors *nfxB* or *mexS,* or in genes that affected growth rate, such as a ribosomal protein, a C4-dicarboxylate transporter, and a cell-wall synthesis gene (S4 Table). Mutations in *nfxB* or *mexS* were also found in the fully-resistant isolates (S4 Table), albeit at different loci compared to the partially-resistant isolates. Notably, *nfxB* is considered a "pathoadaptive gene" in which mutations tend to accumulate during chronic infections (Marvig, Sommer, *et al.*, 2015; Marvig, Dolce, *et al.*, 2015). Mutations in *mexS* are less common, but have also been detected in clinical isolates (Richardot *et al.*, 2016). Slow-growing small colony variant mutants of *P. aeruginosa* have likewise been isolated from patients (Häussler *et al.*, 1999; Malone *et al.*, 2010). Thus, the growth benefits conferred by PYO-induced defenses during antibiotic selection could be relevant to a variety of clinically-adapted strains.

That PYO increases μ_{app} at least in part by promoting the growth of pre-existing partially-resistant mutants was further supported by the alternative approach of evaluating the fit of our data to different mathematical models. Specifically, Pearson's chi-square test indicated that our data closely fit the Hamon and Ycart model (Hamon and Ycart, 2012) (Fig. 4B, S9 Fig, S3 Table), which allows for differential fitness of mutants compared to WT cells, but assumes that all mutants arise pre-plating. However, we could not unequivocally rule out the possibility that post-plating mutations contributed to the increases in μ_{app}, as a subset of our data also fit a mixed LD-Poisson model that assumes some mutations occurred during the antibiotic selection step (Lang and Murray, 2008) (Fig. 4B, S9 Fig, S3 Table). We also performed growth curves under the culture conditions used in our fluctuation tests prior to the antibiotic selection step, with the addition of the live-cell-impermeable DNA-binding dye propidium iodide as a marker for cell death. As expected from a previous study on PYO toxicity (Meirelles and Newman, 2018), cell death was undetectable prior to the sampling time point used in most of the fluctuation tests (S8D-E Fig). Thus, while increased population turnover due to stress can also lead to increases in μ_{app} (Frenoy and Bonhoeffer, 2018), this is unlikely to underlie the effect of PYO on μ_{app}. Together, these results suggest that the most probable explanation for the PYO-mediated increases in apparent mutation rates is a combined effect of increased detection of partially-resistant mutants (the proposed scenario A) and increased occurrence of post-plating mutations resulting from elevated survival on the antibiotic plates (the proposed scenario B).

Importantly, previous studies based on *in vitro* evolution experiments have demonstrated that even modest increases in mutation rates, in the range of two- to five-fold, significantly affect the maximum achievable level of antibiotic resistance for diverse bacterial pathogens (Orlén and Hughes, 2006; Ragheb *et al.*, 2019). Moreover, it is well-established that partial resistance can rapidly lead to acquisition of full resistance via secondary mutations (Toprak *et al.*, 2011; Baym *et al.*, 2016). Indeed, several putative mutants appeared fully resistant to ciprofloxacin in our CFU-recovery assay despite having been enriched by exposure to PYO in the fluctuation tests (S8C Fig). This discrepancy could be a result of acquiring secondary mutations either during growth on the original fluctuation test plates or during the pre-growth for the CFU-recovery assay. Thus, our results suggest that PYO may significantly affect the rate at which high-level resistance emerges in populations of *P. aeruginosa* undergoing long-term antibiotic exposure.

PYO promotes antibiotic tolerance in other opportunistic pathogens

While the above experiments were performed with single-species cultures, *P. aeruginosa* is found in polymicrobial communities in both natural environments (e.g. soil) and clinical contexts (e.g. chronic infections) (Green *et al.*, 1974; Fierer and Jackson, 2006; Lipuma, 2010; Stressmann *et al.*, 2012). We hypothesized that microbes that frequently interact with *P. aeruginosa* would have evolved inducible defense mechanisms against PYO toxicity, and that production of PYO by *P. aeruginosa* might therefore also increase tolerance and resistance to clinical antibiotics in these community members. To test this hypothesis, we focused on the genera *Burkholderia* and *Stenotrophomonas*, both of which are (i) soil-born gram-negative opportunistic pathogens that are frequently refractory to clinical antibiotic treatments (Berg *et al.*, 2005; Rhodes and Schweizer, 2016; Adegoke *et al.*, 2017), and (ii) found in co-infections with *P. aeruginosa*, e.g. in CF patients (Chmiel *et al.*, 2014). Specifically, we tested a soil-derived strain, *Burkholderia cepacia* ATCC 25416; a non-CF clinical isolate of *Stenotrophomonas*, *S. maltophilia* ATCC 13637; and several clinical isolates of the three most prevalent *Burkholderia* species found in CF patients (Lipuma, 2010): *B. cenocepacia*, *B. multivorans*, and *B. gladioli* (for descriptions of these strains, see S5 Table).

We first assessed each strain's intrinsic resistance to PYO (Fig. 5A), as we expected that strong defenses against PYO toxicity would be required in order to benefit from exposure to this

natural antibiotic. Indeed, for *S. maltophilia*, which was sensitive to PYO (Fig. 5A), the effects of PYO on antibiotic tolerance were complex: the presence of PYO was only beneficial when ciprofloxacin levels were low (1 µg/mL) (Fig. 5B). At a higher concentration of ciprofloxacin (10 µg/mL), PYO was detrimental in a dose-dependent manner (Fig. 5B), suggesting that the additional stress conferred by PYO outweighed any induction of defense mechanisms against ciprofloxacin.

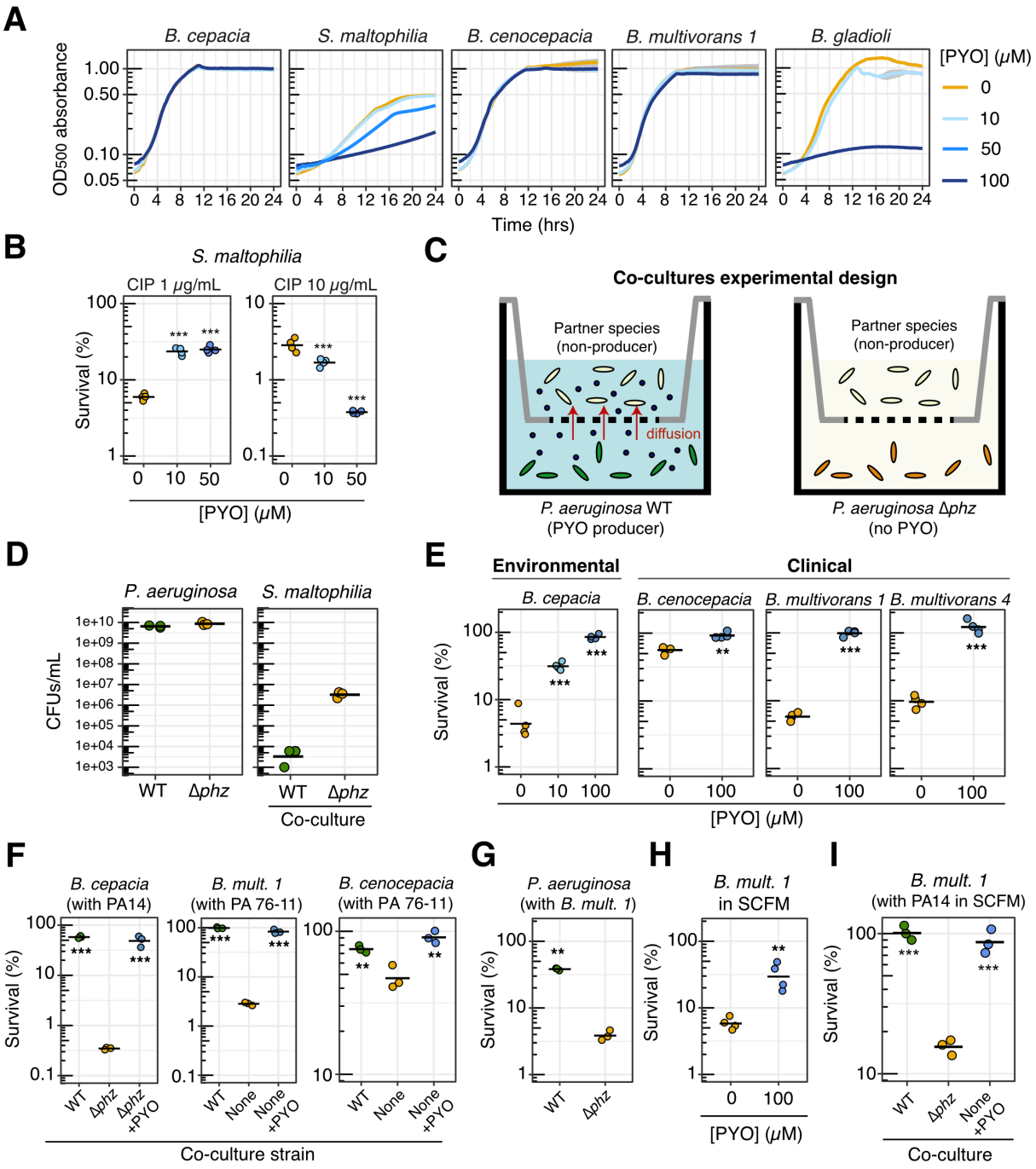

Figure 5 (see next page for legend).

Figure 5: PYO promotes antibiotic tolerance in other opportunistic pathogens.
A. Growth of several strains in the presence of different concentrations of PYO. Plotted lines represent averages of four to six replicates and shaded areas in gray represent the standard deviation. *Burkholderia multivorans 1* = *B. multivorans* AU42096. For complete information on strains, see S5 Table.
B. Tolerance of *S. maltophilia* to different concentrations of ciprofloxacin (CIP; 1 or 10 μg/mL) after growth in the presence of different concentrations of PYO (0, 10 or 50 μM) (n = 4).
C. Schematic depicting the experimental design for co-culture antibiotic tolerance assays (see Methods for details).
D. CFUs recovered from co-cultures of *P. aeruginosa* (PA14 WT and Δ*phz*) and *S. maltophilia* (n = 3), showing that the latter struggled to grow in the presence of *P. aeruginosa.*
E. Effect of PYO on the tolerance to ciprofloxacin (10 μg/mL) of multiple *Burkholderia* species isolated from environmental and clinical samples (n = 4).
F. Effect of PYO produced by *P. aeruginosa* in co-cultures on the tolerance of different *Burkholderia* species to ciprofloxacin (10 μg/mL). PA14 is our model laboratory strain of *P. aeruginosa*, while PA 76-11 is a PYO-producing strain of *P. aeruginosa* isolated from a CF patient. The *Burkholderia* strains were plated separately for CFUs to assess survival following treatment with ciprofloxacin in the co-cultures (n = 3).
G. Tolerance of *P. aeruginosa* PA14 WT and Δ*phz* to ciprofloxacin (1 μg/mL) when grown in co-cultures with *B. multivorans 1* (n = 3).
H. Effect of PYO on the tolerance to ciprofloxacin (10 μg/mL) of *B. multivorans 1* in SCFM (n = 4).
I. Tolerance to ciprofloxacin (1 μg/mL) of *B. multivorans 1* grown in co-cultures with P. *aeruginosa* PA14 WT, Δ*phz* or alone with 100 μM PYO added exogenously (n = 3).
Statistics: B, E, F, G, H, I – One-way ANOVA with Tukey's HSD multiple-comparison test for comparisons of three conditions or Welch's unpaired t-test for comparison of two conditions, with asterisks showing the statistical significance of comparisons with the untreated (no PYO or Δ*phz*) condition (* $p < 0.05$, ** $p < 0.01$, *** $p < 0.001$). In all panels, data points represent independent biological replicates, and black horizontal bars mark the mean values for each condition.

S. maltophilia also struggled to grow with *P. aeruginosa* in co-cultures (Fig. 5C-D), indicating that the conditions under which this species could potentially benefit from PYO are very limited.

B. cepacia, *B. cenocepacia,* and *B. multivorans*, on the other hand, were highly resistant to PYO (Fig. 5A). For these three species, exogenously-added PYO increased tolerance to ciprofloxacin (Fig. 5E). Furthermore, for *B. cepacia*, we confirmed that this effect was PYO dose-dependent (Fig. 5E). We therefore tested whether *P. aeruginosa* could induce tolerance to ciprofloxacin in co-cultures with these *Burkholderia* strains. Using liquid culture plates in which the two species were separated by a permeable membrane (Fig. 5C), we found that PYO-producing *P. aeruginosa* strongly induced tolerance to ciprofloxacin in the *Burkholderia* species, and that the observed tolerance phenotypes were recapitulated by addition of exogenous PYO to co-cultures of *Burkholderia* and the *P. aeruginosa* Δ*phz* mutant, or to control cultures with *Burkholderia* alone in the same setup (Fig. 5F). Notably, for *B. cenocepacia* and *B. multivorans*, increased ciprofloxacin tolerance was also observed in co-cultures with a PYO-producing strain isolated from a CF patient, *P. aeruginosa* PA 76-11 (Fig. 5F). In addition, even when co-cultured with *Burkholderia,* the *P.*

aeruginosa WT strain still showed elevated ciprofloxacin tolerance when compared to the non-PYO-producing Δ*phz* mutant (Fig. 5G). This indicates that the presence of *Burkholderia* did not alter *P. aeruginosa* tolerance patterns under our conditions. Finally, similar results were obtained for experiments performed in SCFM, where either the addition of exogenous PYO (Fig. 5H) or co-culture with *P. aeruginosa* (Fig. 5I) led to increased tolerance levels in *Burkholderia*. Together, these results suggest that PYO produced by *P. aeruginosa* in CF patients may decrease the efficacy of ciprofloxacin as a treatment for multispecies infections.

PYO promotes the evolution of antibiotic resistance in a co-occurring opportunistic pathogen

We next asked whether PYO could mediate an increase in apparent mutation rate for ciprofloxacin resistance in *Burkholderia* species. We chose *B. multivorans* AU42096 (*B. multivorans* 1 in Fig. 5) as our model strain for these experiments because, among the clinical isolates, it displayed the strongest response to PYO in the ciprofloxacin tolerance assays. Remarkably, when selecting *B. multivorans* mutants on ciprofloxacin, we observed PYO-mediated increases in μ_{app} that were far more dramatic than for *P. aeruginosa*: pre-treatment with PYO increased μ_{app} for *B. multivorans* approximately 10-fold, while co-exposure to PYO in the antibiotic plate without pre-exposure increased μ_{app} approximately 40-fold, and the combination of pre- and co-exposure to PYO increased μ_{app} by 230-fold (Fig. 6A, S3 Table). Notably, the magnitude of the latter effect is on par with observed differences between hypermutators, such as mutants deficient in the mismatch repair pathway, and their respective parent strains (Lee *et al.*, 2012; Martina *et al.*, 2014; Nunvar *et al.*, 2017). Moreover, hypermutators of *Burkholderia* isolated from CF infections are associated with clinical ciprofloxacin resistance (Martina *et al.*, 2014). In light of these observations, our results suggest that PYO could significantly affect clinical outcomes for co-infections of *P. aeruginosa* and *B. multivorans* treated with ciprofloxacin.

To verify that the *B. multivorans* colonies growing on ciprofloxacin in the presence of PYO were mutants, and to assess their responses to PYO, we isolated several putative mutants from the fluctuation test antibiotic plates and tested three in our CFU-recovery assay. All three displayed unique profiles of ciprofloxacin resistance in response to PYO treatment, as well as different maximal levels of resistance. However, all were more resistant than the WT parent strain in the presence of PYO, and none were noticeably resistant to ciprofloxacin in this assay without exposure

to PYO (Fig. 6B). MIC tests performed according to clinical standards revealed that the MIC of CipR-1 was indistinguishable from that of the parent strain, while the MIC of CipR-2 was two-fold higher than that of the parent strain in the absence of PYO but identical in the presence of PYO (S7 Table), reflecting the limitations of standard two-fold antibiotic dilution series for revealing mild increases in resistance. The MIC of CipR-7, on the other hand, was eight-fold higher than that of the parent strain, though in the absence of PYO, the MIC of this mutant was still below the ciprofloxacin concentration used in the fluctuation tests. Notably, for all tested *B. multivorans* isolates, including the WT parent, the addition of PYO to the standard MIC tests increased the MIC for ciprofloxacin by four- to eight-fold (S7 Table); however, even in the presence of PYO, the MIC for the parent strain was less than half of the ciprofloxacin concentration used in the tolerance assays, indicating that the observed tolerance phenotype for this strain cannot be fully explained by phenotypic

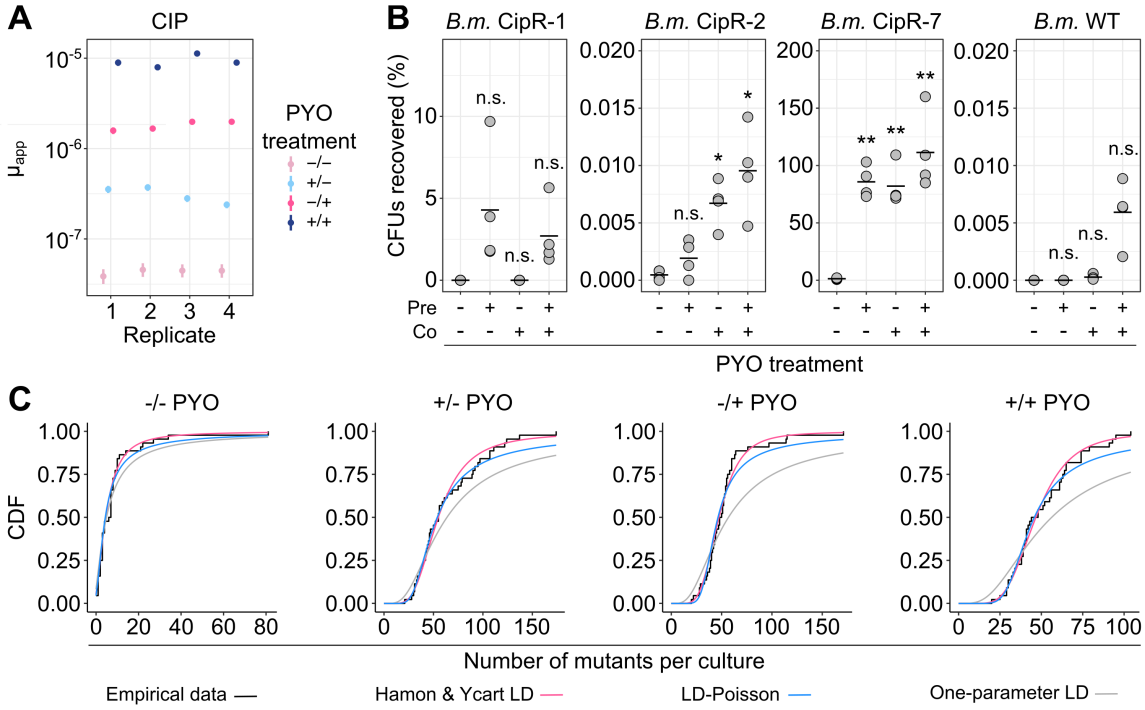

Figure 6. PYO promotes antibiotic resistance in *B. multivorans*.
A. The apparent rate of mutation to resistance when log-phase *B. multivorans 1* cells were plated on MH agar containing ciprofloxacin (8 µg/mL), with or without pre- and/or co-exposure to 100 µM PYO relative to the antibiotic selection step. Each data point represents a biological replicate comprising 44 parallel cultures (n = 4). The vertical lines represent 84% confidence intervals, in which lack of overlap corresponds to statistical significance at the $p < 0.05$ level (Zheng, 2017). The PYO treatments correspond to the following: -/- denotes no PYO pre-treatment (in the liquid culture stage) or co-treatment (in the antibiotic agar plates), +/- denotes PYO pre-treatment but no co-treatment, -/+ denotes PYO co-treatment without pre-treatment, and +/+ denotes both PYO pre-treatment and co-treatment. (*continued on next page*)

B. The percentage of CFUs recovered on ciprofloxacin plates either with or without PYO in the agar, for exponential phase cultures of different partially-resistant *B. multivorans 1* (*B.m.*) mutants that were pre-grown with or without PYO in liquid cultures. Plotted values represent the percentage of CFUs recovered on the ciprofloxacin plates, calculated relative to total CFUs counted on non-selective plates. On the x-axis, "pre" denotes the presence of PYO in the liquid cultures and "co" denotes the presence of PYO in the agar plates. Data points represent independent biological replicates (n = 4), and black horizontal bars mark the mean values for each condition.
C. Goodness-of-fit of different mathematical models for *B. multivorans 1* fluctuation test data. Data are plotted for different combinations of PYO in liquid (pre-treatment) and PYO in agar (co-exposure to antibiotic selection). The empirical cumulative distribution functions of the data (black) are plotted against 1) a variation of the Luria-Delbrück model fit with two parameters, *m* (the expected number of mutations per culture) and *w* (the relative fitness of mutant cells vs. WT), as implemented by Hamon and Ycart (2012) (pink); 2) a mixed Luria-Delbrück and Poisson distribution fit with two parameters, *m* and *d* (the number of generations that occur post-plating), allowing for the possibility of post-plating mutations, as implemented by Lang and Murray (2008) (blue); 3) the basic Luria-Delbrück distribution model fit only with *m*, as implemented by Lang and Murray (2008) (gray). In each condition, the plotted experimental data represent the biological replicate with the lowest chi-square goodness-of-fit *p*-value (i.e. least-good fit) for the Hamon & Ycart model.
Statistics: B – Welch's unpaired t-tests with Benjamini-Hochberg correction for controlling false discovery rate (* $p < 0.05$, ** $p < 0.01$, *** $p < 0.001$).

resistance. Interestingly, the percentage of the parent strain population that could grow on ciprofloxacin in the presence of PYO (Fig. 6B) was approximately equal to what would have been expected from the frequency of colonies detected in the fluctuation tests; moreover, when the CFU recovery assay was performed for the parent strain, the colonies that grew on ciprofloxacin in the presence of PYO exhibited diverse morphologies. This suggests that much of the parent strain growth on ciprofloxacin in the presence of PYO may have in fact reflected the growth of high-frequency spontaneous mutants, rather than background growth of the parent strain itself.

Whole-genome sequencing of the fluctuation test isolates revealed that *B. multivorans* CipR-1 possessed mutations in three uncharacterized regulatory genes (S6 Table). *B. multivorans* CipR-2 possessed mutations in two different homologs of the SpoT/RelA (p)ppGpp synthetase gene, which is known to affect antibiotic tolerance and resistance (Hobbs and Boraston, 2019). Finally, *B. multivorans* CipR-7 possessed a point mutation in DNA gyrase A (S83R), along with a point mutation in a malto-oligosyltrehalose synthase. Given that DNA gyrase A is the target of ciprofloxacin and that the specific mutated residue is likely homologous to the T83 residue that was mutated in a study of fluoroquinolone-resistant mutants in *B. cepacia* (Pope *et al.*, 2008), it is intriguing that this mutant was not able to grow on the original selection concentration of ciprofloxacin in the absence of PYO; however, the specific amino acid substitution in this strain may have resulted in only a mild disruption of ciprofloxacin binding.

Lastly, we asked whether the *B. multivorans* mutants we detected primarily arose prior to or during the antibiotic selection. In all cases, the distribution of mutants closely matched the Hamon and Ycart formulation of the theoretical LD distribution, suggesting that the detected mutants arose prior to the antibiotic exposure (Fig. 6C, S3 Table). Interestingly, the Hamon and Ycart model also predicted the average relative fitness of mutants detected in PYO-treated samples to be significantly lower compared to mutants detected in non-PYO treated samples (S3 Table; $p < 0.05$ for all three comparisons between non-PYO-treated and PYO-treated sample groups, using Welch's paired t-test with Benjamini-Hochberg corrections for controlling the false discovery rate). In addition, unlike for *P. aeruginosa*, the mixed LD-Poisson distribution that allows for post-plating mutations was a poorer fit than the Hamon and Ycart model for all PYO-treated *B. multivorans* samples (Fig. 6C, S3 Table). Together, these results suggest that in *B. multivorans*, PYO increases μ_{app} by promoting growth of a wider range of mutants that arise prior to antibiotic selection, including those with slower growth rates.

Discussion

Many clinical antibiotic resistance genes are thought to have originated in environmental microorganisms as responses to microbial chemical warfare, with subsequent mobilization into human pathogens via horizontal gene transfer (Martinez, 2009; Davies and Davies, 2010; Granato *et al.*, 2019). Here, we have demonstrated that tolerance and resistance to clinically relevant concentrations of synthetic antibiotics can also arise as a collateral benefit of natural antibiotic production by an opportunistic pathogen. *P. aeruginosa* is a particularly relevant example of an opportunistic pathogen whose self-produced natural antibiotics can promote resilience to clinical antibiotics, given the large number of chronic infections caused by this bacterium worldwide (Driscoll *et al.*, 2007) and the fact that PYO has been detected at concentrations up to 130 μM in lung infection sputum samples (Wilson *et al.*, 1988) and 0.31 mg/g in infected wound exudate (Cruickshank and Lowbury, 1953). Notably, treatments for infections caused by *P. aeruginosa* and other opportunistic pathogens often fail even when *in vitro* MIC tests indicate susceptibility to the chosen antibiotic (Chmiel *et al.*, 2014). Previous studies have attributed this discrepancy to metabolic and physiological changes within biofilms (Walters *et al.*, 2003; Olsen, 2015), which represent a major form of bacterial life within infections (Costerton *et al.*, 1999). Our results suggest that cellular defenses induced by bacterially-produced natural antibiotics may also contribute to *in vitro* versus

in vivo differences in antibiotic susceptibility, as standard MIC tests are inoculated at a low cell density (The European Committee on Antimicrobial Susceptibility Testing. Breakpoint tables for interpretation of MICs and zone diameters. Version 10.0, 2020), but *P. aeruginosa* typically does not make PYO *in vitro* until reaching a relatively high cell density (Dietrich *et al.*, 2006). Furthermore, the observation that PYO produced by *P. aeruginosa* strongly promotes antibiotic tolerance and resistance in *Burkholderia* species could hold important ramifications for the treatment of co-infections of these organisms in CF patients, for which clear best practices have yet to be established (Chmiel *et al.*, 2014). In particular, it could be prudent to avoid treating such infections with antibiotics for which PYO is likely to promote increased tolerance and resistance, such as fluoroquinolones, chloramphenicol, and trimethoprim/sulfamethoxazole—the latter two also being known substrates for efflux pumps that we have shown are upregulated by PYO (Driscoll *et al.*, 2007; Lister *et al.*, 2009).

Interestingly, our finding that PYO does not increase tolerance to aminoglycosides (Fig. 2D and S4B Fig) contrasts with the conclusions of two previous studies on phenazine-mediated antibiotic tolerance, which claimed that phenazines broadly increase tolerance to all classes of antibiotics except cationic peptides (Schiessl *et al.*, 2019; Zhu *et al.*, 2019). Importantly, however, these studies did not explore whether or which molecular defense mechanisms are induced by the phenazines and how these defenses might interact with clinical antibiotics. Moreover, the studies were performed under very different experimental setups, including different media, which can profoundly impact the outcomes of antibiotic susceptibility assays. One study focused on colony biofilms of *P. aeruginosa* that produced only phenazine-1-carboxylic acid and phenazine-1-carboxamide (Schiessl *et al.*, 2019), which are less toxic than PYO (Meirelles and Newman, 2018) and consequently may induce a different set of cellular responses. Alternatively, the observed increased tolerance to tobramycin in that study might not be related to molecular defenses induced by phenazines, but rather phenazine-mediated physiological differences under the studied conditions (Schiessl *et al.*, 2019). Phenazines are redox-active molecules that can promote metabolic activity under oxygen limitation, which occurs within biofilms (Dietrich *et al.*, 2013; Schiessl *et al.*, 2019; Saunders *et al.*, 2020); the specific details of how such metabolic activity might affect antibiotic tolerance merit further attention. The other previous study found that PYO increased planktonic culture cell densities in the presence of various antibiotics (Zhu *et al.*, 2019), but these experiments

did not directly demonstrate an effect on antibiotic tolerance (i.e. the ability to survive an otherwise lethal antibiotic treatment) (Brauner *et al.*, 2016). Notably, both studies found that phenazines actually increase sensitivity to cationic peptides, consistent with our observation that WT *P. aeruginosa* is less tolerant to colistin than the Δ*phz* strain. The mechanism of this synergistic lethality warrants further investigation. Our results highlight that identifying the cellular defenses induced by natural antibiotics, not only in the case of *P. aeruginosa* and phenazines, but also potentially other opportunistic pathogens and their endogenously-produced natural antibiotics, is essential for accurately predicting clinical antibiotic efficacy.

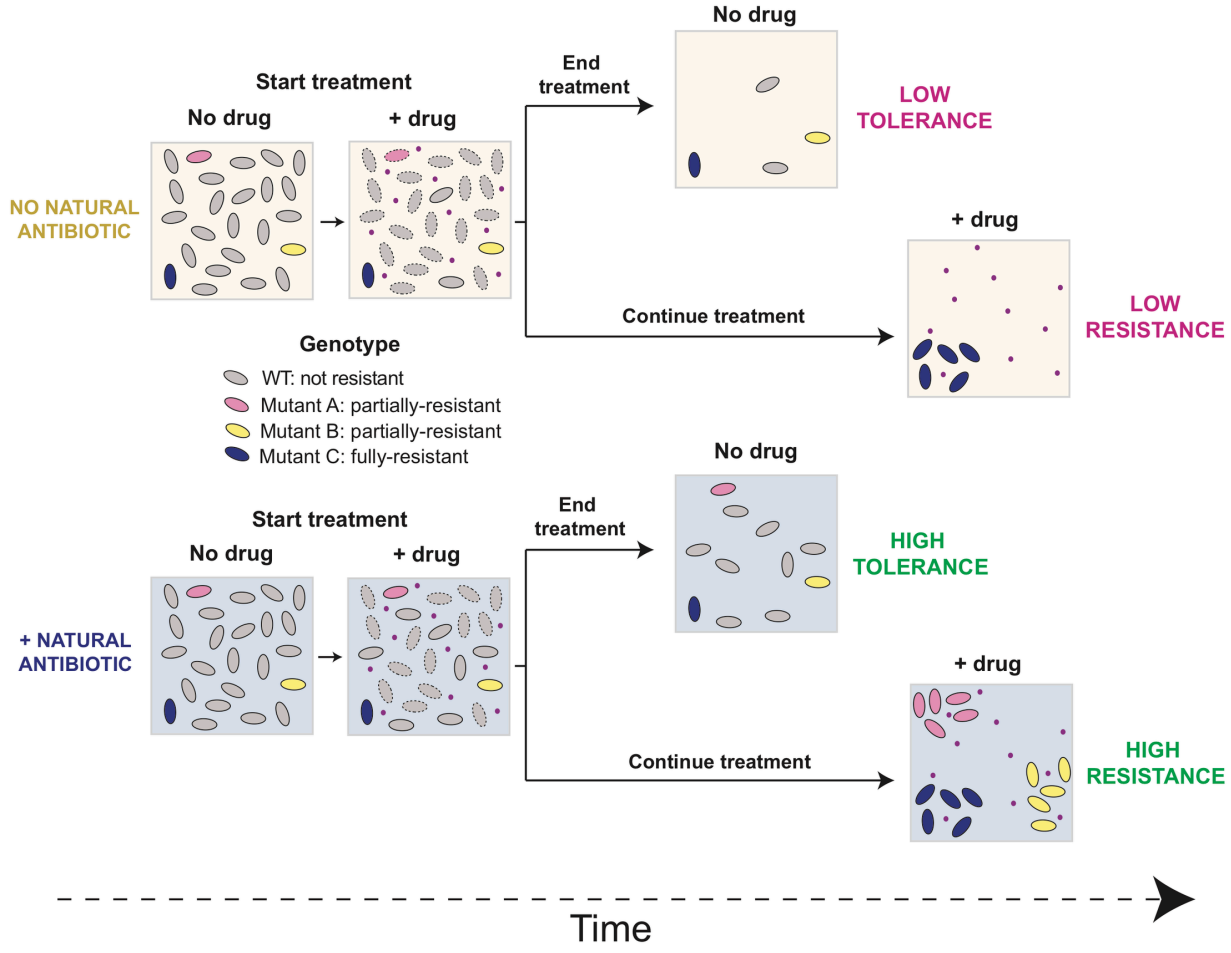

Figure 7: Proposed model for how natural antibiotics increase bacterial tolerance and resistance to clinical drugs.
In the first scenario (tolerance), cells are exposed to the clinical drug (pink dots) for a short period of time. Surviving cells will eventually re-start growth after the drug is removed. The presence of the natural antibiotic (bottom) increases tolerance of both WT and partially-resistant mutants. In the second scenario (resistance), cells are constantly exposed to the drug for an extended period of time, and only mutants are maintained in the population. The presence of the natural antibiotic (bottom) widens the population bottleneck and allows partially-resistant mutants to grow under drug selection, preserving a greater range of genetic diversity in the population.

Our results furthermore suggest that by inducing cellular defenses against specific clinical antibiotics, PYO widens the population bottleneck that occurs during antibiotic selection. This effect occurs via a two-pronged mechanism (Fig. 7). First, PYO increases the proportion of cells that survive short-term antibiotic treatments, which would inherently tend to preserve a greater range of genetic variation in the post-selection population. Second, PYO promotes the establishment of a broader range of resistant mutant lineages, which are likely primed to acquire further step-wise mutations to high-level resistance, yet may otherwise be lost during extended antibiotic treatment. Interestingly, a recent study demonstrated that lineages of spontaneous resistant mutants can be lost through stochastic cell death even at antibiotic concentrations well below the mutants' MICs (Alexander and MacLean, 2020). Thus, besides boosting the growth of partially-resistant mutants whose MICs failed to exceed the antibiotic concentrations used in our fluctuation tests, it is possible that PYO-induced defenses (e.g. enhanced efflux and oxidative stress responses) also increased apparent mutation rates by decreasing the stochastic loss of individual spontaneous mutants with higher MICs. In addition, a recent study in *Staphylococcus aureus* highlighted the important role that pre-existing genetic diversity in the population can play in shaping the evolution of antibiotic resistance (Papkou *et al.*, 2020). In particular, even small variations in efflux-mediated intrinsic resistance of parent strains significantly affected the probability that a population would evolve resistance under ciprofloxacin selection at the clinical breakpoint concentration (Papkou *et al.*, 2020). Multiple studies have also demonstrated additive or synergistic interactions between increased drug efflux and classical ciprofloxacin resistance mutations (Oethinger *et al.*, 2000; Bruchmann *et al.*, 2013; Papkou *et al.*, 2020). We observed a similar phenomenon in our *B. multivorans* CipR-7 strain, which had acquired a mutation in the cellular target of ciprofloxacin (i.e. DNA gyrase A), yet still required exposure to PYO in order to grow at the ciprofloxacin concentration on which it was originally selected (Fig. 6B). Together, these findings suggest that microbial production of natural antibiotics in the context of an infection could dynamically, and in some cases dramatically, affect the evolvability of opportunistic pathogens challenged with clinical drugs.

Beyond *P. aeruginosa* and PYO, our proposed model for collateral benefits of exposure to natural antibiotics (Fig. 7) potentially represents a broader phenomenon among human pathogens than has previously been appreciated. Many opportunistic pathogens originate in environments like

soil (LiPuma *et al.*, 2002; Berg *et al.*, 2005), where they have evolved in the presence of diverse natural antibiotics (Martinez, 2009; Davies and Davies, 2010), and *P. aeruginosa* is not the only pathogen with the capacity to synthesize its own antibiotics. For example, *Burkholderia* species possess the biosynthetic capability to produce a variety of compounds with antibacterial activity, whose potential clinical significance has not been explored (Depoorter *et al.*, 2016). If a given natural antibiotic induces expression of a molecular defense, the only requirement for a consequent increase in tolerance to a clinically-relevant drug would be that the induced defense has some efficacy against the drug—e.g. due to structural similarities like those shared by PYO and fluoroquinolones. This inference is supported by recent evidence that certain food additives and synthetic drugs antagonize the efficacy of specific clinical antibiotics by triggering stress responses in cells, including the induction of efflux pumps (Brochado *et al.*, 2018), and that exposure to a clinical drug to which a strain is already resistant can collaterally affect its development of tolerance and resistance to other drugs (Imamovic *et al.*, 2018). In fact, bacterially-produced toxic metabolites that promote antibiotic tolerance and resistance in human pathogens need not be limited to the types of molecules traditionally thought of as natural antibiotics. For example, indole secretion by highly antibiotic-resistant spontaneous mutants of *Escherichia coli* enables partially-resistant mutants within the same species to grow at drug concentrations above their own MICs, in part by stimulating efflux pump expression (Lee *et al.*, 2010). Unlike PYO, indole is generally thought of as a signaling molecule rather than a natural antibiotic (Kumar and Sperandio, 2019), though it can likewise be toxic to bacteria at high concentrations (Garbe *et al.*, 2000; Kumar and Sperandio, 2019). Efforts to identify and characterize additional examples of such metabolites produced by opportunistic human pathogens could lead to an improved understanding of the modes of antibiotic treatment failure in clinics, and ultimately inform the design of more effective and longer-lived therapies.

Methods

Culture media and incubation conditions

Different culture media were used for different experiments as indicated throughout the Methods. Succinate minimal medium (SMM) composition was: 40 mM sodium succinate (or 20 mM, if specified), 50 mM KH_2PO_4/K_2HPO_4 (pH 7), 42.8 mM NaCl, 1 mM $MgSO_4$, 9.35 mM NH_4Cl, and a trace elements solution (Widdel and Pfennig, 1981). Glucose minimal medium (GMM) was

identical to SMM, except with 10 or 20 mM glucose (as specified for different experiments) instead of succinate. SMM and GMM were prepared by autoclaving all components together for 20 min at 121 °C, except for the carbon source and the 1000x trace elements stock solution, which were filter-sterilized and added separately; interestingly, we found that autoclaving $MgSO_4$ with the other components was crucial for consistent PYO production by WT *Pseudomonas aeruginosa* UCBPP-PA14 in GMM. Luria-Bertani (LB) Miller broth (BD Biosciences) and BBL Cation-Adjusted Mueller-Hinton II (MH) broth (BD Biosciences) were prepared according to the manufacturer's instructions (notably with only a 10 min autoclave step for MH medium), with the addition of 1.5% Bacto agar (BD Biosciences) to make solid media. Synthetic cystic fibrosis sputum medium (SCFM) composition was prepared as described previously (Palmer *et al.*, 2007), with 1.355mM K_2SO_4 and no nitrate. In addition, 3.6 μM $FeSO_4.7H_2O$ and 0.3 mM N-acetyl-glucosamine were added (Turner *et al.*, 2015). All components except for the latter two were dissolved together, sterilized by filtration through a 0.22 μm membrane, and stored for up to two weeks; $FeSO_4.7H_2O$ and N-acetyl-glucosamine solutions were prepared fresh each time or stored at -20 ºC, respectively, and added to SCFM on the day of use. For SCFM agar, a 2x solution of the medium components was prepared and added to a separately autoclaved 3% molten agar solution, for a final concentration of 1x SCFM and 1.5% agar.

Antibiotics were prepared in concentrated stock solutions (100x or greater) and stored at -20 ºC. Ciprofloxacin was dissolved in 0.1 M or 20 mM HCl, while levofloxacin, gentamicin, tobramycin, and colistin were dissolved in sterile deionized water. Phenylalanine-arginine β-naphthylamide (PAβN) dihydrochloride (MedChemExpress) was dissolved in sterile deionized water (50 mg/mL). Pyocyanin (PYO) was synthesized and purified as previously described (Cheluvappa, 2014; Costa *et al.*, 2017) and dissolved in 20 mM HCl to make 10 mM stock solutions. Experiments involving exogenous PYO always included negative controls to which an equivalent volume of 20 mM HCl was added. In addition, MH agar plates were buffered to pH 7 with 10 mM morpholinepropanesulfonic acid (MOPS) to avoid any pH changes upon addition of PYO or HCl; all other media used with exogenous PYO were already inherently buffered. Incubations were always done at 37 ºC, with shaking for liquid cultures (250 rpm), unless mentioned otherwise.

Strain construction

In this study, we use PA14 as an abbreviation for UCBPP-PA14. *P. aeruginosa* PA14 was used for all experiments unless otherwise noted. For a full list of strains made in this study, see S5 Table. Three types of strains were made in different *P. aeruginosa* PA14 backgrounds: (i) unmarked deletions, used for Tn-seq validation experiments; (ii) fluorescent strains for time-lapse microscopy experiments; and (iii) strains overexpressing one of the following three systems: *mexGHI-opmD*, *ahpB*, and *katB*. Established protocols were used for all these procedures (Babin *et al.*, 2016).

Briefly, for unmarked deletions, ~1kb fragments immediately upstream and downstream of the target locus were cloned using Gibson assembly into the pMQ30 suicide vector (Shanks *et al.*, 2006; Gibson *et al.*, 2009). Fragments amplified from *P. aeruginosa* PA14 genomic DNA (gDNA) and cleaned up using the Monarch PCR Purification kit (New England Biolabs) were used for Gibson assembly together with pMQ30 cut with SacI and HindIII. The assembled construct was then transformed into *Escherichia coli* DH10B, with transformants being selected in LB with 20 μg/mL gentamicin. All correctly-assembled plasmids were identified by colony PCR and verified by Sanger sequencing (Laragen). Next, for the insertion of the constructs into *P. aeruginosa* PA14 genome, tri-parental conjugation was performed following Choi and Schweizer (Choi and Schweizer, 2006). All unmarked deletions were done in the *P. aeruginosa* PA14 Δ*phz* background (both *phzA-G1* and *phzA-G2* operons are deleted in this strain (Dietrich *et al.*, 2006)), allowing clean experiments by addition of exogenous phenazines. Merodiploids containing the construct integrated into their genomes were selected on VBMM medium (3 g/L trisodium citrate, 2 g/L citric acid, 10 g/L K_2HPO_4, 3.5 g/L $NaNH_4HPO_4{\cdot}4H_2O$, 1 mM $MgSO_4$, 100 μM $CaCl_2$, pH 7) with 100 μg/mL gentamicin following Choi and Schweizer (Choi and Schweizer, 2006). Finally, merodiploids were then plated on LB lacking NaCl and containing 10% sucrose to select for colonies resulting from homologous recombination. Colonies missing the target locus (unmarked deletions) were identified by PCR. For all primers used, see S5 Table.

Fluorescent strains used in time-lapse microscopy were made using previously published plasmids (Babin *et al.*, 2016; Basta *et al.*, 2017). Constructs containing GFP and mApple florescent proteins under the control of the ribosomal *rpsG* gene were inserted in the *att*Tn7 site of

P. aeruginosa PA14 Δ*phz* chromosome by tetra-parental conjugation, followed with selection on VBMM with 100 µg/mL gentamicin (Choi and Schweizer, 2006).

Finally, overexpressing strains were made as previously described (Babin *et al.*, 2016). The previously-made overexpression construct (pUC18T-miniTn7T-GmR vector containing the arabinose-inducible promoter P_{ara} (Babin *et al.*, 2016)) and the three different targets (*mexGHI-opmD*, *ahpB* and *katB*) were all amplified by PCR. Next, using Gibson assembly, the targets were cloned downstream of P_{ara} in the pUC18T-miniTn7T-GmR vector, resulting in the three different overexpression constructs: P_{ara}*:mexGHI-opmD*, P_{ara}*:ahpB*, and P_{ara}*:katB*. The final constructs were introduced into the *att*Tn7 of the *P. aeruginosa* PA14 Δ*phz* background strain by tetraparental conjugation (Choi and Schweizer, 2006).

Transposon-sequencing (Tn-seq) experiment

The Tn-seq experiment was performed following the design presented in Fig. 1A. Two aliquots of the *P. aeruginosa* PA14 transposon library previously prepared (Basta *et al.*, 2017) were thawed on ice for 15 min, diluted to a starting optical density (OD_{500}) of 0.05 in 50 mL of SMM, and grown aerobically under shaking conditions (250 rpm) at 37 ºC for ~ 4-5 generations to an OD_{500} of 0.8-1. These growing conditions were used for all the stages of the experiment. After growth in SMM, each aliquot was considered an independent replicate. Cells from each replicate were pelleted, washed, and resuspended (5 mL in 18 x 150 mm glass tubes, OD_{500} = 2) in minimal phosphate buffer (MPB - 50 mM KH_2PO_4/ K_2HPO_4[pH 7], 42.8 mM NaCl) with and without 100 µM PYO. Cells were then incubated for 26 hrs under shaking conditions at 37 ºC. Therefore, the experiment consisted of four different samples that were later sequenced: (i) "R1 No PYO," (ii) "R1 + PYO," (iii) "R2 No PYO," and (iv) "R2 + PYO". After the incubation, cultures from all treatments were pelleted, washed again to remove PYO, and resuspended in fresh SMM. Immediately, an aliquot of each sample was diluted to a starting OD_{500} of ~0.05 in 25 mL SMM, followed by outgrowth for ~4-5 generations to an OD_{500} of 0.8-1. After outgrowth, 2.5 mL of each sample was pelleted and stored at -80 ºC.

Genomic DNA was extracted from the pelleted samples using the DNeasy Blood & Tissue kit (Qiagen). All the steps for sequencing library preparation followed exactly the protocol used by

Basta *et al*. (2017), including (i) DNA shearing by sonication (to produce 200-500 bp fragments), (ii) end-repair, (iii) addition of poly(C) tail, and (iv) enrichment of transposon-genome junctions and addition of adapter for Illumina sequencing by PCR (van Opijnen *et al.*, 2014; Basta *et al.*, 2017). The resulting amplified DNA samples were sequenced using 100 bp single-end reads on the Illumina HiSeq 2500 platform at the Millard and Muriel Jacobs Genetics and Genomics Laboratory at Caltech. Data analysis also followed Basta *et al*. (2017). In summary, sequences were mapped to the *P. aeruginosa* UCBPP-PA14 genome sequence using Bowtie 2 (Langmead and Salzberg, 2012) and were analyzed in MATLAB using the ARTIST Tn-seq analysis pipeline (Pritchard *et al.*, 2014), with non-overlapping windows of 100 bp across the genome (Pritchard *et al.*, 2014; Basta *et al.*, 2017). Using the Mann-Whitney U statistical test, the total reads mapping for each gene in the "+PYO" samples were compared to the corresponding reads in the "No PYO" control for each replicate independently (Pritchard *et al.*, 2014; Basta *et al.*, 2017). Next, the read ratio for each replicate was calculated within ARTIST for each gene and then $\log_2$-transformed. Finally, the *p*-values for both replicates were combined using the Fisher's combined probability test as done in Basta *et al.* (2017), and the average of the $\log_2$-ratios of the two replicates are also shown. For the $\log_2$-ratios and *p*-values for all PA14 genes, see S1 Table. For heatmaps shown in Fig. 1A, the average $\log_2$-ratios (fitness) for the selected genes were plotted using the *geom_tile()* function from the ggplot2 package in R (R Core Team, 2018; Wickham, 2016).

Tn-seq datasets correlation analysis

To compare the results of this Tn-seq analysis with a previously published study (Cameron *et al.*, 2018) analyzing fitness determinants for survival during ciprofloxacin treatment in the *P. aeruginosa* PAO1 strain background (Fig. 1E and S1 Table), the data from that study's supplemental Table S1 were used. The normalized average ratio of reads in the treated sample compared to reads in the input sample for each gene (geometric mean of 3 replicates) was $\log_2$-transformed for comparison to the Tn-seq data described above. The list of genes was filtered to include only genes for which ratios were reported in both our PYO Tn-seq experiment and the ciprofloxacin Tn-seq study, and for which there are clear orthologs in both strains (n = 4209 genes). Orthologs were determined using the "pseudomonas.com" database (Winsor *et al.*, 2016).

Tn-seq validation experiments

To validate the Tn-seq results (Fig. 1C), experiments were performed by comparing the survival of four different mutants (Δ*phz*Δ*ackA*Δ*pta*, Δ*phz*Δ*lptA*, Δ*phz*Δ*mexS*, and Δ*phz*Δ*dctBD*) to the survival of the Δ*phz* strain upon exposure to PYO. The experimental design was very similar to the one used for the Tn-seq, with minor adaptations. An overnight culture (5 mL) of each strain was grown in SMM (40 mM succinate) from LB plates. Cells were washed and re-suspended at an OD_{500} of 0.1 (or 0.25 for Δ*phz*Δ*dctBD*) in the same medium to start the new cultures (5 mL), which were grown to OD_{500} ~0.8-1, pelleted, washed, and re-suspended in the same minimal medium without succinate (no carbon source) at OD_{500} of 1. For each strain, the culture was split across 8-12 wells (150 µL cultures) in a 96-well plate, with 100 µM PYO added to half of the cultures. 70 µL of mineral oil was added to the top of the wells to prevent evaporation. Propidium iodide (PI) at 5 µM was also added to the cultures to monitor cell death (Meirelles and Newman, 2018). The plate was then moved to a BioTek Synergy 4 plate reader and incubated under shaking conditions at 37 ºC for 24 hrs. After incubation, cultures were serially diluted in buffer and plated for colony forming units (CFUs) on LB agar, and survival in the presence of PYO was compared to the no-PYO control. Plates were incubated at room temperature (RT) and CFUs were counted after 36-48 hrs. In this study, a stereoscope was always used to count the CFUs. Survival levels were calculated for each mutant (i.e. for each replicate, the % survival for "+PYO" was calculated based on CFUs for "No PYO"). Then, the survival levels for each mutant were normalized by the survival levels of the Δ*phz* parent strain (i.e. % survival for "+PYO" for each mutant was divided by the average % survival for "+PYO" of the Δ*phz* strain); these "fitness" values were $\log_2$-transformed for plotting.

PYO tolerance with efflux inhibitor

Survival assays with efflux inhibition were performed to test the importance of efflux systems in *P. aeruginosa* for tolerance against PYO toxicity. From a Δ*phz* overnight culture pre-grown in SMM (20 mM succinate), a new 7 mL culture was started in fresh SMM at an OD_{500} of 0.05 and was incubated for around 10 hrs (enough to reach stationary phase). Cells were then pelleted, washed, and re-suspended in MPB at an OD_{500} of 1 (10 mL of culture was prepared). The culture was then split into four different treatments: (i) no PYO, no PAβN; (ii) 100 µM PYO, no PAβN; (iii) no PYO, with PAβN (50 µg/mL), and (iv) 100 µM PYO, with PAβN. Each of the

treatments were split across 12 wells containing 150 µL of culture + 70 µL of mineral oil in a 96-well plate. The plate was incubated at 37 ºC under shaking conditions using a BioTek Synergy 4 plate reader. Samples were serially diluted in MPB and plated for CFUs on LB agar after 12, 24, and 48 hrs. Survival for treatments containing PYO were calculated based on the CFUs counted for the negative control without PYO (Fig. 1D). At each time point, four wells were sampled, with each well considered an independent replicate. The experiment was repeated twice with similar results.

Antibiotic tolerance experiments using P. aeruginosa

Tolerance assay for WT, Δ*phz*, and Δ*phz* + PYO. For most antibiotic tolerance assays (except for tolerance using cells harvested during log-phase, see below), the experimental design shown in S4A Fig. was followed. WT and Δ*phz* cells were grown from a plate into overnight cultures in GMM with 20 mM glucose. Next, WT and Δ*phz* cells were pelleted, washed, and re-suspended at an OD_{500} of 0.05 in four independent new cultures (replicates) in GMM (10 mM glucose) per treatment. Three treatments were prepared: WT, Δ*phz* (no PYO), and Δ*phz* + 100 µM PYO, with four independent biological replicates for each. Each of the four individual cultures (replicates) were incubated for around 20 hrs, reaching stationary phase, in 7 mL cultures (18 x 150 mm glass tubes). Each individual culture (replicate) was then split into a negative control (no antibiotic) or antibiotic treatment (2 mL of culture per each treatment, using plastic Falcon tubes, VWR Cat. No. 352059). After addition of the antibiotic from concentrated stocks, cultures were incubated for four hours, serially diluted in MPB, and then plated for CFUs on LB agar. Unless stated otherwise, cells were not washed before plating. We observed that washing the cells did not make any difference in the outcome of the experiments. In addition, washing was not feasible for the tolerance assays using smaller volumes (i.e. in 96-well plates). The only two experiments where washing was performed are described below ("Tolerance assay with PAβN" and "Tolerance assay to measure the lag in CFUs appearance"). In these cases, cells were washed because (i) the ciprofloxacin concentrations were higher (10 µg/mL) and more likely to affect *P. aeruginosa* cells on the plate, and (ii) for the case of the PAβN experiment, we wanted to avoid having cells be in contact with the inhibitor while growing on the plate. Antibiotics were used at the concentrations mentioned in figure legends. Plates were incubated at RT and CFUs were counted after 36-48 hrs. Plates were always checked again after seven days to count any late-arising CFUs. Importantly, for all tolerance experiments performed in

this study (including this and all experiments described below), each experiment was repeated at least twice on different days, with similar results.

The same protocol was followed for the experiment testing different concentrations of PYO (Fig. 2H) and for the experiment testing how PYO impacts tolerance of different *P. aeruginosa* mutants with partial resistance to ciprofloxacin (CipR-21, 25, 33, and 40, S7E Fig). For the experiment testing tolerance after exposure to different phenazines (Fig. 2E), all the phenazines were dissolved in a common solvent (DMSO), which was used as the negative control; these experiments were performed in a Δ*phz** mutant lacking not only the *phzA-G1* and *phzA-G2* operons, but also all phenazine modification genes, to prevent the transformation of phenazine 1-carboxylic acid (PCA) into the other phenazines (see S5 Table). For experiments performed in synthetic cystic fibrosis sputum medium SCFM (Fig. 2D), the same experimental design was followed, with the exception that SCFM was used instead of GMM.

Tolerance assay for strains with arabinose-inducible constructs. For these experiments (Fig. 2I and S6B Fig), the 20 hr cultures of each strain (Δ*phz* P_{ara}*:mexGHI-opmD,* Δ*phz* P_{ara}*:ahpB* and Δ*phz* P_{ara}*:katB*) were grown with and without 20 mM arabinose for induction of the controlled systems, and then exposed to ciprofloxacin the same way described above. To rule out any non-specific interference of the inducer, negative controls with and without 20 mM arabinose using the parent Δ*phz* strain (without the insertions in the *att*Tn7 site) were also done. Adding arabinose to the Δ*phz* strain did not impact tolerance levels (S6 Fig).

Tolerance assay with PAβN. Experiments using the efflux inhibitor PAβN (S4G Fig) were also performed similarly to the way as described above. The only differences were that after the 20 hrs incubation and before the addition of the antibiotic, PAβN was added to the cultures at a final concentration of 50 μg/mL. Cultures were incubated for 15 min and then ciprofloxacin was added, followed by a four-hour incubation. For these experiments, instead of plating cells directly on LB, 1 mL of culture of each replicate/treatment was pelleted (12500 rpm for 2 min), washed in MPB for removal of ciprofloxacin and PAβN, and only then serially diluted in MPB and plated on LB for CFU counting.

Tolerance assay to measure the lag in CFU appearance. This experiment (S4F Fig) followed the same general protocol described above (using 10 μg/mL of ciprofloxacin). The difference was that the reported CFUs were counted after incubation of LB plates for two days and seven days, whereas otherwise only the final counts from the seventh day were reported. This was done to quantify lag in the CFUs' growth under the studied conditions. Similarly to the tolerance assays with PAβN and ciprofloxacin described above, cells were pelleted and washed before plating on LB for CFU counting.

Tolerance assay for cells harvested during log-phase. Δ*phz* cells were grown in overnight cultures in GMM (20 mM glucose). Next, cells were pelleted, washed, and re-suspended into two new cultures, one with PYO (100 μM) and one without PYO, at an OD_{500} of 0.05 in GMM (10 mM glucose, 7 mL cultures). Cultures were grown until OD_{500} = 0.5 (around 5-6 hrs). Cells were then washed and re-suspended in the same medium at an OD_{500} of 0.5, but without the nitrogen source (i.e. no NH_4Cl). PYO was re-added after washes to the culture that was pre-grown with PYO. The cultures, one with and one without PYO, were then split into different treatments: negative control (no antibiotic), ciprofloxacin (0.5 μg/mL), levofloxacin (1 μg/mL), gentamicin (16 μg/mL), and tobramycin (4 μg/mL). Then, they were all transferred to wells in a 96-well plate (three to four wells per treatment, with each well being considered an independent replicate). Cultures within wells contained 150 μL with an additional 70 μL of mineral oil on top to prevent evaporation. The depletion of nitrogen prevented growth in the negative control, which limited overestimation of the antibiotic killing effect (because survival rates were calculated relative to the negative control). The plates were incubated for four hours at 37 ºC under shaking conditions (175 rpm) using a benchtop incubator (VWR incubator orbital shaker). The 96-well plate was kept inside an airtight plastic container with several wet paper towels to maintain high humidity attached to the shaker. After incubation, cells were serially diluted and plated on LB agar for CFU counting (S4B Fig). A similar experiment was also performed with the strains containing arabinose-inducible constructs (Δ*phz* P_{ara}*:mexGHI-opmD,* Δ*phz* P_{ara}*:ahpB* and Δ*phz* P_{ara}*:katB*) and the Δ*phz* background control (S6A Fig), for which tolerance to ciprofloxacin (0.5 μg/mL) was tested. The experiment followed the same protocol described above, with the difference that, instead of presence or absence of PYO, strains were incubated in the presence or absence of 20 mM arabinose.

Time-lapse microscopy experiment and quantification

Fluorescently tagged strains of WT or Δ*phz* were grown in GMM and tolerance experiments were performed as shown in S4D Fig. using ciprofloxacin (10 μg/mL). After the four-hour incubation with the antibiotic, cells were washed and re-suspended in GMM. The two different strains were then mixed and placed on an agarose pad containing GMM (no ciprofloxacin or PYO was added to the pad). Agarose pads were placed into a PELCO Clear Wall Glass Bottom Dish (Cat. No. 14023-20), and the dish was used for imaging within the microscope incubation chamber. Outgrowth was visualized using a Nikon Ti2E microscope with Perfect Focus System 4. Incubation proceeded for 12.5 to 15 hrs at 37 ºC, with imaging every 15 min in bright field (phase contrast), green and red fluorescence channels (50 ms exposure with 470 nm LED lamp and a green-FITC filter [ex = 465-495nm, em = 515-555nm] for GFP; 50 ms exposure with 555 nm LED lamp and a quad band filter [red ex = 543-566nm, red em = 580-611nm] for mApple).

For image analysis, a Fiji macro was used. Briefly, fluorescent channels (GFP/mApple) of the first and last time points were segmented using the "Auto Threshold" function and "Default" setting. The area of the segmented cells was then recorded using the "Analyze Particles" function in Fiji (Schindelin *et al.*, 2012). This allowed for quantification of the total area covered by cells within each channel, with each field of view being processed separately. After that, for each field of view, the total area covered by WT cells (or Δ*phz* + 100 μM PYO, depending on the experiment) was divided by the area covered by Δ*phz* cells to obtain the relative "growth area ratios." This was done for first and last time points. Three experiments were performed, with different fluorescent protein/strain combinations: (i) WT::mApple/Δ*phz*::GFP (n = 13 fields of view, Fig. 2F-G); (ii) Δ*phz*::GFP+PYO /Δ*phz*::mApple (n = 19, Fig. 2G); and (iii) WT::GFP/Δ*phz*::mApple (n = 16, S4E Fig). GFP/mApple were controlled by the *rpsG* promoter for all of the strains (S5 Table).

RNA extraction and quantitative reverse transcriptase PCR (qRT-PCR)

Experiment 1 – measurement of PYO-induced gene expression. Six different treatments were prepared for this qRT-PCR experiment: (i) WT PA14, (ii) Δ*phz*, (iii) Δ*phz* + 1 μM PYO, (iv) Δ*phz* + 10 μM PYO, (v) Δ*phz* + 100 μM PYO, and (vi) Δ*phz* + 200 μM PYO. Cultures of WT or Δ*phz* were grown overnight in GMM (20 mM glucose), then cells were washed and resuspended at an

OD_{500} of 0.05 (three replicates) in fresh GMM (5 mL in culture tubes). Different concentrations of PYO were added to Δ*phz* cultures as mentioned and all cultures were incubated for around 8.5 hrs (until early stationary phase). This was enough time for WT to make PYO (around 50-70 μM, measured by absorbance at OD_{691} (Reszka *et al.*, 2004)). After incubation, cells were pelleted, immediately frozen using liquid nitrogen, and stored at -80 ºC.

Experiment 2 – measuring arabinose induction of *mexGHI-opmD*, *ahpB*, and *katB*. Eight different treatments were prepared for this qRT-PCR experiment, in which each of the four tested strains (Δ*phz*, Δ*phz* P_{ara}:*mexGHI-opmD*, Δ*phz* P_{ara}:*ahpB*, and Δ*phz* P_{ara}:*katB*) were incubated with and without 20 mM arabinose for artificial induction of the constructs. Cultures of the four strains were grown overnight in GMM (20 mM glucose), then cells were washed and resuspended at an OD_{500} of 0.05 (three replicates) in the same medium (5 mL in culture tubes), with and without 20 mM arabinose (for conditions without arabinose, the respective amount of water was added). Cultures were incubated for around 8.5 hrs, then pelleted, immediately frozen using liquid nitrogen, and stored at -80 ºC.

For RNA extraction, previously published protocols were followed (Babin *et al.*, 2016; Meirelles and Newman, 2018). Briefly, samples were thawed on ice for 10 min and re-suspended in 215 μL of TE buffer (30 mM Tris HCl, 1 mM EDTA, pH 8.0) containing 15 mg/mL of lysozyme + 15 μL of proteinase K solution (20 mg/mL, Qiagen), and then incubated for 8–10 min. For lysis steps and RNA extraction, the RNeasy kit (Qiagen) was used. Samples were then treated with TURBO DNA-free kit (Invitrogen) for removal of any contaminant gDNA. Next, cDNA was synthesized using iScript cDNA Synthesis kit (Bio-Rad) (1 μg of total RNA was used). For these kits, the manufacturer's instructions were followed. qRT-PCR reactions were performed using iTaq Universal SYBR Green Supermix (Bio-Rad) in 20 μL reactions using a 7500 Fast Real-Time PCR System machine (Applied Biosystems) following published protocols (Meirelles and Newman, 2018). Standard curves for each primer pair were prepared using *P. aeruginosa* gDNA and were used for calculation of cDNA for each gene studied. The house-keeping gene *oprI* was used as a control gene for normalizations (Babin *et al.*, 2016).

Data showing total *oprI*-normalized cDNA levels (i.e. cDNA measured for a certain gene in a certain sample, divided by the respective cDNA measured for *oprI* in the same sample) and the

log_2-fold change in expression are shown in Fig. 2B and S1, S2, S3, and S5 Figs. Fold changes were calculated relative to the mean value for Δ*phz* samples without added PYO (Fig. 2B and S1B and S3 Figs) or the mean value of samples from the same strain without added arabinose (S5B Fig). cDNA values for replicates within each efflux gene/treatment (shown in S2 Fig) were averaged and used with the *geom_tile()* function in R (R Core Team, 2018; Wickham, 2016) for generation of the heatmap shown in Fig. 2B.

Stenotrophomonas *and* Burkholderia *growth curves and antibiotic tolerance assays*

Stenotrophomonas maltophilia ATCC 13637, *Burkholderia cepacia* ATCC 25416, *B. cenocepacia* AU42085, *B. multivorans* AU42096 (*B. multivorans 1)*, and *B. gladioli* AU42104 were used in the growth experiments shown in Fig. 5A (for strain details, see S5 Table). Each strain was grown overnight in GMM (20 mM glucose, 5 mL culture tubes) supplemented with 1x MEM amino acids (AA) (Sigma, Cat. No. M5550). Cells were pelleted, washed, and re-suspended in new cultures at an OD_{500} of 0.05 in the same medium. Cultures were then split, different concentrations of PYO were added (0, 10, 50 or 100 μM for *S. maltophilia*; 0, 10 or 100 μM for all others), and moved to a 96-well plate (4 to 6 wells per treatment, with each well being considered an independent replicate). Cultures within wells contained 150 μL with an additional 70 μL of mineral oil on top to prevent evaporation. The plates were incubated at 37 ºC under shaking conditions using a BioTek Synergy 4 plate reader with OD_{500} measurements every 15 min for 24 hrs to measure growth. Assays for tolerance to ciprofloxacin with or without exogenous PYO were performed for *S. maltophilia* (sensitive to PYO) and for four *Burkholderia* strains (all resistant to PYO): *B. cepacia*, *B. cenocepacia*, *B. multivorans 1*, and *B. multivorans* AU18358 (*B. multivorans 4*). The experiments followed exactly what was done for *P. aeruginosa* (S4A Fig), except that cultures were grown in GMM + AA, and are shown in Figs 4B and 4E. Finally, a tolerance assay in SCFM with and without PYO was performed for *B. multivorans 1* (Fig. 5H) and followed what was described for the SCFM experiments in *P. aeruginosa* (with the only difference being the ciprofloxacin concentrations, always mentioned in the legends).

Co-culture antibiotic tolerance experiments

To test how PYO produced by *P. aeruginosa* impacts tolerance to ciprofloxacin in other species, co-culture experiments were performed using membrane-separated 12-well tissue culture plates containing 0.1 μm pore PET membranes (VWR Cat. No. 10769-226). Briefly, overnight cultures of the *P. aeruginosa* strain (WT/Δ*phz* PA14 or PA 76-11) and the respective other species tested (*S. maltophilia*, *B. cepacia*, *B. cenocepacia* or *B. multivorans 1*) were prepared in GMM (20 mM glucose) + AA. Cells were pelleted, washed, and re-suspended to different ODs as follows: (i) for any *P. aeruginosa-Burkholderia* assay, *P. aeruginosa* starting OD_{500} = 0.05 and *Burkholderia* starting OD_{500} = 0.025; (ii) for the *P. aeruginosa-S. maltophilia* assay, *P. aeruginosa* starting OD_{500} = 0.01 and *S. maltophilia* starting OD_{500} = 0.1. *P. aeruginosa* was cultured in the bottom part of the well (600 μL), while the other species was cultured in the upper part of the well (100 μL), as shown in Fig. 5C. *B. cepacia* and *S. maltophilia* were cultured either with WT or Δ*phz P. aeruginosa* PA14 (with and without 100 μM PYO exogenously added).

B. cenocepacia and *B. multivorans 1* were cultured either with PA 76-11 (a *P. aeruginosa* strain isolated from CF sputum that produced 50-100 μM PYO in these assays) or alone in the presence or absence of 100 μM PYO. For cases where *Burkholderia* was grown alone, the strain tested was grown in both the bottom and top parts of the membrane-separated wells. In all experiments, co-cultures were grown for around 20 hrs at 37 ºC under shaking conditions (175 rpm) using a benchtop incubator, followed by addition of ciprofloxacin (concentrations were either 1 or 10 μg/mL, as specified in the figure legends) and incubation for four hours. The membrane-separated plates were kept inside an airtight plastic container with several wet paper towels to maintain high humidity attached to the shaker. For every co-culture combination in the membrane-separated plate, three wells were used as a negative control (no antibiotic) and three wells were used for ciprofloxacin treatment; each well was considered an independent replicate. After incubation with ciprofloxacin, cells were serially diluted in MPB and plated for CFUs on LB. In most cases, only *Burkholderia* cells were plated (Fig. 5F). However, to test if our *P. aeruginosa* WT strain was still more tolerant than the Δ*phz* strain when both were grown in the presence of a *Burkholderia* species, we performed an experiment with *P. aeruginosa* PA14 and *Burkholderia multivorans 1* where we treated the co-cultures with ciprofloxacin 1 μg/mL and plated *P. aeruginosa* (Fig. 5G). Finally, we also performed a co-culture experiment in SCFM (*P. aeruginosa* PA14 WT/Δ*phz* with *B. multivorans 1*) to test if PYO produced by PA14 WT increases tolerance in *Burkholderia* in this medium (Fig. 5I). This

experiment in SCFM followed the same overall experimental design used before, except for using SCFM instead of GMM in all steps.

Determination of minimum inhibitory concentrations

The antibiotic concentrations used for selecting *de novo* antibiotic-resistant mutants in the fluctuation tests were chosen based on the results of a modified agar dilution MIC assay. Overnight cultures were grown for each strain in GMM (with 10 mM glucose) or GMM (10 mM glucose) + AA, respectively, then diluted to an OD_{500} of 0.5, from which 3 µL was spotted onto MH agar containing a 2-fold dilution series of the antibiotic. After the spots dried, the antibiotic plates were incubated upside down for 48 hrs at 37 ºC before assessing the spots for growth. We considered the MIC to be the first concentration at which there was neither a lawn of background growth, nor dozens of overlapping colonies visible without magnification. We generally used 2x this MIC as the selection condition for fluctuation tests; for *P. aeruginosa*, this corresponded to the EUCAST (EUCAST, 2003) resistance breakpoints for ciprofloxacin and levofloxacin, while our chosen concentrations of gentamicin and tobramycin were two-fold higher than the EUCAST breakpoints (EUCAST, 2020). EUCAST breakpoints are not available for *Stenotrophomonas* spp. or the *Burkholderia cepacia* complex. The appropriateness of the selection condition was additionally verified by performing a fluctuation test, as described below, and choosing the antibiotic concentration that reliably yielded a countable number of colonies (zero to several dozen, with at least several non-zero counts per 44 parallel cultures) in each well.

Ciprofloxacin MICs for parent strains and isolated mutants from the fluctuation tests were determined according to standard clinical methods for broth microdilution assays (Determination of minimum inhibitory concentrations (MICs) of antibacterial agents by broth dilution, 2003). In brief, cells from either overnight cultures in MH broth or fresh streaks on LB agar (14-16 hrs old) were resuspended to a density of 3-7 x 10^5 CFUs/mL in a two-fold dilution series of ciprofloxacin in MH broth, with or without 100 µM PYO. The dilution series were set up in a final volume of 100 µL per well in 96-well microtiter plates, with appropriate no-antibiotic and cell-free controls. Three biological replicates (independent overnight cultures or cell suspensions) were prepared for each tested strain. Following inoculation, the microtiter plates were sealed with a plastic film to prevent

evaporation and incubated in a single layer at 37 ºC, without shaking. The wells were assessed for growth (turbidity) visible to the naked eye after 18 hrs of incubation.

Fluctuation tests, calculation of mutation rates, and model fitting

For all tested strains and conditions, fluctuation tests were performed by inoculating 200 µL cultures in parallel in a flat-bottomed 96-well plate. All reported fluctuation test data for *P. aeruginosa* are from experiments using the Δ*phz* strain. We also performed fluctuation tests using the *P. aeruginosa* PA14 WT strain, and performed phenotypic and genotypic characterization of partially-resistant mutants detected in those experiments (see below); however, the effect of PYO on apparent mutation rates in WT was difficult to interpret due to inconsistent PYO production in the 96-well plates. For cultures that were grown with PYO (or arabinose in the case of strains with arabinose-inducible constructs), the PYO (or 20 mM arabinose) was added to the medium before inoculation. The cultures were inoculated with a 10^{-6} dilution of a single overnight culture (representing a biological replicate) that had first been diluted to a standard OD_{500} of 1.0, corresponding to an initial cell density of approximately 2000-2500 CFUs/mL (400-500 cells/culture). Each treatment condition consisted of 44 such parallel cultures.

The 96-well plates were placed inside an airtight plastic container with several wet paper towels to maintain high humidity, then incubated at 37 ºC with shaking at 250 rpm. For plating during log-phase, the cultures were incubated until reaching approximately half-maximal density (OD_{500} of 0.4-0.7 for *P. aeruginosa* in GMM with 10 mM glucose, or 0.9-1.2 for *P. aeruginosa* in SCFM or *B. multivorans* in GMM + AA). For plating during stationary phase, the cultures were incubated for 24 hrs. The cultures were then plated by spotting 40-50 µL per culture into single wells of 24-well plates (for any given experiment, the same volume was spotted for all parallel cultures); each well contained 1 mL of MH agar or SFCM agar plus an antibiotic, with or without 100 µM PYO (or 20 mM arabinose for strains with arabinose-inducible constructs). In the case of *B. multivorans* cultures that were spotted onto antibiotic plates containing 100 µM PYO, the cultures were first diluted 1:10 (if not pre-treated with 100 µM PYO) or 1:100 (if pre-treated with 100 µM PYO).

At the same time as plating onto the antibiotic plates, six representative cultures from each treatment were serially diluted and plated on LB agar plates to assess total CFUs. The antibiotic plates were incubated upside down, in stacks of no more than eight, at 37 ºC for 16-24 hrs for *P. aeruginosa* (except for gentamicin plates, which were incubated for 40-48 hrs) or 40-48 hrs for *B. multivorans*. Subsequently, colonies were counted under a stereoscope at the highest magnification for which the field of view still encompassed an entire well; occasionally, a well contained too many colonies to count (a so-called "jackpot" culture (Rosche and Foster, 2000)), in which case that culture was discarded from further analysis. The LB agar plates for total CFU counts were incubated for 30-36 hrs at RT before counting colonies at the same magnification.

Mutation rates reported in the figures were calculated using the function newton.LD.plating from the R package rSalvador (Zheng, 2017) to estimate *m*, the expected number of mutations per culture. This is a maximum likelihood-based method for inferring mutation rates from fluctuation test colony counts, based on the classic Luria-Delbrück (LD) distribution with a correction to account for the effects of partial plating (i.e. plating a portion of each culture rather than the total volume) (Zheng, 2017). We chose this method because it has been shown to be the most accurate estimator of *m* when partial plating is involved (Zheng, 2015; Zheng, 2017). To get μ_{app} (apparent mutation rate per generation) from *m*, we divided *m* by the total number of cells per parallel culture (Zheng, 2017), as estimated from the mean number of CFUs counted for the six representative cultures.

To compare the fits of different formulations of the LD distribution to our data, we generated theoretical cumulative distributions using the parameter values estimated for our data. Specifically, for the Hamon and Ycart version of the LD model (Hamon and Ycart, 2012), we estimated *m* and *w* (relative fitness of mutants compared to the parent strain in the non-selective pre-plating liquid growth medium) using the function GF.est from the R script available at http://ljk.imag.fr/membres/Bernard.Ycart/LD/ (version 1.0; note that in the script, *m* is called alpha and 1/*w* is called rho); then, we used the function pLD from the same script to generate the theoretical distribution. For the mixed LD-Poisson and basic LD models, we wrote and used an R translation of the MATLAB code written by Lang and Murray (2008); the original code is available at https://github.com/AWMurrayLab/FluctuationTest_GregLang. The basic LD model used by Lang and Murray (2008) is equivalent to that available in the rSalvador package (using the function newton.LD), except without the correction for partial plating; the latter is only important when using

the estimate of *m* to infer the mutation rate, not when comparing the fits of different models to the empirical cumulative distribution of the raw colony counts.

Plots of the empirical cumulative distributions of our data against the theoretical models showed that the Hamon and Ycart model was a visually good fit in all cases (see Figs. 4B, 6C, and S9 Fig. for examples). To further assess goodness-of-fit of the Hamon and Ycart model, we performed Pearson's chi-square test in R after binning the data and theoretical distribution such that the expected number of cultures in each bin of mutant counts was at least five (Boe *et al.*, 1994). To compare the goodness-of-fit of the Hamon and Ycart model to the basic LD model, we calculated the negative log-likelihood for each model and performed the likelihood ratio test. To compare the Hamon and Ycart model to the mixed LD-Poisson model, we simply compared the negative log-likelihoods (smaller values indicate a better fit); the likelihood ratio test was not applicable as these two models contain the same number of parameters. Note that although the Hamon and Ycart (or in some cases, LD-Poisson) models were often better fits than the basic LD model, we still used the basic LD model for statistical comparison of mutation rates between conditions, because an accurate method to account for partial plating has not yet been developed for the cases of post-plating mutations or differential fitness between mutants and parent strains (Zheng, 2017). Nevertheless, similar patterns in mutation rates were observed when using an older method of accounting for partial plating to derive μ_{app} from the Hamon and Ycart model (Gillet-Markowska *et al.*, 2015); the Pearson correlation coefficient was 0.98 for mutation rates calculated with the newton.LD.plating function in rSalvador versus the partial-plating-corrected Hamon and Ycart method (S3 Table). We also separately performed non-parametric statistical analysis of the raw mutant frequencies (i.e. mutant colony counts divided by the number of cells per parallel culture), as such analysis is agnostic to any assumptions about the biological processes underlying the data. The statistical significance of this analysis generally corresponded with the statistical significance of a likelihood ratio test based on the newton.LD.plating model of mutation rates, indicating that the effects of PYO were robust to different mathematical approaches to analyzing the fluctuation test data (S2 Table).

Characterization of antibiotic resistance phenotypes

We defined putative ciprofloxacin-resistant mutants as "enriched" by PYO in the fluctuation tests if colonies with a given morphology were at least 2x more numerous on the PYO-containing

ciprofloxacin plate than the respective non-PYO-containing ciprofloxacin plate derived from the same 200 µL culture. These putative mutants could be either from the PYO pre-treated or non-PYO pre-treated branches of the fluctuation test. Putative mutants that were seemingly enriched by PYO were restreaked for purity on PYO-containing agar plates at the same ciprofloxacin concentration on which they were selected in the fluctuation test (0.5 µg/mL for *PA*, 8 µg/mL for *B. multivorans*). Putative mutants that were not enriched by PYO were restreaked on ciprofloxacin agar plates without PYO. Frozen stocks of each restreaked, visually pure isolate were prepared by inoculating cultures with single colonies in 5 mL of liquid LB, incubating to stationary phase, mixing 1:1 with 50% glycerol, and storing at -80 ºC.

The levels of ciprofloxacin resistance of selected isolates, as well as the parent strains, were assessed using a CFU recovery assay as follows. For each isolate, four 5 mL cultures in GMM (for *P. aeruginosa*) or GMM + AA (for *B. multivorans*) were inoculated directly from the frozen stock, to minimize the number of generations in which secondary mutations could be acquired. The cultures were grown to stationary phase overnight, then subcultured to an OD_{500} of 0.05 in 5 mL of fresh GMM (for *P. aeruginosa*) or GMM + AA (for *B. multivorans*), with or without 100 µM PYO. The new cultures were grown to mid log-phase, then serially diluted in GMM or GMM + AA (+/- 100 µM PYO as appropriate) and plated for CFUs (10 µL per dilution step) on 1) plain MH agar, 2) MH agar + ciprofloxacin, and 3) MH agar + ciprofloxacin + 100 µM PYO. The lowest plated dilution was 10^{-1}, making the limit of detection approximately 1000 CFUs/mL.

Identification of mutations by whole-genome sequencing

Genomic DNA was isolated from selected putative mutants and the parent strains using the DNeasy Blood & Tissue kit (Qiagen). Library preparation and 2x150 bp paired-end Illumina sequencing was performed by the Microbial Genome Sequencing Center (Pittsburgh, PA), with a minimum of 300 Mb sequencing output per sample (~50x coverage). Forward and reverse sequencing reads were concatenated into a single file for each isolate and quality control was performed using Trimmomatic (version 0.39) (Bolger *et al.*, 2014) with the following settings: LEADING:27 TRAILING:27 SLIDINGWINDOW:4:27 MINLEN:35. Mutations were then identified using breseq (version 0.34.1) (Deatherage and Barrick, 2014). The annotated reference genome for *P. aeruginosa* UCBPP-PA14 was obtained from BioProject accession number

PRJNA38507. For *B. multivorans* AU42096, no reference genome was available from NCBI. Therefore, a genome scaffold was assembled from the paired-end sequencing data for the parent strain using SPAdes (version 3.14.0) with default parameters (Bankevich *et al.*, 2012). This scaffold was then used as the reference for breseq. Differences between the parent strain and isolates were identified using the gdtools utility that comes with breseq to compare the respective breseq outputs. All sequenced *P. aeruginosa* mutants were derived from the Δ*phz* strain except for CipR-33 and CipR-40, which were derived from the WT strain. In the case of *B. multivorans*, several dozen putative mutations were identified that were common to all three sequenced putative mutants. We assumed that these represented assembly errors in the parent strain genome scaffold, but even if they were genuine mutations, these would not account for the phenotypic differences between the isolates; therefore, S6 Table reports only mutations that were unique to each isolate. The genomic loci containing each putative mutation for the *B. multivorans* isolates were identified by retrieving the surrounding 200 bp from the parent genome scaffold and using the nucleotide BLAST tool on the MicroScope platform (Vallenet *et al.*, 2020) to find the closest match in the *B. multivorans* ATCC 17616 genome.

Growth curves with propidium iodide

To verify that PYO did not increase the population turnover rate (i.e. cell death) in our log-phase fluctuation tests prior to the antibiotic selection step, we performed growth curves in the presence of different concentrations of PYO, with the addition of propidium iodide (PI) as a fluorescent marker for cell death. The use of PI as a marker for PYO-induced cell death has previously been validated under similar conditions (Meirelles and Newman, 2018). The growth curves were performed in GMM and SCFM for *P. aeruginosa* Δ*phz*, and GMM + AA for *B. multivorans 1*. The cultures were prepared and incubated in the same manner as the fluctuation tests, except that 5 μM PI was added at the beginning of the experiment, and measurements for OD_{500} and PI fluorescence (ex = 535 nm, em = 617 nm) were taken periodically using a Spark 10M plate reader (Tecan). Importantly, PI stock concentration (5 mM, 1000x) was prepared in DMSO, and the final concentration of DMSO in the cultures did not exceed 0.1%. In addition, black 96-well plates with clear bottoms were used to minimize the effects of adjacent wells on fluorescence readings.

Statistical analyses

All statistical analyses were performed using R (R Core Team, 2018). Welch's unpaired t-tests or one-way ANOVA with post-hoc Tukey's HSD test for multiple comparisons were used for tolerance assay data. The likelihood ratio test as implemented by the rSalvador function LRT.LD.plating was used to compare mutation rates, alongside the alternative criterion of non-overlapping 84% confidence intervals as a proxy for the $p < 0.05$ threshold for statistical significance. The Mann-Whitney U test was used to compare the distributions of mutant frequencies. Welch's unpaired t-tests were used for comparisons of CFU recovery on ciprofloxacin plates under different PYO treatments. Benjamini-Hochberg corrections were used in all cases to control false discovery rates, except where Tukey's HSD test was performed. For all antibiotic tolerance assays measured by CFUs, survival data were $\log_{10}$-transformed before statistical analyses.

Acknowledgments

We thank members of the Newman lab and Shashank Gandhi for constructive feedback throughout the project and on the manuscript. We also thank Steven Wilbert for assistance with image analysis, David Basta for providing the plasmid used for *lptA* deletion, and The Millard and Muriel Jacobs Genetics and Genomics Laboratory at Caltech and Igor Antoshechkin for support during library preparation and sequencing of the Tn-seq samples. Finally, we thank John LiPuma (CFF *Burkholderia cepacia* Research Laboratory and Repository at the University of Michigan) for providing clinical *Burkholderia* strains and Justin Bois for constructive feedback on our statistical approach.

Data availability

Tn-seq data have been deposited at GEO under accession number GSE148769. Whole genome sequencing data for the parent strains and ciprofloxacin-resistant mutants of *P. aeruginosa* and *B. multivorans* AU42096 have been deposited at NCBI under accession number PRJNA625945. Supplementary tables referred to but not included in this document due to their size and/or format are available through CaltechDATA and are linked to the record of this thesis in CaltechTHESIS. All strains/plasmids used in this study are available from the corresponding author upon request.

References

Adegoke, A.A., Stenström, T.A., and Okoh, A.I. (2017) *Stenotrophomonas maltophilia* as an emerging ubiquitous pathogen: looking beyond contemporary antibiotic therapy. *Front Microbiol* **8**: 2276.

Alexander, H.K., and MacLean, R.C. (2020) Stochastic bacterial population dynamics restrict the establishment of antibiotic resistance from single cells. *Proc Natl Acad Sci USA* **117**: 19455–19464.

Babin, B.M., Bergkessel, M., Sweredoski, M.J., Moradian, A., Hess, S., Newman, D.K., and Tirrell, D.A. (2016) SutA is a bacterial transcription factor expressed during slow growth in *Pseudomonas aeruginosa*. *Proc Natl Acad Sci USA* **113**: E597-605.

Balaban, N.Q., Helaine, S., Lewis, K., Ackermann, M., Aldridge, B., Andersson, D.I., *et al.* (2019) Definitions and guidelines for research on antibiotic persistence. *Nat Rev Microbiol* **17**: 441–448.

Bankevich, A., Nurk, S., Antipov, D., Gurevich, A.A., Dvorkin, M., Kulikov, A.S., *et al.* (2012) SPAdes: a new genome assembly algorithm and its applications to single-cell sequencing. *J Comput Biol* **19**: 455–477.

Basta, D.W., Bergkessel, M., and Newman, D.K. (2017) Identification of fitness determinants during energy-limited growth arrest in *Pseudomonas aeruginosa*. *mBio* **8**: e01170-17.

Baym, M., Lieberman, T.D., Kelsic, E.D., Chait, R., Gross, R., Yelin, I., and Kishony, R. (2016) Spatiotemporal microbial evolution on antibiotic landscapes. *Science* **353**: 1147–1151.

Berg, G., Eberl, L., and Hartmann, A. (2005) The rhizosphere as a reservoir for opportunistic human pathogenic bacteria. *Environ Microbiol* **7**: 1673–1685.

Boe, L., Tolker-Nielsen, T., Eegholm, K.M., Spliid, H., and Vrang, A. (1994) Fluctuation analysis of mutations to nalidixic acid resistance in Escherichia coli. *J Bacteriol* **176**: 2781–2787.

Bolger, A.M., Lohse, M., and Usadel, B. (2014) Trimmomatic: a flexible trimmer for Illumina sequence data. *Bioinformatics* **30**: 2114–2120.

Brauner, A., Fridman, O., Gefen, O., and Balaban, N.Q. (2016) Distinguishing between resistance, tolerance and persistence to antibiotic treatment. *Nat Rev Microbiol* **14**: 320–330.

Bridges, B.A. (1980) The fluctuation test. *Arch Toxicol* **46**: 41–44.

Brochado, A.R., Telzerow, A., Bobonis, J., Banzhaf, M., Mateus, A., Selkrig, J., *et al.* (2018) Species-specific activity of antibacterial drug combinations. *Nature* **559**: 259–263.

Bruchmann, S., Dötsch, A., Nouri, B., Chaberny, I.F., and Häussler, S. (2013) Quantitative contributions of target alteration and decreased drug accumulation to *Pseudomonas aeruginosa* fluoroquinolone resistance. *Antimicrob Agents Chemother* **57**: 1361–1368.

Cameron, D.R., Shan, Y., Zalis, E.A., Isabella, V., and Lewis, K. (2018) A genetic determinant of persister cell formation in bacterial pathogens. *J Bacteriol* **200**.

Cheluvappa, R. (2014) Standardized chemical synthesis of *Pseudomonas aeruginosa* pyocyanin. *MethodsX* **1**: 67–73.

Chmiel, J.F., Aksamit, T.R., Chotirmall, S.H., Dasenbrook, E.C., Elborn, J.S., LiPuma, J.J., *et al.* (2014) Antibiotic management of lung infections in cystic fibrosis. I. The microbiome, methicillin-resistant *Staphylococcus aureus*, gram-negative bacteria, and multiple infections. *Ann Am Thorac Soc* **11**: 1120–1129.

Choi, K.-H., and Schweizer, H.P. (2006) mini-Tn7 insertion in bacteria with single attTn7 sites: example *Pseudomonas aeruginosa*. *Nat Protoc* **1**: 153–161.

Costa, K.C., Glasser, N.R., Conway, S.J., and Newman, D.K. (2017) Pyocyanin degradation by a

tautomerizing demethylase inhibits *Pseudomonas aeruginosa* biofilms. *Science* **355**: 170–173.

Costerton, J.W., Stewart, P.S., and Greenberg, E.P. (1999) Bacterial biofilms: a common cause of persistent infections. *Science* **284**: 1318–1322.

Cruickshank, C.N., and Lowbury, E.J. (1953) The effect of pyocyanin on human skin cells and leucocytes. *Br J Exp Pathol* **34**: 583–587.

Davies, J., and Davies, D. (2010) Origins and evolution of antibiotic resistance. *Microbiol Mol Biol Rev* **74**: 417–433.

Deatherage, D.E., and Barrick, J.E. (2014) Identification of mutations in laboratory-evolved microbes from next-generation sequencing data using breseq. *Methods Mol Biol* **1151**: 165–188.

Depoorter, E., Bull, M.J., Peeters, C., Coenye, T., Vandamme, P., and Mahenthiralingam, E. (2016) *Burkholderia*: an update on taxonomy and biotechnological potential as antibiotic producers. *Appl Microbiol Biotechnol* **100**: 5215–5229.

Dietrich, L.E., Price-Whelan, A., Petersen, A., Whiteley, M., and Newman, D.K. (2006) The phenazine pyocyanin is a terminal signalling factor in the quorum sensing network of *Pseudomonas aeruginosa*. *Mol Microbiol* **61**: 1308–1321.

Dietrich, L.E.P., Okegbe, C., Price-Whelan, A., Sakhtah, H., Hunter, R.C., and Newman, D.K. (2013) Bacterial community morphogenesis is intimately linked to the intracellular redox state. *J Bacteriol* **195**: 1371–1380.

Driscoll, J.A., Brody, S.L., and Kollef, M.H. (2007) The epidemiology, pathogenesis and treatment of Pseudomonas aeruginosa infections. *Drugs* **67**: 351–368.

Fair, R.J., and Tor, Y. (2014) Antibiotics and bacterial resistance in the 21st century. *Perspect Medicin Chem* **6**: 25–64.

Fierer, N., and Jackson, R.B. (2006) The diversity and biogeography of soil bacterial communities. *Proc Natl Acad Sci USA* **103**: 626–631.

Frenoy, A., and Bonhoeffer, S. (2018) Death and population dynamics affect mutation rate estimates and evolvability under stress in bacteria. *PLoS Biol* **16**: e2005056.

Garbe, T.R., Kobayashi, M., and Yukawa, H. (2000) Indole-inducible proteins in bacteria suggest membrane and oxidant toxicity. *Arch Microbiol* **173**: 78–82.

Gibson, D.G., Young, L., Chuang, R.-Y., Venter, J.C., Hutchison, C.A., and Smith, H.O. (2009) Enzymatic assembly of DNA molecules up to several hundred kilobases. *Nat Methods* **6**: 343–345.

Gillet-Markowska, A., Louvel, G., and Fischer, G. (2015) bz-rates: a web tool to estimate mutation rates from fluctuation analysis. *G3 (Bethesda)* **5**: 2323–2327.

Glasser, N.R., Kern, S.E., and Newman, D.K. (2014) Phenazine redox cycling enhances anaerobic survival in *Pseudomonas aeruginosa* by facilitating generation of ATP and a proton-motive force. *Mol Microbiol* **92**: 399–412.

Granato, E.T., Meiller-Legrand, T.A., and Foster, K.R. (2019) The evolution and ecology of bacterial warfare. *Curr Biol* **29**: R521–R537.

Green, S.K., Schroth, M.N., Cho, J.J., Kominos, S.K., and Vitanza-jack, V.B. (1974) Agricultural plants and soil as a reservoir for *Pseudomonas aeruginosa*. *Appl Microbiol* **28**: 987–991.

Hamon, A., and Ycart, B. (2012) Statistics for the Luria-Delbrück distribution. *Electron J Stat* **6**: 1251–1272.

Häussler, S., Tümmler, B., Weissbrodt, H., Rohde, M., and Steinmetz, I. (1999) Small-colony variants of *Pseudomonas aeruginosa* in cystic fibrosis. *Clin Infect Dis* **29**: 621–625.

Hobbs, J.K., and Boraston, A.B. (2019) (p)ppGpp and the stringent response: an emerging threat to antibiotic therapy. *ACS Infect Dis* **5**: 1505–1517.

Imamovic, L., Ellabaan, M.M.H., Dantas Machado, A.M., Citterio, L., Wulff, T., Molin, S., *et al.* (2018) Drug-driven phenotypic convergence supports rational treatment strategies of chronic infections. *Cell* **172**: 121–134.e14.

Kester, J.C., and Fortune, S.M. (2014) Persisters and beyond: mechanisms of phenotypic drug resistance and drug tolerance in bacteria. *Crit Rev Biochem Mol Biol* **49**: 91–101.

Kohanski, M.A., DePristo, M.A., and Collins, J.J. (2010) Sublethal antibiotic treatment leads to multidrug resistance via radical-induced mutagenesis. *Mol Cell* **37**: 311–320.

Kopf, S.H., Sessions, A.L., Cowley, E.S., Reyes, C., Van Sambeek, L., Hu, Y., *et al.* (2016) Trace incorporation of heavy water reveals slow and heterogeneous pathogen growth rates in cystic fibrosis sputum. *Proc Natl Acad Sci USA* **113**: E110-6.

Korgaonkar, A., Trivedi, U., Rumbaugh, K.P., and Whiteley, M. (2013) Community surveillance enhances *Pseudomonas aeruginosa* virulence during polymicrobial infection. *Proc Natl Acad Sci USA* **110**: 1059–1064.

Kumar, A., and Sperandio, V. (2019) Indole signaling at the host-microbiota-pathogen interface. *mBio* **10**: e01031-19.

Lang, G.I., and Murray, A.W. (2008) Estimating the per-base-pair mutation rate in the yeast *Saccharomyces cerevisiae*. *Genetics* **178**: 67–82.

Langmead, B., and Salzberg, S.L. (2012) Fast gapped-read alignment with Bowtie 2. *Nat Methods* **9**: 357–359.

Laursen, J.B., and Nielsen, J. (2004) Phenazine natural products: biosynthesis, synthetic analogues, and biological activity. *Chem Rev* **104**: 1663–1686.

Lee, H., Popodi, E., Tang, H., and Foster, P.L. (2012) Rate and molecular spectrum of spontaneous mutations in the bacterium *Escherichia coli* as determined by whole-genome sequencing. *Proc Natl Acad Sci USA* **109**: E2774-83.

Lee, H.H., Molla, M.N., Cantor, C.R., and Collins, J.J. (2010) Bacterial charity work leads to population-wide resistance. *Nature* **467**: 82–85.

Levin-Reisman, I., Brauner, A., Ronin, I., and Balaban, N.Q. (2019) Epistasis between antibiotic tolerance, persistence, and resistance mutations. *Proc Natl Acad Sci USA* **116**: 14734–14739.

Levin-Reisman, I., Ronin, I., Gefen, O., Braniss, I., Shoresh, N., and Balaban, N.Q. (2017) Antibiotic tolerance facilitates the evolution of resistance. *Science* **355**: 826–830.

Lipuma, J.J. (2010) The changing microbial epidemiology in cystic fibrosis. *Clin Microbiol Rev* **23**: 299–323.

LiPuma, J.J., Spilker, T., Coenye, T., and Gonzalez, C.F. (2002) An epidemic *Burkholderia cepacia* complex strain identified in soil. *Lancet* **359**: 2002–2003.

Lister, P.D., Wolter, D.J., and Hanson, N.D. (2009) Antibacterial-resistant *Pseudomonas aeruginosa*: clinical impact and complex regulation of chromosomally encoded resistance mechanisms. *Clin Microbiol Rev* **22**: 582–610.

Liu, J., Gefen, O., Ronin, I., Bar-Meir, M., and Balaban, N.Q. (2020) Effect of tolerance on the evolution of antibiotic resistance under drug combinations. *Science* **367**: 200–204.

Llanes, C., Hocquet, D., Vogne, C., Benali-Baitich, D., Neuwirth, C., and Plésiat, P. (2004) Clinical strains of *Pseudomonas aeruginosa* overproducing MexAB-OprM and MexXY efflux pumps simultaneously. *Antimicrob Agents Chemother* **48**: 1797–1802.

Luria, S.E., and Delbrück, M. (1943) Mutations of bacteria from virus sensitivity to virus resistance. *Genetics* **28**: 491–511.

Malone, J.G., Jaeger, T., Spangler, C., Ritz, D., Spang, A., Arrieumerlou, C., *et al.* (2010) YfiBNR mediates cyclic di-GMP dependent small colony variant formation and persistence in *Pseudomonas aeruginosa. PLoS Pathog* **6**: e1000804.

Martina, P., Feliziani, S., Juan, C., Bettiol, M., Gatti, B., Yantorno, O., *et al.* (2014) Hypermutation in *Burkholderia cepacia* complex is mediated by DNA mismatch repair inactivation and is highly prevalent in cystic fibrosis chronic respiratory infection. *Int J Med Microbiol* **304**: 1182–1191.

Martinez, J.L. (2009) The role of natural environments in the evolution of resistance traits in pathogenic bacteria. *Proc Biol Sci* **276**: 2521–2530.

Marvig, R.L., Dolce, D., Sommer, L.M., Petersen, B., Ciofu, O., Campana, S., *et al.* (2015) Within-host microevolution of *Pseudomonas aeruginosa* in Italian cystic fibrosis patients. *BMC Microbiol* **15**: 218.

Marvig, R.L., Sommer, L.M., Molin, S., and Johansen, H.K. (2015) Convergent evolution and adaptation of *Pseudomonas aeruginosa* within patients with cystic fibrosis. *Nat Genet* **47**: 57–64.

Meirelles, L.A., and Newman, D.K. (2018) Both toxic and beneficial effects of pyocyanin contribute to the lifecycle of *Pseudomonas aeruginosa*. *Mol Microbiol* **110**: 995–1010.

Muller, M. (2002) Pyocyanin induces oxidative stress in human endothelial cells and modulates the glutathione redox cycle. *Free Radic Biol Med* **33**: 1527–1533.

Nunvar, J., Capek, V., Fiser, K., Fila, L., and Drevinek, P. (2017) What matters in chronic *Burkholderia cenocepacia* infection in cystic fibrosis: insights from comparative genomics. *PLoS Pathog* **13**: e1006762.

Oethinger, M., Kern, W.V., Jellen-Ritter, A.S., McMurry, L.M., and Levy, S.B. (2000) Ineffectiveness of topoisomerase mutations in mediating clinically significant fluoroquinolone resistance in *Escherichia coli* in the absence of the AcrAB efflux pump. *Antimicrob Agents Chemother* **44**: 10–13.

Olaitan, A.O., Morand, S., and Rolain, J.-M. (2014) Mechanisms of polymyxin resistance: acquired and intrinsic resistance in bacteria. *Front Microbiol* **5**: 643.

Olsen, I. (2015) Biofilm-specific antibiotic tolerance and resistance. *Eur J Clin Microbiol Infect Dis* **34**: 877–886.

Opijnen, T. van, Lazinski, D.W., and Camilli, A. (2014) Genome-wide fitness and genetic interactions determined by Tn-seq, a high-throughput massively parallel sequencing method for microorganisms. *Curr Protoc Mol Biol* **106**: 7.16.1-24.

Orlén, H., and Hughes, D. (2006) Weak mutators can drive the evolution of fluoroquinolone resistance in *Escherichia coli*. *Antimicrob Agents Chemother* **50**: 3454–3456.

Palmer, K.L., Aye, L.M., and Whiteley, M. (2007) Nutritional cues control *Pseudomonas aeruginosa* multicellular behavior in cystic fibrosis sputum. *J Bacteriol* **189**: 8079–8087.

Papkou, A., Hedge, J., Kapel, N., Young, B., and MacLean, R.C. (2020) Efflux pump activity potentiates the evolution of antibiotic resistance across *S. aureus* isolates. *Nat Commun* **11**: 3970.

Pope, C.F., Gillespie, S.H., Pratten, J.R., and McHugh, T.D. (2008) Fluoroquinolone-resistant mutants of *Burkholderia cepacia. Antimicrob Agents Chemother* **52**: 1201–1203.

Prayle, A., Watson, A., Fortnum, H., and Smyth, A. (2010) Side effects of aminoglycosides on the kidney, ear and balance in cystic fibrosis. *Thorax* **65**: 654–658.

Pritchard, J.R., Chao, M.C., Abel, S., Davis, B.M., Baranowski, C., Zhang, Y.J., *et al.* (2014) ARTIST: high-resolution genome-wide assessment of fitness using transposon-insertion

sequencing. *PLoS Genet* **10**: e1004782.
R Core Team (2018) R: A language and environment for statistical computing.
Rada, B., and Leto, T.L. (2013) Pyocyanin effects on respiratory epithelium: relevance in *Pseudomonas aeruginosa* airway infections. *Trends Microbiol* **21**: 73–81.
Ragheb, M.N., Thomason, M.K., Hsu, C., Nugent, P., Gage, J., Samadpour, A.N., *et al.* (2019) Inhibiting the evolution of antibiotic resistance. *Mol Cell* **73**: 157–165.e5.
Reszka, K.J., O'Malley, Y., McCormick, M.L., Denning, G.M., and Britigan, B.E. (2004) Oxidation of pyocyanin, a cytotoxic product from *Pseudomonas aeruginosa*, by microperoxidase 11 and hydrogen peroxide. *Free Radic Biol Med* **36**: 1448–1459.
Rhodes, K.A., and Schweizer, H.P. (2016) Antibiotic resistance in *Burkholderia* species. *Drug Resist Updat* **28**: 82–90.
Richardot, C., Juarez, P., Jeannot, K., Patry, I., Plésiat, P., and Llanes, C. (2016) Amino acid substitutions account for most MexS alterations in clinical *nfxC* mutants of *Pseudomonas aeruginosa*. *Antimicrob Agents Chemother* **60**: 2302–2310.
Rosche, W.A., and Foster, P.L. (2000) Determining mutation rates in bacterial populations. *Methods* **20**: 4–17.
Saunders, S.H., Tse, E.C.M., Yates, M.D., Otero, F.J., Trammell, S.A., Stemp, E.D.A., *et al.* (2020) Extracellular DNA promotes efficient extracellular electron transfer by pyocyanin in *Pseudomonas aeruginosa* biofilms. *Cell* **182**: 919–932.e19.
Schiessl, K.T., Hu, F., Jo, J., Nazia, S.Z., Wang, B., Price-Whelan, A., *et al.* (2019) Phenazine production promotes antibiotic tolerance and metabolic heterogeneity in *Pseudomonas aeruginosa* biofilms. *Nat Commun* **10**: 762.
Schindelin, J., Arganda-Carreras, I., Frise, E., Kaynig, V., Longair, M., Pietzsch, T., *et al.* (2012) Fiji: an open-source platform for biological-image analysis. *Nat Methods* **9**: 676–682.
Shanks, R.M.Q., Caiazza, N.C., Hinsa, S.M., Toutain, C.M., and O'Toole, G.A. (2006) *Saccharomyces cerevisiae*-based molecular tool kit for manipulation of genes from gram-negative bacteria. *Appl Environ Microbiol* **72**: 5027–5036.
Smith, C.R., Lipsky, J.J., Laskin, O.L., Hellmann, D.B., Mellits, E.D., Longstreth, J., and Lietman, P.S. (1980) Double-blind comparison of the nephrotoxicity and auditory toxicity of gentamicin and tobramycin. *N Engl J Med* **302**: 1106–1109.
Sobel, M.L., Neshat, S., and Poole, K. (2005) Mutations in PA2491 (*mexS*) promote MexT-dependent mexEF-oprN expression and multidrug resistance in a clinical strain of *Pseudomonas aeruginosa*. *J Bacteriol* **187**: 1246–1253.
Stressmann, F.A., Rogers, G.B., Gast, C.J. van der, Marsh, P., Vermeer, L.S., Carroll, M.P., *et al.* (2012) Long-term cultivation-independent microbial diversity analysis demonstrates that bacterial communities infecting the adult cystic fibrosis lung show stability and resilience. *Thorax* **67**: 867–873.
The European Committee on Antimicrobial Susceptibility Testing (EUCAST). (2003) Determination of minimum inhibitory concentrations (MICs) of antibacterial agents by broth dilution. *Clin Microbiol Infect* **9**: 1-7.
The European Committee on Antimicrobial Susceptibility Testing (EUCAST). Breakpoint tables for interpretation of MICs and zone diameters. Version 10.0 (2020) http://www.eucast.org. Accessed April 7, 2020.
Toprak, E., Veres, A., Michel, J.-B., Chait, R., Hartl, D.L., and Kishony, R. (2011) Evolutionary paths to antibiotic resistance under dynamically sustained drug selection. *Nat Genet* **44**: 101–105.

Turner, K.H., Wessel, A.K., Palmer, G.C., Murray, J.L., and Whiteley, M. (2015) Essential genome of *Pseudomonas aeruginosa* in cystic fibrosis sputum. *Proc Natl Acad Sci USA* **112**: 4110–4115.

Vallenet, D., Calteau, A., Dubois, M., Amours, P., Bazin, A., Beuvin, M., *et al.* (2020) MicroScope: an integrated platform for the annotation and exploration of microbial gene functions through genomic, pangenomic and metabolic comparative analysis. *Nucleic Acids Res* **48**: D579–D589.

Walters, M.C., Roe, F., Bugnicourt, A., Franklin, M.J., and Stewart, P.S. (2003) Contributions of antibiotic penetration, oxygen limitation, and low metabolic activity to tolerance of *Pseudomonas aeruginosa* biofilms to ciprofloxacin and tobramycin. *Antimicrob Agents Chemother* **47**: 317–323.

Wang, Y., Wilks, J.C., Danhorn, T., Ramos, I., Croal, L., and Newman, D.K. (2011) Phenazine-1-carboxylic acid promotes bacterial biofilm development via ferrous iron acquisition. *J Bacteriol* **193**: 3606–3617.

Wickham, H. (2016) *ggplot2 - Elegant Graphics for Data Analysis*. Springer-Verlag New York, New York, NY.

Widdel, F., and Pfennig, N. (1981) Studies on dissimilatory sulfate-reducing bacteria that decompose fatty acids. *Arch Microbiol* **129**: 395–400.

Wilson, R., Sykes, D.A., Watson, D., Rutman, A., Taylor, G.W., and Cole, P.J. (1988) Measurement of *Pseudomonas aeruginosa* phenazine pigments in sputum and assessment of their contribution to sputum sol toxicity for respiratory epithelium. *Infect Immun* **56**: 2515–2517.

Windels, E.M., Michiels, J.E., Fauvart, M., Wenseleers, T., Van den Bergh, B., and Michiels, J. (2019) Bacterial persistence promotes the evolution of antibiotic resistance by increasing survival and mutation rates. *ISME J* **13**: 1239–1251.

Winsor, G.L., Griffiths, E.J., Lo, R., Dhillon, B.K., Shay, J.A., and Brinkman, F.S.L. (2016) Enhanced annotations and features for comparing thousands of *Pseudomonas* genomes in the *Pseudomonas* genome database. *Nucleic Acids Res* **44**: D646-53.

Winstanley, C., O'Brien, S., and Brockhurst, M.A. (2016) *Pseudomonas aeruginosa* evolutionary adaptation and diversification in cystic fibrosis chronic lung infections. *Trends Microbiol* **24**: 327–337.

Zheng, Q. (2015) A new practical guide to the Luria-Delbrück protocol. *Mutat Res* **781**: 7–13.

Zheng, Q. (2017) rSalvador: an R package for the fluctuation experiment. *G3 (Bethesda)* **7**: 3849–3856.

Zhu, K., Chen, S., Sysoeva, T.A., and You, L. (2019) Universal antibiotic tolerance arising from antibiotic-triggered accumulation of pyocyanin in *Pseudomonas aeruginosa. PLoS Biol* **17**: e3000573.

Supplementary Tables and Figures

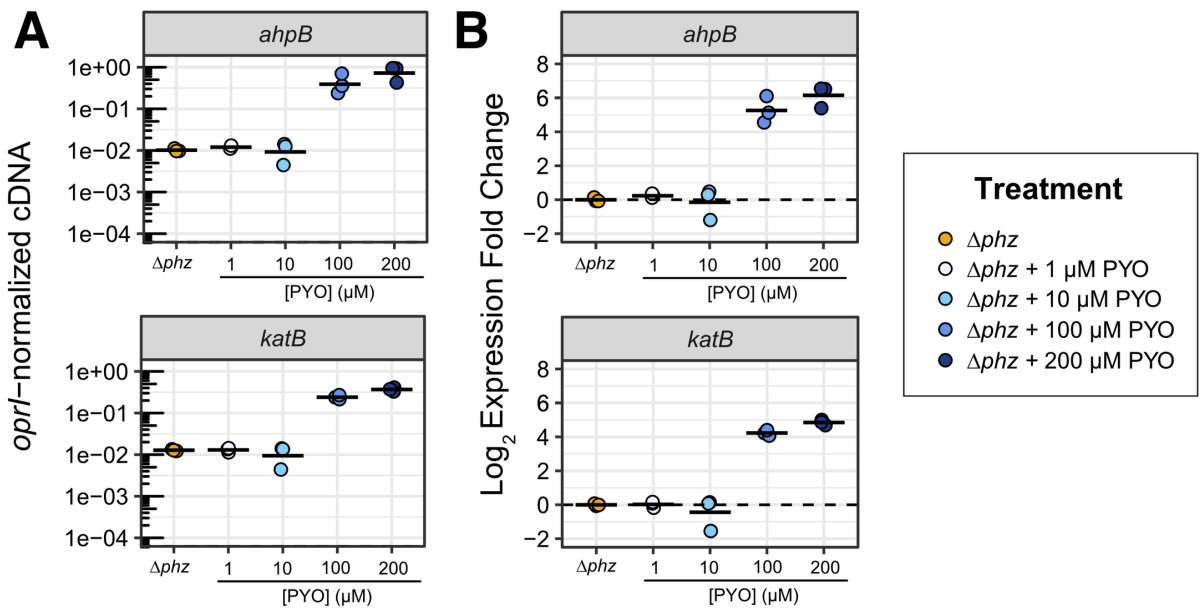

S1 Figure: Effects of different concentrations of PYO on the expression of the *P. aeruginosa* oxidative stress response genes *ahpB* and *katB*.
A. Normalized cDNA levels measured by qRT-PCR. cDNA measurements were normalized by levels of the housekeeping gene *oprI* (see Methods).
B. Fold change in expression upon PYO treatment, relative to the measurements in untreated Δ*phz*. *ahpB*: alkyl hydroperoxide reductase B; *katB*: catalase B. Black horizontal lines mark the mean value for independent biological cultures (n = 3).

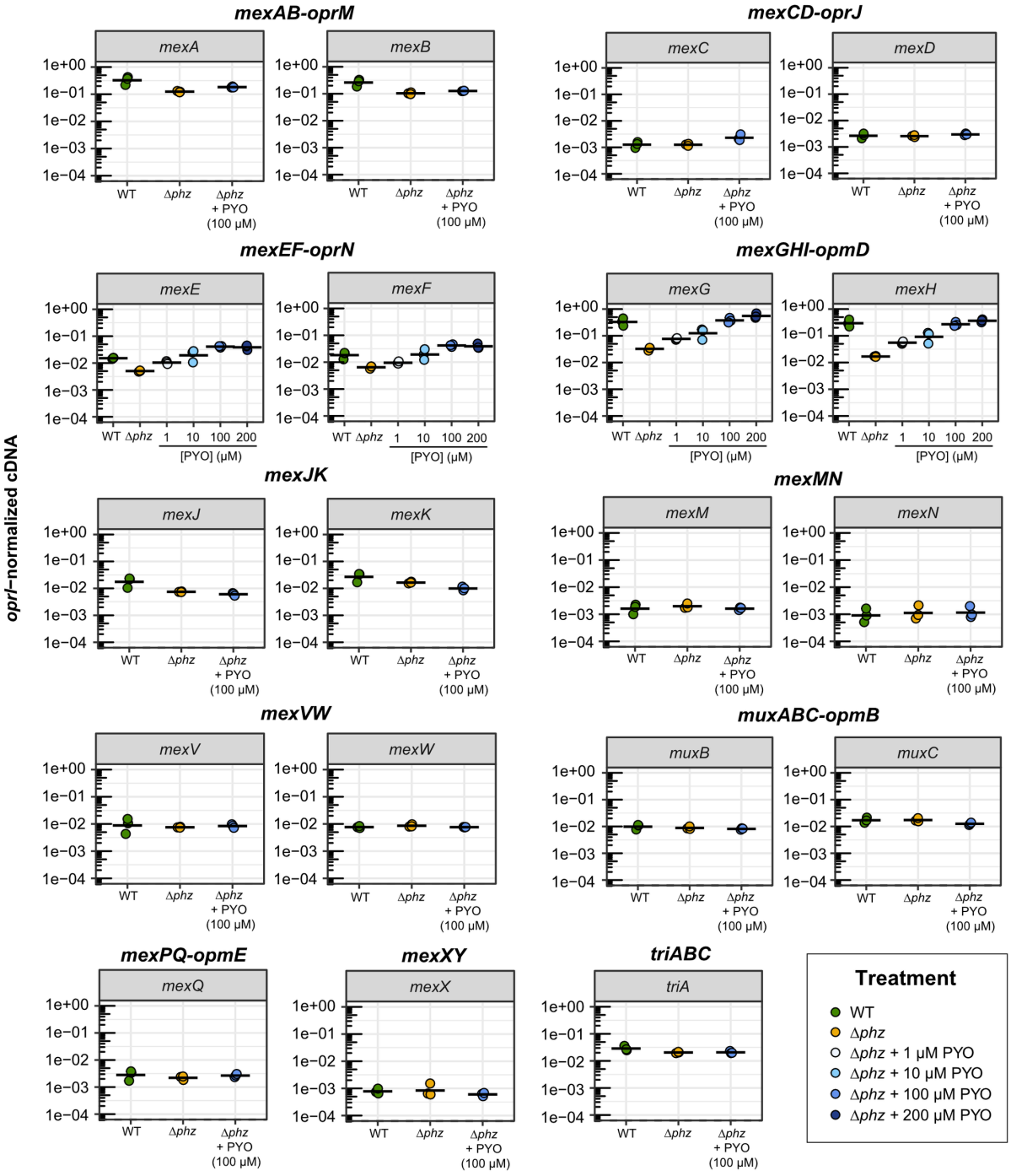

S2 Figure: Effects of PYO on the expression of *P. aeruginosa* RND efflux systems (normalized cDNA levels). The normalized cDNA levels for genes within operons coding for the 11 main RND efflux systems in *P. aeruginosa* are shown. cDNA levels for each gene were measured by qRT-PCR during early stationary phase and normalized by the levels of the housekeeping gene *oprI* (see Methods). This dataset was used to make the heatmap presented in Fig. 2B. Black horizontal lines mark the mean value for independent biological cultures (n = 3).

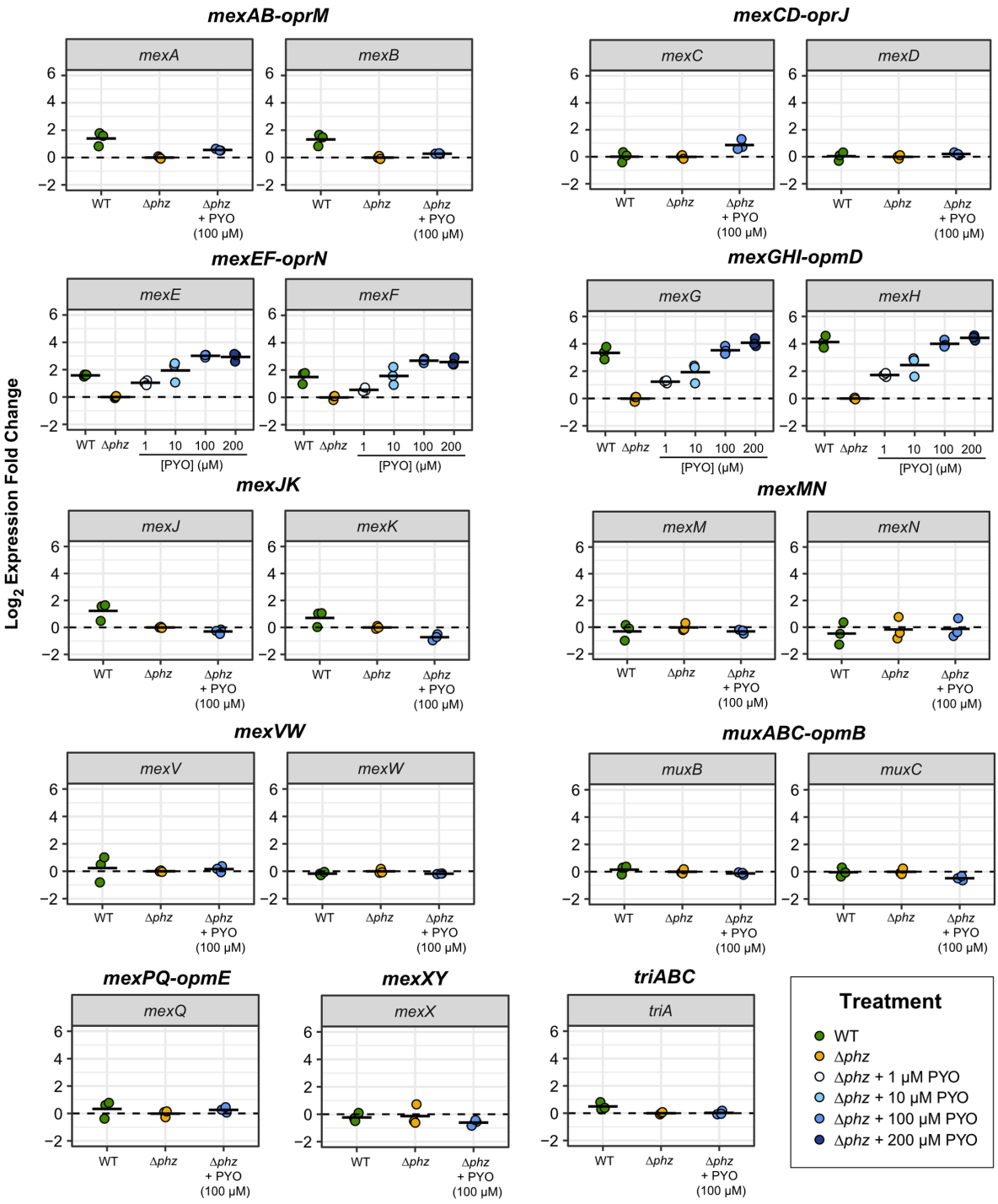

S3 Figure: Effects of PYO on the expression of *P. aeruginosa* RND efflux systems (fold change).
The PYO-induced changes in expression for genes within operons coding for the 11 main RND efflux systems in *P. aeruginosa* are shown. These plots are derived from the normalized cDNA dataset shown in S2 Fig. Here, the values for Δ*phz* were used as the basis for calculation of changes of expression (shown as $\log_2$ fold change). Black horizontal lines mark the mean value for independent biological cultures (n = 3).

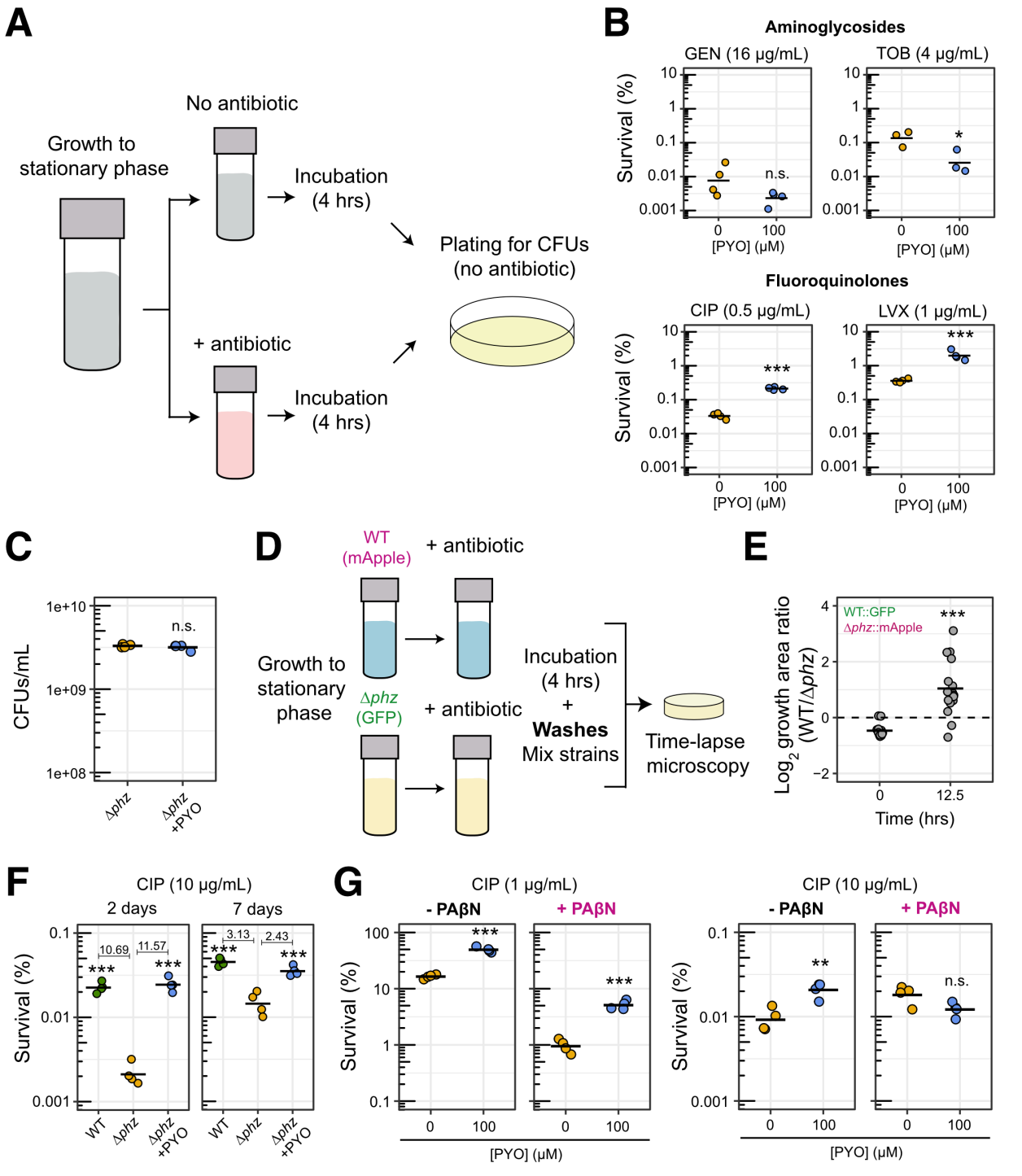

S4 Figure: Effects of PYO on *P. aeruginosa* tolerance to different antibiotics.
A. Experimental design for survival assay to measure tolerance to clinical antibiotics. In conditions with exogenous PYO, the PYO was added when cultures were inoculated. PYO itself was not lethal under these experimental conditions (see panel C in this Fig).
B. Tolerance levels of Δ*phz* cells harvested in log phase, following growth in the presence or absence of PYO (100 µM), to different aminoglycosides and fluoroquinolones (GEN = gentamicin, TOB = tobramycin, CIP =

ciprofloxacin, and LVX = levofloxacin). Data points represent replicates (n = 4 for all except tobramycin, for which n = 3). Stationary phase tolerance experiments are not shown for the aminoglycosides (gentamicin and tobramycin), as treatment with tobramycin in stationary phase under our conditions at this clinically-relevant concentration (EUCAST, 2020) did not result in cell death, regardless of the presence of PYO. However, for experiments performed with stationary phase cells in SCFM, killing did happen (see Fig. 2D).

C. Representative data showing CFUs counted for Δ*phz* grown for 20 hrs (glucose minimal medium, see Methods) in the presence and absence of PYO in our tolerance assays, showing that PYO itself was not toxic under the studied conditions (n = 4). These are the CFUs for the negative control (no antibiotic) for the experiment performed with CIP in Fig. 2C.

D. Experimental design for time-lapse microscopy experiments, in which cells were grown on agarose pads after exposure to CIP (10 μg/mL). The strain/fluorescent protein examples shown (i.e. WT::mApple, Δ*phz*::GFP) are the ones used in the images of Fig. 2F.

E. Quantification of microscopy data as done in Fig. 2G, but for the experiment with swapped fluorescent proteins.

F. Experiment quantifying how PYO affects lag for CFUs appearing after treatment with CIP (10 μg/mL, see Methods). Treating *P. aeruginosa* cells with 10 μg/mL resulted in high killing levels (see panel G), and we observed an increased lag in the absence of PYO (this supports microscopy data presented in Figs 2F-G and S4E Fig). The survival levels were calculated for CFUs counted after two days (too early, since more CFUs appeared later, changing the calculated survival levels) and seven days (no CFUs appeared after this time point; correct survival rate) of the LB plates incubation. Few new CFUs arose for WT and Δ*phz*+PYO treatments after two days, while several appeared for Δ*phz*. Numbers represent the mean survival ratio of WT/Δ*phz* and Δ*phz*+PYO/Δ*phz*. For survival calculated after two days, PYO's presence gave the impression of a ~10-fold higher survival rate. However, this was mostly due to lag of Δ*phz*, and the real survival difference was around ~2-3-fold (calculated after seven days) (n = 4).

G. Effects of the efflux inhibitor PAβN on tolerance levels to CIP of Δ*phz* cells grown in the presence or absence of PYO (100 μM). Cultures were treated with low (left) and high (right) CIP concentrations. Experiments for all the conditions were done in parallel (see Methods for full protocol) (n = 4).

Statistics: B, C, E, G – Welch's unpaired t-tests. F – One-way ANOVA with Tukey's HSD multiple-comparison test, with asterisks showing the statistical significance of comparisons with the Δ*phz* (no PYO) (* $p < 0.05$, ** $p < 0.01$, *** $p < 0.001$, n.s. $p > 0.05$). Black horizontal lines mark the mean value for independent cultures (or fields of view, for E).

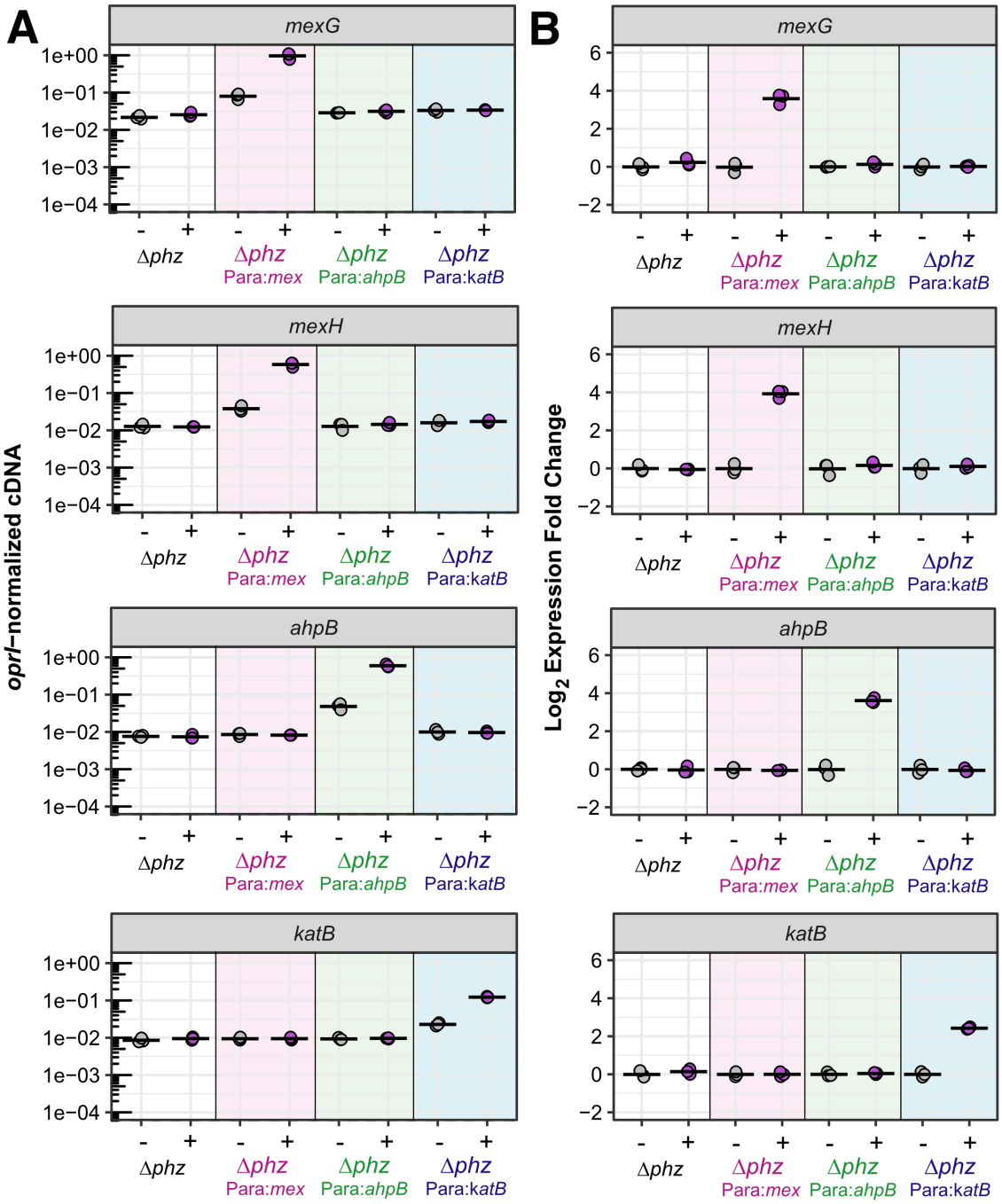

S5 Figure: Artificial induction of *mexGHI-opmD*, *ahpB* and *katB*.
A. Normalized cDNA levels measured by qRT-PCR. cDNA levels were normalized by the housekeeping gene *oprI*.
B. Fold change in expression upon arabinose induction. This dataset can be compared to the PYO-mediated induction of the same genes as shown in Figs. 2B, and S1, S2 and S3 Figs. The four strains shown are: 1) the parent Δ*phz* (white background), 2) Δ*phz* P_{ara}:*mexGHI-opmD* (magenta background), 3) Δ*phz* P_{ara}:*ahpB* (green background) and 4) Δ*phz* P_{ara}:*katB* (blue background). +/- represent addition or not of 20 mM arabinose to the cultures for the artificial induction of expression. For additional experimental details and strain information, see Methods and S5 Table. Black horizontal lines mark the mean value for independent biological cultures (n = 3).

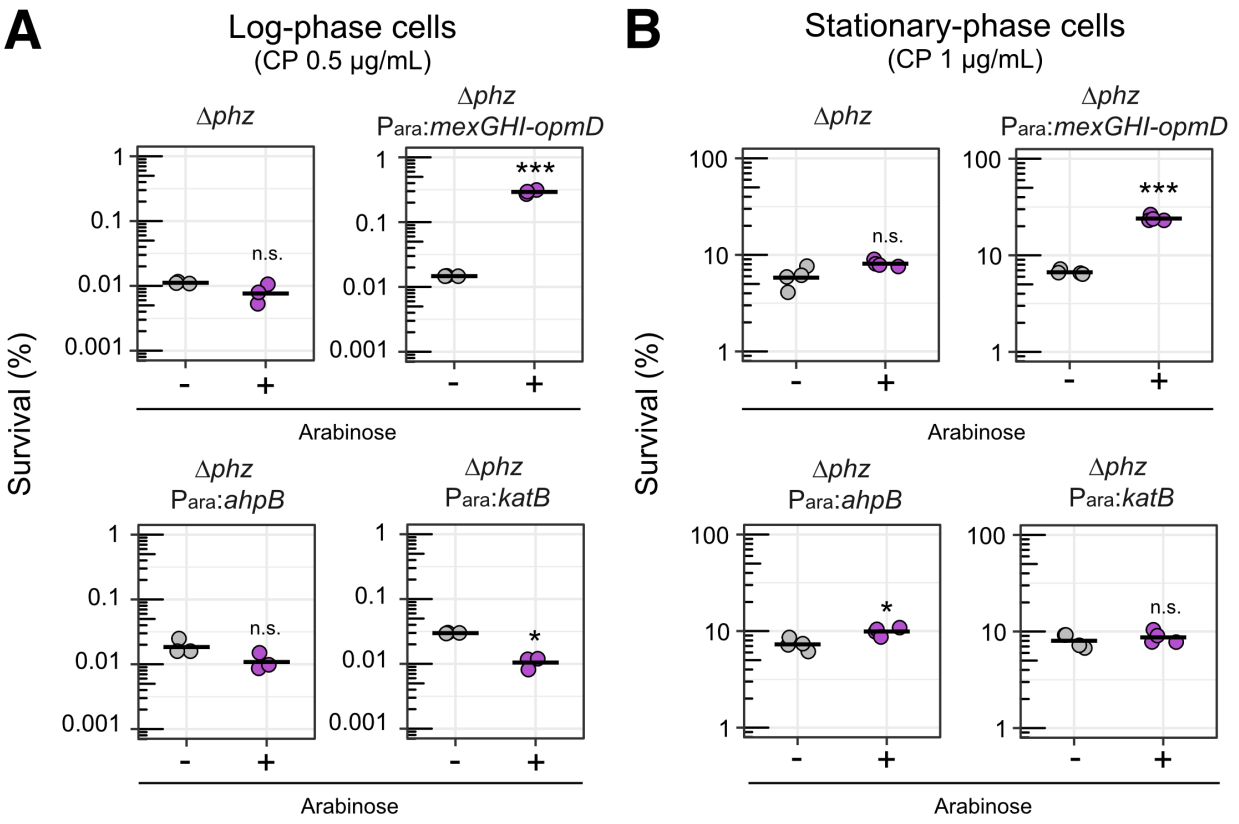

S6 Figure: Effect of artificial induction of PYO-induced genes on tolerance to ciprofloxacin.
Survival relative to the no-antibiotic control is shown for the parent Δ*phz* strain and the three arabinose-inducible strains (in which the PYO-inducible genes *mexGHI-opmD, ahpB,* or *katB* are under control of an arabinose-inducible promoter) grown in the presence or absence of 20 mM arabinose, without exposure to PYO. The tolerance experiments were performed for cultures in both log phase (A, n = 3) and stationary phase (B, n = 4). In B, the experiment for *mexGHI-opmD* is the same as in Fig. 2I, but is also shown here for ease of comparison. Statistics: Welch's unpaired t-tests (* $p < 0.05$, ** $p < 0.01$, *** $p < 0.001$, n.s. $p > 0.05$). Black horizontal lines mark the mean value for independent cultures.

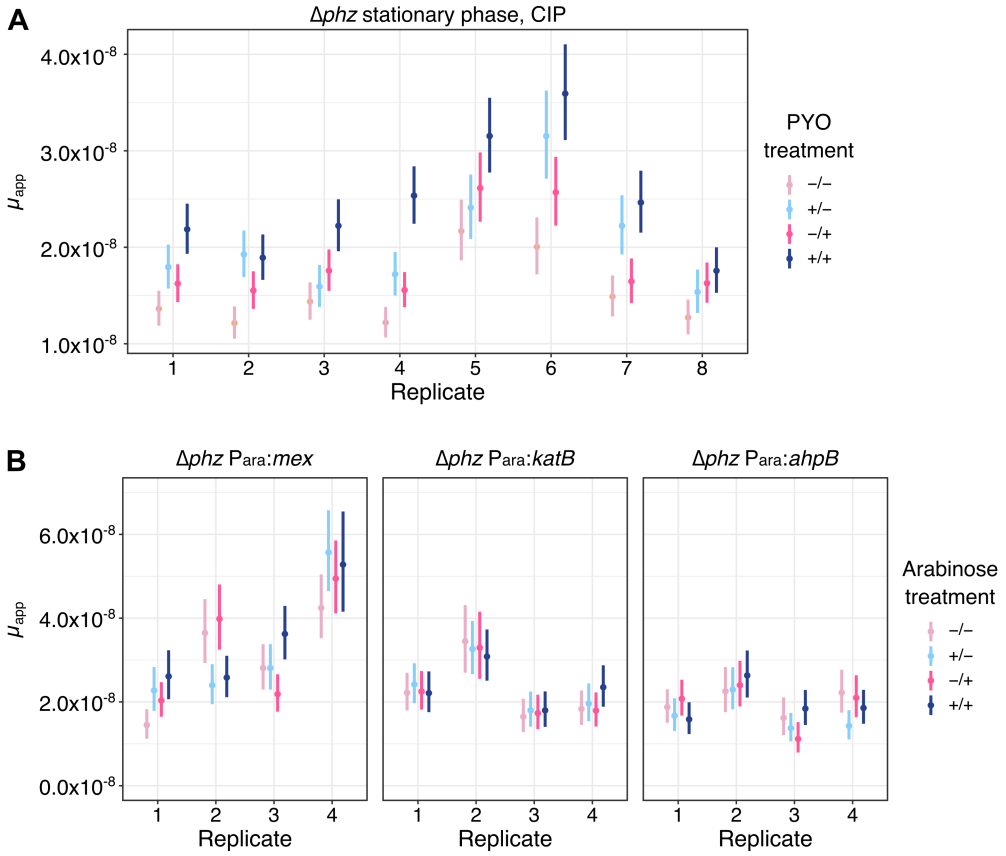

S7 Figure: Effect of PYO or PYO-induced genes on apparent mutation rates in *P. aeruginosa*.
A. Apparent mutation rates of stationary-phase Δ*phz* grown in liquid minimal medium and plated onto MH agar containing ciprofloxacin (CIP, 0.5 µg/mL), with or without pre- and/or co-exposure to 100 µM PYO relative to the antibiotic selection step (n = 8).
B. Apparent mutation rates of log-phase cells grown in glucose minimal medium and plated onto MH agar containing CIP (0.5 µg/mL), with or without pre- and/or co-exposure to 20 mM arabinose relative to the antibiotic selection step. Data are shown for Δ*phz* P_{ara}:*mexGHI-opmD,* Δ*phz* P_{ara}:*katB* and Δ*phz* P_{ara}:*ahpB* (n = 4). In all panels, each data point represents 44 parallel cultures from a single biological replicate, and the vertical lines represent 84% confidence intervals, for which lack of overlap corresponds to statistical significance at the $p < 0.05$ level (Zheng, 2017). The PYO treatments correspond to the following: -/- denotes no PYO pre-treatment (in the liquid culture stage) or co-treatment (in the antibiotic agar plates), +/- denotes PYO pre-treatment but no co-treatment, -/+ denotes PYO co-treatment without pre-treatment, and +/+ denotes both PYO pre-treatment and co-treatment.

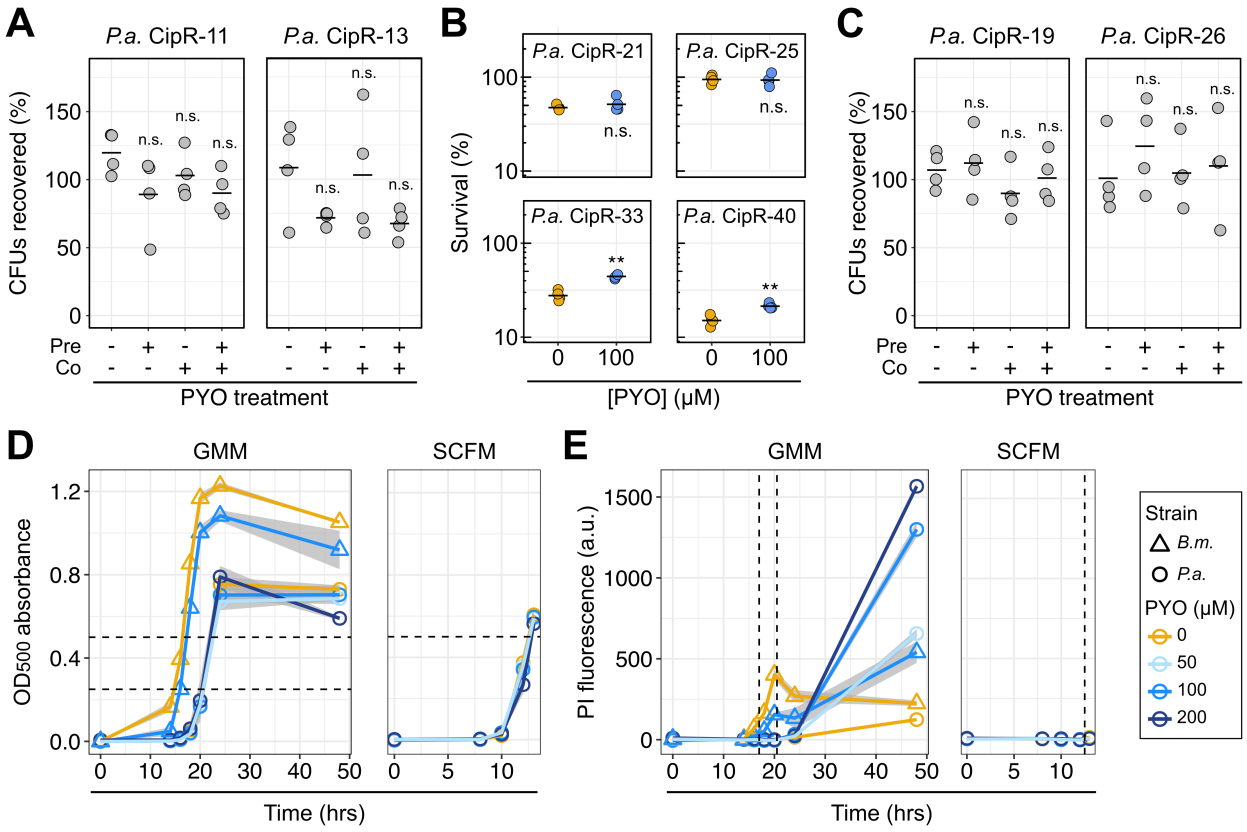

S8 Figure: Effect of PYO on resistance phenotypes and antibiotic tolerance of *P. aeruginosa* mutants.
A. The percentage of CFUs recovered on CIP (0.5 μg/mL) either with or without 100 μM PYO in the agar, for log-phase cultures of representative resistant mutants of *P. aeruginosa* (*P.a.*) that were not enriched by exposure to PYO in the fluctuation tests. The mutants were pre-grown with or without 100 μM PYO in glucose minimal medium before plating. On the x-axis, "pre" denotes the presence of PYO in the liquid cultures and "co" denotes the presence of PYO in the agar plates. Percentage recovery was calculated relative to total CFUs counted on non-selective plates (n = 4). **B.** Tolerance to CIP (1 μg/mL) of partially-resistant mutants grown in glucose minimal medium to stationary phase with or without 100 μM PYO (n = 4). Experiments were performed as shown in S5A Fig.
C. The percentage of CFUs recovered on CIP (0.5 μg/mL) for log-phase cultures of representative resistant mutants that were enriched by exposure to PYO in the fluctuation tests (n = 4). Experiments were performed in the same way as in panel A.
D-E. Growth curves performed for *P. aeruginosa* Δ*phz* (*P.a.*) and *B. multivorans 1* (*B.m.*) in glucose minimal medium (with the addition of amino acids for *B. multivorans*; see Methods) or SCFM, with different concentrations of PYO in the presence of 5 μM propidium iodide (PI), which is a fluorescent marker for cell death. OD_{500} (cell density) is plotted in G, while PI fluorescence is plotted in H. Gray shaded regions represent the standard deviation of four biological replicates. In G, the dashed horizontal lines mark the cell density at which *P. aeruginosa* (lower line in left panel) or *B. multivorans* (upper line in left panel) would have been plated in our fluctuation tests. Note that these OD_{500} values differ from those reported in the Methods section for fluctuation tests due to the use of a microtiter plate reader in this experiment, whereas a different spectrophotometer was used in the fluctuation tests. In H, the vertical dashed lines mark the time at which the cultures would have been plated in the fluctuation tests (in the left panel, left line = *B.m.* sampling time, right line = *P.a.* sampling time). The increase in fluorescence seen for *B. multivorans* prior to stationary phase likely reflects the production of a fluorescent metabolite rather than early cell death, as fluorescence was initially higher for the cultures not treated with PYO and the exponential phase growth rates were identical regardless of PYO treatment.

Statistics: A-C – Welch's unpaired t-tests (* $p < 0.05$, ** $p < 0.01$, *** $p < 0.001$, n.s. $p > 0.05$). Unless indicated otherwise with brackets, statistical significance is shown for the comparison with the untreated (no PYO) condition. In A-C, data points represent independent biological cultures, with horizontal black lines marking the mean value for each condition.

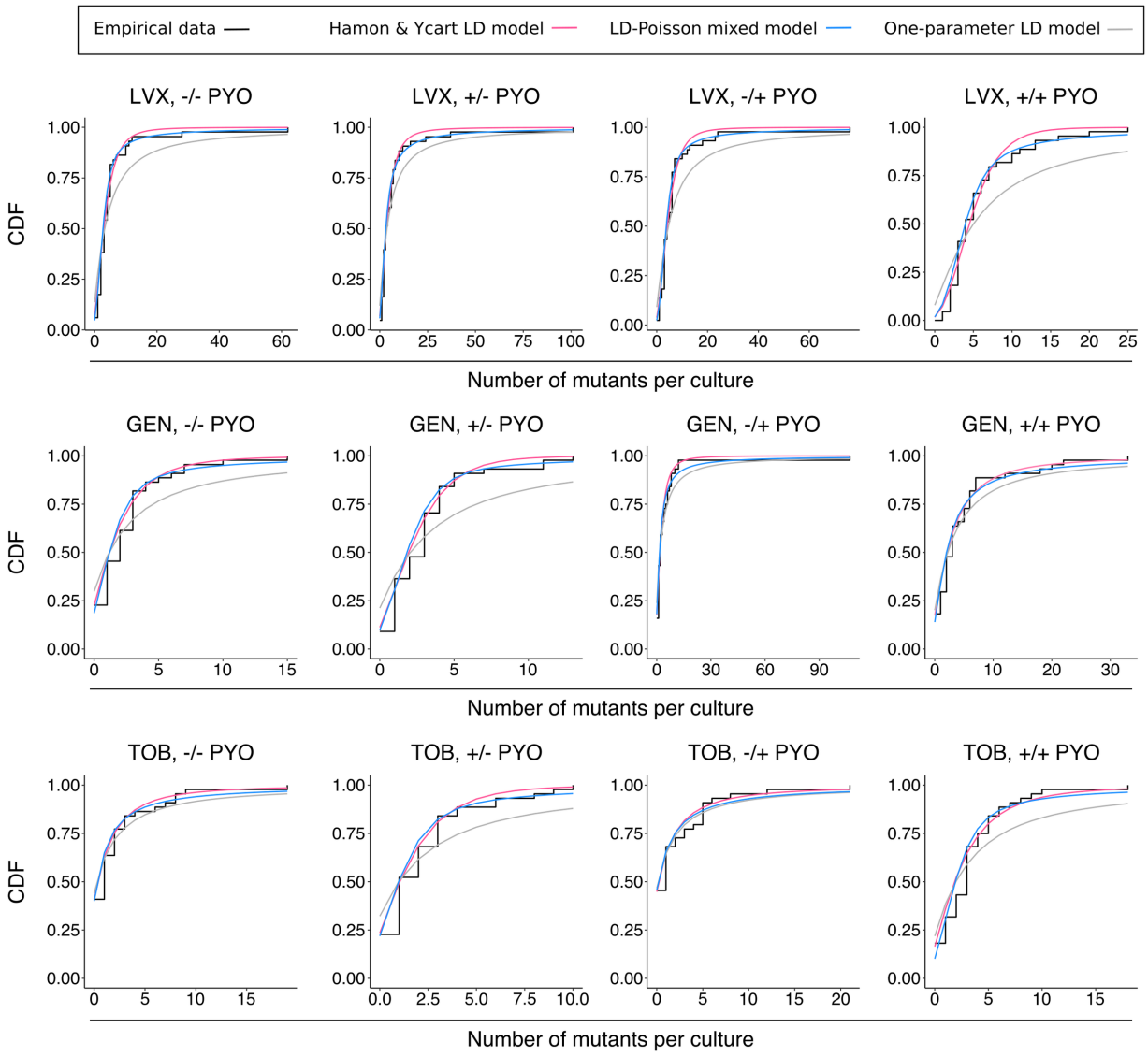

S9 Figure: Goodness-of-fit of different mathematical models for *P. aeruginosa* Δ*phz* fluctuation test data. Data are plotted for different combinations of PYO in liquid (pre-treatment) and PYO in agar (co-exposure to antibiotic selection). LVX = levofloxacin, GEN = gentamicin, and TOB = tobramycin. The empirical cumulative distribution functions of the data (black) are plotted against 1) a variation of the Luria-Delbrück model fit with two parameters, *m* (the expected number of mutations per culture) and *w* (the relative fitness of mutant cells vs. WT), as implemented by Hamon and Ycart (2012) (pink); 2) a mixed Luria-Delbrück and Poisson distribution fit with two parameters, *m* and *d* (the number of generations that occur post-plating), allowing for the possibility of post-plating mutations, as implemented by Lang and Murray (2008) (blue); 3) the basic Luria-Delbrück distribution model fit only with *m*, as implemented by Lang and Murray (2008) (gray). In each condition, the plotted data represent the biological replicate with the lowest chi-square goodness-of-fit *p*-value (i.e. least-good fit) for the Hamon & Ycart model.

S1 Table: Read ratios for each gene (PA14 genome) in the PYO tolerance Tn-seq experiment. Analysis was done using ARTIST software (see Methods). Ratios = reads + PYO conditions / reads no PYO condition (log_2-transformed), where high ratio values = increased fitness, and low ratio values = decreased fitness. Ciprofloxacin Tn-seq values are from: Cameron *et al*. (2018) (see Methods). NA = not applicable. NR =

not reported, meaning that there were no reads from the gene/locus within the replicate (or in at least one of the replicates, when displayed in the "average log2-tranformed ratio" column).

S2 Table: Statistical significance of comparisons of mutation rates and mutant frequencies. Mutation rates reported in this table were calculated using the rSalvador function newton.LD.plating and were compared using the LRT.LD.plating function to determine statistical significance. Mutant frequencies were compared using the Mann-Whitney U test. Reported *p*-values were adjusted with the Benjamini-Hochberg correction to control the false discovery rate.

S3 Table: Fluctuation test analysis results for all log-phase experiments conducted in minimal medium. Model parameters: μ = apparent mutation rate per generation; m = expected number of mutational events per cultures; w = fitness ratio of mutants/WT; d = number of post-plating generations. Abbreviations: HY = Hamon & Ycart; LD = Luria-Delbrück; score = negative log likelihood; LRT = likelihood ratio test; CIP = ciprofloxacin; LVX = levofloxacin; GEN = gentamicin; TOB = tobramycin. See Methods for details on the different mathematical models.

S4 Table: Mutations detected in ciprofloxacin-resistant isolates of *Pseudomonas aeruginosa* PA14. Mutations were detected using breseq, with the reference set as the *P. aeruginosa* UCBPPPA14 genome obtained from BioProject accession number PRJNA38507. Pseudogenes and synonymous substitution mutations were omitted from the table.

S5 Table: Strains, plasmids, and primers used in this study.

S6 Table: Mutations detected in partially ciprofloxacin-resistant isolates of *Burkholderia multivorans* AU42096.
Mutations were detected using breseq, with a draft assembly of the genome for *B. multivorans* AU42096 as the reference. Only mutations unique to each isolate are included.

S7 Table: Ciprofloxacin MICs for fluctuation test isolates and parent strains. MICs were determined in a microbroth dilution assay according to standard clinical methods (see Methods). Where a range of values is presented, this indicates that the observed MIC sometimes varied depending on the initial cell density of the inoculum, even within the clinically-acceptable range of 3-7 x 10^5 CFUs/mL.

Chapter 4

IMPACTS OF BACTERIAL SECONDARY METABOLITES ON ANTIBIOTIC TOLERANCE AND RESISTANCE

This chapter has been submitted for publication as:

Perry, E.K.*, Meirelles, L.A.*, and Newman, D.K. From the soil to the clinic: the impact of microbial secondary metabolites on antibiotic tolerance and resistance. (Submitted)

Abstract

Secondary metabolites profoundly impact microbial physiology, metabolism, and stress responses. While these molecules can modulate microbial susceptibility to commonly used antibiotics, secondary metabolites are typically excluded from standard antimicrobial susceptibility assays. This longstanding oversight may in part account for why infections by diverse opportunistic bacteria that produce secondary metabolites often exhibit discrepancies between clinical antimicrobial susceptibility testing results and clinical treatment outcomes. Here, we synthesize the evidence for which types of secondary metabolites alter antimicrobial susceptibility, as well as how and why this phenomenon occurs. We discuss examples of molecules that opportunistic and enteric pathogens either make themselves or are exposed to from their neighbors, and the nuanced impacts these molecules can have on tolerance and resistance to certain antibiotics. Notably, many opportunists hail from the soil, where secondary metabolites have been used for millennia to wage microbial chemical warfare. That numerous secondary metabolites interact with known routes of antibiotic tolerance and resistance suggests that the ecological history of opportunistic pathogens underpins their notoriously high intrinsic antibiotic resilience. Considering the worldwide need to optimize antibiotic treatment strategies to mitigate the growing antibiotic resistance crisis, we hope this review will stimulate further research on how secondary metabolites impact antibiotic resilience.

Introduction

A vast number of organisms produce a wide range of molecules classified as “secondary metabolites” (Maplestone *et al.*, 1992; Demain and Fang, 2000). Usually defined as organic

compounds that are not directly involved in the producer's growth and development, secondary metabolites can be made by Eukarya (e.g. plants and fungi), Bacteria, and Archaea (Keller *et al.*, 2005; Tyc *et al.*, 2017; Wang and Lu, 2017). In microbial planktonic cultures, they are typically produced during stationary phase, once doubling times have slowed (Price-Whelan *et al.*, 2006; Davies, 2013). As a result, these compounds were for many years assumed to be waste products of metabolism (Haslam, 1986). However, a more nuanced view of the biological functions of microbial secondary metabolites has emerged over the past two decades. Indeed, the moniker "secondary" is something of a misnomer, as these molecules have been shown to play key roles in multiple physiological processes that are critical for microbial survival (Price-Whelan *et al.*, 2006; Davies, 2013), including but not limited to the acquisition of nutrients (such as iron or phosphate), cell-cell signaling, and energy conservation in the absence of oxygen (Demain and Fang, 2000; Dietrich *et al.*, 2006; Wang *et al.*, 2011; Glasser *et al.*, 2014; McRose and Newman, 2021).

In addition to conferring such pleiotropic benefits, many microbial secondary metabolites are also toxic, both to their producers and to neighboring organisms (Haslam, 1986; Maplestone *et al.*, 1992; Demain and Fang, 2000). It is therefore not surprising that antibiotic development pipelines have driven the majority of secondary metabolite characterization and purification efforts, dating back to the discoveries of penicillin and streptomycin in the early 20th century. Most modern clinical antibiotics are the synthetic descendants of natural products that originated from soil microbes, and even today, environmental microbes are still being exploited productively as a source of novel molecules with potent antimicrobial properties (Ling *et al.*, 2015; Tortorella *et al.*, 2018; Chevrette *et al.*, 2019; Fukuda *et al.*, 2021). Yet while the soil-to-clinic axis continues to inspire natural product chemists in their search for and design of new drugs, microbiologists have ironically neglected to consider the potential for unintended consequences of this pipeline, particularly with respect to antibiotic efficacy against opportunistic pathogens that evolved in the same environment. Microbes are rarely, if ever, found in isolation, and therefore the presence of secondary metabolites in a microbial community puts a strong evolutionary pressure both on secondary-metabolite-producing and non-producing members to develop means to withstand them. These defenses can in turn have collateral activity against clinical antibiotics.

In this Review, we highlight the growing body of evidence connecting bacterial secondary metabolites to the problem of clinical antibiotic tolerance (i.e. ability to survive transient antibiotic

exposure) and resistance (i.e. ability to grow in the presence of antibiotics) (Kester and Fortune, 2014; Brauner *et al.*, 2016; Balaban *et al.*, 2019). Emphasizing examples of secondary metabolites produced by opportunistic or enteric pathogens (Table 1), we discuss common modes of action through which these molecules can alter clinical antibiotic efficacy in both single-species and polymicrobial communities. Specifically, we draw attention to secondary metabolites that regulate multidrug resistance efflux systems, secondary metabolites that modulate the toxicity of antibiotics through interactions with reactive oxygen species, and the potential for secondary-metabolite-induced antibiotic tolerance to provide an overlooked route for the evolution of antibiotic resistance in bacterial infections. We offer suggestions for future experiments to explore the breadth of relevance of these observations (Box 1) and discuss the implications that secondary metabolite production can have for the diagnosis of antibiotic resistance (Box 2). Finally, we consider how knowledge of interactions between secondary metabolites and antibiotic efficacy could be applied to optimize the use of existing antimicrobial drugs and generate targets for novel therapeutic strategies.

Secondary-metabolite-mediated regulation of multidrug resistance efflux pumps

Activation of efflux pumps that export toxins out of the cell is a powerful mechanism used by diverse bacteria to thrive during clinical antibiotic treatment (Piddock, 2006b; Li *et al.*, 2015). However, efflux pumps long predate human use of synthetic antibiotics, and therefore are presumed to have originally evolved to transport other, naturally-occurring substrates (Piddock, 2006a; Martinez *et al.*, 2009). Indeed, efflux transport systems can help bacterial cells tolerate stress caused by toxic secondary metabolites produced by themselves (Tahlan *et al.*, 2007; Sakhtah *et al.*, 2016; Wolloscheck *et al.*, 2018; Meirelles and Newman, 2018), by competitor species (including other bacteria) (Benomar *et al.*, 2019), or by a host (e.g. plant or animal (Shafer *et al.*, 1998; Bina and Mekalanos, 2001; Burse *et al.*, 2004; Buckley *et al.*, 2006)), directly impacting fitness (Piddock, 2006a). Efflux pumps also play a key role in the export of metabolites, such as siderophores or signaling molecules, that are not toxic at normal physiological concentrations, but must be secreted in order to confer benefits to their producers (Martinez *et al.*, 2009; Imperi *et al.*, 2009). Extensive details about the types and components of efflux pumps can be found in other recent reviews (Mousa

and Bruner, 2016; Du *et al.*, 2018). Here, we focus instead on how the induction of efflux systems as a response to self-produced secondary metabolites can impact antibiotic tolerance and resistance in pathogenic bacteria (Fig. 1A). The examples we discuss fall mostly within the resistance-nodulation-division (RND) efflux systems, which use the proton-motive force to power substrate transport by working as H^+-coupled antiporters (Li *et al.*, 2015). However, the same principles are,

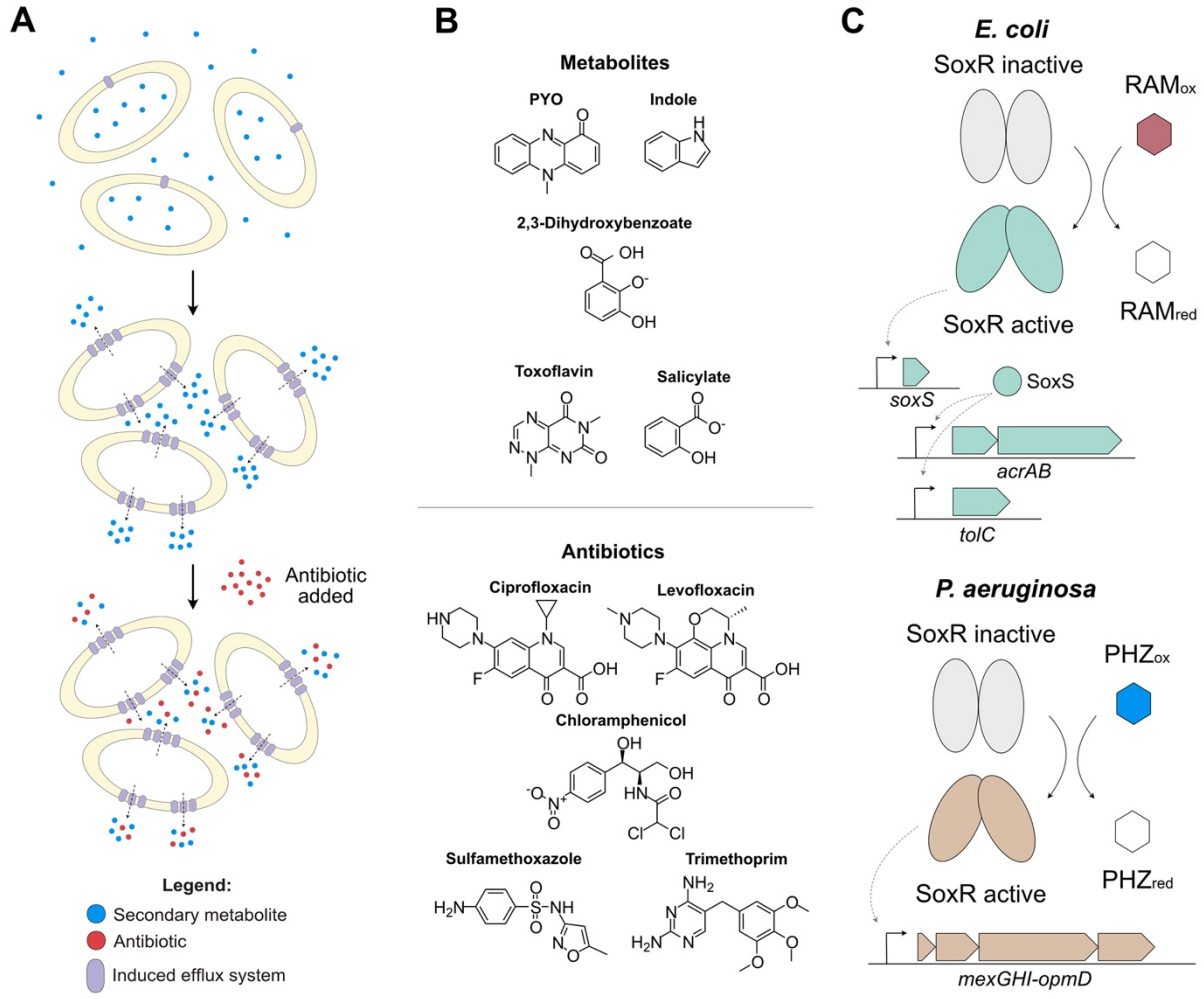

Figure 1: Secondary-metabolite-mediated regulation of multidrug resistance efflux pumps.
A. Schematic showing how secondary metabolites, through the induction of efflux systems used to transport the metabolite, can provide collateral resilience to antibiotics used in the clinic.
B. Structures of known efflux-regulating secondary metabolites and selected clinical antibiotics, showing the shared prevalence of aromatic and/or heterocyclic ring motifs. **C.** SoxR-regulated efflux systems in *E. coli* and *P. aeruginosa*. Each SoxR monomer contains a Fe-S cluster that can be directly oxidized by redox-active molecules, leading to its activation and transcriptional induction of efflux systems (Dietrich *et al.*, 2008; Imlay, 2013). In *E. coli* (top), several molecules can induce transcription of the efflux system AcrAB-TolC through SoxR activation (Gu and Imlay, 2011; Imlay, 2013; Singh *et al.*, 2013). In *P. aeruginosa* (bottom), SoxR activation is mediated by two endogenous phenazines, 5-Me-PCA and PYO, and leads to the induction of the efflux system MexGHI-OpmD (Dietrich *et al.*, 2006; Dietrich *et al.*, 2008; Sakhtah *et al.*, 2016; Meirelles and Perry *et al.*, 2021). PYO, Pyocyanin; PHZ, phenazine; RAM, redox-active molecule.

in theory, applicable to other types of efflux systems, as long as they are regulated by secondary metabolites. Importantly, efflux pumps vary in their specificity, with regard to both their regulation and their substrate affinity (Du *et al.*, 2018). Therefore, to predict whether a secondary metabolite will increase antibiotic resilience in its producer through the induction of a particular efflux system, it is essential to understand how the secondary metabolite interacts with the transcriptional regulation of the system, as well as which classes of drugs the system can transport. More broadly, many known efflux-regulating secondary metabolites have at least one aromatic or heterocyclic ring (Fig. 1B), possibly suggesting that secondary metabolites with this structural motif are particularly likely to affect antibiotic resilience through the induction of multidrug efflux systems.

In the enteric bacterium *Escherichia coli*, one of the best-studied multidrug resistance efflux systems is AcrAB-TolC, which has a complex regulatory system and forms part of a general stress response (Du *et al.*, 2018). While AcrAB-TolC is generally expressed at high intrinsic levels (Li and Nikaido, 2016; Du *et al.*, 2018), numerous molecules have been shown to further upregulate its transcription. These inducers include not only factors produced by animal hosts (e.g. bile salts and fatty acids (Rosenberg *et al.*, 2003)) and synthetic redox-active compounds (e.g. paraquat and phenazine methosulfate (Miller *et al.*, 1994; Gu and Imlay, 2011; Gerstel *et al.*, 2020)), but also self-produced secondary metabolites such as the compound 2,3-dihydroxybenzoate, an intermediate in the biosynthesis of the siderophore enterobactin (Ruiz and Levy, 2014). In fact, 2,3-dihydroxybenzoate directly binds to MarR (Chubiz and Rao, 2010), a transcriptional repressor that modulates the expression of AcrAB-TolC alongside the redox-sensing SoxRS regulatory system (Du *et al.*, 2018) (Fig. 1C). Although whether production of enterobactin or 2,3-dihydroxybenzoate *per se* increases antibiotic resilience has not been tested, it is well-established that AcrAB-TolC provides protection against many clinical antibiotics (Anes *et al.*, 2015). Another example of a self-produced secondary metabolite in *E. coli* with an efflux-mediated effect on antibiotic susceptibility is indole. Generally considered a signaling molecule, indole triggers activation of certain RND efflux genes in enteric bacteria and the resulting efflux pumps are capable of transporting multiple classes of antibiotics (Hirakawa *et al.*, 2005; Nishino *et al.*, 2005; Nishino *et al.*, 2007; Nikaido *et al.*, 2012). Indeed, the production of high levels of indole by a subpopulation of mutants has been characterized as a "charity" mechanism that induces population-level resistance against norfloxacin and gentamicin in *E. coli*, with the MdtEF-TolC efflux system being upregulated by this secondary

metabolite (Lee *et al.*, 2010). Intriguingly, a connection between TolC and sensitivity to anthraquinone-2,6-disulfonate (an analog of naturally-occurring redox-active humic substances in soils that resembles quinone-containing synthetic antibiotics) was observed in *Shewanella oneidensis* (Shyu *et al.*, 2002), reinforcing the point that functional relationships between these classes of molecules may be common.

Besides being activated by diverse compounds, efflux pumps can also confer collateral resilience to clinical antibiotics when serving as a self-defense response against secondary metabolites that are toxic to their producers. For example, multiple RND efflux systems capable of exporting clinical drugs are regulated in the opportunistic pathogen *Pseudomonas aeruginosa* by toxic self-produced secondary metabolites called phenazines (Dietrich *et al.*, 2006; Sakhtah *et al.*, 2016; Meirelles and Newman, 2018; Meirelles and Perry *et al.*, 2021). Phenazines are redox-active compounds known to play important roles both in natural environments (e.g. by protecting plants against fungal pathogens) as well as in infections (e.g. by increasing *P. aeruginosa* virulence in the lungs of cystic fibrosis (CF) patients) (Lau *et al.*, 2004; Mavrodi *et al.*, 2006). *P. aeruginosa* produces several different phenazines, including phenazine-1-carboxylic acid (PCA), pyocyanin (PYO), 5-methylphenazine-1-carboxylate (5-Me-PCA, an intermediate in PYO synthesis (Laursen and Nielsen, 2004)), phenazine-1-carboxamide (PCN), and 1-hydroxy-phenazine (1-OH-PHZ). Toxicity to the producing cells varies across the different phenazines, but all can cause auto-poisoning, particularly under nutrient-limited conditions (Meirelles and Newman, 2018). In the presence of PYO or 5-Me-PCA, the *mexGHI-opmD* efflux pump operon is positively regulated by the redox-sensing transcription factor SoxR (Price-Whelan *et al.*, 2006) (Fig. 1C), whereas expression of this pump is minimal in the absence of these phenazines (Sakhtah *et al.*, 2016; Meirelles and Perry *et al.*, 2021). PYO also induces a second RND efflux operon, *mexEF-oprN* (Meirelles and Newman, 2018; Meirelles and Perry *et al.*, 2021), which is known to be clinically relevant (Llanes *et al.*, 2011; Richardot *et al.*, 2016). The regulation of this efflux system is similarly thought to be impacted by redox sensing (Fargier *et al.*, 2012), though the details of how this works are still unclear. The substrate specificities of these systems overlap, and both can transport phenazines; however, MexGHI-OpmD does so more efficiently (Wolloscheck *et al.*, 2018). Experiments with a broad-spectrum efflux pump inhibitor as well as a knockout mutant lacking *mexGHI-opmD* have confirmed that efflux is a major mechanism underlying the tolerance and resistance of *P. aeruginosa* to its own

phenazines (Sakhtah *et al.*, 2016; Wolloscheck *et al.*, 2018; Meirelles and Perry *et al.*, 2021). Importantly, both PYO-regulated efflux pumps are also known to efficiently transport fluoroquinolones, and multiple studies have reported a strong antagonistic effect of phenazines on fluoroquinolone efficacy (Wolloscheck *et al.*, 2018; Schiessl *et al.*, 2019; Zhu *et al.*, 2019; Meirelles and Perry *et al.*, 2021). For example, *P. aeruginosa* cells exposed to PYO (either self-produced or exogenously added) display increased tolerance against the fluoroquinolones ciprofloxacin and levofloxacin (Meirelles and Perry *et al.*, 2021). This phenotype was recapitulated in one study by artificially overexpressing MexGHI-OpmD in a phenazine-null mutant to a level similar to that achieved in the presence of PYO, suggesting that drug efflux drives PYO-mediated increases in fluoroquinolone tolerance (Meirelles and Perry *et al.*, 2021). Interestingly, besides fluoroquinolones and chloramphenicol, MexEF-OprN is also thought to transport trimethoprim and sulfamethoxazole—to which *P. aeruginosa* is intrinsically resistant (Lister *et al.*, 2009)—but not aminoglycosides (Lister *et al.*, 2009), against which phenazines have demonstrated mixed effects on tolerance (Schiessl *et al.*, 2019; Zhu *et al.*, 2019; Meirelles and Perry *et al.*, 2021). Like phenazines, but unlike aminoglycosides, all of the known antibiotic substrates for MexEF-OprN have at least one aromatic ring (Fig. 1B), suggesting that when a secondary metabolite regulates an efflux pump with a relatively limited range of substrates, analysis of shared structural motifs may enable prediction of which clinical antibiotics will be most affected.

Besides MexGHI-OpmD and MexEF-OprN, *P. aeruginosa* possesses at least nine other RND efflux systems, many of which are expressed at very low levels under typical laboratory conditions (Lister *et al.*, 2009). Whether any *P. aeruginosa*-produced secondary metabolites regulate these other efflux systems under clinically-relevant circumstances remains to be determined. Notably, however, phenazines are not the only secondary metabolites produced by *P. aeruginosa* that promote increased resilience against antibiotics by inducing efflux. Recent work showed that production of the secondary metabolite paerucumarin likewise stimulates transcription of the MexEF-OprN efflux system in *P. aeruginosa*, with consequent increases in resistance to both chloramphenicol and ciprofloxacin (Clarke-Pearson and Brady, 2008; Iftikhar *et al.*, 2020). These findings underscore the potential for self-produced secondary metabolites to promote clinical antibiotic resilience in opportunistic pathogens by triggering upregulation of efflux pumps.

Other bacterial opportunistic pathogens inhabiting soils or plant roots also produce secondary metabolites that promote efflux and decrease antibiotic susceptibility. For example, several strains of "*Burkholderia cepacia* complex" species isolated from CF patients can produce salicylate (Sokol *et al.*, 1992; Darling *et al.*, 1998). Salicylate has Fe-chelating properties and is used as a siderophore by the producing cells (Visca *et al.*, 1993; Bakker *et al.*, 2014), but it also induces specific efflux systems in *Burkholderia* species (e.g. CeoAB-OpcM in *B. cenocepacia*), leading to increased antibiotic resistance (Nair *et al.*, 2004). Moreover, the salicylate-derived antibiotic resistance effect is not limited to the *Burkholderia* genus; for example, in enterobacteria, salicylate binds to and inactivates MarR, leading to upregulation of efflux pump expression and increased resistance to multiple clinical antibiotics (Cohen *et al.*, 1993; Brochado *et al.*, 2018). *Burkholderia* species also produce several other secondary metabolites that could affect antibiotic resilience, including many natural antibiotics with strong inhibitory capacities relevant during plant host colonization (Burkhead *et al.*, 1994; Jeong *et al.*, 2003; Depoorter *et al.*, 2016; Depoorter *et al.*, 2021). One intriguing example is toxoflavin, which is made by several *Burkholderia* species including *Burkholderia gladioli*, a common species in CF patients (Lipuma, 2010). Although it is still unknown whether toxoflavin auto-poisons producing cells, it is redox-active (Latuasan and Berends, 1961; Gencheva *et al.*, 2018), presumably causing oxidative stress through the generation of H_2O_2 (Latuasan and Berends, 1961), and it is toxic to other bacteria and fungi (Latuasan and Berends, 1961; Li *et al.*, 2019). More importantly, like PYO, toxoflavin induces a specific RND efflux system, ToxFGHI, which is used for its export (Kim *et al.*, 2004). It is not yet known if *B. gladioli* or other opportunistic pathogens within the *Burkholderia* genus produce toxoflavin during infections, or if the toxoflavin-induced RND efflux system ToxFGHI can transport any of the currently used clinical antibiotics; however, it would not be surprising if it were to do so, given that toxoflavin, like PYO, bears structural similarity to fluoroquinolones. Taken together, the examples discussed in this section highlight the rich diversity of bacterial secondary metabolites that induce efflux activity in their producers, consequently threatening the efficacy of clinical antibiotic treatments.

Effects of secondary metabolites on oxidative-stress-related antibiotic toxicity

More than a decade ago, it was proposed that bactericidal antibiotics exert their lethal effects in part by inducing oxidative stress, regardless of the specific cellular targets of different antibiotic classes (Kohanski *et al.*, 2007). While this hypothesis has engendered controversy (Keren *et al.*,

2013; Liu and Imlay, 2013), ample evidence reviewed elsewhere (Dwyer *et al.*, 2015) strongly suggests that bactericidal antibiotics impact cellular redox states, and that the resulting increases in reactive oxygen species (ROS) and oxidative stress can be lethal, even though other mechanisms also contribute to cell death. Bacteria exhibit increased resilience to bactericidal antibiotics when pretreated with antioxidants (Dwyer *et al.*, 2014), when respiration is attenuated (Lobritz *et al.*, 2015), and following pre-exposure to hydrogen peroxide or superoxide-generating redox-cycling drugs, which induce protective oxidative stress responses (Vega *et al.*, 2013; Mosel *et al.*, 2013; Dwyer *et al.*, 2014; Martins *et al.*, 2020). Conversely, antibiotic toxicity can be potentiated by the loss of oxidative stress response genes (Wang and Zhao, 2009; Dwyer *et al.*, 2014), or by alterations in cellular metabolism that increase endogenous ROS generation (Brynildsen *et al.*, 2013). Importantly, many secondary metabolites also interface with cellular redox homeostasis and oxidative stress responses. Here, we discuss three different modes of action by which these metabolites can affect the potency of clinical antibiotics (Fig. 2A): 1) upregulation of oxidative stress response genes, 2) direct detoxification of ROS, and 3) increased endogenous ROS generation.

Secondary metabolites that upregulate defenses against oxidative stress

Secondary metabolites that upregulate the expression of oxidative stress responses can prime bacterial cells for tolerance and/or resistance to clinical antibiotics, analogous to the protective effects of exposure to sub-lethal concentrations of oxidants like H_2O_2. Among this class of metabolites, indole is perhaps the best-studied. As mentioned above, indole can also influence antibiotic susceptibility by upregulating efflux pump expression. However, this effect is thought to happen primarily at high concentrations of indole (>1 mM) (Hirakawa *et al.*, 2005; Nikaido *et al.*, 2012); indole concentrations in human feces tend to be somewhat lower (Zuccato *et al.*, 1993), though measurements up to the equivalent of 1100 μM have been recorded (Karlin *et al.*, 1985). At these lower concentrations, indole is non-toxic to its producer, *E. coli*, but still induces oxidative stress response genes regulated by OxyR, including alkyl hydroperoxide reductases, thioredoxin reductase, and the DNA binding protein Dps (Vega *et al.*, 2012). While exposure to indole increases the frequency of *E. coli* persisters to antibiotics belonging to three different classes (fluoroquinolones, aminoglycosides, and beta-lactams) by at least an order of magnitude, deletion of *oxyR* significantly diminishes this effect, demonstrating that upregulation of oxidative stress responses by a secondary metabolite can contribute to bacterial persistence (Vega *et al.*, 2012). The

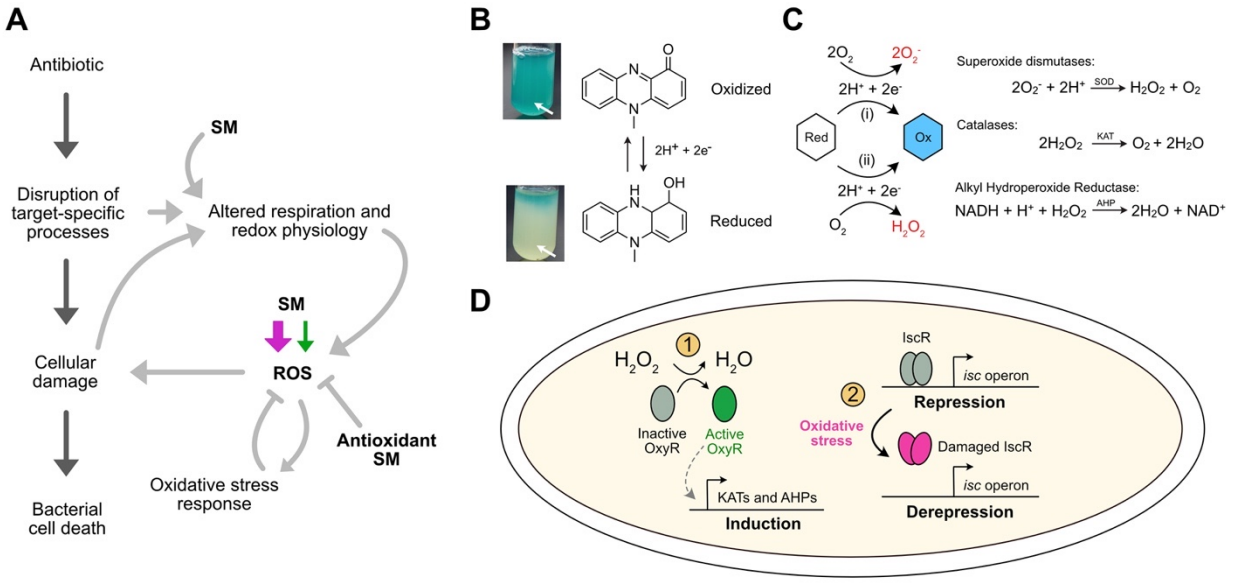

Figure 2: Secondary metabolite interactions with oxidative stress.
A. Schematic depicting how bactericidal antibiotics can cause cell death both by directly disrupting target-specific processes, and by indirectly promoting the formation of reactive oxygen species as a consequence of altered respiration and cellular damage. Secondary metabolites can interface with these pathways at multiple points, including by interfering with respiration and redox homeostasis, directly generating ROS through redox-cycling, and detoxifying ROS via one-electron reactions. Secondary metabolites that promote oxidative stress can either antagonize or potentiate antibiotic toxicity, likely depending on whether the resulting increases in ROS are moderate (green arrow) or severe (purple). Moderate increases in ROS may induce protective oxidative stress responses that can counteract antibiotic toxicity, whereas severe increases in ROS may overwhelm the cell's defenses, leading to synergistic effects with bactericidal antibiotics.
B. The redox-active nature of PYO is visually apparent as it undergoes a color change from blue (oxidized) to colorless (reduced) upon gaining two electrons and two protons from cellular reductants. This reaction is reversible under physiological conditions.
C. Many redox-active secondary metabolites can donate electrons to molecular oxygen in the process of cycling from a reduced (Red) to an oxidized (Ox) state, leading to the formation of superoxide or hydrogen peroxide. Cells can detoxify these forms of ROS through enzymatic reactions catalyzed by superoxide dismutase, catalase, and alkyl hydroperoxide reductase (Imlay, 2013).
D. Bacterial oxidative stress responses are typically regulated through multiple pathways. Shown here is the example of *Pseudomonas aeruginosa*, in which the H_2O_2-sensing transcription factor OxyR controls the expression of catalases (KATs) and alkyl hydroperoxide reductases (AHPs) (Ochsner *et al.*, 2000; Wei *et al.*, 2012), and IscR upregulates the biosynthesis of iron-sulfur clusters in response to oxidative stress (Romsang *et al.*, 2016).

molecular pathway through which indole activates OxyR remains unclear, but indole readily undergoes one-electron reduction to a radical form in the presence of hydroxyl radicals or other strong oxidants (Shen *et al.*, 1987), suggesting that it might interact with and potentially amplify endogenous ROS generated as a byproduct of respiration. Indole has also been proposed to disrupt the arrangement of membrane lipids, allowing direct interaction of respiratory quinones with dioxygen and thereby leading to superoxide generation (Garbe *et al.*, 2000).

PYO is another example of a bacterial secondary metabolite that induces oxidative stress responses. As a redox-active metabolite that can gain and lose electrons reversibly under physiological conditions (Fig. 2B), PYO can generate ROS under aerobic conditions through direct reduction of oxygen to superoxide (Fig. 2C), in addition to interfering with respiration (Voggu *et al.*, 2006; Perry and Newman, 2019). In its producer, *P. aeruginosa*, PYO increases superoxide dismutase activity (Hassett *et al.*, 1992) and upregulates the transcription of several other oxidative stress response genes, including those encoding alkyl hydroperoxide reductases, thioredoxin reductase, catalase, and iron-sulfur cluster biogenesis machinery (Meirelles and Newman, 2018) (Fig. 2C-D). Intriguingly, PYO has been shown to increase the frequency of gentamicin-resistant mutants in *P. aeruginosa* cultures in a manner that is independent of drug efflux, as PYO does not upregulate aminoglycoside-transporting efflux pumps (Meirelles and Perry *et al.*, 2021). Given that gentamicin is known to promote intracellular ROS formation through the formation of complexes with iron (Priuska and Schacht, 1995; Prayle *et al.*, 2010), and that pre-treating cells with oxidants can prime them to tolerate antibiotics (Mosel *et al.*, 2013), a plausible explanation for this phenomenon is that PYO-induced oxidative stress responses counteract ROS-related gentamicin toxicity. This in turn could decrease the rate at which spontaneous mutants are stochastically lost from the population (Alexander and MacLean, 2020), leading to the observed increase in the frequency of resistant mutants. PYO can also promote the growth of *P. aeruginosa* in the presence of other aminoglycosides (kanamycin, streptomycin, and tobramycin) and a beta-lactam antibiotic (carbenicillin) (Zhu *et al.*, 2019). Like gentamicin, these antibiotics are not known to be substrates for PYO-regulated efflux systems (Lister *et al.*, 2009; Meirelles and Perry *et al.*, 2021), but do belong to classes of drugs that have been shown to perturb cellular redox states (Dwyer *et al.*, 2014; Belenky *et al.*, 2015), again suggesting that the observed decreases in antibiotic efficacy could be related to PYO-induced oxidative stress responses.

Microbial metabolites that detoxify ROS

In contrast to ROS-generating redox-active secondary metabolites that induce enzymatic oxidative stress responses, secondary metabolites that possess antioxidant activity (i.e. the ability to neutralize highly reactive free radicals) can protect against antibiotic assaults by directly detoxifying antibiotic-derived ROS. One example is ergothioneine, which is one of two major sulfur-containing redox buffers in mycobacteria, along with mycothiol. Loss of ergothioneine biosynthesis genes in

Mycobacterium tuberculosis significantly decreases minimum inhibitory concentrations (MICs) for rifampicin, isoniazid, bedaquiline, and clofazimine, in addition to decreasing survival under treatment at the wildtype MICs by at least 30-60% (Saini *et al.*, 2016). Other secondary metabolites with antioxidant activity have been shown to be important for resistance to ROS generated by host immune cells, including macrophages and neutrophils. One such metabolite is staphyloxanthin, a membrane-embedded carotenoid pigment that protects *Staphylococcus aureus* against ROS (Clauditz *et al.*, 2006; Hall *et al.*, 2017) and consequently decreases killing by neutrophils (Clauditz *et al.*, 2006). Carotenoids produced by group B *Streptococcus* (Liu *et al.*, 2004) and the dental pathogen *Streptococcus mutans* (Wu *et al.*, 2010) have likewise been implicated in resistance to ROS. The antioxidant capacity of these pigments has been attributed to their highly conjugated polyene backbones (Edge and Truscott, 2018), though the exact mechanisms by which different carotenoids scavenge ROS remain unclear (Young and Lowe, 2018). Importantly, antioxidant agents need not necessarily be located in the cytoplasm in order to protect against antibiotic-induced ROS accumulation, as exogenous catalase has been shown to increase bacterial survival following exposure to trimethoprim (Hong *et al.*, 2019). Thus, while most studies on membrane-embedded carotenoids have focused on interactions with extracellular sources of ROS, these pigments might also be able to dampen oxidative stress that originates inside the cell during treatment with bactericidal antibiotics. Considering the growing body of evidence that redox imbalance and oxidative stress are downstream effects of many antimicrobial drugs (Dwyer *et al.*, 2015), the possibility that staphyloxanthin or other membrane-associated pigments promote resilience to clinical antibiotics is worthy of further investigation.

In addition to the above examples, certain microbially-produced compounds that are not classical secondary metabolites—either because they are inorganic or are not always dispensable for normal growth—also contribute to antibiotic tolerance or resistance by enhancing the antioxidant capacity of bacterial cells. For example, endogenously generated H_2S protects a diverse range of bacteria, including *E. coli*, *P. aeruginosa*, and *S. aureus*, against the toxicity of antibiotics known to exert oxidative stress, such as gentamicin (Shatalin *et al.*, 2011). This phenomenon has been proposed to stem from a dual-action mechanism whereby H_2S both inhibits the Fenton reaction and stimulates the activities of catalase and superoxide dismutase (Shatalin *et al.*, 2011). Polyamines have also been shown to protect bacteria from antibiotic toxicity by counteracting oxidative stress.

This is thought to be due in part to their capacity to neutralize free radicals (Tkachenko and Fedotova, 2007; El-Halfawy and Valvano, 2014), though physical protection of cellular components and indirect upregulation of other oxidative stress responses may also be involved (Tkachenko and Fedotova, 2007; El-Halfawy and Valvano, 2013). *E. coli* upregulates production of putrescine and spermidine upon exposure to antibiotics under aerobic conditions, and these polyamines in turn significantly increase viability under antibiotic treatment by decreasing ROS production and oxidative damage (Tkachenko *et al.*, 2012). Similarly, putrescine secreted by *Burkholderia cenocepacia* protects its producer against oxidative stress arising from treatment with polymyxin B, norfloxacin, or rifampicin (El-Halfawy and Valvano, 2014). Finally, in *P. aeruginosa*, the BqsRS regulatory system drives increased polyamine production upon sensing ferrous iron, which is prevalent in the lungs of CF patients, thereby promoting survival in the presence of cationic antibiotics such as polymyxins and aminoglycosides (Kreamer *et al.*, 2015). Together, these examples demonstrate how interactions between bacterial metabolites and oxidative stress can lead to increased resilience against clinical antibiotics.

Synergistic interactions between ROS-generating secondary metabolites and antibiotics

Besides the examples in which secondary metabolites decrease antibiotic efficacy by attenuating oxidative stress, it is also important to note that in some cases, secondary metabolites that increase ROS generation can amplify the toxicity of clinical antibiotics. One example is 2-heptyl-3-hydroxy-4-quinolone, also known as the *Pseudomonas* quinolone signal (PQS), which is produced by *P. aeruginosa*. PQS is a redox-active molecule capable of reducing not only free radicals but also metal ions, and consequently possesses both antioxidant properties and pro-oxidant activity (i.e. the ability to induce oxidative stress), as reduction of iron promotes ROS formation through the Fenton reaction (Häussler and Becker, 2008). The pro-oxidant activity appears to dominate in cells, as PQS induces oxidative stress responses and increases sensitivity to hydrogen peroxide and ciprofloxacin (Bredenbruch *et al.*, 2006; Häussler and Becker, 2008). The pro-oxidant activity of PQS is also evidenced by the fact that overproduction of PQS acts synergistically with impairment of superoxide dismutase and catalase activity to increase endogenous oxidative stress and antibiotic susceptibility (Nguyen *et al.*, 2011). Notably, abolishment of PQS production increases tolerance to ciprofloxacin, imipenem, and gentamicin (Häussler and Becker, 2008). Another redox-active secondary metabolite that increases antibiotic susceptibility under certain

conditions is PYO. While pre-exposure of *P. aeruginosa* to PYO increases tolerance to fluoroquinolones and promotes the establishment of gentamicin-resistant mutants, PYO and other phenazines have also been shown to increase the sensitivity of *P. aeruginosa* to cationic antimicrobial peptides, including colistin (Schiessl *et al.*, 2019; Meirelles and Perry *et al.*, 2021) and polymyxin B (Zhu *et al.*, 2019). The underlying mechanism of this synergistic interaction has yet to be determined, but it is notable that polymyxin B precipitates severe oxidative stress in *P. aeruginosa* and other Gram-negative opportunistic pathogens (Sampson *et al.*, 2012; Han *et al.*, 2019). Moreover, unlike fluoroquinolones or aminoglycosides, cationic antimicrobial peptides also permeabilize the outer membrane (Trimble *et al.*, 2016) and consequently are almost certain to increase phenazine uptake, which would accelerate ROS generation even further. Thus, the lethal synergy between phenazines and cationic antimicrobial peptides may ultimately be driven by an overwhelming cascade of oxidative stress. Given that ROS-generating secondary metabolites can both potentiate and diminish antibiotic efficacy depending on the circumstances, future studies focused on revealing which effects take precedence during infections will be critical to better understanding how such secondary metabolites may affect clinical treatment outcomes.

Secondary metabolites as interspecies modulators of antibiotic resilience

So far, we have discussed examples of secondary metabolites that either are known to affect their producer's susceptibility to clinical antibiotics, or have the potential to do so based on their interactions with established mechanisms of antibiotic tolerance and resistance. Equally important, however, is the fact that many secondary metabolites—in particular those that are secreted—are also capable of acting as interspecies modulators of antibiotic resilience (Fig. 3). Indeed, significant attention has recently been called to how interactions among members of a polymicrobial infection might affect antibiotic treatment outcomes (Welp and Bomberger, 2020; Bottery *et al.*, 2020). Such infections are common in chronic respiratory disease (such as in CF patients) and in chronic wounds, with a wide range of microbial species often being acquired over time (Rhoads *et al.*, 2012; Einarsson *et al.*, 2019; Welp and Bomberger, 2020). Many of these organisms originate from soil (LiPuma *et al.*, 2002; Berg *et al.*, 2005) and therefore are likely to have a long history of evolving defense mechanisms to cope with each other's toxins (Martinez, 2009; Davies and Davies, 2010). Interspecies microbial interactions are also thought to be important in gastrointestinal infections, where enteric pathogens are surrounded by the resident commensal microbiota (Vega *et al.*, 2013).

While our understanding of how exchangeable secondary metabolites impact community-level antibiotic resilience is still in its infancy, there have been several reports on this subject. For example, indole has been identified as an interspecies modulator of antibiotic tolerance between *E. coli* and *Salmonella typhimurium* (Nikaido *et al.*, 2012; Vega *et al.*, 2013). *S. typhimurium*, which likely interacts with commensal *E. coli* during infections, does not itself produce indole, yet its tolerance to ciprofloxacin increased by greater than threefold in the presence of exogenously-added indole, as well as in co-cultures with indole-producing *E. coli* (Vega *et al.*, 2013). Similarly to its effect in *E. coli*, indole induces OxyR-regulated oxidative stress responses in *S. typhimurium*, and deletion of *oxyR* abolished the indole-mediated increase in ciprofloxacin tolerance (Vega *et al.*, 2013). Interestingly, indole has also been reported to increase resistance to ampicillin in the indole non-producer *P. aeruginosa*, not by inducing oxidative stress responses but rather by stimulating the expression of efflux pumps and a chromosomal beta-lactamase (Kim *et al.*, 2017). These examples highlight the potential for secreted secondary metabolites to have both conserved and mechanistically divergent effects on antibiotic resilience in neighboring species.

Other secondary metabolites besides indole have shown potential as interspecies modulators of antibiotic resilience. For example, the protective effect against polymyxin B of putrescine secreted by *B. cenocepacia* extends not only to the producer, but also to neighboring species in co-cultures, including *E. coli* and *P. aeruginosa* (El-Halfawy and Valvano, 2013). Similarly, PYO produced by *P. aeruginosa* dramatically increases the tolerance of multiple clinically-relevant *Burkholderia* species to ciprofloxacin in co-cultures (Meirelles and Perry *et al.*, 2021). In yet another opportunistic pathogen, *Acinetobacter baumanii*, exposure to PYO increases the frequency of persisters to amikacin and carbenicillin by three- to four-fold (Bhargava *et al.*, 2014), possibly through the upregulation of superoxide dismutase and catalase (Heindorf *et al.*, 2014; Bhargava *et al.*, 2014). Finally, quorum sensing signals produced by *P. aeruginosa* induce fluconazole resistance in the yeast *Candida albicans* (Bandara *et al.*, 2020), indicating that bacterial secondary metabolites can mediate not only interspecies but also interkingdom effects on antimicrobial efficacy. So far, these interactions have only been demonstrated *in vitro*. However, given that *Burkholderia* species, *Acinetobacter* species, and fungal pathogens can all be found together with *P. aeruginosa* in chronic infections (Lipuma, 2010; Chmiel *et al.*, 2014; Schwab *et al.*, 2014), these findings suggest that

valuable insights could be gained from future studies focused on the *in vivo* relevance of secondary-metabolite-mediated interspecies induction of antibiotic resilience.

Importantly, while the above examples suggest that certain secreted secondary metabolites have the potential to raise the community-wide level of antibiotic resilience in polymicrobial infections, a secondary metabolite that promotes antibiotic resilience in one species will not always do so in others. One key consideration is that in order for a secondary metabolite to trigger cross-species induction of clinical antibiotic resilience, the non-producing species must be able to tolerate any stress caused by the secondary metabolite. Otherwise, the added toxicity of the secondary metabolite may outweigh the benefit of any induced defenses or collateral antibiotic detoxification, and the secondary metabolite might even act synergistically with the clinical antibiotic (Wood and Cluzel, 2012). Examples of this type of interaction have been found between *S. aureus* and *P. aeruginosa*, two species that often co-occur in CF patients (Briaud *et al.*, 2020; Yung *et al.*, 2021; Camus *et al.*, 2021). *S. aureus* is sensitive to several secondary metabolites secreted by *P. aeruginosa* (Noto *et al.*, 2017; Radlinski *et al.*, 2017), and some of these can increase the susceptibility of *S. aureus* to clinical antibiotics. For example, *P. aeruginosa*-produced rhamnolipids potentiate tobramycin toxicity in *S. aureus* by increasing membrane permeability (Radlinski *et al.*, 2017). Another *P. aeruginosa*-produced secondary metabolite, 2-n-heptyl-4-hydroxyquinoline N oxide (HQNO), was recently shown to increase the sensitivity of *S. aureus* biofilms to fluoroquinolones and membrane-targeting antibiotics via a similar mechanism (Orazi *et al.*, 2019). However, the toxic effects of *P. aeruginosa* secondary metabolites on *S. aureus* are not always synergistic with clinical antibiotics. By inhibiting growth, HQNO promotes tolerance in *S. aureus* biofilms specifically to antibiotics targeting cell wall synthesis and protein synthesis (Orazi and O'Toole, 2017), contrary to its effect on other classes of antibiotics, while in planktonic cultures of *S. aureus*, HQNO can induce multidrug tolerance by inhibiting respiration and depleting intracellular ATP (Radlinski *et al.*, 2017). The interference of PYO with respiration in *S. aureus* similarly selects for non-respiring small colony variants (Biswas *et al.*, 2009; Noto *et al.*, 2017), which are often resistant to antibiotic treatment (McNamara and Proctor, 2000). In such cases where different secondary metabolites produced by one species seem to have conflicting and condition-dependent effects on a neighboring species, *in vivo* studies and co-culture experiments are particularly necessary to determine the overall impact on clinical antibiotic efficacy.

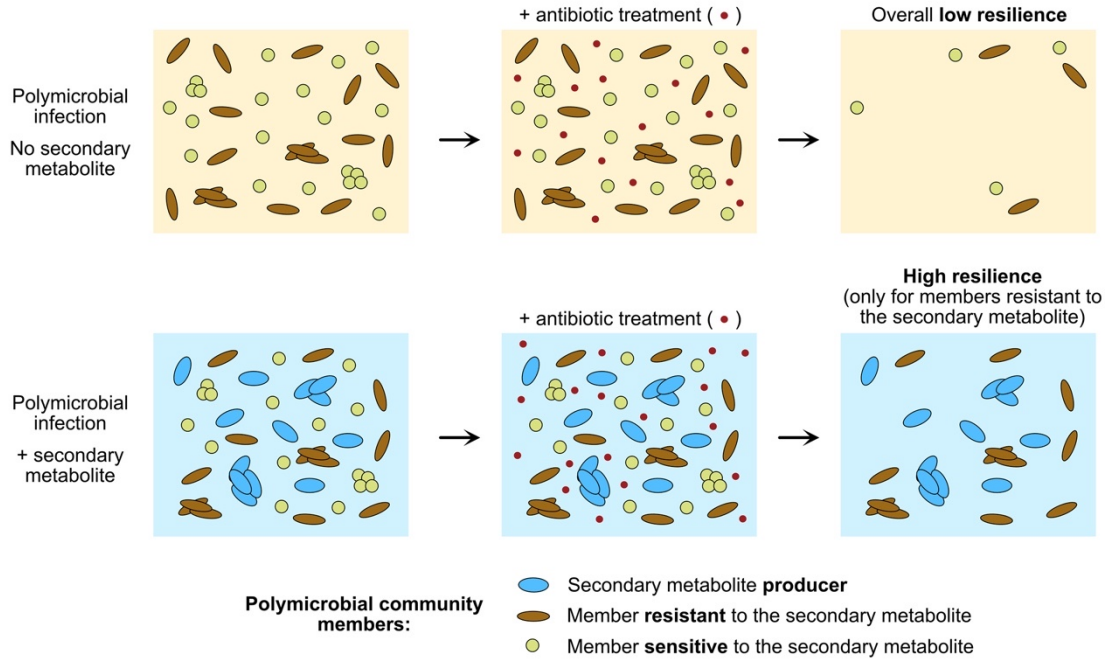

Figure 3: Secondary metabolites as interspecies modulators of antibiotic resilience. The presence of secondary metabolite producers in polymicrobial infections can alter the community susceptibility profile to antibiotic treatment. When the producer is not present (top), overall resilience levels upon treatment are low. However, through the secretion of the secondary metabolite, the producer's presence (bottom, blue cells) can have distinct effects on different community members. For members intrinsically resistant to the secondary metabolite (brown cells), the molecule's presence can increase resilience to antibiotic treatment. However, if a member is sensitive to the secondary metabolite (yellow cells), the added toxicity can overwhelm cellular defenses, potentiating the killing by the clinical drug.

The potential for *P. aeruginosa*-produced secondary metabolites to have complex effects on antibiotic resilience has also been observed in another opportunistic pathogen, *Stenotrophomonas maltophilia*. Compared to members of the *Burkholderia cepacia* complex, which strongly benefit from exposure to PYO during treatment with ciprofloxacin, *S. maltophilia* is more sensitive to PYO toxicity, exhibiting growth inhibition at concentrations as low as 50 µM (Meirelles and Perry *et al.*, 2021). At a relatively low but still lethal dose of ciprofloxacin, PYO at concentrations up to 50 µM significantly increased survival of *S. maltophilia*, suggesting that defenses active against fluoroquinolones are indeed induced by PYO in this species (Meirelles and Perry *et al.*, 2021). Yet at a ten-fold higher dose of ciprofloxacin, even 10 µM PYO was detrimental. Notably, while *in situ* levels of PYO can vary greatly across patients infected with *P. aeruginosa*, PYO has been detected in infected sputum and wound exudates at concentrations up to 130 µM or 0.31 mg/g, respectively (Cruickshank and Lowbury, 1953; Wilson *et al.*, 1988). Thus, the example of PYO and

S. maltophilia suggests that in order to predict how a secondary metabolite will impact community-wide levels of clinical antibiotic resilience during a polymicrobial infection, it may be necessary to characterize the directionality and magnitude of interspecies effects over a range of clinically-relevant concentrations of both the secondary metabolite and the clinical antibiotic.

Implications of secondary-metabolite-induced antibiotic tolerance for the evolution of resistance

In recent years, it has increasingly become appreciated that antibiotic tolerance can not only directly contribute to infection treatment failure, but also promote the establishment of heritable resistance mutations (Levin-Reisman *et al.*, 2017; Windels *et al.*, 2019; Levin-Reisman *et al.*, 2019; Liu *et al.*, 2020; Santi *et al.*, 2021). The latter observation raises the possibility that secondary-metabolite-induced antibiotic tolerance could promote the evolution of *de novo* antibiotic resistance during the course of an infection, especially considering the fact that the stimulatory effect of tolerance on the acquisition of resistance is thought to occur via multiple mechanisms that are largely agnostic to the specific mode of tolerance. First, tolerance results in a larger pool of surviving cells following transient or intermittent antibiotic treatments, inherently broadening the window of opportunity for rare spontaneous resistance mutations to occur (Levin-Reisman *et al.*, 2017). Second, tolerance raises the likelihood that a spontaneous mutation conferring low-level resistance will become established in the population rather than being stochastically lost during the antibiotic treatment. That tolerance can promote resistance in this manner was first proposed more than 30 years ago by Moreillon and Tomasz, who sought to explain the empirical correlation between penicillin tolerance and penicillin resistance in clinical isolates of pneumococci (Moreillon and Tomasz, 1988), and has recently been confirmed with a combination of *in vitro* evolution experiments, mathematical modeling, and simulations (Levin-Reisman *et al.*, 2017). Importantly, another recent study demonstrated that even at antibiotic concentrations less than 1/8 the MIC of a resistant strain, fewer than 5% of single resistant cells produce detectable outgrowth (Alexander and MacLean, 2020), suggesting considerable scope for tolerance to promote the evolution of resistance by raising this frequency. Moreover, while this effect of tolerance is most impactful for spontaneous mutants with low-level resistance (Levin-Reisman *et al.*, 2017), such mutations significantly increase the probability of subsequently acquiring high-level resistance (Toprak *et al.*, 2011; Baym *et al.*, 2016; Santi *et al.*, 2021). Finally, antibiotic tolerance and slow growth have also been proposed

to be epistatically linked to genome-wide mutation rates (Nishimura *et al.*, 2017; Windels *et al.*, 2019); slow growth is itself a common mechanism of tolerance by virtue of decreasing the opportunity for interactions between bactericidal antibiotics and their targets, which generally are components of core biosynthetic machinery (Pontes and Groisman, 2020). In one study, expression levels of the AcrAB efflux pump in *E. coli* were not only positively correlated with the frequency of mutation to resistance against diverse clinical antibiotics (which could potentially be explained by the aforementioned mechanisms), but were also inversely correlated with growth rate and levels of the DNA mismatch repair protein MutS (El Meouche and Dunlop, 2018). This observation suggests that induced antibiotic tolerance could in some cases affect the inherent mutability of a strain, in addition to promoting the fixation of spontaneous resistance mutations.

To date, exploration of the connection between antibiotic tolerance and the evolution of resistance has largely focused on tolerance resulting from spontaneous mutations that are selected by treatment with clinical antibiotics (Levin-Reisman *et al.*, 2017; Levin-Reisman *et al.*, 2019; Liu *et al.*, 2020; Santi *et al.*, 2021). However, effects on the establishment of heritable resistance mutations have already been demonstrated for at least one antibiotic-tolerance-inducing secondary metabolite produced by an opportunistic pathogen—namely, PYO. Experiments based on classical fluctuation tests revealed that PYO increases the rate of mutation to antibiotic resistance not only in the producing species, *P. aeruginosa*, but also in a clinical isolate of a co-occurring opportunist, *Burkholderia multivorans* (Meirelles and Perry *et al.*, 2021). Importantly, the impact of PYO on the acquisition of heritable resistance varied across different classes of antibiotics, with particularly strong effects for drugs against which PYO-induced defenses confer increased tolerance, suggesting that this phenomenon is indeed driven by tolerance as opposed to a mutagenic effect of PYO. Remarkably, in *B. multivorans*, treatment with PYO increased mutation rates for ciprofloxacin resistance to a level rivaling clinical hypermutator strains (Martina *et al.*, 2014; Meirelles and Perry *et al.*, 2021). In addition, in both *P. aeruginosa* and *B. multivorans*, pre-treatment with PYO prior to antibiotic selection was sufficient to increase the rate at which resistant mutants became established, even without continued exposure to high levels of PYO. These findings collectively reveal the potential for tolerance-inducing secondary metabolites to significantly impact the evolution of antibiotic resistance during infections.

Concluding remarks and future directions

While direct connections between bacterial secondary metabolite production or exposure and resilience to clinical antibiotics have only been pursued in a handful of studies, many more secondary metabolites are known to interface with cellular functions that are relevant to antibiotic tolerance and resistance—especially drug efflux and oxidative stress responses. We hope the examples discussed in this Review stimulate further investigation into the conditions under which these and related secondary metabolites alter the efficacy of clinical antibiotics. Moreover, we expect that deliberately searching for such molecules across a broad range of opportunistic pathogens (Box 1) will reveal additional as-yet-uncharacterized secondary metabolites that have the potential to meaningfully affect antibiotic treatment outcomes. Soil-borne opportunistic pathogens in particular often possess the biosynthetic capacity to produce a great variety of secondary metabolites (Ryan *et al.*, 2009; Smith *et al.*, 2013; Walterson and Stavrinides, 2015; Depoorter *et al.*, 2016), perhaps as a consequence of needing to cope with the extraordinary complexity and heterogeneity that typifies the soil environment (König *et al.*, 2020). In most cases, the biological functions of these secondary metabolites, as well as whether they are produced during infections, remain unknown. However, biosynthetic gene clusters for secondary metabolites are often located near or co-transcribed with genes encoding efflux pumps (Martín *et al.*, 2005; Severi and Thomas, 2019; Crits-Christoph *et al.*, 2020), and numerous microbial secondary metabolites are redox-active and therefore have the potential to generate or detoxify ROS (Glasser *et al.*, 2017; McRose and Newman, 2021), suggesting that interactions with clinical antibiotic efficacy are likely to be far more common than is currently appreciated.

Importantly, understanding the molecular mechanisms involved in the cellular responses triggered by a secondary metabolite, as well as the chemical properties of the secondary metabolite itself, can provide practical insights regarding which clinical antibiotics are likely to be affected. With this knowledge in hand, combined with an understanding of other environmental and physiological factors that affect antibiotic susceptibility (Ersoy *et al.*, 2017; Yan and Bassler, 2019), we posit that it will be possible to optimize the use of existing antibiotics so as to better minimize the risk of treatment failure and prevent the evolution of resistance *in vivo*. For example, if a pathogen produces a secondary metabolite that upregulates efflux pumps specific to fluoroquinolones and other aromatic molecules, the chances of successful treatment would likely be higher with another

class of antibiotics that is not susceptible to this defense, such as aminoglycosides. The biosynthetic pathways for these secondary metabolites, or even the molecules themselves, could also serve as targets for the development of new adjuvants for antimicrobial drugs. Such efforts are already underway for secondary metabolites such as PYO and staphyloxanthin (Liu *et al.*, 2008; Song *et al.*, 2009; Costa *et al.*, 2017; VanDrisse *et al.*, 2021), which are also known to act as virulence factors (Liu and Nizet, 2009). Finally, retooling clinical antimicrobial susceptibility testing protocols to account for the impact of secondary metabolites on antibiotic efficacy (Box 2) could potentially significantly improve the predictive value of these assays—especially in the case of secondary-metabolite-producing opportunistic pathogens, such as members of the *Burkholderia cepacia* complex, that often exhibit discrepancies between *in vitro* minimum inhibitory concentration measurements and clinical treatment outcomes (Abbott and Peleg, 2015).

In conclusion, our ability to address the vexing challenges posed by antibiotic tolerance and resistance in the future has much to gain by reflecting on the past. The evolutionary and ecological history of natural antibiotics intersects directly with the history of clinical antibiotic discovery. While the soil has continued to provide a rich reservoir for natural product mining efforts, what has gotten lost is the fact that alongside the evolution of pathways that synthesize these molecules, other pathways have co-evolved that respond to them. Remembering this shared historical context is important for predicting how secondary metabolites might impact the response of polymicrobial communities to conventional antibiotics, and compels creative thinking about novel ways to manage such responses.

Box 1: Guidelines for establishing causal links between secondary metabolite production and increased antibiotic tolerance or resistance.

Here we propose a few steps for the investigation of secondary-metabolite-mediated changes in antibiotic susceptibility:

1. Identifying the candidate secondary metabolite. This can be done in multiple ways, including based on molecular structure or its physiological effects on the cells. Genomic analysis could also be used to reveal potentially relevant secondary metabolites produced by pathogens (Blin *et al.*, 2019). Researchers should investigate

whether the putative secondary metabolite of interest shows any toxicity to the producer, as well as the molecular responses induced upon exposure to it. Transcriptomics approaches, such as RNA-seq, can be used to reveal such responses. Importantly, in order to have appropriate negative controls for such experiments, it will often be necessary to construct a mutant strain lacking the biosynthetic genes for production of the secondary metabolite.

2. Detecting the secondary metabolite. It is essential to use an accurate and quantitative detection method because the secondary metabolite concentration might directly impact how it changes antibiotic susceptibility. Depending on the secondary metabolite, possible detection methods may include ultraviolet or visible light spectroscopy or mass spectrometry, both of which can be coupled to high-performance liquid chromatography in the case of analyzing complex samples (e.g. extracts of microbial cultures or clinical samples). Investigators should attempt to detect the secondary metabolite in the relevant clinical context (e.g. in infected sputum, wound exudates, or stool samples), and physiologically-relevant concentrations of the secondary metabolite should always be used in *in vitro* experiments.

3. Considering the effects on nearby species. Beyond understanding how secondary metabolites might change the producer's response to antibiotics, it is critical to account for the impacts on the entire microbial community in the case of polymicrobial infections. Thus, investigators should consider which species are most commonly found together with the secondary metabolite producer and perform experiments in which the producer and non-producers are cocultured, or the non-producers are separately exposed to controlled concentrations of the secondary metabolite. Understanding how the non-producers are impacted, including the molecular mechanisms involved, is essential for predicting how the secondary metabolite might change the overall antibiotic susceptibility profile of a microbial community.

4. Testing the secondary-metabolite-mediated effects on antibiotic susceptibility. Tolerance and resistance are two different modes of antibiotic resilience that should be tested separately (Kester and Fortune, 2014; Brauner *et al.*, 2016; Balaban *et al.*,

2019) (see the figure below, part A); the former can be measured by determining the percentage of surviving cells following a temporary exposure to the antibiotic, while the latter calls for assessing the ability to grow in the presence of the antibiotic. There are also a variety of assays available for testing secondary-metabolite-mediated effects on drug susceptibility in multispecies communities (see the figure below, part B). In liquid cocultures, the species can be grown with or without separation by a permeable membrane that restricts interactions to those mediated by diffusible small molecules. For biofilms, experiments can be done in (i) macroscopic assays (e.g. colony biofilms, with species mixed or separated), or (ii) microscopic assays (e.g. microfluidics (Liu *et al.*, 2015; Liu *et al.*, 2017) or alternatives assays like the agar block biofilm assay (ABBA) (Costa *et al.*, 2017; Spero and Newman, 2018), to which concomitant measurements of microenvironment variables – such as pH or O_2 levels – have been applied). Importantly, the decision to perform experiments on liquid cultures versus biofilms can directly influence the results, as some secondary-metabolite-mediated tolerance mechanisms are specific to biofilms. For example, secondary-metabolite-mediated increases in extracellular DNA release can stimulate biofilm formation, resulting in elevated tolerance levels (Hazan *et al.*, 2016). In addition, redox-active secondary metabolites, such as phenazines, significantly impact metabolism within biofilms (Schiessl *et al.*, 2019; Saunders *et al.*, 2020). Metabolic activity in turn is known to dramatically affect antimicrobial drug efficacy (Dwyer *et al.*, 2015).

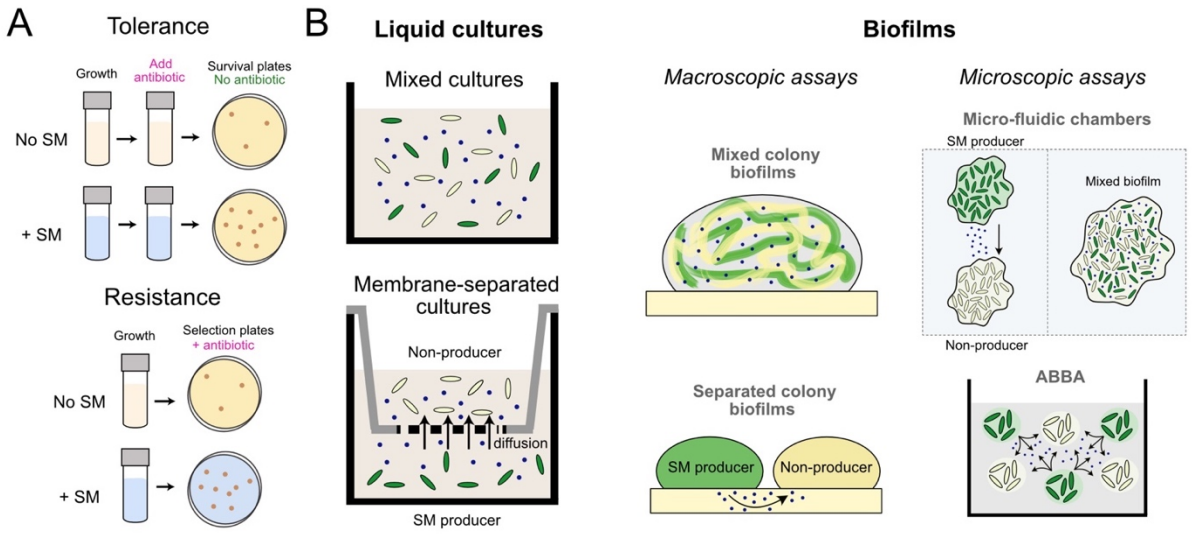

Accordingly, recent work demonstrated that redox-active secondary metabolites can lead to metabolism-mediated increases in antibiotic tolerance within biofilms (Schiessl *et al.*, 2019). On the other hand, planktonic cultures provide better control for testing specific secondary-metabolite-mediated responses and more sophisticated methods when evaluating resistance, such as fluctuation tests to measure mutation rates (Rosche and Foster, 2000; Zheng, 2015). The investigators should therefore decide what is more appropriate for their particular questions.

Box 2: Accounting for secondary metabolite production during antimicrobial susceptibility testing.

As the traditional basis for determining appropriate courses of treatment for infections, antimicrobial susceptibility testing (AST) is a cornerstone of clinical microbiology. However, in many clinical contexts, such as chronic lung infections in cystic fibrosis patients, there is little to no correlation between AST results and treatment outcomes (Hurley *et al.*, 2012; Somayaji *et al.*, 2019). This discrepancy may stem in some cases from the fact that standard AST conditions generally preclude detection of interactions between secondary metabolites and antimicrobial drugs. Regardless of the specific method employed (disk diffusion, microbroth dilution, agar dilution, E-test, or automated systems), clinical AST relies on a readout of absence of growth in cultures that are inoculated at low cell densities (Jorgensen and Ferraro, 2009), whereas secondary metabolites are typically not produced until at least late log-phase or early stationary phase (Davies, 2013). Moreover, AST is routinely performed on single-species cultures even in the case of polymicrobial infections, eliminating the possibility of detecting secondary-metabolite-mediated interspecies interactions that could affect antimicrobial efficacy.

Here, we suggest four possible modifications to clinical AST protocols that would help account for the effects of microbial secondary metabolites produced during infections. Given that secondary metabolites can significantly affect antimicrobial efficacy, the proposed modifications could potentially improve the empirical correlation between *in vitro* AST results and the success of clinical treatments. However, these approaches will need to be validated in animal models of infection and in clinical trials comparing patient outcomes against the use of traditional AST for antimicrobial drug selection. In addition, if studies indicate that secondary-metabolite-related

modifications improve the predictive value of AST, scalability in terms of cost and throughput will likely need to be further optimized before widespread implementation becomes possible in clinical microbiology laboratories.

Proposed modifications to AST protocols

1. Use filtered supernatants from overnight cultures of the infective microorganism(s). By setting up AST assays using a 1:1 dilution of fresh growth media (prepared at 2x concentration) and filtered supernatant from an overnight culture of the infective agent, the effects of any secondary metabolites produced during late log phase or stationary phase could be accounted for without needing to modify other aspects of standard AST protocols (e.g. the use of visible growth as a readout). A key advantage of this approach is that it is agnostic to which secondary metabolite is produced, avoiding the need for prior knowledge of the biosynthetic capabilities of the infective agent, as well as allowing for the combined effects of multiple secondary metabolites to be considered. However, this approach would significantly increase the time between receiving a clinical sample and producing an AST result. In addition, mixing spent supernatant with fresh growth media might dilute the concentrations of the secondary metabolite(s) below clinically relevant levels. The concentrations of different nutrients in the media would also be affected, possibly in unpredictable ways across different strains, which in turn could also impact antibiotic susceptibility (Brown, 1977).

2. Add purified secondary metabolites exogenously to cultures. If it is known that the infective species is capable of producing specific secondary metabolites that have been validated as clinically relevant (e.g. PYO in *P. aeruginosa* or indole in *E. coli*), purified forms of the secondary metabolite(s) could be added to traditional AST assays. An advantage of this approach is the ability to control the level of exposure to the secondary metabolite(s), which would make it possible to ensure that the concentrations in the AST assay are similar to those detected in clinical samples. However, this approach requires that the secondary metabolite(s) be commercially available or otherwise economically viable to synthesize or purify from cultures. In addition, prior knowledge of the biosynthetic capabilities of the infective agent would

be necessary. An important caveat in this regard is that microbial secondary metabolite production can vary greatly from strain to strain within the same species. Thus, basing the working concentration of a secondary metabolite on an average across strains or patient samples may lead to over- or underestimation of the effects of the secondary metabolite in individual cases.

3. Adjust antibiotic "breakpoint" guidelines according to *in situ* levels of secondary metabolites. For secondary metabolites that are commonly found in infections and can be procured in purified form, *in vitro* testing could lead to the development of mathematical models that quantitatively relate the concentration of the secondary metabolite to the change in the producing species' resistance to different antimicrobial drugs. Once validated across a range of different strains, such models could potentially enable secondary-metabolite-based adjustments to the standard "breakpoint" antibiotic concentrations used by clinicians to classify microorganisms as susceptible or resistant. Assays for the quantification of the secondary metabolite in patient samples could then be combined with traditional AST testing. Such an approach would enable taking into account strain variability in secondary metabolite production and avoid necessitating modifications to existing AST protocols. However, this approach might also lead to underestimation of secondary metabolite effects in some cases, as bulk measurements of a secondary metabolite in a patient sample may obscure heterogeneity at the micron scale.

4. Grow multiple species together if they are co-isolated from a polymicrobial infection. Secreted secondary metabolites produced by one species can significantly affect antimicrobial efficacy in neighboring species. Thus, in the case of polymicrobial infections, inoculating multiple species together in AST assays may improve prediction of the overall community response to antimicrobial drugs. To account for the production of secondary metabolites, this approach would still need to be combined with other modifications, such as those proposed above in options 1-3. In addition, the optimal ratios at which to inoculate different species would need to be investigated and standardized. Alternatively, it may be possible to perform AST using mixed cultures

derived directly from patient samples, either bypassing or in parallel to the step in which individual isolates are obtained and identified.

Table 1: Secondary metabolites produced by opportunistic or enteric pathogens and their impacts on antibiotic efficacy. ND = not determined; these are molecules whose effects on antibiotics have not been directly tested. * = for aminoglycosides, PYO has been shown to increase or decrease antibiotic resilience, depending on the studied conditions. ** = hypothesized mechanisms by which the molecule might affect susceptibility.

Metabolite	Producer	Antibiotic affected	Mechanism	References
Pyocyanin (PYO)	*Pseudomonas aeruginosa*	Fluoroquinolones, aminoglycosides*, chloramphenicol, carbenicillin	Efflux induction, oxidative stress response induction	(Schiessl *et al.*, 2019; Zhu *et al.*, 2019; Meirelles and Perry *et al.*, 2021)
Phenazine 1-carboxylic acid (PCA), phenazine 1-carboxamide (PCN)	*P. aeruginosa*	Ciprofloxacin, tobramycin, carbenicillin	Metabolic changes	(Schiessl *et al.*, 2019)
Paerucumarin	*P. aeruginosa*	Chloramphenicol, ciprofloxacin	Efflux induction	(Iftikhar *et al.*, 2020)
Indole	*Escherichia coli*	Fluoroquinolones, gentamicin, ampicillin, carbenicillin	Efflux induction, oxidative stress response induction	(Hirakawa *et al.*, 2005; Lee *et al.*, 2010; Vega *et al.*, 2012; Vega *et al.*, 2013)
Salicylate	*Burkholderia* spp.	Chloramphenicol, trimethoprim, ciprofloxacin	Efflux induction	(Nair *et al.*, 2004)
HQNO	*P. aeruginosa*	Meropenem	Increased extracellular DNA release and biofilm formation	(Hazan *et al.*, 2016)
Ergothioneine	*Mycobacterium tuberculosis*	Rifampicin, isoniazid, bedaquiline, clofazimine	Direct ROS detoxification, redox buffering	(Saini *et al.*, 2016)
Polyamines (putrescine, spermidine)	*E. coli, Burkholderia cenocepacia, P. aeruginosa*	Levofloxacin, amikacin, cefotaxime, polymyxin B, norfloxacin, rifampicin, tobramycin	Direct ROS detoxification, decreased drug penetration	(Tkachenko *et al.*, 2012; El-Halfawy and Valvano, 2014)
Pseudomonas quinolone signal (PQS)	*P. aeruginosa*	Ciprofloxacin, oxofloxacin, imipenem, meropenem, gentamicin, colistin	Increased ROS generation	(Häussler and Becker, 2008; Nguyen *et al.*, 2011)
H_2S	Diverse microbes	Gentamicin, amikacin, nalidixic acid, ciprofloxacin, ampicillin	Oxidative stress response induction, Fe^{2+} sequestration, redox buffering	(Shatalin *et al.*, 2011; Shukla *et al.*, 2017)
Staphyloxanthin	*Staphylococcus aureus*	ND	Direct ROS detoxification	(Clauditz *et al.*, 2006; Hall *et al.*, 2017)
Carotenoids	*Streptococcus* spp.	ND	Direct ROS detoxification	(Liu *et al.*, 2004; Wu *et al.*, 2010)
2,3-dihydroxybenzoate	*E. coli*	ND	Efflux induction	(Ruiz and Levy, 2014)
Toxoflavin	*Burkholderia* spp.	ND	Efflux induction**, oxidative stress response induction**	(Latuasan and Berends, 1961; Kim *et al.*, 2004)

Phthiocol	*M. tuberculosis*	ND	Oxidative stress response induction**	(Anderson and Newman, 1933; Gardner, 1996)
D-alanylgriseoluteic acid	*Pantoea agglomerans*	ND	Oxidative stress response induction**	(Giddens *et al.*, 2002; Giddens and Bean, 2007)
β-3H-indolydenopyruvate	*Achromobacter* sp.	ND	ND	(Krishnamurthi *et al.*, 1969)
Anthraquinones (e.g., emodin, endocrocin)	*Aspergillus* spp.	ND	ND	(Wells *et al.*, 1975; Lim *et al.*, 2012)

Acknowledgements

This work was supported by grants to D.K.N. from the NIH (1R01AI127850-01A1, 1R01HL152190-01), ARO (W911NF-17-1-0024) and the Doren Family Foundation. E.K.P. was supported by a National Science Foundation Graduate Research Fellowship under Grant No. DGE-1745301.

References

Abbott, I.J., and Peleg, A.Y. (2015) *Stenotrophomonas*, *Achromobacter*, and nonmelioid *Burkholderia* species: antimicrobial resistance and therapeutic strategies. *Semin Respir Crit Care Med* **36**: 99–110.

Alexander, H.K., and MacLean, R.C. (2020) Stochastic bacterial population dynamics restrict the establishment of antibiotic resistance from single cells. *Proc Natl Acad Sci USA* **117**: 19455–19464.

Anderson, R.J., and Newman, M.S. (1933) The chemistry of the lipids of tubercle bacilli. *J Bio Chem* **103**: 405–412.

Anes, J., McCusker, M.P., Fanning, S., and Martins, M. (2015) The ins and outs of RND efflux pumps in *Escherichia coli. Front Microbiol* **6**: 587.

Bakker, P.A.H.M., Ran, L., and Mercado-Blanco, J. (2014) Rhizobacterial salicylate production provokes headaches! *Plant Soil* **382**: 1–16.

Balaban, N.Q., Helaine, S., Lewis, K., Ackermann, M., Aldridge, B., Andersson, D.I., *et al.* (2019) Definitions and guidelines for research on antibiotic persistence. *Nat Rev Microbiol* **17**: 441–448.

Bandara, H.M.H.N., Wood, D.L.A., Vanwonterghem, I., Hugenholtz, P., Cheung, B.P.K., and Samaranayake, L.P. (2020) Fluconazole resistance in *Candida albicans* is induced by *Pseudomonas aeruginosa* quorum sensing. *Sci Rep* **10**: 7769.

Baym, M., Lieberman, T.D., Kelsic, E.D., Chait, R., Gross, R., Yelin, I., and Kishony, R. (2016) Spatiotemporal microbial evolution on antibiotic landscapes. *Science* **353**: 1147–1151.

Belenky, P., Ye, J.D., Porter, C.B.M., Cohen, N.R., Lobritz, M.A., Ferrante, T., *et al.* (2015) Bactericidal antibiotics induce toxic metabolic perturbations that lead to cellular damage. *Cell Rep* **13**: 968–980.

Benomar, S., Evans, K.C., Unckless, R.L., and Chandler, J.R. (2019) Efflux pumps in

Chromobacterium species increase antibiotic resistance and promote survival in a coculture competition model. *Appl Environ Microbiol* **85**: e00908-19.

Berg, G., Eberl, L., and Hartmann, A. (2005) The rhizosphere as a reservoir for opportunistic human pathogenic bacteria. *Environ Microbiol* **7**: 1673–1685.

Bhargava, N., Sharma, P., and Capalash, N. (2014) Pyocyanin stimulates quorum sensing-mediated tolerance to oxidative stress and increases persister cell populations in *Acinetobacter baumannii*. *Infect Immun* **82**: 3417–3425.

Bina, J.E., and Mekalanos, J.J. (2001) *Vibrio cholerae* tolC is required for bile resistance and colonization. *Infect Immun* **69**: 4681–4685.

Biswas, L., Biswas, R., Schlag, M., Bertram, R., and Götz, F. (2009) Small-colony variant selection as a survival strategy for *Staphylococcus aureus* in the presence of *Pseudomonas aeruginosa*. *Appl Environ Microbiol* **75**: 6910–6912.

Blin, K., Shaw, S., Steinke, K., Villebro, R., Ziemert, N., Lee, S.Y., *et al.* (2019) antiSMASH 5.0: updates to the secondary metabolite genome mining pipeline. *Nucleic Acids Res* **47**: W81–W87.

Bottery, M.J., Pitchford, J.W., and Friman, V.-P. (2020) Ecology and evolution of antimicrobial resistance in bacterial communities. *ISME J* **15**: 939-948.

Brauner, A., Fridman, O., Gefen, O., and Balaban, N.Q. (2016) Distinguishing between resistance, tolerance and persistence to antibiotic treatment. *Nat Rev Microbiol* **14**: 320–330.

Bredenbruch, F., Geffers, R., Nimtz, M., Buer, J., and Häussler, S. (2006) The *Pseudomonas aeruginosa* quinolone signal (PQS) has an iron-chelating activity. *Environ Microbiol* **8**: 1318–1329.

Briaud, P., Bastien, S., Camus, L., Boyadjian, M., Reix, P., Mainguy, C., *et al.* (2020) Impact of coexistence phenotype between *Staphylococcus aureus* and *Pseudomonas aeruginosa* isolates on clinical outcomes among cystic fibrosis patients. *Front Cell Infect Microbiol* **10**: 266.

Brochado, A.R., Telzerow, A., Bobonis, J., Banzhaf, M., Mateus, A., Selkrig, J., *et al.* (2018) Species-specific activity of antibacterial drug combinations. *Nature* **559**: 259–263.

Brown, M.R. (1977) Nutrient depletion and antibiotic susceptibility. *J Antimicrob Chemother* **3**: 198–201.

Brynildsen, M.P., Winkler, J.A., Spina, C.S., MacDonald, I.C., and Collins, J.J. (2013) Potentiating antibacterial activity by predictably enhancing endogenous microbial ROS production. *Nat Biotechnol* **31**: 160–165.

Buckley, A.M., Webber, M.A., Cooles, S., Randall, L.P., La Ragione, R.M., Woodward, M.J., and Piddock, L.J.V. (2006) The AcrAB-TolC efflux system of *Salmonella enterica* serovar Typhimurium plays a role in pathogenesis. *Cell Microbiol* **8**: 847–856.

Burkhead, K.D., Schisler, D.A., and Slininger, P.J. (1994) Pyrrolnitrin production by biological control agent *Pseudomonas cepacia* B37w in culture and in colonized wounds of potatoes. *Appl Environ Microbiol* **60**: 2031–2039.

Burse, A., Weingart, H., and Ullrich, M.S. (2004) The phytoalexin-inducible multidrug efflux pump AcrAB contributes to virulence in the fire blight pathogen, *Erwinia amylovora*. *Mol Plant Microbe Interact* **17**: 43–54.

Camus, L., Briaud, P., Vandenesch, F., and Moreau, K. (2021) How bacterial adaptation to cystic fibrosis environment shapes interactions between *Pseudomonas aeruginosa* and *Staphylococcus aureus*. *Front Microbiol* **12**: 617784.

Chevrette, M.G., Carlson, C.M., Ortega, H.E., Thomas, C., Ananiev, G.E., Barns, K.J., *et al.* (2019)

The antimicrobial potential of *Streptomyces* from insect microbiomes. *Nat Commun* **10**: 516.
Chmiel, J.F., Aksamit, T.R., Chotirmall, S.H., Dasenbrook, E.C., Elborn, J.S., LiPuma, J.J., *et al.* (2014) Antibiotic management of lung infections in cystic fibrosis. I. The microbiome, methicillin-resistant *Staphylococcus aureus,* Gram-negative bacteria, and multiple infections. *Ann Am Thorac Soc* **11**: 1120–1129.
Chubiz, L.M., and Rao, C.V. (2010) Aromatic acid metabolites of *Escherichia coli* K-12 can induce the marRAB operon. *J Bacteriol* **192**: 4786–4789.
Clarke-Pearson, M.F., and Brady, S.F. (2008) Paerucumarin, a new metabolite produced by the pvc gene cluster from *Pseudomonas aeruginosa*. *J Bacteriol* **190**: 6927–6930.
Clauditz, A., Resch, A., Wieland, K.-P., Peschel, A., and Götz, F. (2006) Staphyloxanthin plays a role in the fitness of *Staphylococcus aureus* and its ability to cope with oxidative stress. *Infect Immun* **74**: 4950–4953.
Cohen, S.P., Levy, S.B., Foulds, J., and Rosner, J.L. (1993) Salicylate induction of antibiotic resistance in *Escherichia coli*: activation of the mar operon and a mar-independent pathway. *J Bacteriol* **175**: 7856–7862.
Costa, K.C., Glasser, N.R., Conway, S.J., and Newman, D.K. (2017) Pyocyanin degradation by a tautomerizing demethylase inhibits *Pseudomonas aeruginosa* biofilms. *Science* **355**: 170–173.
Crits-Christoph, A., Bhattacharya, N., Olm, M.R., Song, Y.S., and Banfield, J.F. (2020) Transporter genes in biosynthetic gene clusters predict metabolite characteristics and siderophore activity. *Genome Res* **31**: 239-250.
Cruickshank, C.N., and Lowbury, E.J. (1953) The effect of pyocyanin on human skin cells and leucocytes. *Br J Exp Pathol* **34**: 583–587.
Darling, P., Chan, M., Cox, A.D., and Sokol, P.A. (1998) Siderophore production by cystic fibrosis isolates of *Burkholderia cepacia*. *Infect Immun* **66**: 874–877.
Davies, J. (2013) Specialized microbial metabolites: functions and origins. *J Antibiot* **66**: 361–364.
Davies, J., and Davies, D. (2010) Origins and evolution of antibiotic resistance. *Microbiol Mol Biol Rev* **74**: 417–433.
Demain, A.L., and Fang, A. (2000) The natural functions of secondary metabolites. *Adv Biochem Eng Biotechnol* **69**: 1–39.
Depoorter, E., Bull, M.J., Peeters, C., Coenye, T., Vandamme, P., and Mahenthiralingam, E. (2016) *Burkholderia*: an update on taxonomy and biotechnological potential as antibiotic producers. *Appl Microbiol Biotechnol* **100**: 5215–5229.
Depoorter, E., De Canck, E., Coenye, T., and Vandamme, P. (2021) *Burkholderia* bacteria produce multiple potentially novel molecules that inhibit carbapenem-resistant Gram-negative bacterial pathogens. *Antibiotics (Basel)* **10**: 147.
Dietrich, L.E., Price-Whelan, A., Petersen, A., Whiteley, M., and Newman, D.K. (2006) The phenazine pyocyanin is a terminal signalling factor in the quorum sensing network of *Pseudomonas aeruginosa*. *Mol Microbiol* **61**: 1308–1321.
Dietrich, L.E.P., Teal, T.K., Price-Whelan, A., and Newman, D.K. (2008) Redox-active antibiotics control gene expression and community behavior in divergent bacteria. *Science* **321**: 1203–1206.
Du, D., Wang-Kan, X., Neuberger, A., Veen, H.W. van, Pos, K.M., Piddock, L.J.V., and Luisi, B.F. (2018) Multidrug efflux pumps: structure, function and regulation. *Nat Rev Microbiol* **16**: 523–539.
Dwyer, D.J., Belenky, P.A., Yang, J.H., MacDonald, I.C., Martell, J.D., Takahashi, N., *et al.* (2014)

Antibiotics induce redox-related physiological alterations as part of their lethality. *Proc Natl Acad Sci USA* **111**: E2100-9.

Dwyer, D.J., Collins, J.J., and Walker, G.C. (2015) Unraveling the physiological complexities of antibiotic lethality. *Annu Rev Pharmacol Toxicol* **55**: 313–332.

Edge, R., and Truscott, T.G. (2018) Singlet oxygen and free radical reactions of retinoids and carotenoids – a review. *Antioxidants (Basel)* **7**: 5.

Einarsson, G.G., Zhao, J., LiPuma, J.J., Downey, D.G., Tunney, M.M., and Elborn, J.S. (2019) Community analysis and co-occurrence patterns in airway microbial communities during health and disease. *ERJ Open Research* **5**: 00128-2017.

El Meouche, I., and Dunlop, M.J. (2018) Heterogeneity in efflux pump expression predisposes antibiotic-resistant cells to mutation. *Science* **362**: 686–690.

El-Halfawy, O.M., and Valvano, M.A. (2013) Chemical communication of antibiotic resistance by a highly resistant subpopulation of bacterial cells. *PLoS One* **8**: e68874.

El-Halfawy, O.M., and Valvano, M.A. (2014) Putrescine reduces antibiotic-induced oxidative stress as a mechanism of modulation of antibiotic resistance in *Burkholderia cenocepacia*. *Antimicrob Agents Chemother* **58**: 4162–4171.

Ersoy, S.C., Heithoff, D.M., Barnes, L., Tripp, G.K., House, J.K., Marth, J.D., *et al.* (2017) Correcting a fundamental flaw in the paradigm for antimicrobial susceptibility testing. *EBioMedicine* **20**: 173–181.

Fargier, E., Mac Aogáin, M., Mooij, M.J., Woods, D.F., Morrissey, J.P., Dobson, A.D.W., *et al.* (2012) MexT functions as a redox-responsive regulator modulating disulfide stress resistance in *Pseudomonas aeruginosa*. *J Bacteriol* **194**: 3502–3511.

Fukuda, T.T.H., Helfrich, E.J.N., Mevers, E., Melo, W.G.P., Van Arnam, E.B., Andes, D.R., *et al.* (2021) Specialized metabolites reveal evolutionary history and geographic dispersion of a multilateral symbiosis. *ACS Cent Sci* **7**: 292-299.

Garbe, T.R., Kobayashi, M., and Yukawa, H. (2000) Indole-inducible proteins in bacteria suggest membrane and oxidant toxicity. *Arch Microbiol* **173**: 78–82.

Gardner, P.R. (1996) Superoxide production by the mycobacterial and pseudomonad quinoid pigments phthiocol and pyocyanine in human lung cells. *Arch Biochem Biophys* **333**: 267–274.

Gencheva, R., Cheng, Q., and Arnér, E.S.J. (2018) Efficient selenocysteine-dependent reduction of toxoflavin by mammalian thioredoxin reductase. *Biochim Biophys Acta Gen Subj* **1862**: 2511-2517.

Gerstel, A., Zamarreño Beas, J., Duverger, Y., Bouveret, E., Barras, F., and Py, B. (2020) Oxidative stress antagonizes fluoroquinolone drug sensitivity via the SoxR-SUF Fe-S cluster homeostatic axis. *PLoS Genet* **16**: e1009198.

Giddens, S.R., and Bean, D.C. (2007) Investigations into the in vitro antimicrobial activity and mode of action of the phenazine antibiotic D-alanylgriseoluteic acid. *Int J Antimicrob Agents* **29**: 93–97.

Giddens, S.R., Feng, Y., and Mahanty, H.K. (2002) Characterization of a novel phenazine antibiotic gene cluster in *Erwinia herbicola* Eh1087. *Mol Microbiol* **45**: 769–783.

Glasser, N.R., Kern, S.E., and Newman, D.K. (2014) Phenazine redox cycling enhances anaerobic survival in *Pseudomonas aeruginosa* by facilitating generation of ATP and a proton-motive force. *Mol Microbiol* **92**: 399–412.

Glasser, N.R., Saunders, S.H., and Newman, D.K. (2017) The colorful world of extracellular electron shuttles. *Annu Rev Microbiol* **71**: 731–751.

Gu, M., and Imlay, J.A. (2011) The SoxRS response of *Escherichia coli* is directly activated by redox-cycling drugs rather than by superoxide. *Mol Microbiol* **79**: 1136–1150.

Hall, J.W., Yang, J., Guo, H., and Ji, Y. (2017) The *Staphylococcus aureus* AirSR two-component system mediates reactive oxygen species resistance via transcriptional regulation of staphyloxanthin production. *Infect Immun* **85**: e00838-16.

Han, M.-L., Zhu, Y., Creek, D.J., Lin, Y.-W., Gutu, A.D., Hertzog, P., *et al.* (2019) Comparative metabolomics and transcriptomics reveal multiple pathways associated with polymyxin killing in *Pseudomonas aeruginosa*. *mSystems* **4**: e00149-18.

Haslam, E. (1986) Secondary metabolism – fact and fiction. *Nat Prod Rep* **3**: 217.

Hassett, D.J., Charniga, L., Bean, K., Ohman, D.E., and Cohen, M.S. (1992) Response of *Pseudomonas aeruginosa* to pyocyanin: mechanisms of resistance, antioxidant defenses, and demonstration of a manganese-cofactored superoxide dismutase. *Infect Immun* **60**: 328–336.

Häussler, S., and Becker, T. (2008) The Pseudomonas quinolone signal (PQS) balances life and death in *Pseudomonas aeruginosa* populations. *PLoS Pathog* **4**: e1000166.

Hazan, R., Que, Y.A., Maura, D., Strobel, B., Majcherczyk, P.A., Hopper, L.R., *et al.* (2016) Auto poisoning of the respiratory chain by a quorum-sensing-regulated molecule favors biofilm formation and antibiotic tolerance. *Curr Biol* **26**: 195–206.

Heindorf, M., Kadari, M., Heider, C., Skiebe, E., and Wilharm, G. (2014) Impact of *Acinetobacter baumannii* superoxide dismutase on motility, virulence, oxidative stress resistance and susceptibility to antibiotics. *PLoS One* **9**: e101033.

Hirakawa, H., Inazumi, Y., Masaki, T., Hirata, T., and Yamaguchi, A. (2005) Indole induces the expression of multidrug exporter genes in *Escherichia coli*. *Mol Microbiol* **55**: 1113–1126.

Hong, Y., Zeng, J., Wang, X., Drlica, K., and Zhao, X. (2019) Post-stress bacterial cell death mediated by reactive oxygen species. *Proc Natl Acad Sci USA* **116**: 10064–10071.

Hurley, M.N., Ariff, A.H.A., Bertenshaw, C., Bhatt, J., and Smyth, A.R. (2012) Results of antibiotic susceptibility testing do not influence clinical outcome in children with cystic fibrosis. *J Cyst Fibros* **11**: 288–292.

Iftikhar, A., Asif, A., Manzoor, A., Azeem, M., Sarwar, G., Rashid, N., and Qaisar, U. (2020) Mutation in pvcABCD operon of *Pseudomonas aeruginosa* modulates MexEF-OprN efflux system and hence resistance to chloramphenicol and ciprofloxacin. *Microb Pathog* 104491.

Imlay, J.A. (2013) The molecular mechanisms and physiological consequences of oxidative stress: lessons from a model bacterium. *Nat Rev Microbiol* **11**: 443–454.

Imperi, F., Tiburzi, F., and Visca, P. (2009) Molecular basis of pyoverdine siderophore recycling in *Pseudomonas aeruginosa*. *Proc Natl Acad Sci USA* **106**: 20440–20445.

Jeong, Y., Kim, J., Kim, S., Kang, Y., Nagamatsu, T., and Hwang, I. (2003) Toxoflavin produced by *Burkholderia glumae* causing rice grain rot is responsible for inducing bacterial wilt in many field crops. *Plant Dis* **87**: 890–895.

Jorgensen, J.H., and Ferraro, M.J. (2009) Antimicrobial susceptibility testing: a review of general principles and contemporary practices. *Clin Infect Dis* **49**: 1749–1755.

Karlin, D.A., Mastromarino, A.J., Jones, R.D., Stroehlein, J.R., and Lorentz, O. (1985) Fecal skatole and indole and breath methane and hydrogen in patients with large bowel polyps or cancer. *J Cancer Res Clin Oncol* **109**: 135–141.

Keller, N.P., Turner, G., and Bennett, J.W. (2005) Fungal secondary metabolism – from biochemistry to genomics. *Nat Rev Microbiol* **3**: 937–947.

Keren, I., Wu, Y., Inocencio, J., Mulcahy, L.R., and Lewis, K. (2013) Killing by bactericidal antibiotics does not depend on reactive oxygen species. *Science* **339**: 1213–1216.

Kester, J.C., and Fortune, S.M. (2014) Persisters and beyond: mechanisms of phenotypic drug resistance and drug tolerance in bacteria. *Crit Rev Biochem Mol Biol* **49**: 91–101.

Kim, J., Kim, J.-G., Kang, Y., Jang, J.Y., Jog, G.J., Lim, J.Y., *et al.* (2004) Quorum sensing and the LysR-type transcriptional activator ToxR regulate toxoflavin biosynthesis and transport in *Burkholderia glumae*. *Mol Microbiol* **54**: 921–934.

Kim, J., Shin, B., Park, C., and Park, W. (2017) Indole-induced activities of β-lactamase and efflux pump confer ampicillin resistance in *Pseudomonas putida* KT2440. *Front Microbiol* **8**: 433.

Kohanski, M.A., Dwyer, D.J., Hayete, B., Lawrence, C.A., and Collins, J.J. (2007) A common mechanism of cellular death induced by bactericidal antibiotics. *Cell* **130**: 797–810.

König, S., Vogel, H.-J., Harms, H., and Worrich, A. (2020) Physical, chemical and biological effects on soil bacterial dynamics in microscale models. *Front Ecol Evol* **8**: 53.

Kreamer, N.N., Costa, F., and Newman, D.K. (2015) The ferrous iron-responsive BqsRS two-component system activates genes that promote cationic stress tolerance. *mBio* **6**: e02549.

Krishnamurthi, V.S., Buckley, P.J., and Duerre, J.A. (1969) Pigment formation from l-tryptophan by a particulate fraction from an *Achromobacter* species. *Arch Biochem Biophys* **130**: 636–645.

Latuasan, H.E., and Berends, W. (1961) On the origin of the toxicity of toxoflavin. *Biochim Biophys Acta* **52**: 502–508.

Lau, G.W., Hassett, D.J., Ran, H., and Kong, F. (2004) The role of pyocyanin in *Pseudomonas aeruginosa* infection. *Trends Mol Med* **10**: 599–606.

Laursen, J.B., and Nielsen, J. (2004) Phenazine natural products: biosynthesis, synthetic analogues, and biological activity. *Chem Rev* **104**: 1663–1686.

Lee, H.H., Molla, M.N., Cantor, C.R., and Collins, J.J. (2010) Bacterial charity work leads to population-wide resistance. *Nature* **467**: 82–85.

Levin-Reisman, I., Brauner, A., Ronin, I., and Balaban, N.Q. (2019) Epistasis between antibiotic tolerance, persistence, and resistance mutations. *Proc Natl Acad Sci USA* **116**: 14734–14739.

Levin-Reisman, I., Ronin, I., Gefen, O., Braniss, I., Shoresh, N., and Balaban, N.Q. (2017) Antibiotic tolerance facilitates the evolution of resistance. *Science* **355**: 826–830.

Li, X., Li, Y., Wang, R., Wang, Q., and Lu, L. (2019) Toxoflavin produced by *Burkholderia gladioli* from *Lycoris aurea* is a new broad-spectrum fungicide. *Appl Environ Microbiol* **85**.

Li, X.-Z., and Nikaido, H. (2016) Antimicrobial drug efflux pumps in *Escherichia coli*. In *Efflux-Mediated Antimicrobial Resistance in Bacteria*. Li, X.-Z., Elkins, C.A., and Zgurskaya, H.I. (eds). Springer International Publishing, Cham. pp. 219–259.

Li, X.-Z., Plésiat, P., and Nikaido, H. (2015) The challenge of efflux-mediated antibiotic resistance in Gram-negative bacteria. *Clin Microbiol Rev* **28**: 337–418.

Lim, F.Y., Hou, Y., Chen, Y., Oh, J.-H., Lee, I., Bugni, T.S., and Keller, N.P. (2012) Genome-based cluster deletion reveals an endocrocin biosynthetic pathway in *Aspergillus fumigatus*. *Appl Environ Microbiol* **78**: 4117–4125.

Ling, L.L., Schneider, T., Peoples, A.J., Spoering, A.L., Engels, I., Conlon, B.P., *et al.* (2015) A new antibiotic kills pathogens without detectable resistance. *Nature* **517**: 455–459.

Lipuma, J.J. (2010) The changing microbial epidemiology in cystic fibrosis. *Clin Microbiol Rev* **23**: 299–323.

LiPuma, J.J., Spilker, T., Coenye, T., and Gonzalez, C.F. (2002) An epidemic *Burkholderia cepacia* complex strain identified in soil. *Lancet* **359**: 2002–2003.

Lister, P.D., Wolter, D.J., and Hanson, N.D. (2009) Antibacterial-resistant *Pseudomonas aeruginosa*: clinical impact and complex regulation of chromosomally encoded resistance

mechanisms. *Clin Microbiol Rev* **22**: 582–610.
Liu, C.-I., Liu, G.Y., Song, Y., Yin, F., Hensler, M.E., Jeng, W.-Y., *et al.* (2008) A cholesterol biosynthesis inhibitor blocks *Staphylococcus aureus* virulence. *Science* **319**: 1391–1394.
Liu, G.Y., Doran, K.S., Lawrence, T., Turkson, N., Puliti, M., Tissi, L., and Nizet, V. (2004) Sword and shield: linked group B streptococcal beta-hemolysin/cytolysin and carotenoid pigment function to subvert host phagocyte defense. *Proc Natl Acad Sci USA* **101**: 14491–14496.
Liu, G.Y., and Nizet, V. (2009) Color me bad: microbial pigments as virulence factors. *Trends Microbiol* **17**: 406–413.
Liu, J., Gefen, O., Ronin, I., Bar-Meir, M., and Balaban, N.Q. (2020) Effect of tolerance on the evolution of antibiotic resistance under drug combinations. *Science* **367**: 200–204.
Liu, J., Martinez-Corral, R., Prindle, A., Lee, D.-Y.D., Larkin, J., Gabalda-Sagarra, M., *et al.* (2017) Coupling between distant biofilms and emergence of nutrient time-sharing. *Science* **356**: 638–642.
Liu, J., Prindle, A., Humphries, J., Gabalda-Sagarra, M., Asally, M., Lee, D.D., *et al.* (2015) Metabolic co-dependence gives rise to collective oscillations within biofilms. *Nature* **523**: 550–554.
Liu, Y., and Imlay, J.A. (2013) Cell death from antibiotics without the involvement of reactive oxygen species. *Science* **339**: 1210–1213.
Llanes, C., Köhler, T., Patry, I., Dehecq, B., Delden, C. van, and Plésiat, P. (2011) Role of the MexEF-OprN efflux system in low-level resistance of *Pseudomonas aeruginosa* to ciprofloxacin. *Antimicrob Agents Chemother* **55**: 5676–5684.
Lobritz, M.A., Belenky, P., Porter, C.B.M., Gutierrez, A., Yang, J.H., Schwarz, E.G., *et al.* (2015) Antibiotic efficacy is linked to bacterial cellular respiration. *Proc Natl Acad Sci USA* **112**: 8173–8180.
Maplestone, R.A., Stone, M.J., and Williams, D.H. (1992) The evolutionary role of secondary metabolites – a review. *Gene* **115**: 151–157.
Martín, J.F., Casqueiro, J., and Liras, P. (2005) Secretion systems for secondary metabolites: how producer cells send out messages of intercellular communication. *Curr Opin Microbiol* **8**: 282–293.
Martina, P., Feliziani, S., Juan, C., Bettiol, M., Gatti, B., Yantorno, O., *et al.* (2014) Hypermutation in *Burkholderia cepacia* complex is mediated by DNA mismatch repair inactivation and is highly prevalent in cystic fibrosis chronic respiratory infection. *Int J Med Microbiol* **304**: 1182–1191.
Martinez, J.L. (2009) The role of natural environments in the evolution of resistance traits in pathogenic bacteria. *Proc Biol Sci* **276**: 2521–2530.
Martinez, J.L., Sánchez, M.B., Martínez-Solano, L., Hernandez, A., Garmendia, L., Fajardo, A., and Alvarez-Ortega, C. (2009) Functional role of bacterial multidrug efflux pumps in microbial natural ecosystems. *FEMS Microbiol Rev* **33**: 430–449.
Martins, D., McKay, G.A., English, A.M., and Nguyen, D. (2020) Sublethal paraquat confers multidrug tolerance in *Pseudomonas aeruginosa* by inducing superoxide dismutase activity and lowering envelope permeability. *Front Microbiol* **11**: 576708.
Mavrodi, D.V., Blankenfeldt, W., and Thomashow, L.S. (2006) Phenazine compounds in fluorescent *Pseudomonas* spp. biosynthesis and regulation. *Annu Rev Phytopathol* **44**: 417–445.
McNamara, P.J., and Proctor, R.A. (2000) *Staphylococcus aureus* small colony variants, electron transport and persistent infections. *Int J Antimicrob Agents* **14**: 117–122.
McRose, D.L., and Newman, D.K. (2021) Redox-active antibiotics enhance phosphorus

bioavailability. *Science* **371**: 1033–1037.
Meirelles, L.A., and Newman, D.K. (2018) Both toxic and beneficial effects of pyocyanin contribute to the lifecycle of *Pseudomonas aeruginosa*. *Mol Microbiol* **110**: 995–1010.
Meirelles, L.A., Perry, E.K., Bergkessel, M., and Newman, D.K. (2021) Bacterial defenses against a natural antibiotic promote collateral resilience to clinical antibiotics. *PLoS Biol* **19**: e3001093.
Miller, P.F., Gambino, L.F., Sulavik, M.C., and Gracheck, S.J. (1994) Genetic relationship between *soxRS* and *mar* loci in promoting multiple antibiotic resistance in *Escherichia coli. Antimicrob Agents Chemother* **38**: 1773–1779.
Moreillon, P., and Tomasz, A. (1988) Penicillin resistance and defective lysis in clinical isolates of pneumococci: evidence for two kinds of antibiotic pressure operating in the clinical environment. *J Infect Dis* **157**: 1150–1157.
Mosel, M., Li, L., Drlica, K., and Zhao, X. (2013) Superoxide-mediated protection of *Escherichia coli* from antimicrobials. *Antimicrob Agents Chemother* **57**: 5755–5759.
Mousa, J.J., and Bruner, S.D. (2016) Structural and mechanistic diversity of multidrug transporters. *Nat Prod Rep* **33**: 1255–1267.
Nair, B.M., Cheung, K.-J., Griffith, A., and Burns, J.L. (2004) Salicylate induces an antibiotic efflux pump in *Burkholderia cepacia* complex genomovar III (*B. cenocepacia*). *J Clin Invest* **113**: 464–473.
Nguyen, D., Joshi-Datar, A., Lepine, F., Bauerle, E., Olakanmi, O., Beer, K., *et al.* (2011) Active starvation responses mediate antibiotic tolerance in biofilms and nutrient-limited bacteria. *Science* **334**: 982–986.
Nikaido, E., Giraud, E., Baucheron, S., Yamasaki, S., Wiedemann, A., Okamoto, K., *et al.* (2012) Effects of indole on drug resistance and virulence of *Salmonella enterica* serovar Typhimurium revealed by genome-wide analyses. *Gut Pathog* **4**: 5.
Nishimura, I., Kurokawa, M., Liu, L., and Ying, B.-W. (2017) Coordinated changes in mutation and growth rates induced by genome reduction. *mBio* **8**: e00676-17.
Nishino, K., Honda, T., and Yamaguchi, A. (2005) Genome-wide analyses of *Escherichia coli* gene expression responsive to the BaeSR two-component regulatory system. *J Bacteriol* **187**: 1763–1772.
Nishino, K., Nikaido, E., and Yamaguchi, A. (2007) Regulation of multidrug efflux systems involved in multidrug and metal resistance of *Salmonella enterica* serovar Typhimurium. *J Bacteriol* **189**: 9066–9075.
Noto, M.J., Burns, W.J., Beavers, W.N., and Skaar, E.P. (2017) Mechanisms of pyocyanin toxicity and genetic determinants of resistance in *Staphylococcus aureus*. *J Bacteriol* **199**: e00221-17.
Ochsner, U.A., Vasil, M.L., Alsabbagh, E., Parvatiyar, K., and Hassett, D.J. (2000) Role of the *Pseudomonas aeruginosa* oxyR-recG operon in oxidative stress defense and DNA repair: OxyR-dependent regulation of katB-ankB, ahpB, and ahpC-ahpF. *J Bacteriol* **182**: 4533–4544.
Orazi, G., and O'Toole, G.A. (2017) *Pseudomonas aeruginosa* alters *Staphylococcus aureus* sensitivity to vancomycin in a biofilm model of cystic fibrosis infection. *mBio* **8**: e00873-17.
Orazi, G., Ruoff, K.L., and O'Toole, G.A. (2019) *Pseudomonas aeruginosa* increases the sensitivity of biofilm-grown *Staphylococcus aureus* to membrane-targeting antiseptics and antibiotics. *mBio* **10**: e01501-19.
Perry, E.K., and Newman, D.K. (2019) The transcription factors ActR and SoxR differentially affect

the phenazine tolerance of *Agrobacterium tumefaciens*. *Mol Microbiol* **112**: 199–218.
Piddock, L.J.V. (2006a) Multidrug-resistance efflux pumps – not just for resistance. *Nat Rev Microbiol* **4**: 629–636.
Piddock, L.J.V. (2006b) Clinically relevant chromosomally encoded multidrug resistance efflux pumps in bacteria. *Clin Microbiol Rev* **19**: 382–402.
Pontes, M.H., and Groisman, E.A. (2020) A physiological basis for nonheritable antibiotic resistance. *mBio* **11**: 00817-20.
Prayle, A., Watson, A., Fortnum, H., and Smyth, A. (2010) Side effects of aminoglycosides on the kidney, ear and balance in cystic fibrosis. *Thorax* **65**: 654–658.
Price-Whelan, A., Dietrich, L.E.P., and Newman, D.K. (2006) Rethinking "secondary" metabolism: physiological roles for phenazine antibiotics. *Nat Chem Biol* **2**: 71–78.
Priuska, E.M., and Schacht, J. (1995) Formation of free radicals by gentamicin and iron and evidence for an iron/gentamicin complex. *Biochem Pharmacol* **50**: 1749–1752.
Radlinski, L., Rowe, S.E., Kartchner, L.B., Maile, R., Cairns, B.A., Vitko, N.P., *et al.* (2017) *Pseudomonas aeruginosa* exoproducts determine antibiotic efficacy against *Staphylococcus aureus. PLoS Biol* **15**: e2003981.
Rhoads, D.D., Wolcott, R.D., Sun, Y., and Dowd, S.E. (2012) Comparison of culture and molecular identification of bacteria in chronic wounds. *Int J Mol Sci* **13**: 2535–2550.
Richardot, C., Juarez, P., Jeannot, K., Patry, I., Plésiat, P., and Llanes, C. (2016) Amino acid substitutions account for most MexS alterations in clinical nfxC mutants of *Pseudomonas aeruginosa. Antimicrob Agents Chemother* **60**: 2302–2310.
Romsang, A., Dubbs, J.M., and Mongkolsuk, S. (2016) The iron-sulfur cluster biosynthesis regulator IscR contributes to iron homeostasis and resistance to oxidants in *Pseudomonas Aeruginosa*. In *Stress and environmental regulation of gene expression and adaptation in bacteria*. Bruijn, F.J. de (ed.). John Wiley & Sons, Inc., Hoboken, NJ, USA. pp. 1090–1102.
Rosche, W.A., and Foster, P.L. (2000) Determining mutation rates in bacterial populations. *Methods* **20**: 4–17.
Rosenberg, E.Y., Bertenthal, D., Nilles, M.L., Bertrand, K.P., and Nikaido, H. (2003) Bile salts and fatty acids induce the expression of *Escherichia coli* AcrAB multidrug efflux pump through their interaction with Rob regulatory protein. *Mol Microbiol* **48**: 1609–1619.
Ruiz, C., and Levy, S.B. (2014) Regulation of acrAB expression by cellular metabolites in *Escherichia coli. J Antimicrob Chemother* **69**: 390–399.
Ryan, R.P., Monchy, S., Cardinale, M., Taghavi, S., Crossman, L., Avison, M.B., *et al.* (2009) The versatility and adaptation of bacteria from the genus *Stenotrophomonas*. *Nat Rev Microbiol* **7**: 514–525.
Saini, V., Cumming, B.M., Guidry, L., Lamprecht, D.A., Adamson, J.H., Reddy, V.P., *et al.* (2016) Ergothioneine maintains redox and bioenergetic homeostasis essential for drug susceptibility and virulence of *Mycobacterium tuberculosis. Cell Rep* **14**: 572–585.
Sakhtah, H., Koyama, L., Zhang, Y., Morales, D.K., Fields, B.L., Price-Whelan, A., *et al.* (2016) The *Pseudomonas aeruginosa* efflux pump MexGHI-OpmD transports a natural phenazine that controls gene expression and biofilm development. *Proc Natl Acad Sci USA* **113**: E3538-47.
Sampson, T.R., Liu, X., Schroeder, M.R., Kraft, C.S., Burd, E.M., and Weiss, D.S. (2012) Rapid killing of *Acinetobacter baumannii* by polymyxins is mediated by a hydroxyl radical death pathway. *Antimicrob Agents Chemother* **56**: 5642–5649.
Santi, I., Manfredi, P., Maffei, E., Egli, A., and Jenal, U. (2021) Evolution of antibiotic tolerance

shapes resistance development in chronic *Pseudomonas aeruginosa* infections. *mBio* **12**: e03482-20.

Saunders, S.H., Tse, E.C.M., Yates, M.D., Otero, F.J., Trammell, S.A., Stemp, E.D.A., *et al.* (2020) Extracellular DNA promotes efficient extracellular electron transfer by pyocyanin in *Pseudomonas aeruginosa* biofilms. *Cell* **182**: 919–932.e19.

Schiessl, K.T., Hu, F., Jo, J., Nazia, S.Z., Wang, B., Price-Whelan, A., *et al.* (2019) Phenazine production promotes antibiotic tolerance and metabolic heterogeneity in *Pseudomonas aeruginosa* biofilms. *Nat Commun* **10**: 762.

Schwab, U., Abdullah, L.H., Perlmutt, O.S., Albert, D., Davis, C.W., Arnold, R.R., *et al.* (2014) Localization of *Burkholderia cepacia* complex bacteria in cystic fibrosis lungs and interactions with *Pseudomonas aeruginosa* in hypoxic mucus. *Infect Immun* **82**: 4729–4745.

Severi, E., and Thomas, G.H. (2019) Antibiotic export: transporters involved in the final step of natural product production. *Microbiology (Reading, Engl)* **165**: 805–818.

Shafer, W.M., Qu, X., Waring, A.J., and Lehrer, R.I. (1998) Modulation of *Neisseria gonorrhoeae* susceptibility to vertebrate antibacterial peptides due to a member of the resistance/nodulation/division efflux pump family. *Proc Natl Acad Sci USA* **95**: 1829–1833.

Shatalin, K., Shatalina, E., Mironov, A., and Nudler, E. (2011) H2S: a universal defense against antibiotics in bacteria. *Science* **334**: 986–990.

Shen, X., Lind, J., and Merenyi, G. (1987) One-electron oxidation of indoles and acid-base properties of the indolyl radicals. *J Phys Chem* **91**: 4403–4406.

Shukla, P., Khodade, V.S., SharathChandra, M., Chauhan, P., Mishra, S., Siddaramappa, S., *et al.* (2017) "On demand" redox buffering by H2S contributes to antibiotic resistance revealed by a bacteria-specific H2S donor. *Chem Sci* **8**: 4967–4972.

Shyu, J.B.H., Lies, D.P., and Newman, D.K. (2002) Protective role of tolC in efflux of the electron shuttle anthraquinone-2,6-disulfonate. *J Bacteriol* **184**: 1806–1810.

Singh, A.K., Shin, J.-H., Lee, K.-L., Imlay, J.A., and Roe, J.-H. (2013) Comparative study of SoxR activation by redox-active compounds. *Mol Microbiol* **90**: 983–996.

Smith, D.D.N., Kirzinger, M.W.B., and Stavrinids, J. (2013) Draft genome sequence of the antibiotic-producing cystic fibrosis isolate *Pantoea agglomerans* Tx10. *Genome Announc* **1**: e00904-13.

Sokol, P.A., Lewis, C.J., and Dennis, J.J. (1992) Isolation of a novel siderophore from Pseudomonas cepacia. *J Med Microbiol* **36**: 184–189.

Somayaji, R., Parkins, M.D., Shah, A., Martiniano, S.L., Tunney, M.M., Kahle, J.S., *et al.* (2019) Antimicrobial susceptibility testing (AST) and associated clinical outcomes in individuals with cystic fibrosis: a systematic review. *J Cyst Fibros* **18**: 236–243.

Song, Y., Liu, C.-I., Lin, F.-Y., No, J.H., Hensler, M., Liu, Y.-L., *et al.* (2009) Inhibition of staphyloxanthin virulence factor biosynthesis in *Staphylococcus aureus*: in vitro, in vivo, and crystallographic results. *J Med Chem* **52**: 3869–3880.

Spero, M.A., and Newman, D.K. (2018) Chlorate specifically targets oxidant-starved, antibiotic-tolerant populations of *Pseudomonas aeruginosa* biofilms. *mBio* **9**: e01400-18.

Tahlan, K., Ahn, S.K., Sing, A., Bodnaruk, T.D., Willems, A.R., Davidson, A.R., and Nodwell, J.R. (2007) Initiation of actinorhodin export in *Streptomyces coelicolor. Mol Microbiol* **63**: 951–961.

Tkachenko, A.G., Akhova, A.V., Shumkov, M.S., and Nesterova, L.Y. (2012) Polyamines reduce oxidative stress in *Escherichia coli* cells exposed to bactericidal antibiotics. *Res Microbiol* **163**: 83–91.

Tkachenko, A.G., and Fedotova, M.V. (2007) Dependence of protective functions of *Escherichia coli* polyamines on strength of stress caused by superoxide radicals. *Biochemistry (Mosc)* **72**: 109–116.

Toprak, E., Veres, A., Michel, J.-B., Chait, R., Hartl, D.L., and Kishony, R. (2011) Evolutionary paths to antibiotic resistance under dynamically sustained drug selection. *Nat Genet* **44**: 101–105.

Tortorella, E., Tedesco, P., Palma Esposito, F., January, G.G., Fani, R., Jaspars, M., and Pascale, D. de (2018) Antibiotics from deep-sea microorganisms: current discoveries and perspectives. *Mar Drugs* **16**: 355.

Trimble, M.J., Mlynárčik, P., Kolář, M., and Hancock, R.E.W. (2016) Polymyxin: alternative mechanisms of action and resistance. *Cold Spring Harb Perspect Med* **6**: a025288.

Tyc, O., Song, C., Dickschat, J.S., Vos, M., and Garbeva, P. (2017) The ecological role of volatile and soluble secondary metabolites produced by soil bacteria. *Trends Microbiol* **25**: 280–292.

VanDrisse, C.M., Lipsh-Sokolik, R., Khersonsky, O., Fleishman, S.J., and Newman, D.K. (2021) Computationally designed pyocyanin demethylase acts synergistically with tobramycin to kill recalcitrant *Pseudomonas aeruginosa* biofilms. *Proc Natl Acad Sci USA* **118**: e2022012118.

Vega, N.M., Allison, K.R., Khalil, A.S., and Collins, J.J. (2012) Signaling-mediated bacterial persister formation. *Nat Chem Biol* **8**: 431–433.

Vega, N.M., Allison, K.R., Samuels, A.N., Klempner, M.S., and Collins, J.J. (2013) Salmonella typhimurium intercepts Escherichia coli signaling to enhance antibiotic tolerance. *Proc Natl Acad Sci USA* **110**: 14420–14425.

Visca, P., Ciervo, A., Sanfilippo, V., and Orsi, N. (1993) Iron-regulated salicylate synthesis by *Pseudomonas* spp. *J Gen Microbiol* **139**: 1995–2001.

Voggu, L., Schlag, S., Biswas, R., Rosenstein, R., Rausch, C., and Götz, F. (2006) Microevolution of cytochrome *bd* oxidase in staphylococci and its implication in resistance to respiratory toxins released by *Pseudomonas*. *J Bacteriol* **188**: 8079–8086.

Walterson, A.M., and Stavrinides, J. (2015) *Pantoea*: insights into a highly versatile and diverse genus within the Enterobacteriaceae. *FEMS Microbiol Rev* **39**: 968–984.

Wang, S., and Lu, Z. (2017) Secondary metabolites in archaea and extreme environments. In *Biocommunication of Archaea*. Witzany, G. (ed.). Springer International Publishing, Cham. pp. 235–239.

Wang, X., and Zhao, X. (2009) Contribution of oxidative damage to antimicrobial lethality. *Antimicrob Agents Chemother* **53**: 1395–1402.

Wang, Y., Wilks, J.C., Danhorn, T., Ramos, I., Croal, L., and Newman, D.K. (2011) Phenazine-1-carboxylic acid promotes bacterial biofilm development via ferrous iron acquisition. *J Bacteriol* **193**: 3606–3617.

Wei, Q., Minh, P.N.L., Dötsch, A., Hildebrand, F., Panmanee, W., Elfarash, A., *et al.* (2012) Global regulation of gene expression by OxyR in an important human opportunistic pathogen. *Nucleic Acids Res* **40**: 4320–4333.

Wells, J.M., Cole, R.J., and Kirksey, J.W. (1975) Emodin, a toxic metabolite of *Aspergillus wentii* isolated from weevil-damaged chestnuts. *Appl Microbiol* **30**: 26–28.

Welp, A.L., and Bomberger, J.M. (2020) Bacterial community interactions during chronic respiratory disease. *Front Cell Infect Microbiol* **10**: 213.

Wilson, R., Sykes, D.A., Watson, D., Rutman, A., Taylor, G.W., and Cole, P.J. (1988) Measurement of *Pseudomonas aeruginosa* phenazine pigments in sputum and assessment of their

contribution to sputum sol toxicity for respiratory epithelium. *Infect Immun* **56**: 2515–2517.
Windels, E.M., Michiels, J.E., Fauvart, M., Wenseleers, T., Van den Bergh, B., and Michiels, J. (2019) Bacterial persistence promotes the evolution of antibiotic resistance by increasing survival and mutation rates. *ISME J* **13**: 1239–1251.
Wolloscheck, D., Krishnamoorthy, G., Nguyen, J., and Zgurskaya, H.I. (2018) Kinetic control of quorum sensing in *Pseudomonas aeruginosa* by multidrug efflux pumps. *ACS Infect Dis* **4**: 185–195.
Wood, K.B., and Cluzel, P. (2012) Trade-offs between drug toxicity and benefit in the multi-antibiotic resistance system underlie optimal growth of *E. coli*. *BMC Syst Biol* **6**: 48.
Wu, C., Cichewicz, R., Li, Y., Liu, J., Roe, B., Ferretti, J., *et al.* (2010) Genomic island TnSmu2 of *Streptococcus mutans* harbors a nonribosomal peptide synthetase-polyketide synthase gene cluster responsible for the biosynthesis of pigments involved in oxygen and H_2O_2 tolerance. *Appl Environ Microbiol* **76**: 5815–5826.
Yan, J., and Bassler, B.L. (2019) Surviving as a community: antibiotic tolerance and persistence in bacterial biofilms. *Cell Host Microbe* **26**: 15–21.
Young, A.J., and Lowe, G.L. (2018) Carotenoids – antioxidant properties. *Antioxidants (Basel)* **7**: 28.
Yung, D.B.Y., Sircombe, K.J., and Pletzer, D. (2021) Friends or enemies? The complicated relationship between *Pseudomonas aeruginosa* and *Staphylococcus aureus*. *Mol Microbiol*. Epub ahead of print. PMID: 33576132.
Zheng, Q. (2015) A new practical guide to the Luria-Delbrück protocol. *Mutat Res* **781**: 7–13.
Zhu, K., Chen, S., Sysoeva, T.A., and You, L. (2019) Universal antibiotic tolerance arising from antibiotic-triggered accumulation of pyocyanin in *Pseudomonas aeruginosa. PLoS Biol* **17**: e3000573.
Zuccato, E., Venturi, M., Di Leo, G., Colombo, L., Bertolo, C., Doldi, S.B., and Mussini, E. (1993) Role of bile acids and metabolic activity of colonic bacteria in increased risk of colon cancer after cholecystectomy. *Dig Dis Sci* **38**: 514–519.

Chapter 5

PREVALENCE OF PHENAZINE RESISTANCE IN CULTURABLE BACTERIA FROM A DRYLAND WHEAT FIELD

Abstract

Phenazines are a class of bacterially-produced natural antibiotics that have demonstrated potential as a sustainable alternative to traditional pesticides for the control of fungal crop diseases in agriculture. However, the prevalence of bacterial resistance to agriculturally-relevant phenazines is poorly understood, limiting the ability to assess the risk of off-target negative effects on native rhizosphere communities. In addition, it is currently not known whether there are conserved genetic markers that could be used to predict bacterial resistance or susceptibility to phenazines. Here, we describe profiles of susceptibility to an agriculturally-relevant phenazine across more than 100 bacterial strains isolated from a wheat field where phenazine producers are indigenous. Our results shed light on which classes of bacteria are most likely to be susceptible to phenazine toxicity, depending on the environmental pH. These insights will be useful for investigating whether the effects of phenazine producers on rhizosphere communities are consistent with the incidence of bacterial resistance to this family of natural antibiotics. In addition, the taxonomic and phenotypic diversity of our strain collection lays a foundation for the future development of models that could enable prediction of phenazine resistance in diverse bacterial taxa.

Introduction

Diverse microorganisms produce natural antibiotics that can kill or inhibit the growth of other microbes (Bérdy, 2012; Granato *et al.*, 2019). Several such compounds have been commercialized as antimicrobial drugs for the treatment of infections, beginning with penicillin in the 1940s (Aminov, 2010; Hutchings *et al.*, 2019). Unfortunately, the selective pressures exerted by the widespread use of antibiotics in medicine and agriculture have led to worrisome increases in the prevalence of antimicrobial resistance among human and animal pathogens over the past several decades (Davies and Davies, 2010; Manyi-Loh *et al.*, 2018). Yet while this repercussion of human antibiotic use has been well documented, comparatively little is known about the ecological roles of

microbially-produced antibiotics in natural environments (Aminov, 2009; Sengupta *et al.*, 2013). Recent studies have suggested that natural antibiotics may serve a variety of functions for their producers beyond the suppression of competing microbes (Davies, 2006; Davies *et al.*, 2006), including nutrient acquisition (Wang and Newman, 2008; McRose and Newman, 2021), conservation of energy in the absence of oxygen (Glasser *et al.*, 2014; Glasser *et al.*, 2017), and cell-cell signaling (Dietrich *et al.*, 2006; Linares *et al.*, 2006). At the same time, toxicity to one or more microorganisms is by definition a feature of these molecules, but the extent to which this trait shapes their influence on microbial communities is unclear (Demain and Fang, 2000; Davies and Ryan, 2012; Bérdy, 2012). In addition, for many if not most natural antibiotics, the determinants and prevalence of susceptibility or resistance to their toxicity remain unknown or poorly characterized (Handelsman and Stabb, 1996). These gaps in knowledge hinder our ability to understand and predict the impacts of these metabolites on microbial communities of interest.

One environmental context in which natural antibiotics are thought to be particularly abundant and ecologically relevant is the rhizosphere—the narrow plane of soil immediately adjacent to plant roots (Haas and Défago, 2005; Mavrodi *et al.*, 2012; Tyc *et al.*, 2017). Natural antibiotics such as phenazines and 2,4-diacetylphloroglucinol have been directly detected in the rhizospheres of multiple crops, including wheat, potato, and sugar beet (Thomashow *et al.*, 1990; Bergsma-Vlami *et al.*, 2005; Mavrodi *et al.*, 2012), and phenazines have been shown to increase the fitness of their producers when competing with other microbes in the rhizosphere (Mazzola *et al.*, 1992; Yu *et al.*, 2018). Production of these molecules has also been demonstrated to underpin the ability of certain bacteria to control fungal crop diseases (Thomashow and Weller, 1988; Thomashow *et al.*, 1990; Haas and Keel, 2003; Mazurier *et al.*, 2009; Yu *et al.*, 2018), further indicating that natural antibiotics can act as agents of microbe-microbe antagonism in the rhizosphere. As a result of this activity, phenazine-producing *Pseudomonas* strains have received attention as potential "biocontrol agents" that could serve as a more sustainable alternative to traditional synthetic pesticides in agriculture (Handelsman and Stabb, 1996; Haas and Keel, 2003). However, several challenges remain with respect to the practical application of these strains, including inconsistent efficacy under field conditions (Haas and Keel, 2003; Haas and Défago, 2005), limited understanding of the mechanisms and evolutionary dynamics of resistance to

phenazines (Mazzola *et al.*, 1995; Handelsman and Stabb, 1996), and the possibility of off-target effects (Haas and Keel, 2003).

Importantly, with regard to the latter concern, phenazines are toxic not only to fungi, but also to some bacteria (Baron and Rowe, 1981; Turner and Messenger, 1986; Costa *et al.*, 2015). Yet while the utility of phenazine-producing pseudomonads for biocontrol of fungal crop diseases has been extensively investigated, the potential impact of these strains on non-target bacterial residents of the rhizosphere is less well understood. One study found that inoculation of *Pseudomonas* biocontrol strains shifted the rhizosphere community of maize seedlings, pushing the ratio of Gram-positive to Gram-negative bacteria in favor of the latter; however, this analysis was based on profiling colony growth rates and whole-cell fatty acids from pooled cultured isolates, greatly limiting the taxonomic resolution and making it difficult to rule out whether the Gram-negative biocontrol strains might themselves have directly contributed to the shift (Kozdrój *et al.*, 2004). On the other hand, at least three studies found no notable or consistent effects of introduced *Pseudomonas* species on the rhizosphere bacterial communities of wheat or potato (Gagliardi *et al.*, 2001; Bankhead *et al.*, 2004; Roquigny *et al.*, 2018), albeit the studies in wheat employed methods with limited discriminatory power (namely, carbon source utilization profiling and terminal restriction fragment length polymorphism). Given these mixed results and the lack of fine-grained spatial or taxonomic resolution in most studies on this topic, whether phenazine-producing bacteria actively shape the surrounding rhizosphere bacterial community through antibiosis, potentially at the micron or millimeter scale, remains an open question.

In addition to the lack of clarity regarding the effects of phenazines on rhizosphere bacterial communities, the genetic and phylogenetic correlates of phenazine resistance in bacteria remain incompletely understood. The toxicity of phenazines is generally ascribed to the generation of reactive oxygen species (ROS) and interference with respiration (Hassan and Fridovich, 1980; Baron and Rowe, 1981; Voggu *et al.*, 2006; Perry and Newman, 2019). Previous studies have suggested that efflux pump expression, cell permeability, oxidative stress responses, and the composition of the respiratory electron transport chain can affect bacterial susceptibility to phenazines (Voggu *et al.*, 2006; Khare and Tavazoie, 2015; Noto *et al.*, 2017; Wolloscheck *et al.*, 2018; Perry and Newman, 2019; Meirelles and Perry *et al.*, 2021). In addition, a comparison of 14 bacterial strains indicated that Gram-negative bacteria as a group may be more resistant to phenazine toxicity than

Gram-positive bacteria (Baron and Rowe, 1981). However, all of these studies focused on a specific phenazine, pyocyanin, that is particularly toxic (Meirelles and Newman, 2018) and best known for its role as a virulence factor during infections of humans and animals (Lau *et al.*, 2004; Liu and Nizet, 2009). Whether the same observations hold true for more agriculturally-relevant phenazines such as phenazine-1-carboxylic acid (PCA) (Thomashow and Weller, 1988; Thomashow *et al.*, 1990; Mavrodi *et al.*, 2012; Dar *et al.*, 2020) is unknown, and no consensus set of predictive genetic markers of phenazine resistance exists that has been validated across different microorganisms.

In this study, we set out to lay a foundation for addressing unresolved questions about the ecological impact of phenazine toxicity in the rhizosphere by determining the prevalence of phenazine resistance among bacteria isolated from a wheat field in the Inland Pacific Northwest, a region where phenazine production and the biocontrol potential of indigenous *Pseudomonas* species have been studied for decades (Thomashow and Weller, 1988; Thomashow *et al.*, 1990; Mazzola *et al.*, 1992; Mavrodi *et al.*, 2012). We designed a culture-based assay to measure sensitivity to PCA, which is the best-studied and one of the most abundant phenazines in this environment (Thomashow *et al.*, 1990; Mavrodi *et al.*, 2012; Dar *et al.*, 2020). We also performed full-length 16S rRNA gene sequencing of our isolates in order to assess the relationship between taxonomy and PCA resistance. Our strain collection is taxonomically diverse and encompasses a wide range of phenotypes with respect to PCA resistance. This work thereby opens the door to identifying conserved genetic markers of resistance to phenazines, if any exist.

Results

Taxonomy of culturable bacteria from dryland wheat rhizospheres and bulk soil

A total of 175 strains of bacteria were isolated from 12 soil samples collected from a wheat field at Washington State University's Lind Dryland Research Station in early August 2019, shortly after the wheat harvest. The samples comprised 4 replicates each of wheat rhizosphere ("Wheat"), bulk soil collected between planted rows ("Between"), and bulk soil from a virgin patch of uncultivated soil adjacent to the field ("Virgin"). Full-length 16S rRNA gene sequencing revealed that the isolates represented 21 genera across 4 phyla: Actinobacteria, Bacteroidetes, Firmicutes, and Proteobacteria. The vast majority of isolates from the bulk soil samples (both Between and Virgin)

were Actinobacteria or Firmicutes. In Wheat samples, on the other hand, the combined proportions of these two phyla were lower, accounting for 18-50% and 10-25% of isolates respectively, while Proteobacteria accounted for approximately 25-60% of isolates depending on the replicate, and 1-3 strains of Bacteroidetes were also detected in each replicate (5-12% of isolates) (Fig. 1).

Development of a phenotypic screen for PCA resistance

The toxicity of PCA to diverse organisms is known to vary depending on pH, with generally minimal toxicity above pH 6 and increasing toxicity with increasing acidity (Brisbane *et al.*, 1987; Cezairliyan *et al.*, 2013). This phenomenon has been attributed to the fact that the deprotonated form of PCA is negatively charged (Fig. 2A); the negative charge on bacterial cell walls and the outer membrane of Gram-negative bacteria (or the negative membrane potential of eukaryotic cells) likely hinders uptake of this species. The protonated form of PCA, on the other hand, is neutral and presumably can passively diffuse across cell membranes given the small size and hydrophobic nature of the molecule (Price-Whelan *et al.*, 2006; Cezairliyan *et al.*, 2013). The pKa of PCA is 4.24 at 25 °C; thus, at pH 7, only 0.17% of PCA in solution is protonated compared to 14.8% at pH 5, leading to greater toxicity at the lower pH (Brisbane *et al.*, 1987). Given this pH dependency and the fact that the bulk soil and rhizosphere pH of wheat fields in the Inland Pacific Northwest can vary by >3 units (pH 4.3-8.0) depending on geographic location and fertilizer treatment status (Smiley

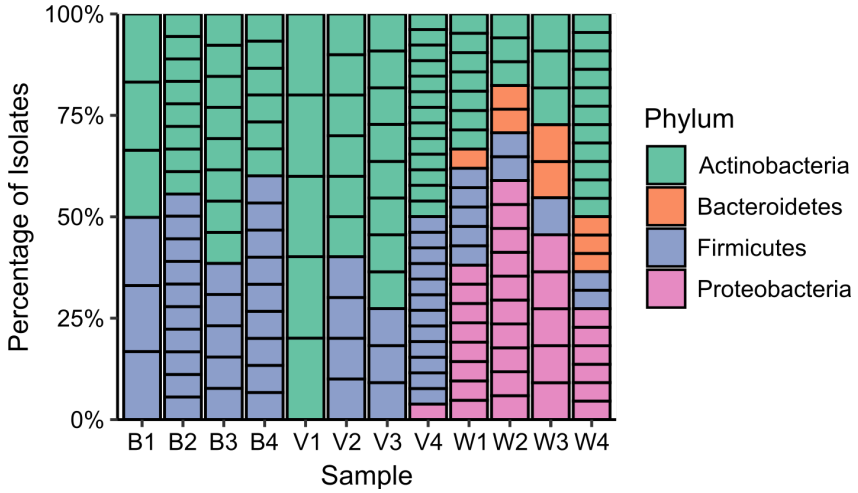

Figure 1: Taxonomic distribution of bacterial isolates from wheat rhizosphere and bulk soil samples. This plot depicts the proportion of isolates from each sample that belonged to the 4 represented phyla. Each column represents one soil sample, and each box within the columns represents an individual isolate colored by the phylum to which it belongs (e.g. 6 boxes comprising one column indicates that 6 strains were isolated from that sample). B = Between (bulk soil), V = Virgin (bulk soil), W = Wheat (rhizosphere).

and Cook, 1973), we decided to screen our isolates for resistance to PCA at both circumneutral and acidic pH (7.3 and 5.1, respectively). We chose 100 µM as the working concentration of PCA as this is likely to be in a physiologically relevant range based on concentrations measured both in pure cultures and in the field. In broth cultures of biocontrol strains of *Pseudomonas*, PCA accumulates to concentrations ranging from dozens to hundreds of micromolar (Séveno *et al.*, 2001; Tagele *et al.*, 2019). In natural wheat rhizospheres, PCA has been detected at nanomolar concentrations (Mavrodi *et al.*, 2012), but these bulk measurements almost certainly underestimate local concentrations at the micron scale given that bacteria colonize the rhizosphere in a patchy manner (Thomashow *et al.*, 1990). Notably, PCA can accumulate in biofilms to concentrations 360-fold greater on a per volume basis compared to broth cultures (Séveno *et al.*, 2001), suggesting that local concentrations of PCA in the rhizosphere, where biocontrol strains form robust biofilms (LeTourneau *et al.*, 2018), may be orders of magnitude higher than the reported values.

We initially attempted to perform our screen in liquid cultures in 96-well plates, in order to quantitatively track growth of the isolates using optical density over time. However, we found that for the majority of our isolates, even the untreated controls did not grow well under this condition—either they grew as clumps or showed minimal growth after 3 days, despite robustly forming visible colonies on agar plates in the same timeframe. We therefore turned instead to an agar-based assay,

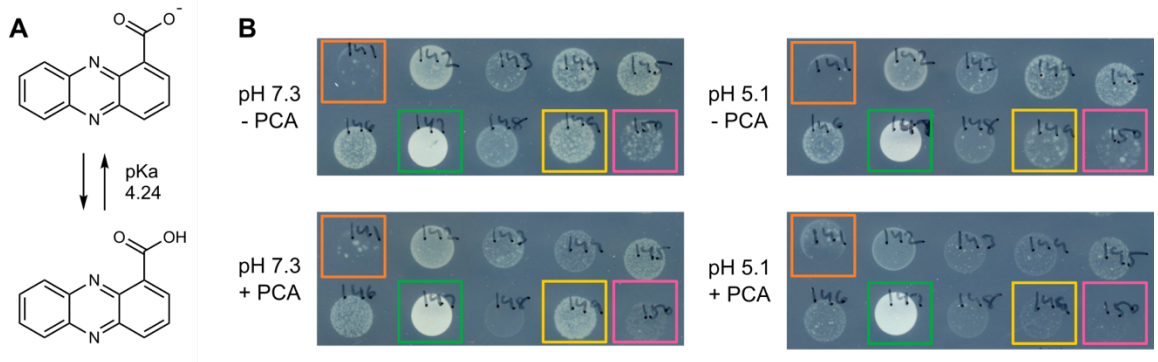

Figure 2: Design and examples of readouts from a first-round PCA resistance screen.
A. Structure of oxidized PCA in deprotonated and protonated states.
B. In the first round of screening, resuspended cells of individual strains were spotted next to each other on 10 cm agar plates under the four depicted conditions (pH 7.3 or pH 5.1, with or without 100 µM PCA). The relative positions of individual strains are consistent across the conditions. These images were taken after 72 hrs. The colored boxes highlight different types of outcomes. Orange: a strain that was inhibited by an unidentified antibiotic secreted by its neighbor (the strain marked "146"). Green: a strain that was completely resistant to PCA at both pH 7.3 and pH 5.1. Yellow: a strain that was resistant to PCA at pH 7.3, but mildly inhibited by PCA at pH 5.1. Pink: a strain that was mildly inhibited by PCA at both pH 7.3 and pH 5.1.

whereby cells of each isolate were resuspended to a low density in liquid medium (or diluted from overnight cultures) and the suspensions were spotted onto agar plates containing either 100 μM PCA or a solvent control. In the first round of this assay, we used 10 cm petri dishes and spotted up to 40 strains on the same plate. The plates were imaged once per day for 3 days using a flatbed scanner and the growth of each strain on the PCA plates relative to the controls was qualitatively scored by eye. This approach clearly revealed that certain strains were sensitive to PCA while others were resistant (Fig. 2B). However, one confounding factor was that several isolates produced their own antibiotics that inhibited the growth of their neighbors, and PCA appeared to alter antibiotic production in some of these strains, leading to cases where neighboring strains grew better on the PCA plates than on the control plates (Fig. 2B). In addition, we had used 0.1x tryptic soy agar (TSA) for the pH 7.3 condition and 0.1x potato dextrose agar (PDA) for the pH 5.1 condition; while these two media naturally have the desired pH, this raised the possibility that other nutritional differences between the conditions might also have affected sensitivity to PCA toxicity.

To address these shortcomings, we performed a second, optimized round of the screen using 24-well plates and 0.1x TSA that was either left unadjusted (pH 7.3) or adjusted to pH 5.1 with HCl. Each isolate in this round was spotted onto agar in separate wells (one spot per well) to prevent crosstalk and antagonism between the strains, and image analysis was used to derive quantitative information about the growth of each strain. Since several strains among our isolates appeared to be duplicates of each other, we restricted this round to strains that we judged likely to be unique (Table S1), as determined by the combination of 16S rRNA gene sequence, colony morphology, and response to PCA in the first round of screening (data not shown); where multiple strains appeared identical, we chose a representative strain. We also included 13 strains from the U.S. Department of Agriculture's Agriculture Research Service Culture Collection (NRRL) that represented species found among our isolates (Table S1), in order to investigate the extent to which PCA resistance phenotypes are consistent across different strains of the same species. Finally, in this round we imaged the plates for up to 7 days in order to allow for the possibility that some sensitive strains would eventually grow in the presence of PCA. While performing the image analysis, it became evident that accurate quantification of growth would not be possible for certain strains that formed transparent colonies or secreted dark pigments. Nevertheless, this assay enabled us to derive detailed profiles of PCA sensitivity and resistance for the vast majority of our strains.

Distribution of PCA resistance phenotypes

We began our analysis by focusing on a single-timepoint snapshot of each strain's phenotype, taken at the equivalent of late log or early stationary phase (i.e. around the time that the spots on non-PCA control plates reached their maximal density; see Methods for details). In accordance with previous reports of the pH dependency of PCA toxicity, we found that more of our strains were sensitive to PCA at pH 5.1 than at pH 7.3, and strains that were mildly inhibited by PCA at pH 7.3 were typically inhibited more strongly at pH 5.1 (Fig. 3A-B). At pH 5.1, sensitivity or resistance to PCA largely fell along a Gram-positive / Gram-negative divide (Fig. 3A): most strains of Actinobacteria and Firmicutes were strongly inhibited by PCA, while most Proteobacteria were relatively resistant, and members of Bacteroidetes were either resistant or fell in the middle of the range. Interestingly, three strains of Proteobacteria (W1I13, W2I6, and W3I7, representing *Paraburkholderia graminis*, *Pseudomonas brenneri*, and *Pseudomonas fluorescens*, respectively) even appeared to grow slightly better on PCA plates compared to the control at pH 5.1. At pH 7.3, there was considerably more phenotypic variation among the Actinobacteria (Fig. 3B), particularly within the genera *Agromyces* and *Streptomyces*; for example, the top two rows of the heat map in Fig. 3B represent two species of *Agromyces* with dramatically different sensitivities to PCA. In some cases, there was even significant variation within the same species of *Streptomyces* (Fig. 3C). In addition, two strains of *Microbacterium* (W2I7 and W4I20) and two strains of *Arthrobacter* (B2I5 and W3I6) grew significantly better in the presence of PCA at pH 7.3 compared to the control condition, perhaps suggesting that they can use PCA as a carbon source or otherwise benefit from its presence at a pH where toxicity is limited; one strain of *Streptomyces* (B-2570) also had higher calculated growth on the PCA plate compared to the control, but visual examination indicated that this was likely due to pigment production on the control plate. On the other hand, in contrast to the phenotypic variation seen among Actinobacteria, Firmicutes remained universally sensitive to PCA at pH 7.3 (albeit somewhat less so than at pH 5.1), and Proteobacteria and Bacteroidetes remained relatively resistant (Fig. 3B)—the latter more so than at pH 5.1. The one exception among the Proteobacteria was a strain of *Sphingomonas faeni*, isolate W4I17, that appeared to be mildly inhibited by PCA; surprisingly, the degree of inhibition for this strain appeared greater at pH 7.3 than at pH 5.1.

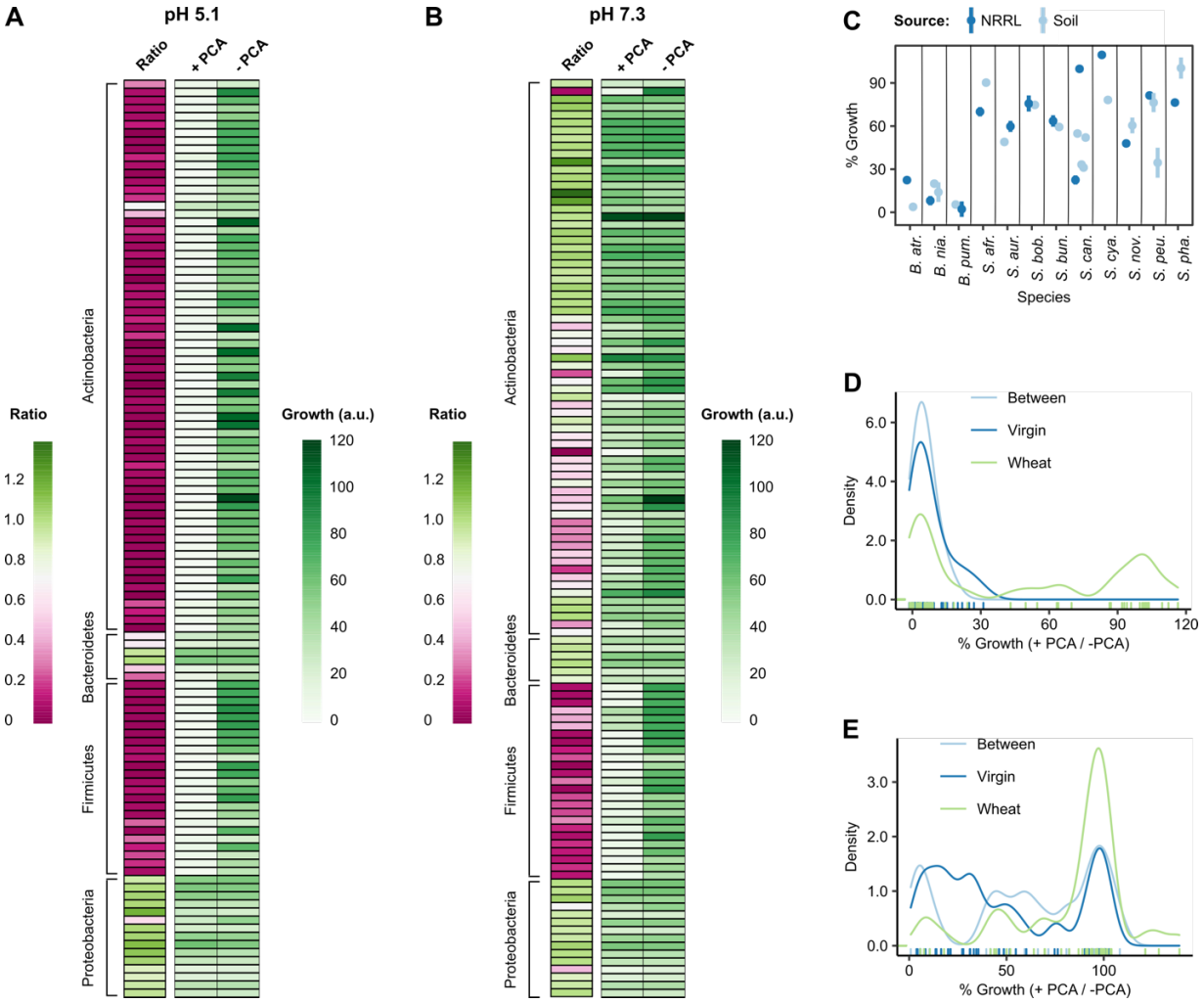

Figure 3: Distribution of PCA resistance phenotypes across phyla and soil sample type.
A-B. Heat maps depicting the growth of the strains at pH 5.1 (A) and pH 7.3 (B) in the optimized second round of screening for PCA resistance. Each row represents a strain. The leftmost columns are colored according to the ratio of growth on PCA-containing agar versus PCA-free agar; magenta indicates sensitivity to PCA while green indicates resistance to PCA. The right two columns in each heat map are colored according to the separate values for growth on PCA-containing agar (+ PCA) or solvent control agar (- PCA), with darker green indicating more growth; values are the average of three technical replicates. See Methods for a description of how growth was quantified. The rows in A roughly align with the rows in B; however, a few strains in B were not included in A due to poor growth at pH 5.1 in the PCA-free control condition.
C. PCA sensitivity at pH 7.3 of different strains belonging to the same species of *Bacillus* or *Streptomyces*. Dots represent the mean of three technical replicates for one strain and vertical lines represent the standard deviation. % Growth = percentage of growth on PCA-containing agar compared to PCA-free agar. *B. atr.* = *B. atrophaeus*; *B. nia.* = *B. niacini*; *B. pum.* = *B. pumilus*; *S. afr.* = *S. africanus*; *S. aur.* = *S. aurantiacus*; *S. bob.* = *S. bobili*; *S. can.* = *S. canus* (synonymous with *S. ciscaucasicus*); *S. cya.* = *S. cyaneofuscatus*; *S. nov.* = *S. novaecaesareae*; *S. peu.* = *S. peucetius*; *S. pha.* = *S. phaeochromogenes*.
D-E. Density plots (i.e. smoothed histograms) representing the distribution of PCA resistance phenotypes at pH 5.1 (D) and pH 7.3 (E) among strains isolated from Between (bulk), Virgin (bulk), or Wheat (rhizosphere) soil**.** Higher values along the x-axis indicate greater resistance to PCA. If multiple identical strains were isolated from the same soil type, only one representative was counted; thus, 26 strains were counted for Between, 39 for Virgin, and 45 for Wheat. Colored tick marks above the x-axis represent where individual isolates fall along the range of PCA resistance phenotypes.

We next examined whether there was any evidence of correlation between PCA resistance phenotypes and which type of soil each strain was isolated from (Between, Virgin, or Wheat). A previous study based on samples taken from the same wheat field found that the relative abundance of phenazine producers was higher in the wheat rhizosphere compared to adjacent bulk soil (Dar *et al.*, 2020). We therefore hypothesized that if PCA-mediated antibiosis had shaped the bacterial community composition of this field, the prevalence of PCA resistance would be higher among isolates from the rhizosphere samples. Indeed, the Wheat samples clearly had the highest proportion

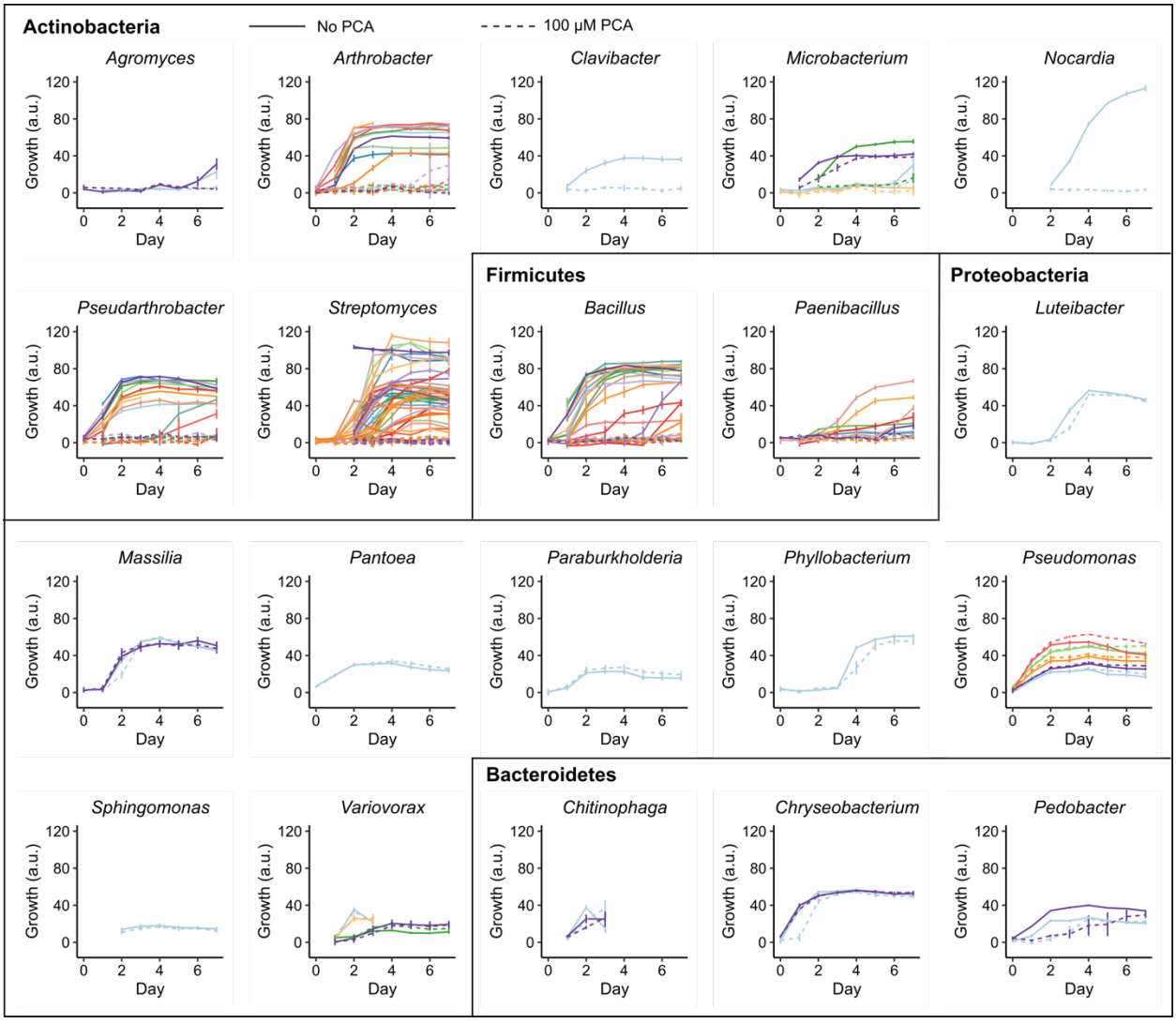

Figure 4: Growth of strains over time with and without PCA at pH 5.1.
Growth was quantified as described in the Methods. Solid lines represent the growth of spotted cultures on PCA-free agar, and dashed lines represent the growth of spotted cultures on agar containing 100 µM PCA. Each color within a panel corresponds to one strain. Data points are the mean of three technical replicates and vertical error bars are the standard deviation. Strains of *Chitinophaga* and two strains of *Variovorax* were only tracked for 3 days instead of 7 because these strains became highly mucoid and appeared to lyse starting on day 3.

of PCA-resistant isolates, regardless of whether resistance was assessed at pH 5.1 (Fig. 3D) or pH 7.3 (Fig. 3E). By contrast, all strains from Between or Virgin samples were highly sensitive to PCA at pH 5.1, though at pH 7.3, the resistance phenotypes of isolates from either type of bulk soil spanned the full range from highly sensitive to completely resistant. However, these findings are conflated with the fact that all of our Bacteroidetes strains, and all but one strain of Proteobacteria, were exclusively isolated from the Wheat samples, and that the members of these two phyla were

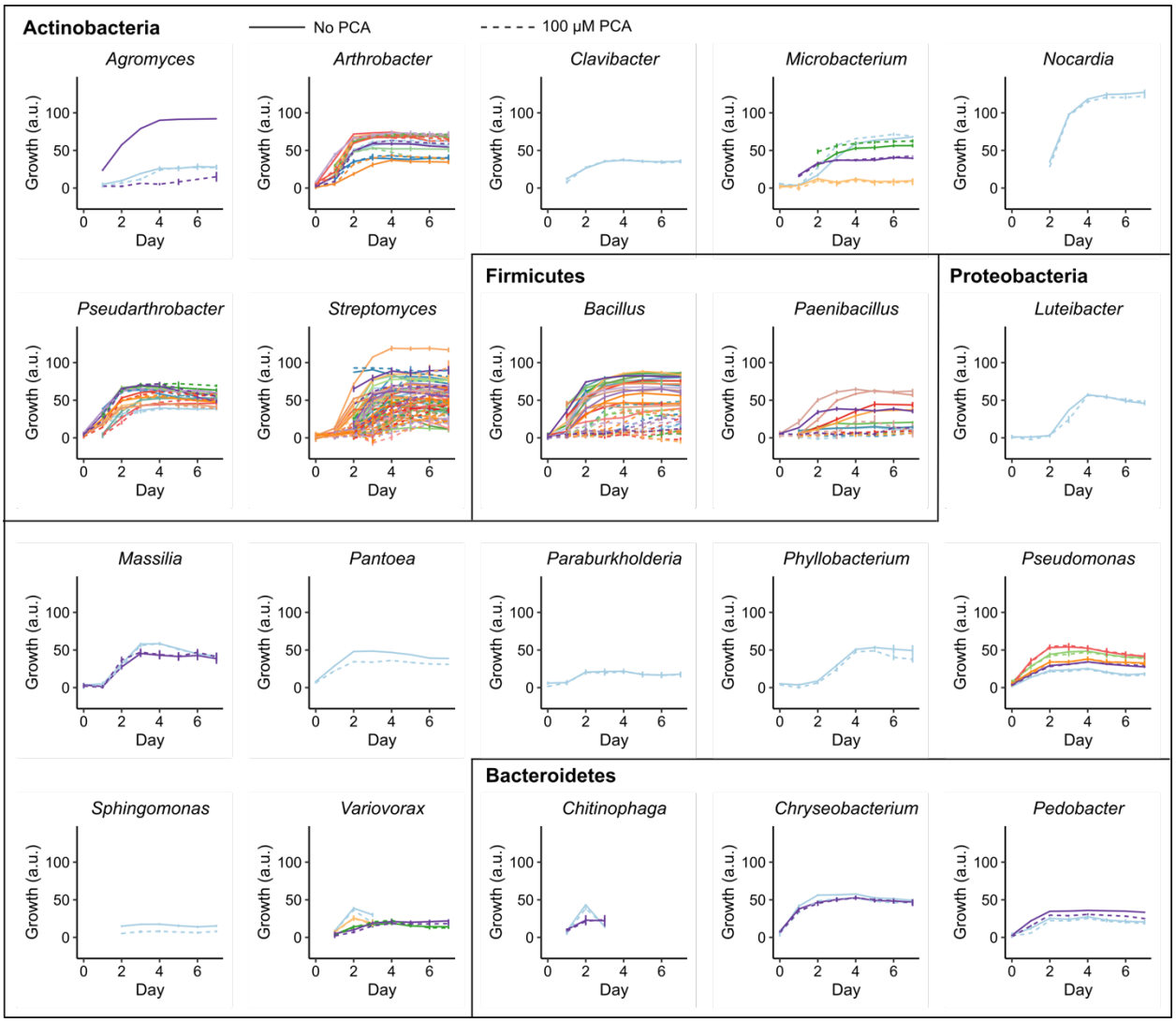

Figure 5: Growth of strains over time with and without PCA at pH 7.3.
Growth was quantified as described in the Methods. Solid lines represent the growth of spotted cultures on PCA-free agar, and dashed lines represent the growth of spotted cultures on agar containing 100 µM PCA. Each color within a panel corresponds to one strain. Data points are the mean of three technical replicates and vertical error bars are the standard deviation. Strains of *Chitinophaga* and two strains of *Variovorax* were only tracked for 3 days instead of 7 because these strains became highly mucoid and appeared to lyse starting on day 3.

generally relatively resistant to PCA. Further experiments will be necessary in order to distinguish whether the enrichment of PCA-resistant phenotypes in the rhizosphere samples is a consequence of PCA-mediated antibiosis or merely an indirect reflection of other factors that favor the growth of Proteobacteria and Bacteroidetes in the rhizosphere.

Finally, plotting the growth of each strain over time revealed more nuanced variations among the PCA resistance phenotypes at pH 5.1 and pH 7.3 (Figs. 4 and 5, respectively). For example, strains of *Chryseobacterium* and *Pedobacter* (both in the Bacteroidetes phylum), as well as one strain of *Microbacterium* (Actinobacteria), displayed increased lag in the presence of PCA at pH 5.1, but the growth on the PCA plates eventually caught up to the controls. In addition, one strain of *Arthrobacter* eventually started to grow on PCA at pH 5.1 but only after 5 days, with variable lag across the three technical replicates (Fig. S1A). At pH 7.3, the effect of PCA on *Bacillus* species was a combination of increased lag, slower growth rate, and lower final cell density, as compared to no growth at all on PCA at pH 5.1. A few strains of *Bacillus*, as well as *Paenibacillus*, appeared to be still unable to grow on PCA at pH 7.3 based on the values shown in Fig. 5. However, examination of the plate images by eye revealed that this reflected a limitation in the sensitivity of our imaging and quantification methods to low levels of growth, as well as underestimation of growth due to color changes, rather than a true lack of growth (Fig. S1B).

Other phenotypic interactions with PCA

In the course of examining the plates from both rounds of our screen, we noticed two other interesting phenomena that appeared related to the presence of PCA, besides simple growth inhibition of sensitive strains. First, as alluded to above, the production of pigment or antibiotics by certain *Streptomyces* strains appeared to be altered by PCA (Fig. 6A-B); for a few strains, this was likely directly tied to growth inhibition by PCA, but in other cases where growth was not clearly altered, generalized stress responses or specific signaling interactions might be involved. In some cases, PCA inhibited pigment production, while in others, it seemed to act as a stimulant. Thus, besides directly suppressing strains that are sensitive to PCA toxicity, PCA producers could potentially indirectly modulate other interspecies microbial interactions by altering the secondary metabolite profiles of other species; this is already evident from the examples where PCA rescued the growth of one strain by suppressing antibiotic production in a neighboring strain (Fig. 6B).

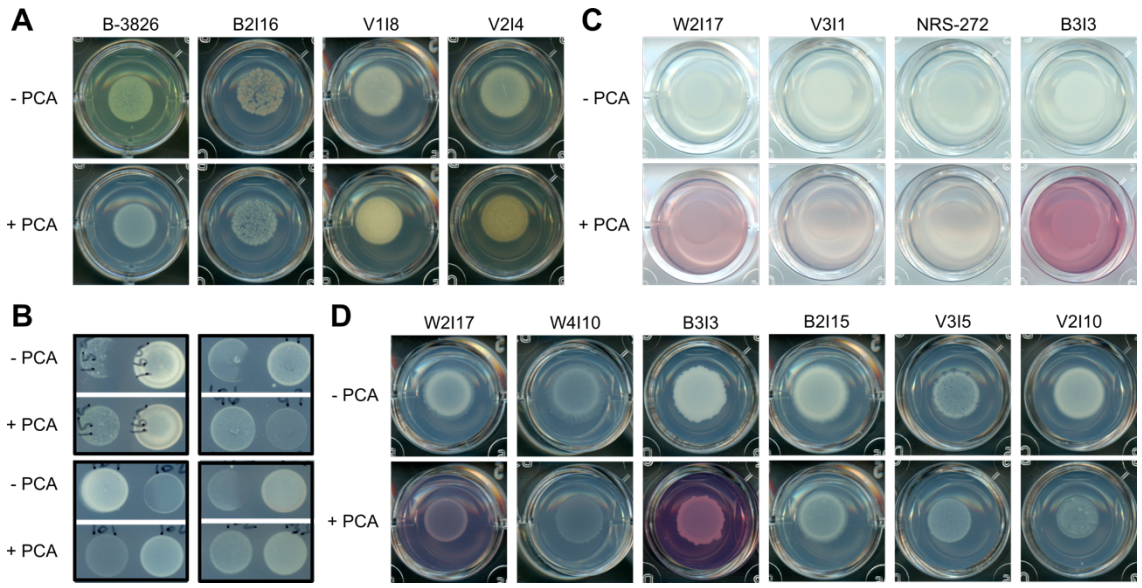

Figure 6: Interactions between PCA and *Streptomyces*, *Bacillus*, and *Paenibacillus* species.
A. *Streptomyces* strains for which PCA affected pigment production at pH 7.3. PCA suppressed pigment production in B-3826 (*S. peucetius*) and B2I16 (*S. aurantiacus/glomeraurantiacus*), but stimulated it in V1I8 (*S. phaeochromogenes*) and V2I4 (*S. ederensis*).
B. Examples of PCA-mediated suppression of antibiotic production at pH 7.3 in various *Streptomyces* strains. In each of the displayed pairs of strains, one strain was partially suppressed by the other in the absence of PCA, but recovered growth in the presence of PCA.
C. Strains of *Bacillus* and *Paenibacillus* that catalyzed the development of a pink color in PCA-containing plates at pH 7.3. W2I17 = *P. mobilis*, V3I1 = *B. atrophaeus*, NRS-272 = *B. pumilus*, B3I3 = *B. pumilus*.
D. Comparison of growth after 7 days at pH 7.3 with and without PCA, for selected strains of *Paenibacillus* and *Bacillus* that did or did not catalyze the pink color change. W2I17 = *P. mobilis*, W4I10 = *P. mobilis*, B3I3 = *B. pumilus*, B2I15 = *B. simplex*, V3I5 = *B. drentensis*, V2I10 = *B. idriensis*.

Second, certain strains of *Bacillus* and *Paenibacillus* catalyzed a color change in the presence of PCA, turning the surrounding medium pink over the course of several days (Fig. 6C). Typically, the color change first became visible after 4 days of incubation, when growth also became visible, and the color continued to intensify in subsequent days as the colonies grew. In addition, the color change only happened at pH 7.3, as none of these strains grew in the presence of PCA at pH 5.1. However, while the color change is striking, the evidence does not particularly suggest that it is related to a mechanism of detoxifying PCA: several strains of *Bacillus* that did not catalyze the color change were similarly able to grow to a moderate density on PCA at pH 7.3 within 7 days (Fig. 6D).

We have so far been unable to confirm whether PCA itself is enzymatically transformed into another compound by these strains, whether the strains secrete another compound that directly reacts with PCA or indirectly causes PCA to react with a component of the medium, or whether PCA stimulates the production of an unrelated molecule. We attempted to perform reverse phase liquid

chromatography-mass spectrometry (LC-MS) on pink supernatant from one of these strains to identify the colored compound, but this was unsuccessful due to clogging of the column, even after centrifuging and filtering the sample to remove cells. We were also unable to extract the pink compound using ethyl acetate or dichloromethane, solvents that work well for PCA and pyocyanin, respectively, although whether PCA is depleted by these strains could be inferred by attempting instead to extract PCA from the pink supernatant. The insolubility of the pink compound in ethyl acetate and dichloromethane suggests that it is hydrophilic, which is consistent with the properties of at least one group of red phenazines derived from PCA: aeruginosins A and B (Turner and Messenger, 1986). However, it seems unlikely that the compound is specifically aeruginosin A or B, as these compounds have been described as reddish-brown rather than bright pink (Ogunnariwo and Hamilton-Miller, 1975). In the future, a simple test of whether the compound is potentially an aeruginosin would be to transfer the cultures to airtight containers after the color has turned pink; if it is an aeruginosin, it should be reversibly reduced to a colorless form as the bacteria consume the oxygen in the culture (Turner and Messenger, 1986). Even if it is not an aeruginosin, its apparently hydrophilic nature suggests that techniques that have been used to purify aeruginosin A may also be useful for extraction of this compound.

Notably, the ability to catalyze the color change varied even across strains that appeared relatively closely related to each other. For example, isolates W2I17 and W4I10 both have high 16S sequence similarity to *Paenibacillus mobilis* strain S8 (99.63% and 99.64%, respectively), but only W2I17 catalyzed the color change (Fig. 6D). Similarly, isolate B3I3 matched to the 16S sequence of *Bacillus pumilus* NRS-272 with 100% identity, but B3I3 catalyzed the color change to a far greater degree than NRS-272 under identical conditions (Fig. 6C). The strain-specificity of the phenotype suggests that comparative genomics and/or a genetic screen might prove fruitful in identifying the underlying mechanism of the color change.

Discussion

In this study, we have characterized profiles of resistance to an agriculturally-relevant phenazine across taxonomically diverse bacteria isolated from a wheat field where phenazine producers are indigenous. One of our more notable findings is that the previously reported pH dependency of PCA toxicity varies across bacterial taxonomic groups. For most Actinobacteria and

Firmicutes, sensitivity to PCA was clearly higher at pH 5.1 than at pH 7.3, indicating greater toxicity at the lower pH as expected according to the pKa of PCA. On the other hand, nearly all tested Proteobacteria were completely resistant to 100 μM PCA regardless of pH, at least down to pH 5.1. Consequently, at pH 5.1, PCA resistance phenotypes largely correlated with phylum—and more broadly, a Gram-positive versus Gram-negative divide, which has previously been reported for the toxicity of another phenazine, pyocyanin (Baron and Rowe, 1981). The Gram-positive versus Gram-negative divide at pH 5.1 is perhaps not surprising, as at this pH, a significant proportion (~14%) of PCA in solution is protonated and therefore would not be repelled by the negatively charged cell wall. Under this condition, the outer membrane of Gram-negative species presumably presents an additional barrier to the entry of PCA, helping to limit the intracellular accumulation of the toxin in the same manner as for numerous other antibiotics (Nikaido, 1989). Less expected, however, was the considerably greater within-phylum and even within-species variation in PCA resistance phenotypes at pH 7.3, at least among the Actinobacteria. In particular, it was surprising that several *Streptomyces* strains exhibited at least some PCA-dependent growth inhibition even at pH 7.3, considering that many *Streptomyces* species are capable of producing their own toxic phenazines (Turner and Messenger, 1986; Dar *et al.*, 2020). Given that the major limit on PCA toxicity at circumneutral pH is thought to be its ability to enter cells, the phenotypic variability at pH 7.3 may indicate the presence of transporters or channels capable of phenazine uptake in some PCA-sensitive Actinobacteria. Alternatively, it is possible that PCA-sensitive strains acidified the growth medium, which was not buffered.

Importantly, despite the general Gram-positive versus Gram-negative divide in sensitivity to PCA at pH 5.1, possessing an outer membrane is evidently not a leakproof shield against PCA toxicity. Proteobacteria as a group were more resistant to PCA at pH 5.1 compared to strains of Bacteroidetes, most of which exhibited increased lag in the presence of PCA, even though both phyla are comprised of Gram-negative bacteria. Intriguingly, one major difference between these clades is that Proteobacteria generally utilize ubiquinone as an electron carrier during aerobic growth (Collins and Jones, 1981), while the Bacteroidetes genera screened in this study (*Chitinophaga*, *Chryseobacterium*, and *Pedobacter*) utilize menaquinone (Lin *et al.*, 2015; Singh *et al.*, 2017; Kong *et al.*, 2019). Menaquinones have a lower reduction potential compared to ubiquinones (White *et al.*, 2012). Although the standard reduction potential of menaquinone is still higher than that of PCA

(-74 mV compared to -177 mV) (Price-Whelan *et al.*, 2006; White *et al.*, 2012), indicating that PCA likely is not reduced by menaquinol, this difference with ubiquinone nevertheless raises the possibility that PCA may interact differently, and perhaps more readily, with the aerobic respiratory electron transport chain of menaquinone-utilizing Bacteroidetes strains compared to Proteobacteria, thereby generating more ROS and/or interfering with the generation of ATP. Interestingly, another study has shown that the reduced form of different phenazine with a low reduction potential, neutral red (3-amino-7-dimethylamino-2-methylphenazine), can directly transfer electrons to menaquinone, bypassing the proton-pumping NADH dehydrogenase complex that normally transfers electrons from NADH to menaquinone and thereby "robbing" the electron transport chain of energy that normally would be used to power ATP synthesis. We hypothesize that a similar phenomenon may occur with PCA in strains that rely on menaquinone. In future studies, this hypothesis could be tested by 1) performing *in vitro* experiments with purified menaquinone, ubiquinone, and reduced PCA to directly test whether quinones oxidize the latter and if so, whether the kinetics differ between menaquinone and ubiquinone, 2) measuring ROS production and steady-state ATP pools in selected strains of Bacteroidetes and Proteobacteria both in the presence and absence of PCA, and 3) forcing species of Proteobacteria (such as *Escherichia coli*) that utilize both ubiquinone and menaquinone in different branches of their electron transport chains to rely only on latter (for example, by deleting the genes for ubiquinone biosynthesis), followed by reassessing their sensitivity to PCA.

Beyond the specific strains screened in this study, our larger goal for the risk assessment of phenazine-producing biocontrol strains, and the understanding of phenazine biology in general, is to develop a platform for the prediction of phenazine resistance phenotypes from genomic or phylogenetic information. The results of this study already indicate that, depending on the environmental pH, phylogenetic information may be of limited utility for prediction of PCA resistance, given the variation in phenotypes for Actinobacteria at circumneutral pH. However, this variability may also hold the key to identifying genome-based predictive markers of phenazine resistance. We envision sequencing whole genomes for our isolates and using comparative genomics to search for such markers. The latter could potentially be accomplished through a machine-learning approach such as sparse logistic regression, based on the presence/absence or counts of certain orthologs or functional gene groups, such as multidrug efflux pumps, components of the respiratory electron transport chain, redox-sensing transcription factors (e.g. SoxR), oxidative stress responses,

and enzymes that modify structural or chemical properties of the cell wall or membrane. Predicted genomic markers of phenazine resistance, if any, could be validated through classical genetic approaches (i.e. knockouts, overexpression, and heterologous expression) in both intrinsically resistant and sensitive strains. In parallel to the comparative genomics approach, phenotypic traits that are expected to correlate with PCA resistance (e.g. efflux activity, ROS generation, and PCA uptake and reduction rates) could also be screened through fluorescence-based assays to identify which cellular properties are most relevant for resistance (Price-Whelan *et al.*, 2007; Sullivan *et al.*, 2011; Blair and Piddock, 2016; McBee *et al.*, 2017).

In addition to identifying genetic markers and physiological determinants of phenazine resistance, it will be important to relate PCA resistance phenotypes to how PCA shapes rhizosphere bacterial communities. On the millimeter-to-meter scale, this question could be addressed in part by metagenomic sequencing of bulk and rhizosphere soil samples from wheat fields to determine whether there are trends in the relative abundances of putative phenazine producers and putative PCA-sensitive or -resistant bacteria in different samples, following the example of Dar *et al.* (2020); such efforts are currently underway for the original soil samples used in this study. However, this approach can only reveal correlation, not causation. To probe the latter, it may be useful to start with reductionist model systems, such as *in vitro* co-cultures of selected strains from among our isolates with differing PCA resistance phenotypes. Culture setups that promote biofilm growth may be particularly relevant to modeling microbial interactions in the rhizosphere (LeTourneau *et al.*, 2018), and could reveal whether PCA producers affect the spatial organization of the strains in addition to, or perhaps instead of, the overall taxonomic composition of the community. Wheat seedlings could also be grown *in vitro* with the selected strains to see which ones successfully colonize the roots in the presence or absence of a PCA producer, and how the strains organize themselves along the root surface; one might hypothesize that PCA producers would most likely be surrounded by PCA-resistant strains, with PCA-sensitive bacteria potentially colonizing other regions of the root. Notably, the impact of PCA toxicity may be affected by environmental conditions; for example, PCA is likely to be less toxic in waterlogged soils in which oxygen has been depleted.

In summary, the findings presented in this study have established a basis for inferring whether intrinsic resistance is a factor that affects how phenazine production shapes bacterial communities in the rhizosphere, as it will now be possible to test data-driven predictions regarding

which strains, species, or even phyla are most likely to be affected by phenazine-mediated antibiosis. This work has thus laid the groundwork for rectifying a major gap in studies of how introduction of a phenazine-producing biocontrol strain affects rhizosphere bacterial communities. Previous studies have lacked information about the baseline prevalence of resistance in the native communities (Gagliardi *et al.*, 2001; Bankhead *et al.*, 2004; Kozdrój *et al.*, 2004; Roquigny *et al.*, 2018), and in the absence of such information, it is impossible to determine whether a negative result (lack of change in the rhizosphere community) reflects a high prevalence of resistance to PCA that is particular to the studied community, versus a general lack of toxicity of PCA to most bacteria or fundamental abiotic constraints on the antibacterial activity of PCA in the rhizosphere (e.g. limited diffusion, adsorption to soil particles, etc.). Distinguishing between these scenarios is key to assessing the risk of unwanted side effects in rhizosphere communities upon the application of phenazine-producing biocontrol strains. In addition, recent studies have demonstrated that phenazines produced by the opportunistic pathogen *Pseudomonas aeruginosa* can promote bacterial tolerance and resistance to clinical antibiotics (Schiessl *et al.*, 2019; Zhu *et al.*, 2019; Meirelles and Perry *et al.*, 2021; VanDrisse *et al.*, 2021), and that these effects can extend to other opportunistic pathogens that are resistant to phenazines (Meirelles and Perry *et al.*, 2021). Thus, understanding the prevalence and genetic determinants of resistance to phenazines may have implications not only for agriculture but also for human medicine and beyond, as we continue to uncover new ecological roles for these multifaceted bacterial metabolites.

Methods

Isolation of bacteria from wheat rhizosphere and bulk soil samples

Three types of samples were collected from a non-irrigated wheat field at Washington State University's Lind Dryland Research Station on August 9, 2019: wheat plants and surrounding soil, bulk soil from in between the planted rows, and bulk soil from a "virgin" hillside site that has never been farmed. The wheat had been harvested a few weeks prior to sample collection. All samples were immediately stored on ice in clean plastic bags, and subsequently at 4 °C for four days until processing. Rhizosphere soil samples were obtained by shaking the wheat roots until only 1-2 mm of tightly-adhering soil remained, followed by excising the roots at the crown with a sterile razor blade. The roots of 2-3 plants per replicate were placed in 50 mL conical tubes with 30 mL of sterile

deionized water, vortexed at top speed for 1 min, and treated in an ultrasonic water bath for 1 min to dislodge bacteria from the roots. Bulk soil samples (1 g per sample) were processed in the same manner. Large soil particles were allowed to settle to the bottom of the tubes on the bench top, and 100 µL each of a 10-fold dilution series of the supernatants was spread onto 0.1x TSA plates containing 50 µg/mL nystatin to inhibit fungal growth. The plates were incubated upside down at room temperature in the dark and monitored for the appearance of new colonies over the course of a week. Colonies that appeared morphologically distinct in each sample were picked and restreaked on 0.1x TSA until visually pure cultures were obtained. Multiple representatives were also picked for the most common colony types in an attempt to account for strain variations that might not be apparent to the eye. Once the streaks yielded uniform single colonies, the isolates were inoculated into 1.5 mL of 0.1x tryptic soy broth (TSB) in 5 mL polycarbonate culture tubes and incubated at 30 °C with shaking at 250 rpm. After 1-3 days of incubation, depending on when the cultures became turbid, 0.5 mL of each culture was mixed with 0.5 mL of 50% glycerol and stored at -80 °C. Some cultures never became turbid under these conditions, but nevertheless yielded viable frozen stocks.

Species identification by 16S rRNA gene sequencing

Single colonies or patches of morphologically pure streaks were picked and resuspended in 20 µL sterile nuclease-free water. Colony PCR was performed using GoTaq Green Master Mix (Promega, Madison, WI) in 50 µL reactions (1 µL of cell suspension) according to the manufacturer's instructions. For putative streptomycetes (isolates that formed hard colonies rooted in agar, often with aerial hyphae), the thermocycling protocol was modified to include a 10 min initial heating step at 95 °C (compared to 2 minutes for other samples). The primers used were 27F (AGAGTTTGATCMTGGCTCAG) and 1492R (TACGGYTACCTTGTTACGACTT) (Lane, 1991). The PCR products were run on a 1% agarose gel to verify the presence of a single band at the expected size (~1500 bp), followed by purification with the Monarch PCR and DNA Cleanup Kit (New England Biolabs). The purified products were submitted for Sanger sequencing at Laragen, Inc., using the same 27F and 1492R primers. The resulting forward and reverse sequences were aligned using MAFFT (Katoh *et al.*, 2019) and subjected to BLAST against the NCBI 16S ribosomal RNA sequences database. For a few strains, either the forward or reverse sequence was unusually short (possibly due to high GC content in the case of streptomycetes) or appeared to contain multiple products. We presumed that the latter was generally due to multiple primer binding sites or other

sequencing artifacts rather than mixed cultures as the corresponding sequence from the other direction was always clean. In these cases, only the clean sequence was submitted to BLAST.

PCA resistance screen

The optimized version of the PCA resistance screen was performed with four conditions: 0.1x TSA (15 g/L agar plus 3 g/L tryptic soy broth no. 2 from MilliporeSigma) with or without 100 µM PCA at pH 7.3 or pH 5.1 (adjusted with HCl). PCA was purchased from Princeton BioMolecular Research and dissolved in filter-sterilized 14 mM NaOH to make 10 mM stock solutions. The PCA stock solution or solvent control (14 mM NaOH) was added at 1% v/v to autoclaved molten 0.1x TSA; we verified that this addition did not noticeably alter the pH of the medium. Subsequently, 1 mL of the medium was pipetted into each well in 24-well polystyrene Cellstar Cell Culture plates (Greiner Bio-One). The plates were allowed to set and dry with the lids off in a biological safety cabinet for 20-30 min, followed by storage upside with the lids on at room temperature in the dark for two days prior to use.

Cell suspensions for inoculation in the screen were prepared in one of two ways. First, individual strains were inoculated into 5 mL TSB cultures in glass culture tubes and incubated at 25 °C with shaking at 250 rpm. Strains that grew overnight were then diluted to an OD_{600} of 0.05. Some strains did not grow well in this condition, especially strains of *Streptomyces* and *Paenibacillus*. For these, we directly scraped cells from streaks grown on 0.1x TSA plates and resuspended the cells in 200 µL TSB with pipetting and brief vortexing at top speed. Subsequently, 10 µL of each cell suspension was pipetted onto the agar in a single well in the 24-well plates. Three adjacent wells per condition were inoculated with each cell suspension, representing technical replicates. After the spots dried, the plates were incubated at room temperature upside in the dark for up to 7 days. Every 24 hrs, the plates were imaged in color at 600 dpi with an Epson Perfection V550 Photo flatbed scanner (Epson).

Image analysis and quantification of growth

Images from the scanner were analyzed using Fiji (Schindelin *et al.*, 2012). Circular regions of interest (ROIs) were drawn around each culture spot and the mean gray value was measured for each ROI. We also measured the mean gray values of equivalent ROIs in the wells of blank,

uninoculated plates for each condition. The latter values were averaged across each 24-well blank plate to give the "background" gray value, which was then subtracted from the mean gray values of the culture spots. The resulting numbers were reported as the metric for growth. Importantly, while this method generally worked well for comparisons across conditions within each strain, there are a few caveats. First, this metric underestimated growth for strains that produced a dark pigment. Second, growth was difficult to quantify for a few strains that grew as nearly transparent colonies. Finally, this metric is not very sensitive to low levels of growth. Nevertheless, for the vast majority of strains, this approach captured visible differences in growth across the four conditions in the screen.

Acknowledgements

We thank Linda Thomashow of the USDA's Agricultural Research Service for supplying the soil samples from the wheat field at Lind Dryland Research Station, and the members of the Newman lab for helpful feedback throughout the process of designing and analyzing the results of the PCA resistance screen. We also thank Zevin Condiotte for assistance with the initial rounds of testing the design of the PCA resistance screen. This material is based upon work supported by the National Science Foundation Graduate Research Fellowship under Grant No. DGE-1745301. This work was also supported by grants to D.K.N. from the ARO (W911NF-17-1-0024) and NIH (1R01AI127850-01A1).

References

Aminov, R.I. (2009) The role of antibiotics and antibiotic resistance in nature. *Environ Microbiol* **11**: 2970–2988.

Aminov, R.I. (2010) A brief history of the antibiotic era: lessons learned and challenges for the future. *Front Microbiol* **1**: 134.

Bankhead, S.B., Landa, B.B., Lutton, E., Weller, D.M., and Gardener, B.B.M. (2004) Minimal changes in rhizobacterial population structure following root colonization by wild type and transgenic biocontrol strains. *FEMS Microbiol Ecol* **49**: 307–318.

Baron, S.S., and Rowe, J.J. (1981) Antibiotic action of pyocyanin. *Antimicrob Agents Chemother* **20**: 814–820.

Bérdy, J. (2012) Thoughts and facts about antibiotics: where we are now and where we are heading. *J Antibiot* **65**: 385–395.

Bergsma-Vlami, M., Prins, M.E., and Raaijmakers, J.M. (2005) Influence of plant species on population dynamics, genotypic diversity and antibiotic production in the rhizosphere by indigenous *Pseudomonas* spp. *FEMS Microbiol Ecol* **52**: 59–69.

Blair, J.M.A., and Piddock, L.J.V. (2016) How to measure export via bacterial multidrug resistance efflux pumps. *mBio* **7**: e00840-16.

Brisbane, P.G., Janik, L.J., Tate, M.E., and Warren, R.F. (1987) Revised structure for the phenazine antibiotic from *Pseudomonas fluorescens* 2-79 (NRRL B-15132). *Antimicrob Agents Chemother* **31**: 1967–1971.

Cezairliyan, B., Vinayavekhin, N., Grenfell-Lee, D., Yuen, G.J., Saghatelian, A., and Ausubel, F.M. (2013) Identification of *Pseudomonas aeruginosa* phenazines that kill *Caenorhabditis elegans*. *PLoS Pathog* **9**: e1003101.

Collins, M.D., and Jones, D. (1981) Distribution of isoprenoid quinone structural types in bacteria and their taxonomic implication. *Microbiol Rev* **45**: 316–354.

Costa, K.C., Bergkessel, M., Saunders, S., Korlach, J., and Newman, D.K. (2015) Enzymatic degradation of phenazines can generate energy and protect sensitive organisms from toxicity. *mBio* **6**: e01520-15.

Dar, D., Thomashow, L.S., Weller, D.M., and Newman, D.K. (2020) Global landscape of phenazine biosynthesis and biodegradation reveals species-specific colonization patterns in agricultural soils and crop microbiomes. *eLife* **9**: e59726.

Davies, J. (2006) Are antibiotics naturally antibiotics? *J Ind Microbiol Biotechnol* **33**: 496–499.

Davies, J., and Davies, D. (2010) Origins and evolution of antibiotic resistance. *Microbiol Mol Biol Rev* **74**: 417–433.

Davies, J., and Ryan, K.S. (2012) Introducing the parvome: bioactive compounds in the microbial world. *ACS Chem Biol* **7**: 252–259.

Davies, J., Spiegelman, G.B., and Yim, G. (2006) The world of subinhibitory antibiotic concentrations. *Curr Opin Microbiol* **9**: 445–453.

Demain, A.L., and Fang, A. (2000) The natural functions of secondary metabolites. *Adv Biochem Eng Biotechnol* **69**: 1–39.

Dietrich, L.E., Price-Whelan, A., Petersen, A., Whiteley, M., and Newman, D.K. (2006) The phenazine pyocyanin is a terminal signalling factor in the quorum sensing network of *Pseudomonas aeruginosa*. *Mol Microbiol* **61**: 1308–1321.

Gagliardi, J.V., Buyer, J.S., Angle, J.S., and Russek-Cohen, E. (2001) Structural and functional analysis of whole-soil microbial communities for risk and efficacy testing following microbial inoculation of wheat roots in diverse soils. *Soil Biol Biochem* **33**: 25–40.

Glasser, N.R., Kern, S.E., and Newman, D.K. (2014) Phenazine redox cycling enhances anaerobic survival in *Pseudomonas aeruginosa* by facilitating generation of ATP and a proton-motive force. *Mol Microbiol* **92**: 399–412.

Glasser, N.R., Saunders, S.H., and Newman, D.K. (2017) The colorful world of extracellular electron shuttles. *Annu Rev Microbiol* **71**: 731–751.

Granato, E.T., Meiller-Legrand, T.A., and Foster, K.R. (2019) The evolution and ecology of bacterial warfare. *Curr Biol* **29**: R521–R537.

Haas, D., and Défago, G. (2005) Biological control of soil-borne pathogens by fluorescent pseudomonads. *Nat Rev Microbiol* **3**: 307–319.

Haas, D., and Keel, C. (2003) Regulation of antibiotic production in root-colonizing *Peudomonas* spp. and relevance for biological control of plant disease. *Annu Rev Phytopathol* **41**: 117–153.

Handelsman, J., and Stabb, E.V. (1996) Biocontrol of soilborne plant pathogens. *Plant Cell* **8**: 1855–1869.

Hassan, H.M., and Fridovich, I. (1980) Mechanism of the antibiotic action pyocyanine. *J Bacteriol*

141: 156–163.
Hutchings, M.I., Truman, A.W., and Wilkinson, B. (2019) Antibiotics: past, present and future. *Curr Opin Microbiol* **51**: 72–80.
Katoh, K., Rozewicki, J., and Yamada, K.D. (2019) MAFFT online service: multiple sequence alignment, interactive sequence choice and visualization. *Brief Bioinform* **20**: 1160–1166.
Khare, A., and Tavazoie, S. (2015) Multifactorial competition and resistance in a two-species bacterial system. *PLoS Genet* **11**: e1005715.
Kong, X.-K., Chen, D., Huang, J.-W., Cheng, X.-K., and Jiang, J.-D. (2019) *Chitinophaga deserti* sp. nov., isolated from desert soil. *Int J Syst Evol Microbiol* **69**: 1783–1788.
Kozdrój, J., Trevors, J.T., and Elsas, J.D. van (2004) Influence of introduced potential biocontrol agents on maize seedling growth and bacterial community structure in the rhizosphere. *Soil Biol Biochem* **36**: 1775–1784.
Lane, D.J. (1991) 16S/23S rRNA sequencing. In *Nucleic acid techniques in bacterial systematics*. Stackebrandt, E., and Goodfellow, M. (eds). John Wiley & Sons, Inc., New York, New York. pp. 115–176.
Lau, G.W., Ran, H., Kong, F., Hassett, D.J., and Mavrodi, D. (2004) *Pseudomonas aeruginosa* pyocyanin is critical for lung infection in mice. *Infect Immun* **72**: 4275–4278.
LeTourneau, M.K., Marshall, M.J., Cliff, J.B., Bonsall, R.F., Dohnalkova, A.C., Mavrodi, D.V., *et al.* (2018) Phenazine-1-carboxylic acid and soil moisture influence biofilm development and turnover of rhizobacterial biomass on wheat root surfaces. *Environ Microbiol* **20**: 2178–2194.
Lin, S.-Y., Hameed, A., Wen, C.-Z., Liu, Y.-C., Shen, F.-T., Hsu, Y.-H., *et al.* (2015) *Chryseobacterium echinoideorum* sp. nov., isolated from sea urchins (*Tripneustes gratilla*). *Int J Syst Evol Microbiol* **65**: 3985–3990.
Linares, J.F., Gustafsson, I., Baquero, F., and Martinez, J.L. (2006) Antibiotics as intermicrobial signaling agents instead of weapons. *Proc Natl Acad Sci USA* **103**: 19484–19489.
Liu, G.Y., and Nizet, V. (2009) Color me bad: microbial pigments as virulence factors. *Trends Microbiol* **17**: 406–413.
Manyi-Loh, C., Mamphweli, S., Meyer, E., and Okoh, A. (2018) Antibiotic use in agriculture and its consequential resistance in environmental sources: potential public health implications. *Molecules* **23**: 795.
Mavrodi, D.V., Mavrodi, O.V., Parejko, J.A., Bonsall, R.F., Kwak, Y.-S., Paulitz, T.C., *et al.* (2012) Accumulation of the antibiotic phenazine-1-carboxylic acid in the rhizosphere of dryland cereals. *Appl Environ Microbiol* **78**: 804–812.
Mazurier, S., Corberand, T., Lemanceau, P., and Raaijmakers, J.M. (2009) Phenazine antibiotics produced by fluorescent pseudomonads contribute to natural soil suppressiveness to Fusarium wilt. *ISME J* **3**: 977–991.
Mazzola, M., Cook, R.J., Thomashow, L.S., Weller, D.M., and Pierson, L.S. (1992) Contribution of phenazine antibiotic biosynthesis to the ecological competence of fluorescent pseudomonads in soil habitats. *Appl Environ Microbiol* **58**: 2616–2624.
Mazzola, M., Fujimoto, D.K., Thomashow, L.S., and Cook, R.J. (1995) Variation in sensitivity of *Gaeumannomyces graminis* to antibiotics produced by fluorescent *Pseudomonas* spp. and effect on biological control of take-all of wheat. *Appl Environ Microbiol* **61**: 2554–2559.
McBee, M.E., Chionh, Y.H., Sharaf, M.L., Ho, P., Cai, M.W.L., and Dedon, P.C. (2017) Production of superoxide in bacteria is stress- and cell state-dependent: a gating-optimized flow cytometry method that minimizes ROS measurement artifacts with fluorescent dyes. *Front*

Microbiol **8**: 459.
McRose, D.L., and Newman, D.K. (2021) Redox-active antibiotics enhance phosphorus bioavailability. *Science* **371**: 1033–1037.
Meirelles, L.A., and Newman, D.K. (2018) Both toxic and beneficial effects of pyocyanin contribute to the lifecycle of *Pseudomonas aeruginosa*. *Mol Microbiol* **110**: 995–1010.
Meirelles, L.A., Perry, E.K., Bergkessel, M., and Newman, D.K. (2021) Bacterial defenses against a natural antibiotic promote collateral resilience to clinical antibiotics. *PLoS Biol* **19**: e3001093.
Nikaido, H. (1989) Role of the Outer Membrane of Gram-Negative Bacteria in Antimicrobial Resistance. In *Microbial resistance to drugs*. Bryan, L.E. (ed.). Springer Berlin Heidelberg, Berlin, Heidelberg. pp. 1–34.
Noto, M.J., Burns, W.J., Beavers, W.N., and Skaar, E.P. (2017) Mechanisms of pyocyanin toxicity and genetic determinants of resistance in *Staphylococcus aureus*. *J Bacteriol* **199**: e00221-17.
Ogunnariwo, J., and Hamilton-Miller, J.M. (1975) Brown- and red-pigmented *Pseudomonas aeruginosa*: differentiation between melanin and pyorubrin. *J Med Microbiol* **8**: 199–203.
Perry, E.K., and Newman, D.K. (2019) The transcription factors ActR and SoxR differentially affect the phenazine tolerance of *Agrobacterium tumefaciens*. *Mol Microbiol* **112**: 199–218.
Price-Whelan, A., Dietrich, L.E.P., and Newman, D.K. (2006) Rethinking "secondary" metabolism: physiological roles for phenazine antibiotics. *Nat Chem Biol* **2**: 71–78.
Price-Whelan, A., Dietrich, L.E.P., and Newman, D.K. (2007) Pyocyanin alters redox homeostasis and carbon flux through central metabolic pathways in *Pseudomonas aeruginosa* PA14. *J Bacteriol* **189**: 6372–6381.
Roquigny, R., Novinscak, A., Léger, G., Marcoux, N., Joly, D.L., and Filion, M. (2018) Deciphering the rhizosphere and geocaulosphere microbiomes of potato following inoculation with the biocontrol agent *Pseudomonas fluorescens* strain LBUM223. *Phytobiomes* **2**: 92–99.
Schiessl, K.T., Hu, F., Jo, J., Nazia, S.Z., Wang, B., Price-Whelan, A., *et al.* (2019) Phenazine production promotes antibiotic tolerance and metabolic heterogeneity in *Pseudomonas aeruginosa* biofilms. *Nat Commun* **10**: 762.
Schindelin, J., Arganda-Carreras, I., Frise, E., Kaynig, V., Longair, M., Pietzsch, T., *et al.* (2012) Fiji: an open-source platform for biological-image analysis. *Nat Methods* **9**: 676–682.
Sengupta, S., Chattopadhyay, M.K., and Grossart, H.-P. (2013) The multifaceted roles of antibiotics and antibiotic resistance in nature. *Front Microbiol* **4**: 47.
Séveno, N.A., Morgan, J.A.W., and Wellington, E.M.H. (2001) Growth of *Pseudomonas aureofaciens* PGS12 and the dynamics of HHL and phenazine production in liquid culture, on nutrient agar, and on plant roots. *Microb Ecol* **41**: 314–324.
Singh, P., Singh, H., Kim, Y.-J., and Yang, D.-C. (2017) *Pedobacter panacis* sp. nov., isolated from Panax ginseng soil. *Antonie Van Leeuwenhoek* **110**: 235–244.
Smiley, R.W., and Cook, R.J. (1973) Relationship between take-all of wheat and rhizosphere pH in soils fertilized with ammonium vs. nitrate-nitrogen. *Phytopathology* **63**: 882–890.
Sullivan, N.L., Tzeranis, D.S., Wang, Y., So, P.T.C., and Newman, D. (2011) Quantifying the dynamics of bacterial secondary metabolites by spectral multiphoton microscopy. *ACS Chem Biol* **6**: 893–899.
Tagele, S.B., Lee, H.G., Kim, S.W., and Lee, Y.S. (2019) Phenazine and 1-undecene producing *Pseudomonas chlororaphis* subsp. *aurantiaca* strain KNU17Pc1 for growth promotion and disease suppression in Korean maize cultivars. *J Microbiol Biotechnol* **29**: 66–78.

Thomashow, L.S., and Weller, D.M. (1988) Role of a phenazine antibiotic from *Pseudomonas fluorescens* in biological control of *Gaeumannomyces graminis* var. *tritici*. *J Bacteriol* **170**: 3499–3508.

Thomashow, L.S., Weller, D.M., Bonsall, R.F., and Pierson, L.S. (1990) Production of the antibiotic phenazine-1-carboxylic acid by fluorescent *Pseudomonas* species in the rhizosphere of wheat. *Appl Environ Microbiol* **56**: 908–912.

Turner, J.M., and Messenger, A.J. (1986) Occurrence, biochemistry and physiology of phenazine pigment production. *Adv Microb Physiol* **27**: 211–275.

Tyc, O., Song, C., Dickschat, J.S., Vos, M., and Garbeva, P. (2017) The ecological role of volatile and soluble secondary metabolites produced by soil bacteria. *Trends Microbiol* **25**: 280–292.

VanDrisse, C.M., Lipsh-Sokolik, R., Khersonsky, O., Fleishman, S.J., and Newman, D.K. (2021) Computationally designed pyocyanin demethylase acts synergistically with tobramycin to kill recalcitrant *Pseudomonas aeruginosa* biofilms. *Proc Natl Acad Sci USA* **118**: e20220128.

Voggu, L., Schlag, S., Biswas, R., Rosenstein, R., Rausch, C., and Götz, F. (2006) Microevolution of cytochrome *bd* oxidase in staphylococci and its implication in resistance to respiratory toxins released by *Pseudomonas*. *J Bacteriol* **188**: 8079–8086.

Wang, Y., and Newman, D.K. (2008) Redox reactions of phenazine antibiotics with ferric (hydr)oxides and molecular oxygen. *Environ Sci Technol* **42**: 2380–2386.

White, D., Drummond, J., and Fuqua, C. (2012) Electron transport. In *The Physiology and Biochemistry of Prokaryotes*. Oxford University Press, New York, New York. pp. 146–174.

Wolloscheck, D., Krishnamoorthy, G., Nguyen, J., and Zgurskaya, H.I. (2018) Kinetic control of quorum sensing in *Pseudomonas aeruginosa* by multidrug efflux pumps. *ACS Infect Dis* **4**: 185–195.

Yu, J.M., Wang, D., Pierson, L.S., and Pierson, E.A. (2018) Effect of producing different phenazines on bacterial fitness and biological control in *Pseudomonas chlororaphis* 30-84. *Plant Pathol J* **34**: 44–58.

Zhu, K., Chen, S., Sysoeva, T.A., and You, L. (2019) Universal antibiotic tolerance arising from antibiotic-triggered accumulation of pyocyanin in *Pseudomonas aeruginosa. PLoS Biol* **17**: e3000573.

Supplementary Table and Figure

Table S1: Strains used in this study. This table is available in CaltechDATA and is linked to the record of this thesis in CaltechTHESIS.

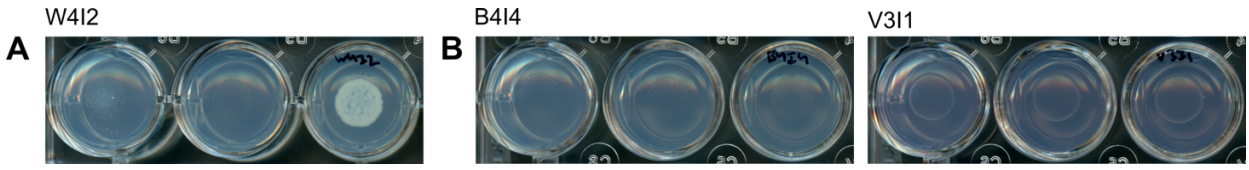

Figure S1: Limitations of image analysis for the quantification of bacterial growth on agar plates
A. Growth of isolate W4I2 (*Arthrobacter woluwensis*) on 100 µM PCA at pH 5.1 after 7 days, showing variable lag across the 3 technical replicates.
B. Growth of isolates B4I4 (*Bacillus drentensis*) and V3I1 (*Bacillus atrophaeus*) on 100 µM PCA at pH 7.3 after 7 days. These are examples of strains for which growth was visible, but image analysis and quantification yielded growth values that were within the range seen for strains with no visible growth (in the case of B4I4, due to the limited sensitivity of our image analysis method) or were below zero (in the case of V3I1, due to the combination of low growth and a color change in the medium).

Chapter 6

CONCLUSIONS

Summary

In this thesis, I have presented new insights into both the molecular mechanisms and broader consequences of intrinsic resistance to phenazines, a class of bacterially-produced natural antibiotics. Below, I synthesize our main findings with regard to bacterial defenses against phenazine toxicity, links between natural antibiotics and clinical antibiotic resistance, and the prevalence of phenazine resistance in soil and the rhizosphere. I also provide some suggestions for future research directions, particularly with an eye towards bridging the gap between reductionist *in vitro* studies and predicting the ecological impacts of phenazines in complex communities and natural environments.

In Chapter 2, by taking a functional genetics approach to dissecting defenses against phenazine toxicity in *A. tumefaciens*, a soil bacterium that is relatively resistant to pyocyanin (PYO), I revealed a dose-dependent interplay between two contrasting yet complementary transcriptional regulation systems. At low doses of PYO, appropriate regulation of the terminal members of the respiratory electron transport chain (ETC) plays a crucial role in tolerance to PYO toxicity; upregulation of oxidative stress responses and multidrug efflux pumps seemingly cannot compensate for disruptions in this system. However, at high doses of PYO, these active resistance mechanisms become equally indispensable. In *P. aeruginosa*, the producer of PYO, the transcriptional responses to PYO are functionally similar to those found in *A. tumefaciens*, including ROS-detoxifying enzymes and specific efflux pumps. As discussed in Chapter 3, the latter are essential for the tolerance of *P. aeruginosa* to physiologically-relevant concentrations of PYO. Interestingly, unlike in *A. tumefaciens*, which displays an all-or-nothing response to PYO, the expression of PYO-regulated efflux pumps in *P. aeruginosa* is PYO dose-dependent. This difference may partially explain why low concentrations of PYO have a mild growth-inhibitory effect on *A. tumefaciens* but not *P. aeruginosa*, as eliminating the burdensome transcriptional response to PYO in *A. tumefaciens* improved growth at low-to-moderate doses (up to 50 μM PYO). In addition, in both *A. tumefaciens* and *P. aeruginosa*, disruptions of genes involved in cell wall or membrane modifications increased susceptibility to PYO toxicity, presumably by increasing cellular permeability and uptake of PYO.

Taken together, the results from both species suggest that minimizing intracellular redox cycling of PYO is key to intrinsic bacterial resistance to this natural antibiotic, and that multiple mechanisms can work in parallel towards this end. Thus, features such as possessing an outer membrane and efflux pumps that are homologous to known transporters of aromatic molecules may prove to be particularly informative when predicting phenazine resistance phenotypes in other bacteria. The composition of the ETC likely also plays an important role in modulating the sensitivity of different organisms to phenazines, but further studies will be necessary to develop a broad understanding of which variants are beneficial or detrimental.

Importantly, the efflux pumps induced by PYO in *P. aeruginosa* not only provide protection against this self-produced toxin, but also confer cross-tolerance to structurally similar clinical antibiotics, such as fluoroquinolones. PYO-mediated increases in antibiotic tolerance in turn promote the fixation of spontaneous antibiotic resistance mutations. This stimulatory effect of PYO on the evolution of heritable antibiotic resistance is robust in *P. aeruginosa*, and can be even more dramatic in other opportunistic pathogens, such as *B. multivorans*, that are known to form polymicrobial infections alongside *P. aeruginosa*. These findings, along with related examples reviewed in Chapter 4, suggest that natural antibiotics and certain other types of bacterial secondary metabolites may have underappreciated effects on clinical antimicrobial treatment outcomes, particularly in the context of opportunistic and/or chronic infections.

Finally, in order for a microorganism to benefit from exposure to a natural antibiotic, it must be able to tolerate any attendant toxicity. Given the pleiotropic effects of phenazines, being able to predict which species are intrinsically resistant to these natural antibiotics could be impactful in a variety of fields, from informing new approaches to antimicrobial therapy in polymicrobial infections, to refining risk assessments for phenazine-based biocontrol of crop diseases, to improving our understanding of which microbes might leverage phenazines for nutrient acquisition or anaerobic survival. As described in Chapter 5, I have advanced this goal by characterizing the phenazine-1-carboxylic acid (PCA) resistance profiles of bacteria isolated from a wheat field where phenazine producers are native members of the rhizosphere microbiota. I found that while Gram-positive bacteria are generally more sensitive to PCA than Gram-negative bacteria, especially under acidic conditions, there are occasional exceptions to the rule, and not all Gram-negative bacteria are equally resistant. Moreover, among *Streptomyces* species, which are a clade of bacteria known to contain

phenazine producers, I observed unexpected variation in the ability to resist PCA when grown at circumneutral pH. Together with the findings presented in Chapters 2 and 3, this work has set the stage for a multifaceted comparative approach that will reveal which genetic and physiological correlates are most predictive of resistance to phenazines and related redox-active natural antibiotics. In addition, with more than 100 taxonomically and phenotypically diverse strains, our collection of soil and wheat rhizosphere isolates will facilitate investigations of whether and how resistance to natural antibiotics shapes their ecological impact in complex microbial communities.

Future directions

Disentangling condition-dependent contributions of different modes of phenazine resistance

While genetic analysis of intrinsic phenazine resistance in *A. tumefaciens* and *P. aeruginosa* suggests that minimizing reactive oxygen species (ROS) production plays a central role in this phenotype, several questions remain open with regard to how different modes of controlling phenazine redox-cycling interact with each other, and which take precedence under different conditions. For example, is proper regulation of the respiratory ETC an essential prerequisite in all bacteria that are intrinsically resistant to phenazines, or is this necessity an idiosyncratic feature of *A. tumefaciens*? Does the robustness of a phenazine resistance phenotype depend on the number of branches in an organism's ETC or the degree of redundancy in ETC regulation? To what extent can enhanced efflux or oxidative stress responses compensate for increased cell permeability? Genetic analysis with combinatorial mutants in *P. aeruginosa* and other intrinsically resistant species, together with comparative genomics and/or heterologous expression of putative resistance genes in phenazine-susceptible organisms, may shed light on these issues. For example, as discussed in Chapter 5, the generally higher susceptibility of Gram-positive bacteria to phenazines compared to Gram-negative bacteria is thought to be related to cell permeability; the outer membrane of Gram-negative bacteria, which Gram-positive bacteria lack, acts as a barrier to the uptake of many other antibiotics, and may limit the uptake of phenazines as well. It would therefore be interesting to determine whether overexpression of a *P. aeruginosa* phenazine-regulated efflux pump in a Gram-positive organism can rescue growth in the presence of phenazines, or whether the inherently greater permeability of Gram-positive cells is an overriding factor that active resistance mechanisms cannot overcome.

It would also be worthwhile to investigate how the contributions of different pillars of phenazine resistance (including efflux, oxidative stress responses, cell wall, or membrane modifications, and ETC regulation) are modulated by oxygen tension, especially since phenazines are important for anaerobic energy conservation in *P. aeruginosa*. Notably, while ROS generation is thought to be the primary mechanism of phenazine toxicity, phenazines such as PYO still retain some of their toxicity under anoxic conditions (Baron and Rowe, 1981; Noto *et al.*, 2017; Meirelles and Newman, 2018). The mechanisms that drive this mode of toxicity are poorly understood, but may include the formation of reactive nitrogen species, oxidation of proteins, damage to iron-sulfur clusters, and/or DNA intercalation. The key resistance mechanisms that enable *P. aeruginosa* to take advantage of the redox-cycling properties of phenazines under oxygen limitation are also unknown. Identifying the relevant targets of phenazine toxicity and protective mechanisms under anoxic or microoxic conditions will require careful experimental design and more sophisticated approaches than those used under oxic conditions, given that phenazines can support anaerobic survival. If performing Tn-seq, for example, it will be necessary to disentangle cell death due to increased phenazine toxicity per se from cell death due to decreased ability to leverage phenazine redox-cycling for survival. One possible approach might be to perform an initial screen to identify mutants with a fitness disadvantage in the presence of phenazines under anoxic conditions, and subsequently monitor NADH/NAD+ ratios in the mutants of interest; if a mutant is unable to efficiently use phenazines as an electron shuttle for anaerobic survival (e.g. due to a defect in phenazine reduction), the NADH/NAD+ ratio should theoretically be higher than that of the wildtype strain, and more similar to that of a phenazine-null mutant in the absence of exogenous phenazines. However, some mechanisms, such as efflux, might be essential both for minimizing intracellular toxicity and for supporting efficient electron shuttling.

Assessing the impact of phenazines on the evolution of antibiotic resistance during infections

Our data indicate that exposure to PYO can significantly increase the rate of antibiotic resistance acquisition via spontaneous mutations, both in *P. aeruginosa* and in certain other opportunistic pathogens that are intrinsically resistant to PYO. However, while our experiments were performed in a clinically-relevant growth medium that mimics the environment of the CF lung, it remains to be seen whether the observed effects also occur in patients, and whether they have any bearing on treatment outcomes. In animal models of infections, it may be possible to perform

controlled experiments to address these questions. Infections could be initiated with otherwise isogenic PYO-producing or PYO-deficient strains of *P. aeruginosa* and the emergence of antibiotic resistant mutants could be monitored over time. The efficacy of different treatment strategies (e.g. using or avoiding drugs that are structurally similar to PYO) could also be interrogated in such models. However, it is important to keep in mind that animal models for CF and chronic wounds have a variety of limitations with regard to how faithfully they capture clinical features of these disorders (Grada *et al.*, 2018; McCarron *et al.*, 2018). In humans, it will only be possible to perform correlative analyses due to ethical considerations. Nevertheless, it may be possible to indirectly infer relationships between PYO production and antibiotic resistance; for example, the PYO production phenotypes of *P. aeruginosa* isolates from various stages of infection could be assessed alongside their clinical antibiotic resistance phenotypes. Ultimately, if there appears to be an empirical correlation between the production of PYO and either antibiotic resistance phenotypes or treatment outcomes, clinical trials could be carried out to determine the utility of accounting for secondary metabolite production during antimicrobial susceptibility testing—for example, by implementing one or more of the approaches discussed in Chapter 4.

Quantifying the production and spatial distribution of phenazines in the rhizosphere

In order to forecast the potential impacts of phenazine production on bacterial communities *in situ*, it will be useful not only to have a predictive understanding of phenazine resistance, but also to know where and to what concentration phenazines accumulate, and how far they can diffuse away from producing organisms. However, addressing these seemingly simple questions presents significant challenges. Existing measurements of phenazines in natural environments are based on organic extraction followed by high-performance liquid chromatography (Wilson *et al.*, 1988; Mavrodi *et al.*, 2012). The results of such analyses are expressed in nonintuitive units (e.g. nanograms of phenazines per gram of fresh roots) that are difficult to relate to the units of concentration (e.g. μM) that are typically used in laboratory experiments. Moreover, such measurements obscure any variation in local concentrations at the micron scale—which is the scale that likely matters to microorganisms.

One approach to measuring phenazine production and diffusion with higher spatial resolution would be to design a system of reporter genes in “producer” and “receiver” bacteria, and apply it to

the rhizosphere. In the producing organism, expression of a fluorescent protein could be coupled to the promoter that controls expression of phenazine biosynthesis genes. On the receiving end, expression of a different fluorescent protein could be placed under control of a phenazine-sensing transcription factor, such as SoxR, in an organism that does not make its own phenazines or other redox-active secondary metabolites. The regulation of the heterologous SoxR copies could further be tuned to yield either a dose-dependent response to phenazines (as is the case for SoxR in *P. aeruginosa*), or an all-or-nothing response (as is the case for SoxR in *A. tumefaciens* due to an autoregulatory positive feedback loop). The former approach could be validated against known concentrations of phenazines to generate a calibration curve, while the latter might offer a more sensitive detector to define the outer reaches of phenazine diffusion. The producers and receivers could then be inoculated into a complex *in vitro* system, such as an EcoFAB (Gao *et al.*, 2018), that recreates the rhizosphere environment while remaining amenable to fluorescence microscopy. However, while this approach would enable detailed characterization of the location of the bacteria in addition to revealing the distribution of phenazines, there are limitations: 1) SoxR is not specific to phenazines and can be activated by a wide range of redox-active metabolites, so it will be important to include control samples without the producer, and 2) it remains difficult to image fluorescently-tagged bacteria in natural soils, except by embedding samples in resin and thin-sectioning. Thus, it would also be worthwhile to develop mass spectrometry imaging techniques for direct detection of phenazines in "wild" rhizosphere samples (Veličković and Anderton, 2017). Conveniently, EcoFABs can also be made amenable to mass spectrometry imaging (Gao *et al.*, 2018), which would enable sample processing methods to be validated based on concordance between expression of phenazine biosynthesis reporter genes and actual detection of phenazines.

Determining effects of phenazine production on rhizosphere microbial communities

Even in the absence of quantitative, spatially-resolved *in situ* measurements of phenazines, it may be possible to empirically determine how phenazine production shapes rhizosphere microbial communities. Effects on overall taxonomic composition could be addressed through 16S and ITS rRNA amplicon sequencing and/or shotgun metagenomics, ideally with an initial focus on rhizospheres in EcoFABs or similar systems where highly controlled introduction of a phenazine-producing strain is possible. This type of analysis could subsequently be extended to more natural scenarios, such as temporally-resolved analysis of taxonomic composition before and after the

introduction of a biocontrol strain to an actual crop field. Meanwhile, effects on the spatial organization of different taxa could be addressed through techniques such as multiplexed, spectral imaging fluorescence *in situ* hybridization (FISH), using probes that are specific for individual genera or species. When paired with information on each taxon's biosynthetic capacity and susceptibility to phenazines, the spatial organization of the visualized taxa could indirectly reveal the extent to which phenazines accumulate and diffuse in the rhizosphere, as well as how different degrees of phenazine susceptibility affect the outcome of competition between strains.

Concluding thoughts

We are at an exciting junction in the study of phenazine biology. New physiological and ecological functions continue to come to light, and the potential impacts on multispecies bacterial communities are just beginning to be appreciated. Much can still be gained from using *in vitro* model systems to further refine the molecular details of how phenazines interface with microbial physiology. However, I believe the next great frontier is to take the insights we have acquired in the laboratory and test their predictive value in real-world environments. Fortunately, new tools and resources are making this ever more achievable, raising the tantalizing possibility that we will one day be able to leverage our knowledge of phenazines and other natural antibiotics not only to uncover fundamental principles of microbial ecology, but also to improve human medicine and agricultural sustainability.

References

Baron, S.S., and Rowe, J.J. (1981) Antibiotic action of pyocyanin. *Antimicrob Agents Chemother* **20**: 814–820.

Gao, J., Sasse, J., Lewald, K.M., Zhalnina, K., Cornmesser, L.T., Duncombe, T.A., *et al.* (2018) Ecosystem fabrication (EcoFAB) protocols for the construction of laboratory ecosystems designed to study plant-microbe interactions. *J Vis Exp* **134**: e57170.

Grada, A., Mervis, J., and Falanga, V. (2018) Research techniques made simple: animal models of wound healing. *J Invest Dermatol* **138**: 2095–2105.e1.

Mavrodi, D.V., Mavrodi, O.V., Parejko, J.A., Bonsall, R.F., Kwak, Y.-S., Paulitz, T.C., *et al.* (2012) Accumulation of the antibiotic phenazine-1-carboxylic acid in the rhizosphere of dryland cereals. *Appl Environ Microbiol* **78**: 804–812.

McCarron, A., Donnelley, M., and Parsons, D. (2018) Airway disease phenotypes in animal models of cystic fibrosis. *Respir Res* **19**: 54.

Meirelles, L.A., and Newman, D.K. (2018) Both toxic and beneficial effects of pyocyanin contribute

to the lifecycle of *Pseudomonas aeruginosa*. *Mol Microbiol* **110**: 995–1010.

Noto, M.J., Burns, W.J., Beavers, W.N., and Skaar, E.P. (2017) Mechanisms of pyocyanin toxicity and genetic determinants of resistance in *Staphylococcus aureus*. *J Bacteriol* **199**: e00221-17.

Veličković, D., and Anderton, C.R. (2017) Mass spectrometry imaging: towards mapping the elemental and molecular composition of the rhizosphere. *Rhizosphere* **3**: 254–258.

Wilson, R., Sykes, D.A., Watson, D., Rutman, A., Taylor, G.W., and Cole, P.J. (1988) Measurement of *Pseudomonas aeruginosa* phenazine pigments in sputum and assessment of their contribution to sputum sol toxicity for respiratory epithelium. *Infect Immun* **56**: 2515–2517.